RUTHENIUM POLYPYRIDYL COMPOUNDS AS LUMINESCENT PROBES FOR BIOLOGICAL MATERIALS.

by

Eleanor M. Ryan, BSc. (Hons), MSc.

A Thesis presented to Dublin City University for the degree of Doctor of Philosophy.

This work was carried out under the supervision of

Dr. J.G. Vos, School of Chemical Sciences

and

Dr R. O'Kennedy, School of Biological Sciences,

at

Dublin City University, Dublin.

October 1991.

To my parents and Mick.

This thesis has not previously been submitted as an exercise for a degree at this or at any other university. Except as otherwise indicated, this work has been carried out by the author alone.

Eleanor Ryan

Eleanor Ryan

Abstract

The synthesis and characterisation of ruthenium (II) bis-(1,10-phenanthroline) and bis-(2,2'-bipyridyl) complexes containing amino and isothiocyanate phenanthroline and pyridine ligands are described. These complexes were characterised using HPLC, UV/vis spectroscopy, electrochemistry, NMR, IR, and emission spectroscopy. HPLC was used to determine the purity of the various complexes.

Electronic spectra and electrochemical measurements indicate that most likely, the 2,2'-bipyridyl and 1,10-phenanthroline ligands are the emitting ligands and the amino and isothiocyanate phenanthroline and pyridine ligands act as the spectator ligands.

These complexes were subsequently conjugated to biological materials, including albumins, immunoglobulins and poly-L-lysine. The complexes were bound at different sites on the biomolecules, via the lysine residues, the carbohydrate moieties and via the tyrosine residues.

The effect of conjugation on the spectroscopic properties of the complexes was examined. The absorption spectra were found to exhibit changes in the MLCT band with the absorption wavelength maximum experiencing slight red shifts together with general band broadening effects. The emission decay behaviour was also investigated. The unbound complexes were found to exhibit single exponential decay behaviour and the bound complexes exhibited essentially double exponential behaviour. From the double exponential decay fits, the first short-lived species was suggested to be a quenched bound species whilst the second species probably arises from a bound species which is considerably protected from the effects of quenching molecules.

The synthesis and characterisation of a number of bis-(1,10-phenanthroline) (phen), and bis-(4,4'-dimethyl-2,2'-bipyridyl) (dmbpy), ruthenium (II) complexes containing a series of pyridyltriazole ligands are described. The ruthenium ion may bind via the $N^{1'}$/ $N^{2'}$ or $N^{4'}$ of the

triazole ring. The most favourable coordination mode being dependent on the position of a substituent on the triazole ring. Coordination isomers were obtained and separated by semi-preparative HPLC methods. The electrochemical results suggest that the phen and dmbpy ligands are the emitting ligands and that the pyridyltriazole ligands are the spectator ligands.

The acid-base chemistry of those pyridyltriazole complexes which can undergo protonation / deprotonation reactions was investigated and the results substantiated the coordination modes proposed using NMR data for the complexes. The ground state pK_a values show that there is a strong σ-donating effect from the triazole ring to the ruthenium ion. Also, the excited state pK_a^* values are lower than the ground state pK_a values which indicates that the pyridyltriazole ligands do not participate in the emission process. This study completes investigations which were initially conducted on the 2,2'-bipyridyl analogues.

Acknowledgements

I wish to thank Dr. Han Vos and Dr. Richard O'Kennedy for their help, encouragement and patience over the past few years. Their assistance in the preparation of this manuscript is greatly appreciated.

I wish to acknowledge the help received from Prof. John Kelly and Martin Feeney, of the Chemistry Dept. at Trinity College Dublin where the emission decay lifetimes were measured by TCSPC. Special thanks go to Martin, without whose help, these lifetimes would never have been measured. Thanks also to Prof. John Kelly for his constructive comments on the measurements.

I wish to express my gratitude to Boris, Koos and Fokke Fennema for allowing me to stay with them during my visit to Holland. Thanks also to Ronald Hage, for assistance in analysing the NMR spectra, and to Dr. J.G. Haasnoot and Prof. J. Reedijk for allowing me use of the lab. facilities whilst I was working in Leiden University.

In my own research group, I wish to thank Renyi Wang and Robert Forster for all their help. Special thanks to Renyi for carrying out lifetime measurements in Tulane University, and for helping with electrochemical measurements. Thanks also to Helen, Barbara, Alan, Andy and Boris, my fellow ruthenium researchers !

To my fellow postgraduates both past and present for their friendship and encouragement particularly Paula, Bernie, Barbara, Mary K, Mary M, Robert, Renyi, Helen, Barry, Gerry, Graham, Joe, Alan and Conor.

Thanks also to the technical staff at D.C.U., again both past and present, Theresa, Mick, Ita, Peig, Maurice, Fintan, Veronica, Orla and Dawn, who were always willing to oblige.

Thanks to Janice for helping me with the photocopying, sticking and pasting.

Thanks to both the Chemistry and Biology Departments for maintenance grants.

I would like to acknowledge Prof. Albert Pratt and Dr. Malcolm Smyth for the use of the Chemistry Dept. facilities and Dr. Richard O'Kennedy for the use of the Biology Dept. facilities.

I wish to acknowledge the support and encouragement received from everyone at the Oncology Labs., Mater Hospital.

Finally, I would like to express my thanks to Mick, my parents, Ricky, Don and Alison who have supported me financially and morally, willingly and otherwise ! during the course of this work, my M.Sc. and B.Sc. studies.

Table of Contents.

Chapter 2 Materials and Methods.

Chapter 4 The Conjugation of Ruthenium Polypyridyl Complexes to Biomolecules.

CHAPTER 1

INTRODUCTION

1.1 Introduction.

The primary concern of this thesis is the application of ruthenium polypyridyl compounds as fluorescent labels in biological systems. The second part involves a study of the synthesis and characterisation of bis-(1,10'-phenanthroline) and bis-(4,4'-dimethyl-2,2'-bipyridyl) ruthenium compounds containing various pyridyltriazole ligands and is a continuation of studies carried out on the analogous bis-(2,2'-bipyridyl compounds). [1,2]

The common factor in both these projects is the use of ruthenium polypyridyl compounds, therefore, it is appropriate to commence with a review of the properties of ruthenium polypyridyl compounds relevant to this thesis. This chapter will also survey the literature in relation to the use of fluorescent labels in biological systems with emphasis on the application of ruthenium compounds in this manner. The literature will also be summarised in regard to the study of the ruthenium coordinated pyridyltriazole complexes.

Hundreds of papers have been published about various aspects of ruthenium polypyridyl spectroscopy, photophysics, photochemistry and electrochemistry, in particular $[Ru(bpy)_3]^{2+}$ where bpy = 2,2'-bipyridyl, has received extensive attention. [3,4,5,6,7]

1.2 The structure and physical properties of ruthenium polypyridyl complexes.

Ru^{2+} is a d^6 system and the polypyridyl ligands are usually colourless molecules possessing σ-donor orbitals localised on the nitrogen atoms and π-dcnor and π^*-acceptor orbitals more or less delocalised on aromatic rings. The compound $[Ru(bpy)_3]^{2+}$ and other $[Ru(L\text{-}L)_3]^{2+}$ compounds where L-L = bidentate polypyridyl ligand, exhibit D_3 symmetry and the π and π^* orbitals of the ligands may be symmetrical (χ) or anti-symmetrical (ψ) with respect to rotation around the C_2 axis retained by each Ru(bpy) unit. [3] The X-ray crystal structure for $[Ru(bpy)_3]^{2+}$ shows that the metal to ligand (Ru-N) bond lengths are short, indicating significant back-bonding between Ru(II) and the π^* orbitals of bpy. [3]

For most Ru(II) polypyridyl complexes, the lowest excited state is a ^{3}MLCT (metal to ligand charge transfer) transition, [8,9,10] which undergoes slow radiationless decay and thus exhibits long lifetime luminescence emission. [4] An important advantage of MLCT excited states is the presence of two distinct redox sites, i.e. an oxidising site on the metal and a reductive site on the ligands. [3] The energy position of the MLCT state depends on the redox properties of the metal and ligands, in particular on the σ-donor or π-acceptor properties of the ligands. [11]

Compounds containing strong σ-donor ligands

donate much electron density into the metal d orbitals, causing lower oxidation potentials and more negative reduction potentials. Strong π-acceptor ligands stabilise the filled metal orbitals giving rise to high oxidation potentials and low reduction potentials. The σ-donor strength of the ligands modulates the metal d orbital energies. Weaker σ-donor ability to a central metal ion results in a higher formal charge on the metal and consequently, the stabilisation of the metal d orbital. The σ-donor ability of the ligand is related to the pK_a of the free ligand. The difference in energy between the filled d orbitals and the lowest unoccupied ligand-based orbital is related to the absorption and emission energy of the complexes. By a judicious choice of ligands in a series of complexes of the same metal ion, the orbital nature of the lowest excited state and, hence, its energy, emission lifetime, emission quantum yield, redox properties, chemical stability and oxidation and reduction potentials can be controlled. [3]

As a consequence of the unique combination of photochemistry, electrochemistry and chemical stability of Ru(II) polypyridyl type compounds, they find application as a) photoluminescent compounds; b) excited state reactants in electron and energy transfer processes and c) excited state products in electron transfer chemiluminescence and electrochemiluminescence. [12]

$[Ru(bpy)_3]^{2+}$ has been recognised as a potential catalyst for the decomposition of water into its

elements by irradiation with solar light. [13] However, a major disadvantage is that $[Ru(bpy)_3]^{2+}$ is not photochemically inert towards ligand substitution. Ligand photosubstitution may be avoided by increasing the energy gap between the ^{3}MLCT and ^{3}MC state. This may be achieved by the choice of other ligands such that the ground and excited state properties of the compounds may be improved. [3] Also, this drawback may be remedied by the use of caged ruthenium polypyridyl complexes which have much better chemical stability and longer excited state lifetimes. [14,15,16] Other problems associated with water splitting systems include problems with the platinum catalyst, inefficient electron transfer processes, the separation of the evolving dihydrogen and dioxygen gases and back reactions. [13]

1.2.1 Absorption spectroscopy.

The absorption spectrum of $[Ru(bpy)_3]^{2+}$ is shown in Figure 1.1. The intense transitions observed in the visible region are due to the metal to ligand charge transfer transition between the metal centred t_{2g} ground state and ligand π^* states. [3,8,9,10] The intense bands in the ultraviolet region have been assigned to intraligand π - π^* transitions by comparison with the spectrum of the protonated bipyridine.

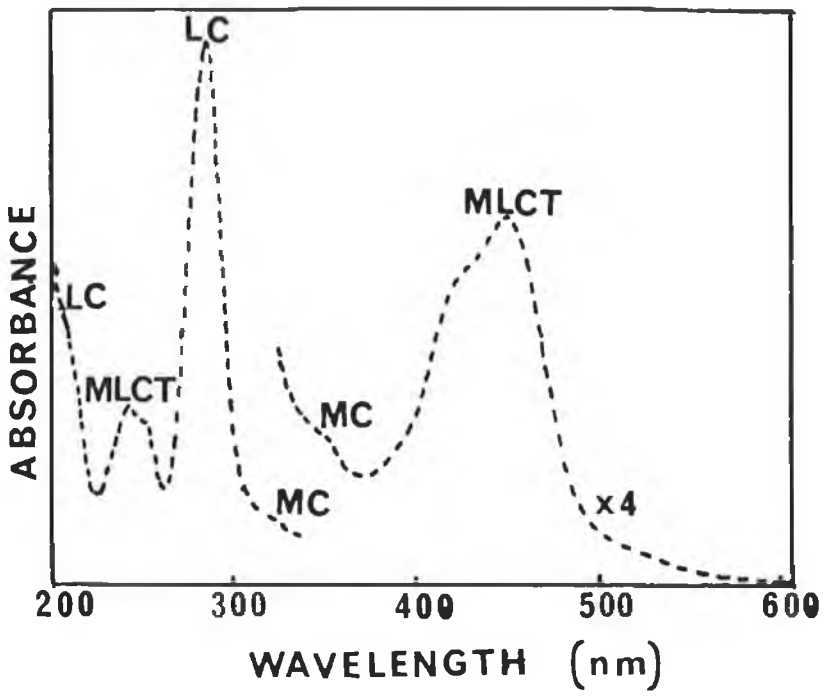

Figure 1.1 Absorption spectrum of $[Ru(bpy)_3]^{2+}$ in aqueous solution, with the assignments for the various bands.

Exact assignment of the multiplicity of levels involved in the MLCT excited state is not possible because of the heavy atom effect where spin-orbit coupling mixes the two spin states. However, it has been established that the electronic transitions of $[Ru(bpy)_3]^{2+}$ may be assigned as either singlet or triplet states. In particular, a singlet character of about 10% has been estimated for the lower lying excited states of $[Ru(bpy)_3]^{2+}$. Excitation leads to a state, which is best defined as ^{1}MLCT from which intersystem crossing occurs with unit efficiency to a lower lying MLCT considered triplet in character and from which emission occurs. [17,18]

The weaker absorption observed to the blue of the visible band has been assigned to a metal centred d-d* transition while the tail at longer wavelengths has been assigned to a weak spin-forbidden MLCT transition. [4,8] It is now believed that the excited electron is delocalised among the ligands in the ^{1}MLCT excited state but that as interaction between the ligands is low, it localises on only one ligand when intersystem crossing to the ^{3}MLCT excited state takes place, Figure 1.2.

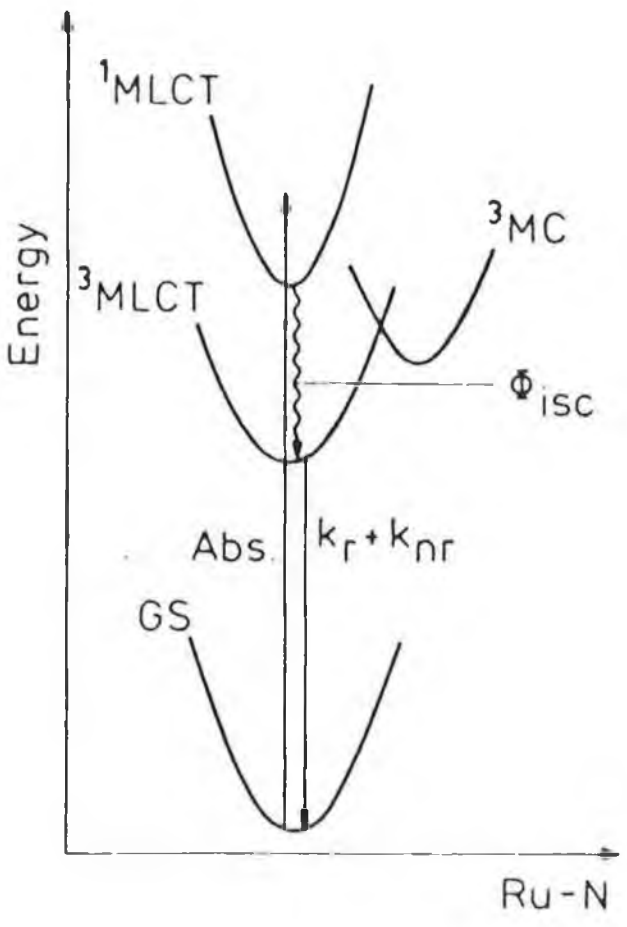

Figure 1.2 Representation of the excited state properties of $[Ru(bpy)_3]^{2+}$.

1.2.2 Emission spectroscopy.

The exact nature of emission in ruthenium polypyridyl compounds is surrounded by controversy and uncertainty. The points of contention are the nature and multiplicity of the levels involved and whether charge transfer results in the electron being localised on one ligand or delocalised over all the ligand orbitals.

The electronic structural model proposed by Kober and Meyer, [8,9,10] seems best to describe the photophysical events in $[Ru(bpy)_3]^{2+}$ and related compounds. This model assumes very little interaction occurs between ligands so that the excited electron is localised on one orbital for the lifetime of the excited state. While including spin-orbit coupling this model finds that the ^{1}MLCT and ^{3}MLCT states are predominantly singlet and triplet in character, respectively.

A second model proposed by Crosby *et al.* [19,20,21], has also been used to explain the nature of the MLCT states involved in emission. This electron ion-pairing model assumes that the terms singlet and triplet become meaningless because of strong spin-orbit coupling. The model also assumes ligand interaction such that the excited electron is delocalised among them. The symmetry of the excited state remains D_3, and the ^{3}MLCT state, which is split into three levels, is populated according to the Boltzmann distribution. All the states have mixed

multiplicities and the emission can be considered as essentially spin-forbidden from a manifold of states.

A general model of the photophysical processes of $[Ru(bpy)_3]^{2+}$ has already been presented in Figure 1.2. The electron is excited to a ligand centred ^{1}MLCT manifold which is singlet in character. Fast intersystem crossing occurs with unit efficiency from the singlet state to the triplet manifold of three closely spaced ^{3}MLCT states, (shown through detailed studies on the temperature dependence of the emission lifetime and quantum yield in the temperature range 2-70 K), with a fourth state occurring several hundred cm^{-1} to higher energy. The presence of the fourth MLCT state in Ru(II) polypyridyl complexes is usually masked by the deactivating ^{3}MC state. The three lowest lying levels are fairly close together (ΔE is about $100cm^{-1}$) and have predominantly triplet character. Calculations on the fourth higher state have shown that this state has more singlet character than the other three lower lying states. [8,9,10]

At higher temperatures all of these states are populated and contribute to the excited state decay so that the excited state manifold may be considered as an average state and on emission, results in a broad band. At low and ambient temperatures the contributions of the upper states (unless they are extremely short lived) are thought to be negligible. At low temperatures, the emission spectrum exhibits a fine structure which has been attributed to a perturbed skeletal vibration of the aromatic ring due to removal of the π^* electron. The maximum wavelength of

emission occurs at higher wavelength (lower energy) at room temperature compared to that at low temperature. This red shift of the emission λ max. in comparison to the emission λ max. at low temperature, is called the rigidochromic effect and has been attributed to relaxation of the rigid matrix perturbation.

Emission from the triplet state to the ground state (K_r) or radiationless decay (K_{nr}) to the ground state can take place. The ^{3}MC state is responsible for a further deactivating pathway giving rise to either radiationless deactivation or photodecomposition of the complex.

Emission intensities are stronger at lower temperature. This may be explained by the energy difference between the emitting ^{3}MLCT state and the deactivating ^{3}MC state. [10,22,23,24,25] At room temperature, thermal population of this deactivating state is possible [4,11,26], and hence K_r will decrease i.e. the emission intensity decreases. At low temperatures, thermal population of the ^{3}MC state is not possible and K_r increases resulting in a more intense emission. The ^{3}MC dd state lies about 4000cm^{-1} above the ^{3}CT manifold, and has a high rate of radiationless decay. In addition to being responsible for thermal deactivation, this ^{3}MC state is accountable for photochemical reactions such as racemisation and photosubstitution. [27,28,29] Non-radiative decay occurs but less efficiently from the ^{3}CT manifold which is important at low temperatures and is dependent on vibrational activity and on the solvent. [30] For most complexes there is a

radiationless deactivation path which is to some extent "frozen" when the solvent matrix is rigid at low temperature and becomes important only as the solvent matrix becomes "fluid" at room temperature. [31]

Studies indicate that there is some CTTS (charge transfer to the solvent) character in the MLCT states and while this has little effect on the radiative decay of the excited state, it does effect the radiationless decay through thermally accessed ^{3}MC states and has an important role in the photochemistry of the ruthenium polypyridyl compounds. [4,6,7,27,30,32]

1.2.3 Emission lifetime and temperature dependence.

Temperature dependence studies of the luminescence behaviour can yield information concerning energy, electronic nature, and deactivation rate of the luminescent and reactive states.

The essential features of the temperature dependence (Figure 1.3) of the luminescence decay of $[Ru(bpy)_3]^{2+}$ are (a) an Arrhenius type behaviour of the luminescence decay in the rigid glass region (84-100 K); (b) a discontinuity in the glass-fluid transition region (about 100-150 K); (c) an Arrhenius type behaviour in the 150-250 K temperature range with essentially the same parameters as in the rigid glass and (d) another steeper Arrhenius type region for $T > 250$ K. This complex behaviour has been accounted for by the equation given

below, where Ko' is a temperature-independent term;

$$1/\tau = K_{o'} + \frac{B_i}{1 + \exp\,[C(1/T-1/T_b]} + A_1 e^{-\Delta E1/RT} + A_2 e^{-\Delta E2/RT}$$

The second term takes care empirically of the behaviour in the glass-fluid transition and the two exponential terms account for the Arrhenius behaviour at low and high temperature. The temperature behaviour of $[Ru(bpy)_3]^{2+}$ has been accounted for as follows: emission originates from a cluster of closely spaced (ΔE about 100 cm^{-1}) MLCT levels having similar but not identical decay properties. When the matrix melts, large amplitude (low frequency) vibrational modes come into play, which enhance the rate of radiationless deactivation processes, with a consequent decrease in lifetime and intensity. Once the glass is completely melted, the slightly activated Arrhenius behaviour continues because the emission always originates from the same cluster of MLCT excited states. As already mentioned, at higher temperatures, a ^3MC excited state which lies about 4000 cm^{-1} above the emitting levels becomes accessible. Since this level is strongly distorted compared with the ground state geometry, it undergoes very fast radiationless decay which includes ligand substitution and racemisation reactions. The fourth MLCT excited state

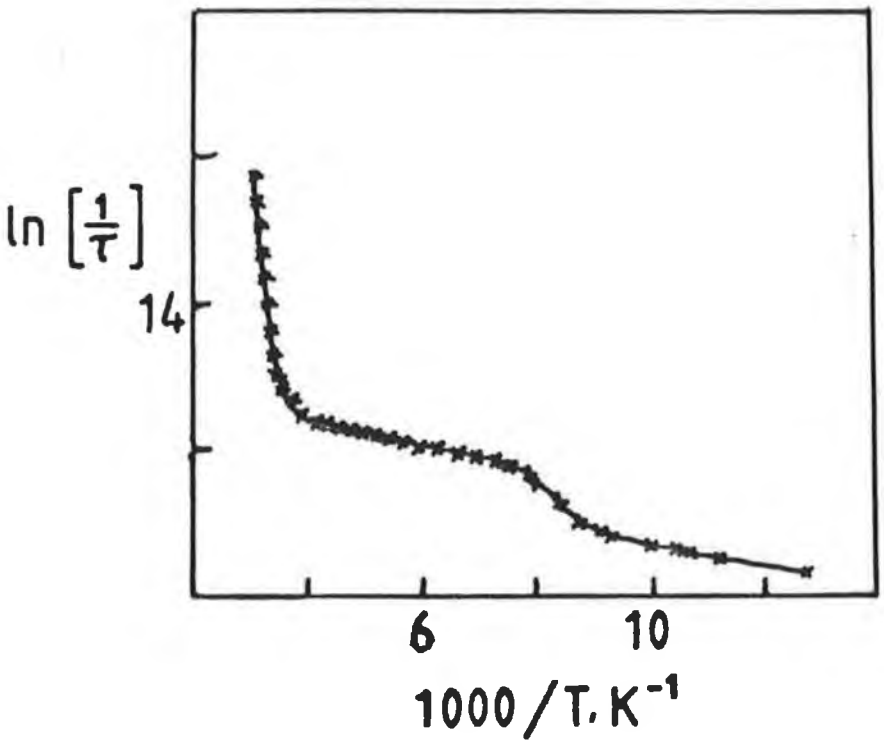

Figure 1.3 Temperature dependence behaviour of $[Ru(bpy)_3]^{2+}$ in nitrile solution.

at several hundred cm^{-1} higher with the largely singlet character does not play a role in the temperature dependence behaviour because it is "masked" by the surface crossing to ^3MC. [3,33]

1.2.4 Electrochemical properties of $[Ru(bpy)_3]^{2+}$.

Four successive reversible one electron cyclic voltammetric responses are observed for $[Ru(bpy)_3]^{2+}$, see Figure 1.4. One couple at positive potential corresponds to a metal based oxidation and three couples at negative potentials correspond to successive bpy reductions.

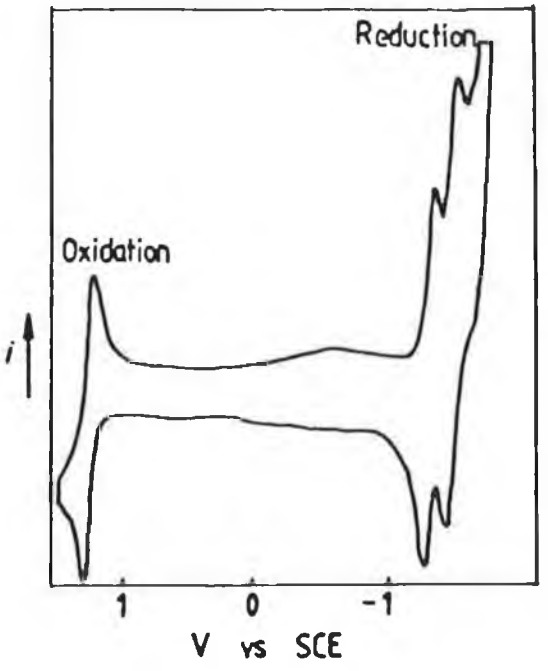

Figure 1.4 Cyclic voltammagram of the oxidation and reduction processes of $[Ru(bpy)_3]^{2+}$ in CH_3CN/0.1 M NEt_4ClO_4 (TEAP).

Oxidation of $[Ru(bpy)_3]^{2+}$ involves a metal centred orbital with formation of a low spin $4d^5$ system which is inert to ligand substitution:

$$[Ru(bpy)_3]^{2+} \rightleftharpoons [Ru(bpy)_3]^{3+} + e^-$$

The oxidation potential of $[Ru(bpy)_3]^{2+}$ occurs at 1.26 V. By substituting one or more of the bpy ligands, the oxidation potential can be changed dramatically. For instance, the substitution of one bpy ligand in $[Ru(bpy)_3]^{2+}$ with two Cl^- ions to give $[Ru(bpy)_2Cl_2]$ lowers the oxidation potential to about 0.35 V vs SCE (saturated calomel electrode), whereas substitution with two strong π^*-acceptor CO molecules increases the oxidation potential above 1.9 V in $[Ru(bpy)_2(CO)_2]^{2+}$. [3] This shows that the oxidation potential of the ruthenium complexes is strongly dependent on the σ-donor or π-acceptor properties of the ligands. [3]

Reduction of $[Ru(bpy)_3]^{2+}$ involves a ligand centred π^* orbital, which is the commonly observed behaviour for Ru(II) polypyridyl compounds where the ligand field is sufficently strong and/or the ligands may be easily reduced.

$$[Ru((bpy)_3]^{2+} + e^- \rightleftharpoons [Ru(bpy)_2(bpy^-)]^+$$

The added electron appears to be localised on a single ligand. Several reduction steps may be observed and up to 6 electrons can be pumped into the complex at low temperature, yielding $[Ru(bpy^{2-})_3]^{4-}$. [3]

The localisation of the acceptor orbitals in the reduction processes is often very clear in mixed ligand compounds involving polypyridyl ligands with different π^* orbital energies. Strong π-accepting ligands have low lying π^* orbitals and compounds containing such ligands are easily reduced. Compounds containing weak π^*-accepting orbitals have a much more negative reduction potential. In mixed ligand complexes the first reduction potential usually involves the ligand with the lowest lying π^* orbital. [3]

1.2.5 Chemistry and quenching reactions of the $[Ru(bpy)_3]^{2+}$ excited state.

The first step in any photochemical and photophysical process is the absorption of a photon by a molecule. The excited state that is formed in this way is a high energy unstable species which must undergo some type of deactivation process. Excited state deactivation can occur in a number of ways, as shown in Figure 1.5.

Deactivation may occur via (i) disappearance of the original molecule which undergoes some photochemical reaction; (ii) emission of light (luminescence); (iii) degradation of the

excess energy into heat (radiationless deactivation) and (iv) some type of interaction with other species present in the solution (quenching processes). [3]

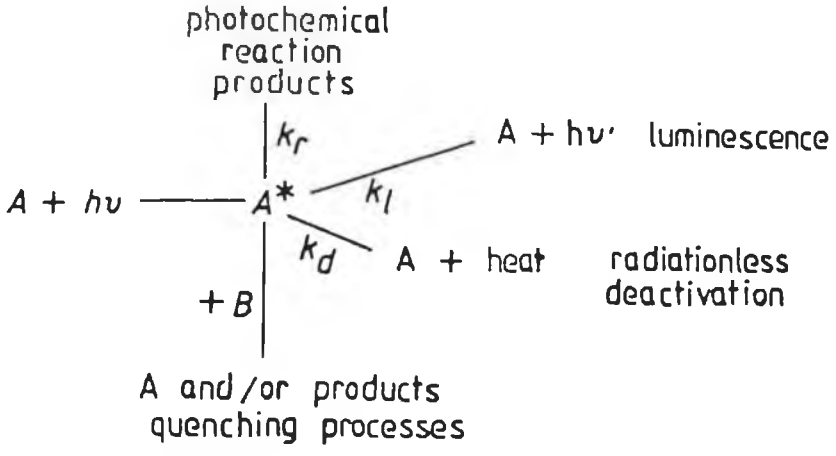

Figure 1.5 Schematic representation of excited state deactivation processes.

Processes involving radiationless deactivation, quenching or photochemical reactions compete with the luminescent decay process of the excited state. The presence of the thermally accessible ^{3}MC state may result in deactivation through photosubstitution and photoracemisation processes. [28,29,30]

When the lifetime of the excited state is sufficiently long, the excited state may have a chance to encounter a molecule of another solute. Interaction may occur bimolecularly, leading to quenching of the excited state.

The lowest ^{3}MLCT excited state of $[Ru(bpy)_3]^{2+}$ lives long enough to encounter other solute molecules and possesses suitable properties to play the role of energy donor, electron donor or electron acceptor. Figure 1.6 shows the energy avaliable to the excited $^*[Ru(bpy)_3]^{2+}$ and its reduction and oxidation potentials.

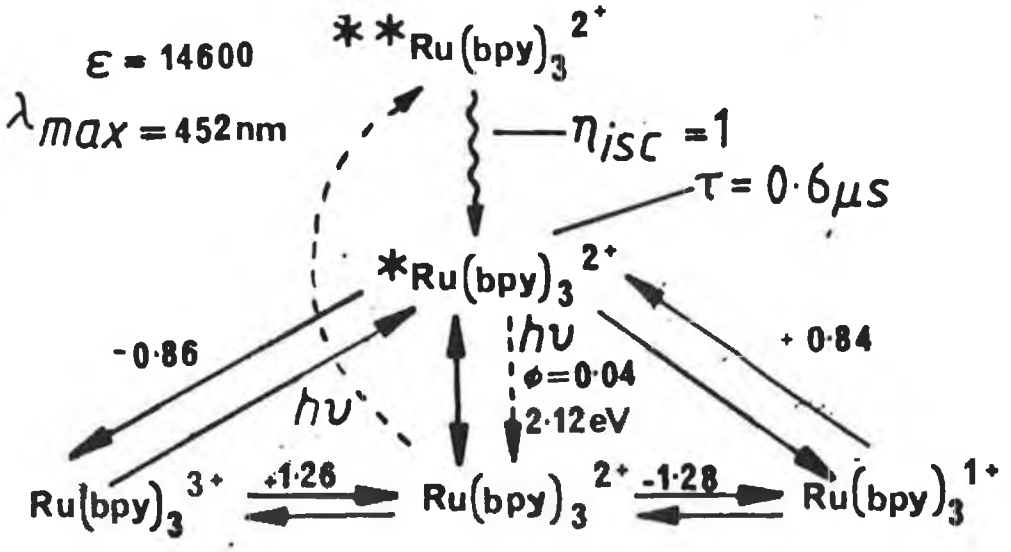

Figure 1.6 Molecular quantities of $[Ru(bpy)_3]^{2+}$ relevant for energy and electron transfer processes. $^{**}[Ru(bpy)_3]^{2+}$ indicates spin-allowed excited states and $^*[Ru(bpy)_3]^{2+}$ indicates the lowest spin-forbidden excited state (^{3}MLCT) $[Ru(bpy)_3]^{2+}$.

The excited state redox potentials estimated from corresponding ground state values and the excited state energy, indicate that the luminescent excited state is a strong reductant as well as a good oxidant. The higher energy content of an excited state means that the excited state is both a stronger reductant and oxidant than the corresponding ground state. [3]

The most important bimolecular processes are energy transfer and electron transfer. [3,4,7]

(1) $^{*}[Ru(bpy)_3]^{2+} + Q \longrightarrow [Ru(bpy)_3]^{2+} + Q^{*}$

(1) Energy transfer

(2) $^{*}[Ru(bpy)_3]^{2+} + Q \longrightarrow [Ru(bpy)_3]^{3+} + Q^{-}$

(2) Oxidative quenching

(3) $^{*}[Ru(bpy)_3]^{2+} + Q \longrightarrow [Ru(bpy)_3]^{+} + Q^{+}$

(3) Reductive quenching

The excited state acts as (i) an energy donor in process (1); (ii) a reductant in process (2) and (iii) an oxidant in process (3).

Energy transfer (process (1)) is a physical process where through contact, an excited state molecule transfers its energy to another molecule. The second and third processes involve electron transfer from/to the excited molecule and simultaneous oxidation or reduction of another species in solution.

The actual quenching mechanism is determined by both thermodynamic and kinetic factors and most often establishment of the actual mechanism is quite difficult. The ability to undergo energy transfer is related to the zero-zero spectroscopic energy E^{0-0} of the donor-acceptor pair (spectral overlap) and that of electron transfer to the redox potentials. The kinetic factors are associated with the activation energy needed to reorganise the inner and outer shells before electron transfer can occur. [4]

The assignment of quenching processes to "energy transfer" requires either direct observation of the acceptor phosphorescence or at least photoreactions arising from the excitation into the acceptor excited sites. The number of authenticated cases of energy transfer from $^{*}[Ru(bpy)_3]^{2+}$ are very few. [3] A clear example of the quenching of $^{*}[Ru(bpy)_3]^{2+}$ by $[Cr(CN)_6]^{3-}$ has been demonstrated by the observation of sensitised phosphorescence from the chromium complex. In this case both reductive and oxidative $^{*}[Ru(bpy)_3]^{2+}$ electron transfer quenchings by $[Cr(CN)_6]^{3-}$ are thermodynamically forbidden, because it is very difficult to oxidize or reduce $[Cr(CN)_6]^{3-}$. [3,4,34]

In contrast, $[Cr(bpy)_3]^{3+}$ can be very easily reduced and with this quencher, oxidative electron transfer prevails over energy transfer, which has been demonstrated by the appearance of the $[Cr(bpy)_3]^{2+}$ absorption spectrum in flash photolysis experiments. [3,4,35] The direct observation of redox products in flash photolysis represents the strongest evidence to support the occurrence of oxidative and reductive quenching mechanisms. [3]
An example of reductive electron transfer quenching is that involving Eu^{2+} as the quencher. [36,37]

$$[Ru(bpy)_3]^{2+} + Eu^{2+}(aq) \longrightarrow [Ru(bpy)_3]^{+} + Eu^{3+}(aq)$$

The absorption spectrum obtained after flash photolysis shows bleaching effects due to depletion of $[Ru(bpy)_3]^{2+}$ and increased absorption due to the formation of $[Ru(bpy)_3]^{+}$. The increased absorption due to the $[Ru(bpy)_3]^{+}$ occurs at the same rate of decay of luminescence emission of $^{*}[Ru(bpy)_3]^{2+}$ and indicates kinetically that reductive quenching has taken place.

Quenching of the excited state of $[Ru(bpy)_3]^{2+}$ has been widely investigated. The excited state has been shown to be quenched by a variety of inorganic species. [3,4]

A useful parameter in considering an excited state is its mean lifetime given by;

$$1/\tau = K_{obs}$$

where τ = lifetime and K_{obs} = decay rate constant. This is the average lifetime for an excited state, decaying by all possible decay mechanisms, each with its own decay constant so that;

$$1/\tau = K_r + K_{nr} + K_q[Q]$$

where K_r = rate constant for emission, K_{nr} = rate constant for internal non-radiative decay and K_q = rate constant for bimolecular quenching with Q, a quencher such as triplet oxygen, $^3O_2$.
From this is derived the Stern-Volmer equation;

$$1/\tau = 1/\tau_o + K_q[Q]$$

where τ and τ_o are the observed lifetimes in the presence and absence of the quencher respectively, [Q] is the concentration (M) of the quencher and K_q is the quenching rate constant.

This describes the effect of a quencher in solution on the lifetime. [38,39,40] A Stern-Volmer plot of $1/\tau$ vs [Q] yields K_q (slope).

Compounds containing unpaired electrons can act as efficient quenching agents. The most important compound of this type is molecular oxygen which is well known as a paramagnetic species and is universally present in solution

in all samples. It is particularly effective in removing the energy from triplet state molecules and is, therefore, a particular problem in phosphorescence and with molecules possessing relatively long fluorescence lifetimes. Oxygen is one of the few molecules which effectively quenches $^{*}[Ru(bpy)_3]^{2+}$ ($K_q = 3.3 \times 10^9 M^{-1}s^{-1}$). Singlet oxygen formation by energy transfer and electron transfer mechanisms has been proposed. The lifetime of $^{*}[Ru(bpy)_3]^{2+}$ is reduced by about a third in aerated aqueous solutions, however, bubbling with nitrogen or argon reduces oxygen quenching to less than 1%. [6]

Although the Stern-Volmer method for the determination of quenching constants is widely used, it is difficult to deduce from a single study which of the three mechanisms is responsible for quenching. Clarification of which process is responsible for Stern-Volmer behaviour may be obtained by examination of the dependence of the quenching constants (K_q), for a given quencher, on the excited state reduction potential of a series of closely related Ru(II) polypyridyl complexes. Dependence of K_q on the excited state potential indicates quenching by electron transfer processes whilst absence of any dependence suggests quenching by energy transfer mechanisms. [7]

Sometimes it is difficult to obtain direct evidence for energy transfer quenching (sensitised luminescence or absorption spectrum of the excited acceptor), or electron transfer quenching (absorption spectrum of redox products). In such cases, it has been shown that free energy correlation

of rate constants are useful in elucidating the quenching rate mechanism. [3]

1.2.6 Acid-base properties of the ground and excited states of ruthenium polypyridyl complexes which undergo proton transfer reactions.

One concern of this thesis was the continuation of studies conducted on various bis-(2,2'-bipyridyl) ruthenium pyridyltriazole compounds. In this work,bis-(4,4'-dimethyl-2,2'-bipyridyl) and bis-(1,10-phenanthroline) ruthenium pyridyltriazole compounds were investigated. Some of these pyridyltriazole compounds may undergo proton transfer reactions. Studies on ruthenium complexes which can undergo proton transfer reactions are of interest since the acid-base properties of the ground state and excited state can often be related to electron density distributions in the compounds and the nature of the lowest unoccupied molecular orbital (LUMO) of the ruthenium complexes. The nature of the LUMO may be revealed by measurement of the ground state pK_a and the excited state pK_a, pK_a^*. This is especially important in mixed ligand complexes where emission can be located on one or other of the ligands.

Usually, upon coordination to ruthenium the pK_a of the ligand decreases because of electrostatic effects due to the positive charge on the metal ion and because of σ-donation from the ligand to the metal. [41,42,43,44]

One exception is $[(NH_3)_5Ru(pyrz)]^{2+}$ where pyrz = pyrazine, which exhibits reverse behaviour and the pK_a of the coordinated pyrazine is higher when coordinated to the ruthenium ion. [45] This has been attributed to the strong back-donation of electron density from the filled metal based t_{2g} orbitals into the unoccupied π^* anti-bonding orbitals of the pyrz ligand, thus making the second nitrogen of this ligand more basic when coordinated. [45]

It is generally accepted that the excited state acidity of a metal complex is related to the nature of its emitting state. [46] If the acidity of the excited state is greater than that of the ground state, the ligand is not expected to be involved in the emission process but acts merely as a spectator ligand. In this case, after excitation the metal ion becomes formally 3+ and more charge is donated from the ligand to the metal ion, less electron density is present on the ligand and its acidity increases. Examples of these compounds are $[Ru(bpy)_2]^{2+}$ complexes with the ligands 4,7-dihydroxy-1,10-phenanthroline [43], imidazoles [47,48,49,50,51], pyrazoles [51,52,53], and 1,2,4-triazoles [54]. The excited states of the bis(-2,2'bipyridyl) ruthenium pyridyltriazole compounds are more acidic than in the ground state, which indicates that the pyridyltriazole ligands do not participate in the luminescence process. [1,2] This is also reflected in the lower oxidation potentials measured for the deprotonated species.

The pyridyltriazole ligands have stronger σ-donor and weaker π-acceptor properties than the bipyridine ligand.

For other complexes, the excited state may be more basic than in the ground state. Here, after excitation more electron density is present on the ligand and it becomes easier to bind a proton. For these complexes, the excited electron is thought to reside on the ligand which is actively involved in the emission process. [42,45,46] Examples include $[Ru(bpy)_2]^{2+}$ complexes with 4,4-dicarboxylic acid -2,2'bipyridine [44,55,56,57,58], bipyrazine [59,60], and 1,4,5,8,-tetraazaphenanthrene. [61]

Recently studies of a combination of the two types of ligand have been conducted using $[Ru(bpy)_2$ complexes with pyrazyltriazoles.[2] The compounds exhibit rather unusual behaviour in that the orbital nature changes upon deprotonation. The combination of the strong π-accepting pyrazine ring together with the strong σ-donor triazole ring is accountable for this interesting behaviour. When the pyrazyltriazole ligand is protonated the LUMO is based on this ligand and hence this ligand is involved in the emission process. When protonated, the filled dπ orbitals as well as the π^* level of the pyrazyltriazole ligand are lowered (below the π^* level of bpy), and a combination of a higher oxidation potential with a less negative reduction potential is observed.

Upon deprotonation of the coordinated pyrazyltriazole ligand, the LUMO is based on the bpy ligand because its π^* level is now lower than that of the pyrazyltriazole ligand, and the emission process originates from the bpy ligand.

This change in orbital nature is unique, as normally the emission originates from one or other of the ligands for both the deprotonated and protonated species. This is the case for the bis-(2,2'-bipyridine) ruthenium pyridyltriazole complexes [1,2] and indeed for the analogous bis-(4,4'-dimethyl-2,2-bipyridine) and bis-(1,10-phenanthroline) complexes.

The excited state pK_a^* may be estimated using the Forster cycle given in the equation below:

$$pK_a^* = pK_a + \frac{0.625}{T} (\nu_b - \nu_a)$$

where T = absolute temperature, ν_a and ν_b are the energies of the zero-zero transition from the ground state to the excited state involved in the deprotonation equilibrium for the acid and base forms, respectively. [62]

Another method may also be used to calculate the pK_a^* and is given in the equation below:

$$pK_a^* = pH_i + \log(\tau_a / \tau_b)$$

where pHi = inflection point of the luminescence titration curve; τ a and τ b are the excited state state lifetimes of the acid and base forms, respectively. [56]

1.3 Ruthenium polypyridyl interactions with DNA.

The interactions of ruthenium polypyridyls with DNA and polynucleotides have been the subject of active investigation over the past few years. Metal complexes are uniquely suited for these studies since their unusual binding properties together with their general photoactivity render them as suitable candidates for (a) the design of site- or conformation-specific probes for recognition of the biopolymer structure; (b) the development of selective DNA cleaving agents for mapping or footprinting experiments and (c) the design of site specific drugs. [63,64,65,66,67,68,69, 70,71]

Ruthenium polypyridyls possess a number of features which are critical to their application as DNA/polynucleotide binders and photocleavage reagents. They are rigid, planar, chiral and contain a coordinatively saturated metal ion at their core. By virtue of their chirality, the complexes have been shown to bind preferentially to right- or left-handed DNA, making them useful probes of DNA helicity. [72]

The complexes display intense MLCT absorptions and emit strongly, with room temperature lifetimes in aqueous

solution in the range 100-600 ns. [3] The strong visible absorption band distinct from the absorption due to DNA or indeed the biomolecules used in this thesis, together with the strong luminescence, provide a spectroscopic tool to monitor the binding process. [3,65]

The complexes also possess a redox active site which is essential for their ability to act as DNA photo-cleaving molecules. [72,73] The nature of the heterocyclic ligands surrounding the Ru(II) centre directly controls the ground and excited state properties of the complexes as well as their binding and probing abilities. [74]

DNA is a polyanion with one negative charge for each nucleotide or a charge of -2 for each step along the α-helix. Thus, the helix is awash with negative charge and electrostatic considerations alone account for a high association of cationic metal centres with nucleic acids. However, further interaction can occur if the aromatic ligands attached to the metal provide a sufficently extended structure where intercalation may occur in the major groove of the DNA helix. [73]. DNA has various sites where a molecule may bind and are depicted in Figure 1.7.

DNA binding molecules tend to interact non-covalently in the following ways, (a) by full intercalation, where the molecule is inserted between the hydrophobic base pairs of the polynucleotide duplex and is stabilised through π stacking; (b) minor groove and major groove binding where a mixture of hydrophobic, electrostatic and hydrogen-bonding interactions stabilise the DNA duplex;

(c) externally, by binding on the outside (surface binding) of the helix. [63].

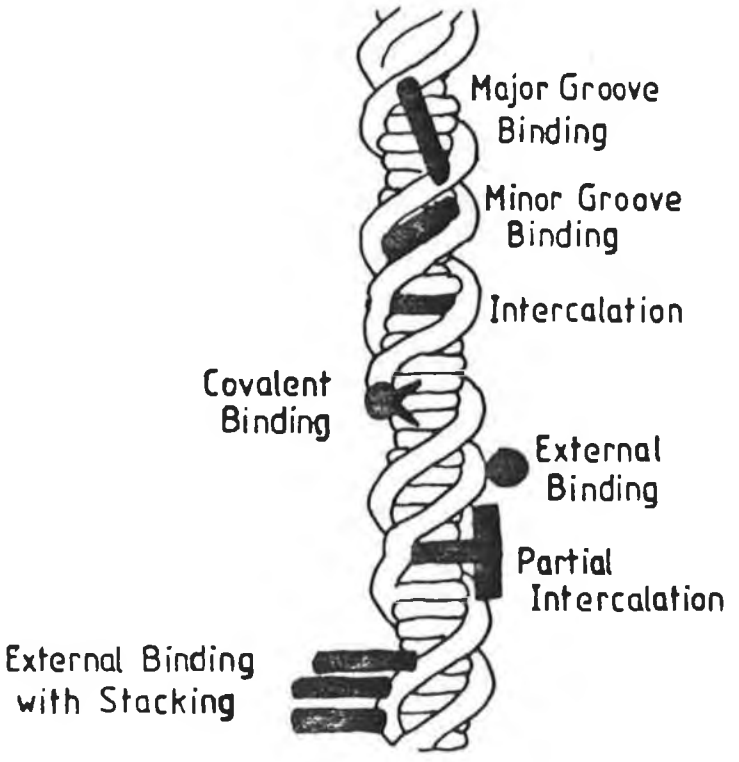

Figure 1.7 **Schematic representation of the available binding sites of DNA.**

Binding to the minor and major groove and externally are essentially electrostatic, reversible interactions, which occur between the negatively charged residues on the DNA and occur rapidly by diffusion and coulombic attraction.

It has been proposed that intercalative binding is a non-covalent stacking interaction, resulting from the insertion of a planar heterocyclic aromatic moiety between the base pairs of the DNA helix. For insertion to occur, the base pairs must separate and the helix must unwind to accommodate the planar intercalator.

Covalent binding may also take place. This is an irreversible type of binding in which the molecules form covalent bonds with atoms in the DNA residues. The classic example is the antitumour drug [cis-$Pt(NH_3)_2Cl_2$], cis-platin. In solution the chlorines are lost and the platinum forms covalent bonds with the base atoms. [75]. Bis(phenanthroline)dichlororuthenium has also been bound to DNA and exhibits striking enantiomeric selectivity, different from that observed upon intercalation. [76] DNA oligomers and duplexes containing a covalently attached derivative of $[Ru(bpy)_3]^{2+}$ have also been reported. [77]

Bathophenanthroline ruthenium (II) complexes have also been covalently attached to DNA. [78,79,80].

Covalent attachment to biomolecules is of particular interest in this thesis because all the binding methods used result in a covalent bond between the protein / polypeptide molecules and the ruthenium (II) polypyridyl complexes. Most of the research reported in the literature

dealing with the interaction of ruthenium polypyridyl complexes with biomolecules concerns electrostatic and intercalative binding modes. In comparison, very little is is reported on covalent attachment of ruthenium polypyridyls to biomolecules. However, it is pertinent to review the literature generally with regard to ruthenium polypyridyl interactions with DNA and polynucleotides.

Firstly, it is useful to distinguish briefly between the various conformational forms of DNA. Much of the literature describes the chiral discrimination of ruthenium polypyridyls in relation to the "handedness" of DNA i.e. whether the ruthenium complexes bind to right-handed DNA or left-handed DNA. Right-handed helical structured DNAs are the A and B forms, left-handed DNA is the Z-form.

Since Crick and Watson [81], first described the double helical structure of DNA in 1953, it has been shown that DNA exists in three helical conformations, A-DNA, B-DNA and Z-DNA. There are also C-DNA and D-DNA but these are considered as modified versions of A-DNA and B-DNA. The overall shapes of the helices are quite different even though each form involves a helix made up of two anti-parallel polymer strands with the bases paired through Watson and Crick hydrogen bonding. Both A-DNA and B-DNA are right-handed helical structures, whereas Z-DNA spirals in a left-handed sense. B-DNA, the predominant form, is a regular right-handed helix with base pairs oriented essentially perpendicular to the helix axis and distinctive major and minor grooves of well defined width and depth. The A-DNA

helical form is the predominant conformation of DNA-RNA hybrids and double-stranded RNA segments, it has a very shallow and wide minor groove. Z-DNA is not a left-handed version of either A or B helices. The Z-DNA helix zig-zags and can best be considered as a long slender helix with a wide and shallow, almost convex, major groove and a minor groove pinched down into a narrow crevice. Along the DNA strands themselves, there are a range of structural variations including cruciforms, bends, hairpin loops, kinks and left-handed sites. The previous discussion has been concerned with double-stranded DNA (dsDNA), but research has also been conducted on ruthenium (II) polypyridyl interactions with single-stranded DNA (ssDNA), RNA and various synthetic "ss" and "ds" polynucleotides of the bases adenosine (A), thymine (T), cytosine (C), guanine (G) and uracil (U). Ruthenium polypyridyl complexes may bind electrostatically to single or double stranded DNA at low ionic strength and also intercalatively in the case of dsDNA. [82]

Secondly, it is beneficial to distinguish between the enantiomeric forms of ruthenium polypyridyl compounds. Octahedral complexes with three bidentate ligands such as phenanthroline do not contain an inversion centre and therefore, two enantiomeric forms are possible. Ruthenium(II) complexes of phenanthroline and derivatives are of interest due to their inertness to racemization. This allows the enantiomers to be resolved. [65,72] The two enantiomeric configurations of $[Ru(phen)_3]^{2+}$ are shown in Figure 1.8.

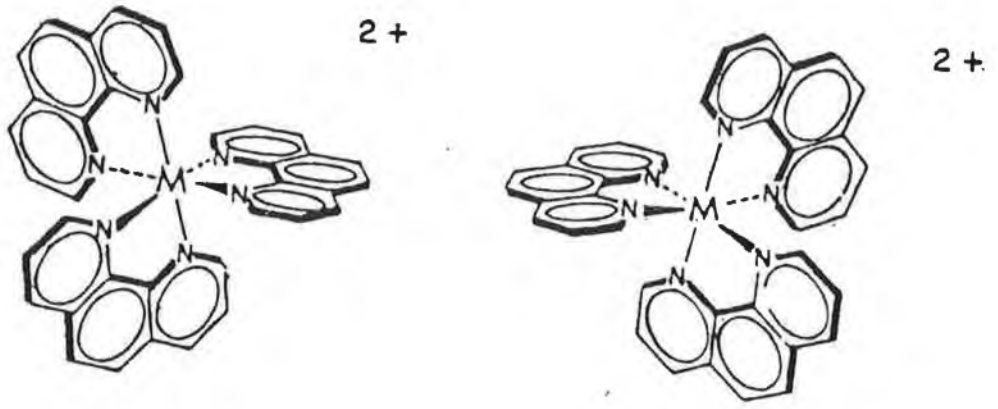

Figure 1.8 Enantiomeric forms of $[Ru(phen)_3]^{2+}$.

The intercalating phenanthroline ligand is coordinated directly to the assymetric metal centre. Due to the proximity of this chiral metal centre to the site of intercalation, the interaction of ruthenium polypyridyls with DNA clearly illustrates stereospecific binding to a similarly asymmetric DNA helix and suggests the use of these complexes as probes for DNA helicity. [65]

Organic cations bearing an extended heteroaromatic system have long been recognised as intercalators of DNA. These intercalators consist of various anti-tumour drugs such as daunomycin and actinomycin, whose pharmacological activity arises from their ability to intercalate into DNA and dyes

such as ethidium bromide, acridine orange and proflavine which serve as DNA stains and probes of nucleic acid structure. [73]

Lippard and co-workers were the first to discover that metal complexes could intercalate into DNA and RNA. [83] The original studies centered on square planar platinum(II) complexes containing aromatic terpyridyl or phenanthroline ligands. X-ray diffraction studies of terpyridylplatinum(II) complexes stacked with nucleotides showed that the platinum complex inserted almost fully between the base pairs. Generally, charged tetra-coordinated planar platinum complexes were found to intercalate into DNA whilst the neutral cis dichloroplatinum complexes could bind covalently to DNA through coordination to its nitrogen bases. The reagent methidiumpropyl-Fe(II)-EDTA, is a well characterised planar intercalator and has also been used in DNA cleavage studies. [72] Metalloporphyrins represent another family of essentially aromatic metal complexes that can intercalate into DNA. [72]

Direct intercalation of metal complexes is not restricted to those metal centres possessing a square planar geometry. Non-planar metal complexes with planar aromatic ligands can bind to DNA by intercalation. One such example is the tetrahedral zinc complex, $Zn(phen)Cl_2$. The analogous complex of cuprous ion, $[Cu(phen)_2]^{1+}$, has been shown to cause efficient DNA strand cleavage. [63,72]

Octahedral transition metal (Ru,Zn,Co,Rh) polypyridyl complexes can interact with DNA and RNA and

synthetic polynucleotides. The literature describes the use of these chiral complexes in designing spectroscopic probes and photoactivated DNA cleaving agents for DNA. The interactions of transition metal polypyridyl complexes with DNA and polynucleotides has been studied by various groups using quite a diverse range of homoleptic and heteroleptic complexes. The common feature of these complexes is the incorporation of planar aromatic ligands which can interact non-covalently, intercalatively and electrostatically with biomolecules. Covalent linkage to DNA has also been described to some degree using ruthenium(II) phenanthroline compounds. [76]

DNA ruthenium polypyridyl interactions will be reviewed conveniently in the following manner. Firstly, in regard to their chirality and their use as probes for DNA handedness. Secondly, in terms of the effects of binding on the physical properties of DNA and the spectroscopic changes which occur to the complexes upon binding to DNA. Thirdly, in relation to their use as sensitisers for the photocleavage of DNA. There will of course be some overlap between these sections but it is hoped that a clear and concise picture of the interactions of polypyridylruthenium(II) complexes with DNA will be presented.

1.3.1 The use of ruthenium polypyridyl complexes as probes for DNA handedness.

Numerous studies of DNA interactions with chiral tris-chelate metal complexes have been inspired by the possibility of discriminating DNA handedness. These complexes are shaped like three-bladed propellers and have two enantiomeric forms corresponding to right (Δ) and left (Λ) handed screws. See Figure 1.8 earlier. [84]

Ruthenium(II) polypyridyl enantiomers may be resolved by diastereometric recrystallisation procedures, [63] by virtue of their inertness to racemisation.

Enantiomeric selectivity has been observed in the ruthenium tris(phenanthroline) complexes with B-DNA. The Δ enantiomer, a right-handed propeller-like structure displays a greater affinity than Λ-$[Ru(phen)_3]^{2+}$ for the right-handed DNA helix. Figure 1.9 illustrates the basis for this selectivity. With one phenanthroline ligand intercalated, the two non-intercalated ligands of the isomer fit closely along the right handed helical groove. The non-intercalated ligands of the Λ isomer are repelled sterically by the phosphate backbone of the duplex. The disposition of the left-handed isomer is opposed to the right-handed helical groove of B-DNA. [65]

Experiments have demonstrated that both enantiomeric isomers of the tris (phenanthroline) ruthenium(II) complex can bind to DNA, one isomer binds in an intercalative manner and the other in a surface bound mode.

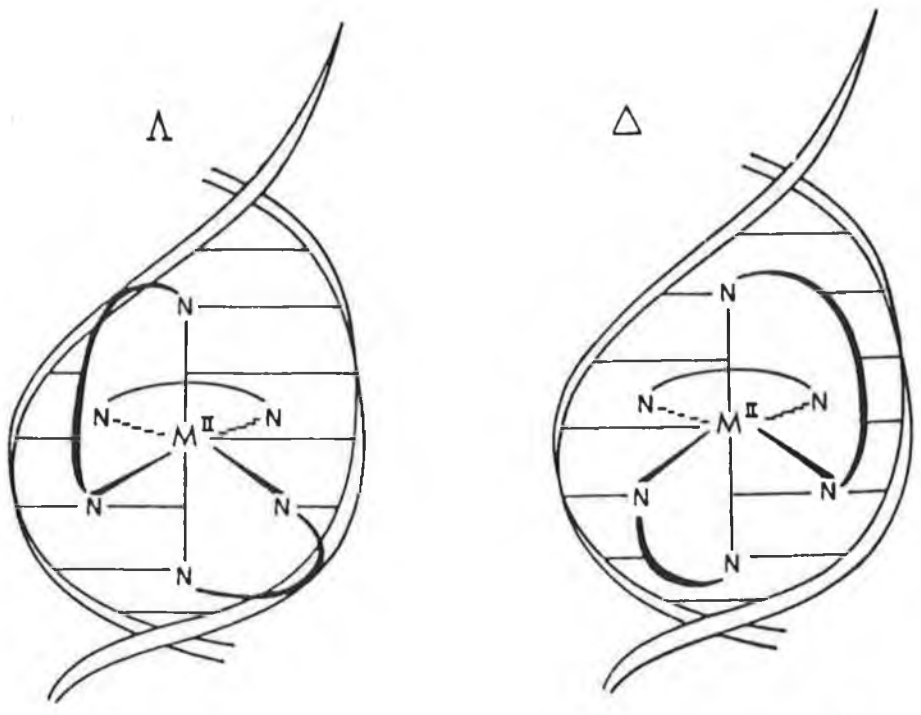

Figure 1.9 Lambda (Λ) and delta (Δ) tris(phenanthroline) metal complexes, a schematic illustration of the complex intercalated into right-handed DNA.

Intercalative binding through the major groove of B-DNA is associated with preferential binding of the Δ isomer to the right-handed helix and surface bound binding with the Λ isomer. It is noteworthy that it is surface groove binding that requires a complementary asymmetry in structures, left-handed Λ-$[Ru(phen)_3]^{2+}$ binds against a right-handed helix, whereas intercalation, inserting into the base pairs of the helix is best when symmetries are matched, as a result Δ-$[Ru(phen)_3]^{2+}$ intercalates selectively into a right-handed helix. This stereochemical criterium has been observed also with respect to the covalent coordination of

bis(phen)Ru(II) species to a B-DNA helix. [76]

The enantiomeric selectivity for intercalation depends on the size of the helical groove relative to the diameter (sterically excluded distance) of the chiral metal complex. If the DNA groove is wider than the metal complex, there is no enantiomeric discrimination. If the complex is much larger than the groove, as for $[Ru(DIP)_3]^{2+}$, the binding is stereospecific. [64]. The level of enantiomeric discrimination is not high for the ruthenium tris-(phenanthroline) enantiomers since both bind to some degree to DNA. In order to amplify the chiral discrimination of the complex, phenyl substituents on the 4 and 7 positions of each of the phenanthroline ligands were incorporated to give $[Ru(DIP)_3]^{2+}$, [64]. See Figure 1.10.

Λ-tris(4,7-diphenyl-1,10-phenanthroline)Ruthenium(II)

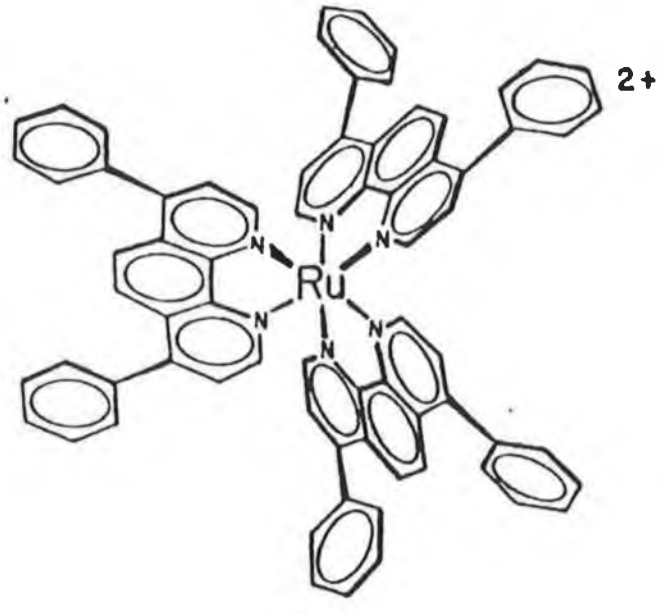

Figure 1.10 Structure of $[Ru(DIP)_3]^{2+}$.

Barton and co-workers have shown that isomers of $[Ru(DIP)_3]^{2+}$ bind B-DNA enantiospecifically. The right-handed isomer Δ-$[Ru(DIP)_3]^{2+}$ binds to B-DNA whereas Λ-$[Ru(DIP)_3]^{2+}$, the left-handed isomer does not. The right-handed isomer is able to bind in the well defined major groove of B-DNA by intercalation of one of the diphenylphenanthroline ligands, because in such an interaction, the two non-intercalated ligands are oriented along the direction of the groove. In contrast, intercalation by the left-handed isomer is prevented by steric clashes between the two non-intercalating ligands and the phosphate backbone of the B-DNA, the bulky substituents on the phenanthroline ligands block completely the intercalation of this isomer into a right-handed helix. This compound has proven to be a useful spectroscopic probe for Z-DNA. A left-handed helix favours the left-handed isomer, but only a slight stereoselectivity in binding Λ-$[Ru(DIP)_3]^{2+}$ to Z-DNA is observed. Z-DNA is not a left-handed DNA and due to its wide and shallow major groove, the Z-helix provides a poor template for discrimination between steric isomers. Thus, both isomers can bind to DNA. However, the comparative binding by $[Ru(DIP)_3]^{2+}$ enantiomers serves as the probe for helix conformation. If only the Δ isomer binds to the polynucleotide, the conformation is likely to be right-handed and B-like. Since the Λ-$[Ru(DIP)_3]^{2+}$ isomer does not bind to B-DNA, then if the unknown DNA binds this isomer, the helical conformation is probably left-handed. If binding occurs

with both isomers, but to a lesser extent with the right-handed isomer, the unknown conformation is likely to be Z-DNA.

A probe for the A-DNA conformation has been reported which targets sites along the strand by shape as well as by symmetry. [85] The complex $[Ru(TMP)_3]^{2+}$ (Figure 1.11), associates with the nucleic acid in a surface or groove bound mode rather than through intercalation. The complex binds against the surface of A-form polynucleo- tides but it is too large to bind against the well defined major groove of B-DNA. In binding against the right-handed A-DNA helix, the complementary symmetry of the left-handed isomer provides for a better fit between the metal complex and the nucleic acid, thus accounting for the chiral discrimination.

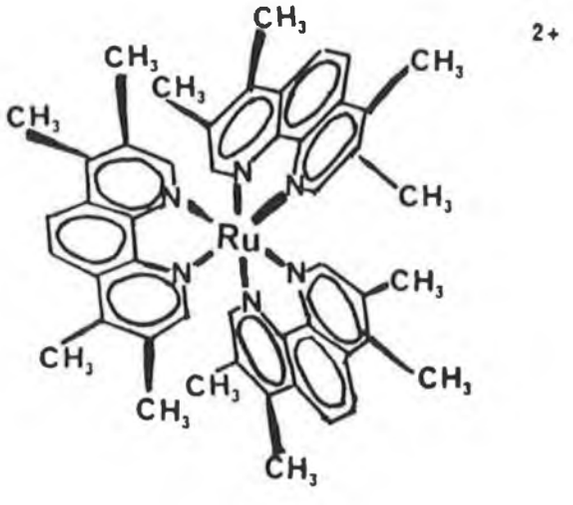

Figure 1.11 Structure of $[Ru(TMP)_3]^{2+}$.

Studies have been conducted on the interaction of mixed ligands complexes of Ru(II) with right-handed B-DNA. Equilibrium dialysis experiments showed that after dialysis of the DNA against the racemic mixture of these mixed ligand complexes, the optical activity observed in the dialysate reflected enrichment in the less favoured enantiomer. For most of the complexes, optical activity was found in the dialysate. The enantiomeric selectivity was compared to the well studied $[Ru(phen)_3]^{2+}$ enantiomers. On the following assumptions, an enrichment of the left-handed Λ isomer in the dialysate and the preferential binding of the right-handed Δ isomer to the right-handed DNA, enantiomeric selectivity was demonstrated for the complexes $[Ru(phen)_2(phi)]^{2+}$, $[Ru(phen)_2(DIP)]^{2+}$, $[Ru(bpy)_2(phi)]^{2+}$ and $[Ru(bpy)_2(DIP)]^{2+}$. [86]. See Figure 1.12 for a diagram of the ligands used in these systems and those described subsequently.

Recently, a report was published stating that both enantiomers of $[Ru(phen)_3]^{2+}$ bind to the major groove but with different geometries owing to steric interactions. It was proposed that the left-handed Λ enantiomer has a single chelate pointing in toward the DNA, lying parallel to the DNA base pairs and that the stability and average orientation of the ruthenium ion with the DNA molecule are mainly determined by interaction of the two remaining wings with phosphates of the strands. For the right-handed Δ complex, an opposite geometry was proposed where two chelates sit in the groove and determine the orientation by closely fitting the helical

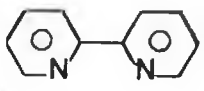

2,2'-bipyridyl
(bpy)

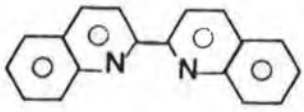

2,2'-biquinoline
(biq)

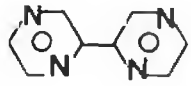

2,2'-bipyrazine
(bpz)

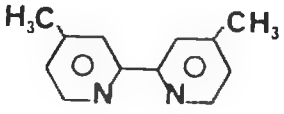

4,4'-dimethyl-2,2'-bipyridyl
(dmb)

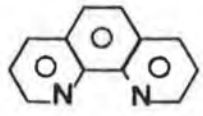

1,10-phenanthroline
(phen)

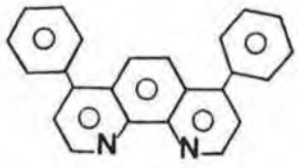

4,7-diphenyl-1,10-phenanthroline
(DIP)

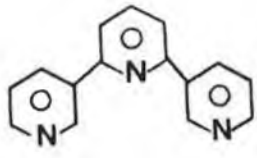

2,2',2''-terpyridine
(terpy)

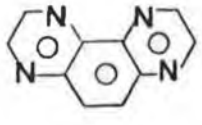

1,4,5,8-tetraazatriphenylene
(TAP)

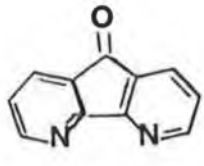

4,5-diazafluorene-9-one
(flone)

Figure 1.12 Structures and abbreviations of the ligands used in studies of ruthenium polypyridyl interactions with DNA and polynucleotides, continued on the following page.

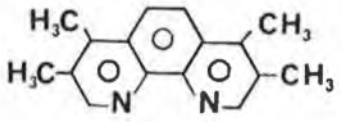

3,4,7,8-tetramethyl-1,10-phenanthroline
(TMP)

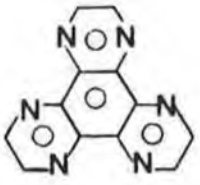

1,4,5,8,9,12-hexaazatriphenylene
(HAT)

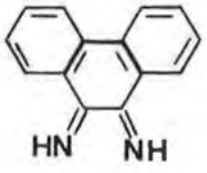

9,10-phenanthrenequinonediimine
(phi)

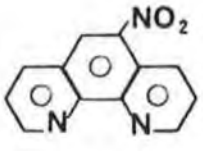

5-nitro-1,10-phenanthroline
(NO2phen)

ethylene diamine
(en)

Figure 1.12 **Structures and abbreviations of the ligands used in studies of ruthenium polypyridyl interactions with DNA and polynucleotides, continued from previous page.**

stack of base pairs. The results indicated that the binding geometry measured through the orientations and chromophoric perturbation of the complex is almost the same for a given enantiomer irrespective of the kind of DNA. In addition, variations in affinity suggested that the enantioselectivity is sensitively dependent on DNA sequence. [84].

This report was quickly followed by another paper disproving these suggestions stating that not enough experimental techniques were used to definitively establish whether or not intercalative or surface binding occurred. [87]

These reports show that the question of whether tris chelate metal complexes can discriminate enantiomerically between different conformational forms of DNA is controversial and details of the DNA / complex interaction are far from being well understood.

The complex $[Ru(phen)_2Cl_2]$ binds covalently to B-DNA, and has been shown to exhibit striking enantiomeric selectivity different from that seen on intercalation. [76,88] The neutral complex contains like cis-platin two cis-oriented chloride ions that are good leaving groups. Racemic $Ru(phen)_2Cl_2$ binds covalently to DNA and optical enrichment studies have indicated that enantiomeric selectivity accompanies the covalent binding of the complex to the helix. Unlike intercalation, where a right-handed isomer stacks best with a right-handed helix, it appears that the left-handed Λ isomer is favoured.

Covalent coordination of $[Ru(phen)_2Cl_2]$ to DNA

seems to resemble the groove bound mode, which favours the left-handed Λ isomer in binding to a right-handed helix. Model building has shown that from an initially intercalated position the Λ left-handed isomer is well oriented for covalent binding to the base positions above and below.

Similar alignment for covalent binding of the right-handed isomer is not possible because the other non-stacked phenanthroline ligand is considerably crowded by the right-handed helical column.

For intercalation by $[Ru(phen)_3]^{2+}$, the right-handed isomer which has the same helical screw sense as the right-handed B-DNA is preferred, while covalent binding seems best to require the left-handed $\Lambda-[Ru(phen)_2Cl_2]$ isomer which is a structure complimentary to the right-handed B-DNA helix.

1.3.2 Spectroscopic properties of DNA bound ruthenium polypyridyl complexes and the effect of binding on the physical properties of DNA.

Intercalative binding allows a close approach of the metal complex to the helix as one of the ligands is sandwiched between the adjacent base pairs. This mode of binding leads to a substantial perturbation in the photophysical properties of the metal complex such as emission lifetimes and intensities as well as steady-state polarisation. In addition, intercalation imposes constraints on rotational

degrees of freedom and can enhance the emission polarisation. The stereoselectivity associated with this binding mode is sensitive to the chirality of the metal complex, matching the symmetry of the metal complex to the helix topography and DNA groove size. In contrast, surface binding provides stabilisation due to hydrophobic and electrostatic interactions. The metal complex is relatively free to diffuse along the helix surface. [89] The stereo-selectivity of this type of binding is also sensitive to the helix topography and DNA groove size.

Numerous methods of probing the intercalation of a DNA molecule with its host in solution are available. The physical effects and characteristics of intercalation on DNA structures have been well studied. The techniques available for studying intercalation are based on some fundamental features of this type of binding, (a) the double helix is stretched by about 3.4 $\mathring{A}$ per input dye at each binding site; (b) the double helix is unwound by 18-26° per input dye; (c) the helix is stabilised by intercalation; (d) the dye is held coplanar with the DNA base and is therefore oriented; (e) the spectroscopic properties of the dye are altered by intercalation. [87] The techniques used to study binding modes are based either on physical changes occurring to the DNA or on spectroscopic changes occurring to the dye.

Intercalating compounds have been shown to unwind and lengthen helical DNA using electrophoretic mobility assays. The electronic interaction of the intercalator with the helix may be investigated using spectroscopic techniques

with the observation of hypochromicity and red shifts in the MLCT band and increased MLCT excited state lifetimes upon binding to DNA. Thermal denaturation of DNA can be used to distinguish between those molecules which bind intercalatively and those which bind externally. Intercalation generally results in a considerable stabilisation (more so than for electrostatic binding) of the DNA helix with a corresponding increase in its T_m, melting temperature. Upon intercalation, there is substantial structural overlap between the base pairs and the intercalator. The intercalator becomes rigidly held and oriented with the planar moiety perpendicular to the helical axis. These effects may be monitored using fluorescence depolarisation and anisotrophic techniques which indicate, only if intercalation occurs, the retention of polarisation of emitted light. [87]

It is recommended that as many of the mentioned techniques as possible are conducted in order to verify whether binding occurs via intercalation or surface binding. [87]

Kelly and Tossi have examined the nature of binding of a series of ruthenium complexes containing various different ligands with calf thymus DNA, poly [(dA-T)] and poly [(dG-C)]. [71] They studied, (a) how the ligands affect the mode of binding using absorption and emission spectroscopy and DNA thermal denaturation techniques, (b) how the photophysical properties of the bound ruthenium complexes were modified by binding and (c) the use of the complexes as

photocleavage agents.

The ligands have already been given in Figure 1.12.

DNA thermal denaturation experiments indicated that three classes of behaviour were observed. $[Ru(phen)_3]^{2+}$, $[Ru(phen)_2(en)]^{2+}$ and $[Ru(bpy)_2(HAT)]^{2+}$ were found to fall into one class with behaviour very similar to the intercalator ethidium bromide. $[Ru(bpy)_3]^{2+}$ and $[Ru(terpy)_3]^{2+}$ fall into a second class with similar behaviour to that of Mg^{2+} which binds electrostatically. The remaining complexes $[Ru(bpy)_2(phen)]^{2+}$, $[Ru(bpy)_2(DIP)]^{2+}$, $[Ru(bpy)_2(biq)]^{2+}$, $[Ru(dmb)_2(phen)]^{2+}$ and $[Ru(TAP)_3]^{2+}$ exhibit intermediate behaviour.

Two complexes, $[Ru(bpy)_2(CN)_2]$ and $[Ru(phen)_2(CN)_2]$, did not have any effect on DNA melting or on the unwinding / lengthening of DNA, nor do they show any change in the absorption or emission spectroscopy upon addition of DNA. These complexes have been termed as non-binders. The fact that these complexes are not affected to any degree upon addition of DNA has been taken as evidence that electrostatic interactions play an important role in the binding of ruthenium(II) polypyridyl complexes to DNA. All of the compounds which bind to DNA are charged and their binding has been shown to be sensitive to the ionic strength of the solution. [71]

$[Ru(bpy)_3]^{2+}$ and $[Ru(terpy)_3]^{2+}$ are external binders and affect the melting of DNA in a similar way to that of Mg^{2+}, and they do not unwind or lengthen

DNA. These facts suggest that these complexes bind mainly through ionic interactions on the outside of the DNA helix.

The other complexes, $[Ru(phen)_3]^{2+}$, $[Ru(phen)_2(en)]^{2+}$ and $[Ru(bpy)_2(HAT)]^{2+}$, in the presence of calf thymus DNA are subject to a hypochromicity at the band maximum and a slight shift of the band to longer wavelengths to a greater or lesser degree depending on the ligand. The largest effects have been observed for $[Ru(bpy)_2(HAT)]^{2+}$, the complexes intercalated HAT ligand, with an additional aromatic ring compared to phenanthroline, can be inserted further into the base pairs than phenanthroline and this allows a greater π electron overlap. $[Ru(TAP)_3]^{2+}$ shows intermediate behaviour which is interesting since the compound is very similar in structure to $[Ru(phen)_3]^{2+}$, which intercalates into the DNA helix. The presence of the two additional nitrogens on the ligands must destabilise the intercalative binding of this complex to DNA. This may be the result of interactions of the lone pair of electrons on the nitrogens with the atoms of the DNA backbone and the increased hydrophobicity of the TAP ligands compared to the phenanthroline ligands. [71]

The complexes containing the biquinoline ligands result in greater stabilisation than for $[Ru(bpy)_3]^{2+}$ and less than for $[Ru(bpy)_2(HAT)]^{2+}$, which is consistent with the more extended ring system for the biquinoline ligand than for the bipyridine ligand and the inability of the additional ligand to obtain as great an overlap as that achieved by the HAT ligand. [71]

Synthetic polynucleotides were used to test for dependence of the binding on base content. It was established that $[Ru(phen)_3]^{2+}$ and $[Ru(bpy)_2(HAT)]^{2+}$ have a marked preference for poly [d(A-T)], while $[Ru(bpy)_3]^{2+}$ and $[Ru(TAP)_3]^{2+}$ bind equally to poly [d(A-T)] and poly [d(G-C)]. This is interesting, since until recently the view was held that intercalators preferred to bind in the doublet pyrimidine (3'-5') purine with an increased preference for DNA rich in GC.

For all the complexes studied except for $[Ru(TAP)_3]^{2+}$ binding to DNA leads to an enhancement of luminescence. This is probably due to an increase in the average lifetime of the complex upon binding to DNA and to protection of the complexes excited state from oxygen. The lifetimes measurements of the bound complexes show non-single exponential decay behaviour, with two decay components. One with a lifetime shorter than the unbound species and the second with a much longer lifetime than the unbound species. The presence of the shorter lived species is under investigation but may be due to self-quenching, if the complexes can move along the DNA strand as proposed by Barton [89,90], or due to triplet-triplet annihilation caused by the high laser excitation intensities, which has been suggested to cause quenching of DNA bound $[Ru(bpy)_3]^{2+}$. [91] The longer lived species is probably the composite of similar decays from the complexes where binding can occur to different base sequences, externally and intercalatively. Also the possibility of the binding of the different

enantiomers can not be excluded. [71]

The complex $[Ru(bpy)_2(HAT)]^{2+}$ showed the most marked enhancement in emission intensity on addition of calf thymus DNA which is unaffected by oxygen concentration or changes in temperature.

$[Ru(TAP)_3]^{2+}$ was the only complex where a marked degree of excited state quenching was observed for the poly [d(G-C)] and calf thymus DNA and not for poly [d(A-T)]. The quenching process has been explained by photoredox interaction with guanines. [71]

The rate of oxygen quenching for $[Ru(phen)_3]^{2+}$ and $[Ru(bpy)_3]^{2+}$ when bound to DNA are quite similar and substantially reduced compared to the unbound compounds. Intercalation is not essential for the protection from this type of quenching since $[Ru(phen)_3]^{2+}$ is known to intercalate DNA whilst $[Ru(bpy)_3]^{2+}$ binds electrostatically to DNA. [71]

Electrostatic interactions of ruthenium polypyridyls with DNA are known to be dependent on the ionic strength of the solution, in addition to the solvent nature and the DNA phosphate/ruthenium(II) ratio. Addition of alkali or alkaline earth salts at very low concentrations, stabilises partial intercalation whereas high salt concentrations leads to a release of the ruthenium complex from the strand. [92]

Gorner and co-workers have proposed that $[Ru(bpy)_3]^{2+}$ may partially intercalate into DNA but this type of binding is sensitive to the ionic strength of the

solution. Therefore, the proportion and lifetimes of the decaying species are probably dependent on the ionic strength of the solution under investigation, which may explain the varying results obtained by different groups. [92]

Various factors may result in the enhancement of the emission intensity in the absence of quenching by electron transfer processes. [93] Among which are (a) the protection from quenchers in the sheltered environment of the DNA; (b) changes in solvent environment; (c) a decrease in the vibrational activity of the bound dye as it is held in a more rigid environment or (d) an increase in the energy gap between the emitting state and the other states involved in deactivation.

The binding of $[Ru(bpy)_3]Cl_2$, $[Ru(phen)_3]Cl_2$ and $[Ru(DIP)_3]Cl_2$ and of various mixed ligands complexes has been investigated by other workers. [86] The mixed ligand complexes include $[Ru(bpy)_2(DIP)]^{2+}$, $[Ru(bpy)_2(phen)]^{2+}$, $[Ru(phen)_2(bpy)]^{2+}$, $[Ru(phen)_2(DIP)]^{2+}$, $[Ru(DIP)_2(phen)]^{2+}$, $[Ru(phi)_2(bpy)]^{2+}$ and $[Ru(phen)_2(phi)]^{2+}$. The ligands used in these systems have already been shown in Figure 1.12. Generally, binding led to hypochromicity in the intense MLCT band which was accompanied by a red shift of this band, the magnitude of which were found to correlate with the strength of the intercalative interaction. [86] The complexes containing the phi ligand exhibit the largest red shifts (about 10 nm), followed by those containing DIP ligands (about 5 nm), phen ligands (about 3 nm) and bpy

ligands (no red shift). If the red shift is taken as a measure of intercalating ability, then the optimal shape for intercalation is phi > DIP > phen > bpy.

This variation in intercalating ability is a reflection of the differing capacity of the ligands to stack and overlap with the base pairs. The phi ligand is flat, large in surface area and has a geometry that permits substantial overlap with the base pairs of the DNA helix. Hence, the phi ligand is well suited for intercalation and in mixed ligand complexes, it would be the phi ligand which would be expected to preferentially intercalate. The DIP ligand is not expected to be flat with phenyl groups twisted out of the plane of the phenanthroline ring which diminishes the ligands favourability for intercalation. However, it is not established whether its greater affinity over the phenanthroline ligand is associated with intercalation or additional stabilisation through hydrophobic surface binding. [86]

The complexes examined with the exception of $[Ru(bpy)_3]^{2+}$, were found to intercalate and to surface bind to DNA. For those that bound appreciably, enantiomeric selectivity was observed. The bipyridine ligand provides insufficent π electron overlap with the DNA base pairs for intercalation to be effective. These conclusions were based upon effects of hypochromism, increases in emission intensities and lifetimes, DNA helical unwinding and excited state resonance Raman experiments.

The effects of ancillary ligands and hydrogen bonding were also investigated. It was found that the primary effect of the ancillary ligand is in altering the extent of enantio-selectivity. This has also been demonstrated in comparisons of $[Ru(phen)_3]^{2+}$ with $[Ru(DIP)_3]^{2+}$. The increased steric bulk of the ancillary ligands of $[Ru(DIP)_3]^{2+}$ ensures that the right-handed isomer intercalates with right-handed DNA, while the left-handed Λ isomer can not intercalate. By investigation of mixed ligand complexes it is possible to establish how different ancillary ligands add or detract from the overall binding affinity for DNA. $[Ru(DIP)_2(phen)]^{2+}$ has a similar binding affinity as $[Ru(phen)_2(DIP)]^{2+}$ which suggests that the presence of one bulky hydrophobic ligand that can intercalate stabilises the bound complex, but that a second bulky ancillary ligand does not further stabilise the bound complex. The complex $[Ru(phi)_2(bpy)]^{2+}$ displays decreased affinity for DNA in comparison with $[Ru(bpy)_2(phi)]^{2+}$. Here, steric interaction may interfere with the insertion of the intercalating ligand into the helix. Also, due to the increased hydrophobicity of the complexes, self-stacking of the complexes may occur which would decrease the binding affinity for DNA. [86]

In comparison of $[Ru(bpy)_2(phen)]^{2+}$ with $[Ru(phen)_3]^{2+}$ and $[Ru(bpy)_2(DIP)]^{2+}$ with $[Ru(phen)_2-(DIP)]^{2+}$, it was noticed that the DNA binding affinity increased with increasing hydrophobicity of the ancillary ligands, with the greater binding affinity being observed

for $[Ru(phen)_3]^{2+}$ and $[Ru(DIP)_2(phen)]^{2+}$. It was thought that hydrogen bonding might further stabilise complexes bound to DNA. To this end, the binding of the complexes $[Ru(5\text{-}NO_2phen)_3]^{2+}$ and $[Ru(phen)_2(flone)]^{2+}$ to DNA was investigated. The structures and abbreviations of these ligands have been presented in Figure 1.12. These complexes were found to bind poorly to DNA.

Space models of $[Ru(5\text{-}NO_2phen)_3]^{2+}$ indicated that for binding intercalatively or via surface binding, the nitro groups on the ancillary ligands would be oriented appropriately for hydrogen bonding. However, the major type of binding was found to be electrostatic. A similar conclusion was drawn for the flone complex. For this ligand, the oxygen atom is aligned appropriately for hydrogen bonding, in a manner different to that of the nitro ligands, but no further stabilisation was observed. It was concluded therefore, that the substitution of potential hydrogen binding acceptors onto the phenanthroline ligands provides no additional source of stabilisation. [86]

Recently, the nature of the interaction of some homo and heteroleptic ruthenium(II) polypyridyl complexes containing bipyridine, bipyrazine, phenanthroline, DIP, TMP, TAP, and HAT has been investigated. [74] The structures and abbreviations of these ligands have been presented in Figure 1.12.

This study was divided into (a) those complexes that bind to and photoinduce redox processes with DNA and (b) those complexes that bind to DNA without any photoredox

processes. The complexes that were capable of photoinducing redox processes were those containing at least two HAT / TAP ligands coordinated to the ruthenium centre. These chelates were $[Ru(bpy)(TAP)_2]^{2+}$, $[Ru(bpy)(TAP)(HAT)]^{2+}$, $[Ru(bpy)(HAT)_2)]^{2+}$, $[Ru(TAP)_2(HAT)]^{2+}$, $[Ru(TAP)(HAT)_2]^{2+}$ and $[Ru(HAT)_3]^{2+}$. These chelates all have excited state reduction potentials of $\geq$ 1.1 V vs SCE and as such were shown to oxidise guanine when bound to DNA with quenching of luminescence and emission lifetimes. At excited state reduction potentials of > 1.40 V, the chelates can oxidise guanine free poly[(dA-T)]. Similar oxidising behaviour has already been described for $[Ru(TAP)_3]^{2+}$, where the excited state potential is 1.35 V (vs SCE). [74]

The quenching process has been shown to be important for the complexes $[Ru(TAP)_3]^{2+}$ and $[Ru(bpy)_2(TAP)]^{2+}$ with regard to their use as sensitisers for photocleavage. Some of the other complexes mentioned above, may also have potential in this regard.

The complexes studied that bound to DNA without redox processes were those possessing excited state reduction potentials lower than 0.80 V (vs SCE) so that photo-oxidation of DNA guanine is not a spontaneous process. These chelates included homoleptic or heteroleptic chelates containing solely bpy, phen, DIP or TMP as well as those incorporating one HAT or TAP ligand. The complexes under investigation were $[Ru(phen)_2(HAT)]^{2+}$, $[Ru(bpy)_2(HAT)]^{2+}$, $[Ru(bpy)_2(TAP)]^{2+}$, $[Ru(bpy)_2(phen)]^{2+}$,

$[Ru(bpy)_2(DIP)]^{2+}$, $[Ru(phen)_3]^{2+}$ and $[Ru(TMP)_3]^{2+}$. Upon the addition of DNA all the complexes with the exception of $[Ru(TMP)_3]^{2+}$ exhibit biexponential emission decay behaviour. It has been established previously that this latter molecule is too large to bind against the well-defined groove of B-DNA, thus the single exponential decay is that of the unbound species.

In every case, the decay of the unbound complex was single exponential, but upon addition of DNA, biexponential behaviour decays were observed with a fast component and a slower component. For the most oxidising complexes i.e. $[Ru(TAP)(HAT)_2]^{2+}$ and $[Ru(HAT)_3]^{2+}$, the fast component was not detected and the decay profile exhibited single exponential decay behaviour. However, when bound to poly [d(A-T)], instead of DNA, the chelates exhibit biexponential (possibly multiexponential in the case of the two most oxidising complexes) decay behaviour.

Thus, those complexes containing two or more TAP / HAT ligands photooxidise the guanine base upon binding to DNA but show emission enhancement and increased emission lifetimes in the presence of poly [d(A-T)], but even the complexes $[Ru(TAP)(HAT)_2]^{2+}$ and $[Ru(HAT)_3]^{2+}$, photooxidise the adenosine base, with quenching of emission in the presence of adenosine or guanine. [74]

The relative contribution of each decay component for the series $[Ru(bpy)_2(L)]^{2+}$ was examined and showed that the contribution of each component was dependent on the structure of L. The effects of the polynucleotide-phosphate

/ Ru(II) ratio, ionic strength of the solution and solvent nature were also examined. It was found that the intercalation of the complexes into DNA increases with (a) decreasing ionic strength of the medium, (b) increasing DNA / Ru(II) and (c) partial replacement of water with glycerol.

The enhancement observed upon partial replacement of water with glycerol is the usual effect observed for Ru(II) polypyridyls when water is replaced by alcohols and other organic solvents. [3] and may be explained by a less efficient energy transfer to the solvent oscillators which influences the non-radiative deactivation rate constant of the ^{3}MLCT excited state.

It was also demonstrated that the use of a mixed solvent medium is a useful tool for the elucidation of binding patterns of Ru(II) polypyridyls to DNA because intercalative, surface bound and free species may be differentiated.

The complex $[Ru(bpy)_2(dppz)]^{2+}$ (Figure 1.13) has been found to be a highly sensitive reporter molecule for double stranded DNA. The compound does not exhibit any luminescence in aqueous solution at ambient temperatures but displays intense emission in the presence of DNA to which the compound binds avidly. [94]

It has been proposed as a molecular "light switch" for DNA. Electrochemical and photophysical measurements in the ground and excited states of this molecule show that the charge transfer is directed from the metal centre to the

phenazine ring and the major non-radiative deactivation pathway for the compound likely involves the protonation of the phenazine nitrogen atoms in the excited state.

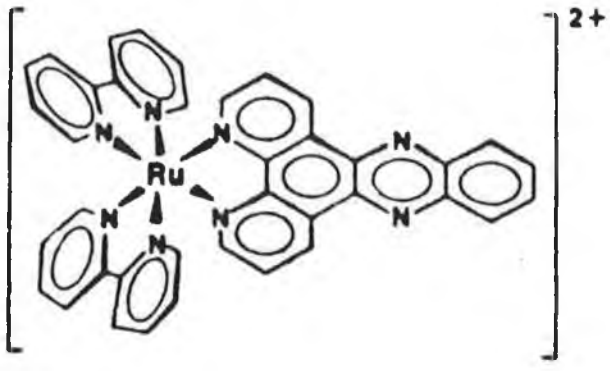

Figure 1.13 Structure of the complex $[Ru(bpy)_2(dppz)]^{2+}$.

The compound binds intercalatively to DNA as expected from the extended planar structure of the dppz ligand. Lifetime decay profiles reveal biexponential decay behaviour with a short-lived component and a long-lived component. Quenching experiments using $[Fe(CN)_6]^{4-}$ as quencher showed that the shorter-lived component is preferentially quenched indicating that the long-lived component may be a less accessible tightly intercalated form. The complex when bound to oligonucleotides may find application as a sensitive non-radioactive DNA probe in heterogenous and homogenous assays.

1.3.3 Ruthenium polypyridyl complexes as sensitisers for the photocleavage of DNA.

In conjunction with studies on the enantiomeric selectivity and changes in the spectroscopic properties of the complexes combined with the effects on the DNA itself upon binding, there has been a great deal of effort involved in the investigation of many of the Ru(II) polypyridyl complexes described as DNA photocleavage agents. Photoactive compounds may act either by sensitising the formation of singlet oxygen which attacks DNA or by direct reaction with the polynucleotide by photoredox processes. [95]

A very simple and effective method of monitoring the photosensitised cleavage of DNA is the use of covalently closed circular (ccc) plasmid DNA, such as pBR322 which is highly supercoiled. This is achieved by monitoring the transition from the naturally occurring, ccc form (Form I) to the open circular (oc) relaxed form (Form II). This occurs when one strand of the ccc plasmid is nicked which may be observed using gel electrophoresis of the plasmid followed by microdensitometric scanning. Extended irradiation results in a build up of nicks on both strands of the plasmid which eventually results in its opening to the linear (lin) form, (Form III).

It is not necessary to enter into a lengthy description of the various transition metal photocleavers in this work. It is suffice to briefly discuss the ruthenium(II) polypyridyls which photosensitise DNA cleavage.

Table 1.1 Summary of some of the metal complexes investigated and reactions that have been used to cleave target sites along the strand.

Compound	Binding Mode	Cleavage Mechanism	Site
$[Rh(phen)_3]^{3+}$	Intercalation/ Surface binding	photoredox	B-DNA
$[Co(phen)_3]^{3+}$	Intercalation/ Surface binding	photoredox	B-DNA
$[Ru(phen)_3]^{2+}$	Intercalation/ Surface binding	singlet oxygen	guanine
Λ-$[Co(DIP)_3]^{2+}$	Intercalation Surface binding	photoredox	Z-DNA
$[Ru(TMP)_3]^{2+}$	Surface binding	singlet oxygen	A-DNA/ guanine
$[Rh(DIP)_3]^{2+}$	Surface binding	photoredox	cruciforms
$[Ru(TAP)_3]^{2+}$	Intercalation/ Surface binding	photoredox	guanine
$[Ru(bpy)_3]^{2+}$	Surface binding	singlet oxygen	guanine

$[Ru(bpy)_3]^{2+}$ and $[Ru(phen)_3]^{2+}$ have been shown to mediate the formation of singlet oxygen with the resultant photocleavage of DNA. [71,95,96] The fact that both of these complexes are capable of sensitising DNA photocleavage shows that the mode of binding does not appear to be a factor in determining whether these complexes sensitise this process, since $[Ru(phen)_3]^{2+}$ intercalates into DNA and $[Ru(bpy)_3]^{2+}$ electrostatically binds to DNA. In the presence of Mg^{2+} (20 mM), these complexes and $[Ru(TAP)_3]^{2+}$ were no longer able to sensitise the cleavage of pBR322 plasmid DNA. This salt concentration is more than sufficient to prevent intercalation of ruthenium complexes into DNA and may effect the release of the complexes from the strand. This observation indicates that binding is essential for cleavage. This is further substantiated by the fact that the neutral complex $[Ru(phen)_2(CN)_2]$, which does not bind to DNA, also does not sensitise its cleavage. [71]

The complex $[Ru(TMP)_3]^{2+}$, which binds preferentially to A-DNA helices, also cleaves these helical forms. Furthermore, as observed in the binding process, enantiomeric selectivity similarly occurs with the cleavage process. The left-handed Λ-$[Ru(TMP)_3]^{2+}$, cleaves the A-DNA form with twice the efficiency of the right-handed Δ isomer. [85]

$[Ru(TAP)_3]^{2+}$ has been found to be the most effective as a photocleavage sensitiser. [71,74,97] For the other complexes mentioned, the sensitiser reacts with triplet

oxygen present in the solution with the formation of singlet oxygen which can attack the DNA. However, for the TAP complex, since the complex is only inefficiently quenched by oxygen and is therefore, expected to be a poor singlet oxygen sensitiser, an alternative mechanism has been proposed. For this complex and also $[Ru(TAP)_2(bpy)]^{2+}$, both of which are strongly oxidising and are capable of oxidising guanine (G), an electron transfer process has been suggested. Consideration of the excited state potentials shows that the following electron transfer reaction is thermodynamically favourable.

$$[Ru(bpy)_n(TAP)_{3-n}]^{2+} + G \longrightarrow [Ru(bpy)_n(TAP)]_{3-n}]^{+} + G^{\bullet+}$$

It is thought that the complexes $[Ru(TAP)(HAT)_2]^{2+}$ and $[Ru(HAT)_3]^{2+}$ which are capable of oxidising both guanine and adenosine, may also act as photocleavage sensitisers through electron transfer processes. In fact, this mechanism has recently been confirmed by the detection of the monoreduced complex in laser flash photolysis experiments in the presence of the mononucleotides. [71,74]

The effects of $[Ru(TMP)_3]^{2+}$ and $[Ru(phen)_3]^{2+}$ on the photocleavage of transfer RNA (tRNA) have recently been reported and reveal that these complexes preferentially photocleave at the guanine residues. [98]

Somewhat different patterns of cleavage were observed despite the fact that both complexes sensitise photocleavage through the formation of singlet oxygen, ($^1O_2$). $[Ru(TMP)_3]^{2+}$ was found to photocleave a subset of those guanine residues cleaved by $[Ru(phen)_3]^{2+}$ and with different relative intensities. It was observed that some of the guanine residues are protected from $[Ru(TMP)_3]^{2+}$, because of its molecular shape, (which governs its binding characteristics). Therefore, given the uniqueness of the sites cleaved, these probes may have application in the assessment of the structural integrity of tRNAs.

A complex which provides a route to double stranded cleavage through a metal-activated mechanism rather than photoactivated cleavage has been described. [99,100] This complex is an analogue of the complex $[Ru(DIP)_3]^{2+}$. One of the three diphenylphenanthroline ligands are modified with two polyamine armlike segments that can themselves complex metal ions. See Figure 1.14. The concept is that the complex will bind to DNA and the two arms of the macro ligand will deliver complexed metal ions to each strand of the DNA helix for double stranded cleavage. The complex has been shown, in the presence of the redox active Cu(II) and the redox inactive Zn(II), though less efficiently for the latter, to efficiently effect the cleavage of double stranded DNA.

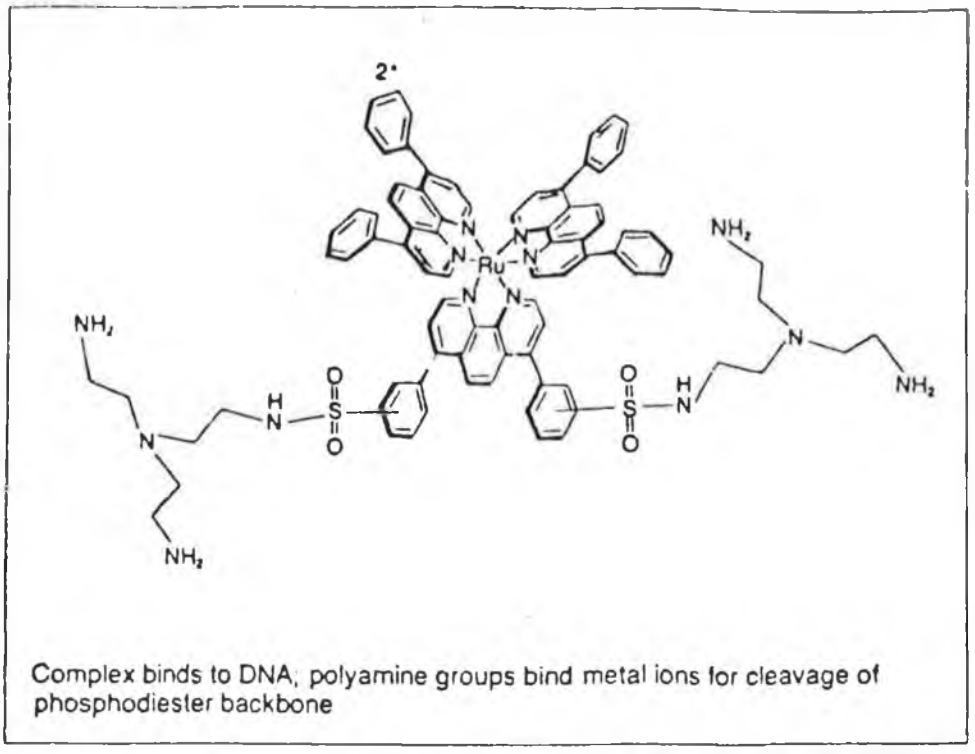

Figure 1.14 The structure of $[Ru(DIP)_2(Macro)]^{n+}$.

The results suggest that the metal-activated cleavage by the $[Ru(DIP)_2(Macro)]^{n+}$ molecule occurs via nucleophilic attack at the phosphodiester backbone leading to hydrolysis of the anionic diester. As a result the possibility of using these types of molecule as artificial restriction enzymes has been proposed. [99,100]

1.4 Fluorescent probes in immunochemistry.

In addition to their use as probes of DNA structure, fluorescent molecules find application as probes in immunochemistry techniques. Immunoassays are based on an immunological reaction between the substance to be measured (antigen) and a specific antibody or antibodies. This interaction is reversible and non-covalent. In order to

detect or quantify this reaction it is usual to label either the antigen or antibody with a probe of some sort, which may be a radioactive species, an enzyme or a fluorescent compound. [101]

Immunological methods for the qualitative and quantitative measurement of many types of molecules, including hormones, antibodies and drugs are employed because of their superior specificity and sensitivity. [102] Fluorescent agents are used in immunofluorescence (IF) and fluorescent immunoassay techniques (FIA, fluoroimmunoassay; IFMA, immunofluorometric assay), where the antigen or antibody is labelled with a fluorescent species.

Fluorescent methods are applied in immunology, mainly in fluorescence microscopy for studying various types of cells, tissues, bacteria, viruses, etc. In these cases, the sample under investigation is detected with an antibody which is labelled with a fluorescent species. This is a qualitative method of analysis, but a microscope that can quantitate fluorescence in an individual cell is available. However, with the recent advances in the use of fluorescence activated cell sorting (FACS), it is also possible to quantify the visual picture obtained under the fluorescence microscope. With this method also, dual labelling using two different fluorescent probes can be used to distinguish between different cell populations. [103]

Other quantitative fluorescent immunoassay techniques include fluorescent polarisation methods, fluorescence quenching methods, fluorescent enhancement

methods and fluorescent excitation transfer methods.

The use of fluorescent probes to replace radioactive isotopes as labels is somewhat hindered because of the decreased sensitivity obtained with fluorescence, which is partially due to the samples own fluorescence, (autofluorescence). The intensity of this background has been overcome by the use of time-resolved fluorescence and labels with a long emission decay, including the lanthanide chelates and some ruthenium(II) polypyridyl complexes. [80,102,104]

Some of the other problems associated with fluorometric analysis include (a) light scattering due to the colloidal nature of the substances under investigation and (b) quenching of the fluorescence by oxygen, heavy atoms and concentration quenching due to the location of probes in close proximity to each other. [105]

The requirements for a suitable fluorescent probe in IF and fluorescent immunoassay techniques are outlined in Table 1.2.

1.4.1 Chemical modification of proteins.

Proteins contain several different chemical groups which can be used for the attachment of reporter molecules. Conjugation usually involves binding to the amino side-chains, in particular the ε-amino group of lysines, the phenolic moiety of tyrosines, carboxyl groups of

Table 1.2 Requirements for a good fluorescent probe.

(1)	The fluorochrome should possess chemical groups which will form stable covalent bonds with protein molecules or be easily convertible to such a reactive form without destroying the fluorescent structure.
(2)	It should be easy to separate the unbound fluorescent probe from the bound probe.
(3)	The probe should possess a high quantum yield of fluorescence, ideally $\phi = 1$ and this efficiency should not decrease upon conjugation.
(4)	For IF procedures, the fluorescent colour should be distinguishable from that of the background.
(5)	Conjugation of the probe to the protein molecule should not adversely affect the antibody-antigen binding process.
(6)	It should be possible to conduct the conjugation reaction under mild conditions so that the conformation of the antibody or antigen is not disturbed.
(7)	The probes should be photostable.
(8)	The probe should exhibit a large Stokes shift so that the scattered analysing light does not interfere with the signal.

glutamate and aspartate and the sulphydryl groups of cysteines. One feature common to all these approaches is the lack of specificity of the reactions, in that the label can not be directed to a particular site on the antibody or antigen. Also for immunoglobulins, the amino groups are located close to the antigenic binding site which may result in a decrease in the affinity of the antibody (Ig) for the antigen. [106] An alternative approach which generates more specificity in the labelling of immunoglobulins and other glycoproteins, is via modification of the carbohydrate moieties, particularly those which are covalently attached to asparagine. Also, the oligosaccharide moieties which are modified using this method, are not involved in the process of antigenic binding and are far removed from the site of binding. [106]

Some probes are themselves not fluorescent or only weakly fluorescent but become highly fluorescent upon conjugation. One such probe is 9-maleimidoacridine (Figure 1.15), which couples with the protein and in doing so the conjugating group can no longer act as an intramolecular quenching species since its reaction with a nucleophile destroys its quenching ability. [107]

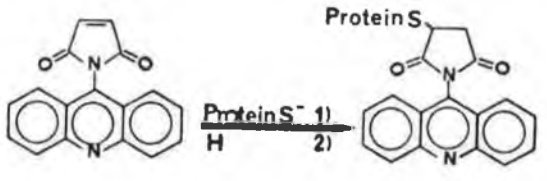

Figure 1.15 Reaction of 9-maleimidoacridine with protein via the sulphydryl group on the protein. [107]

Some intercalating dyes may also fall in this category and include the $[Ru(bpy)_2(dppz)]^{2+}$ complex described earlier. [94]

Intercalating dyes which themselves are fluorescent include ethidium bromide and acridine orange and are used in immunofluorescence techniques for staining cells, to determine cell viability and measurement of DNA. [108]

Some probes require light for activation and are converted to the reactive species upon absorption of a photon of appropriate energy. The most common photoactivating functional group is the aromatic azide ion ($R-N_3$). Upon photolysis azides are converted to nitrenes (R-N). Electron deficient nitrenes are extremely reactive and have broad reaction specificity. [108] They can potentially react with a variety of chemical bonds including NH, OH, CH and C=C via addition and insertion reactions. [109] Some of the azide fluorochromes are shown in Figure 1.16.

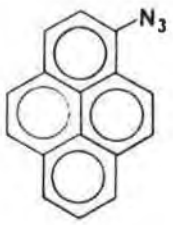

Azidopyrene

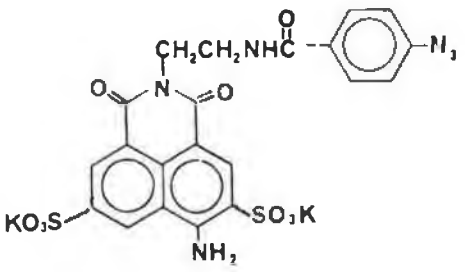

Lucifer Yellow AB

Figure 1.16 Some photoactivatable fluorescent azide probes.

Other photoactivatable fluorochromes include the furan and o-nitrobenzyl compounds shown in Figure 1.17.

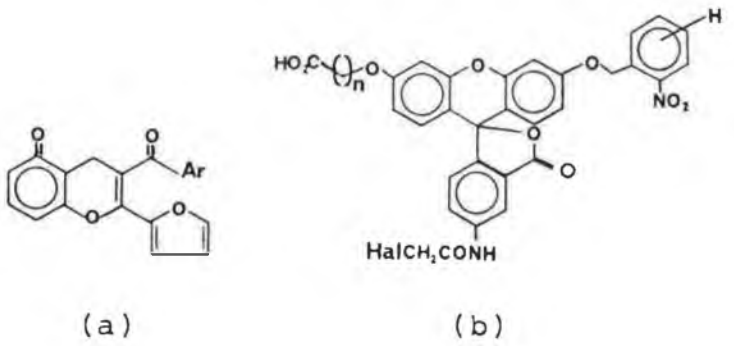

Figure 1.17 Two photoactivatable probes, (a) a furan compound and (b) an o-nitrobenzyl compound. [107]

Upon photolysis the furan under goes photoinduced rearrangement giving a highly fluorescent species. The o-nitrobenzyl derivative undergoes photofragmentation to give the fluorescent species. [107]

1.4.1.1 Conjugation reactions via modification of the amine groups of proteins.

Amine groups are common targets for modification in conjugation procedures. Fluorochromes which modify these groups include the isothiocyanates, succinimidyl esters,

isocyanates and sulphonyl halides (chlorides). Examples of some of these types of fluororchrome are presented in Figure 1.18.

Isocyanates (N=C=O), yield ureas on reaction with amines but are unstable and are no longer commonly used as probes. Fluorescein isocyanate was first described by Coons et al.. [110] The isothiocyanate analogue of this compound (FITC), was introduced by Riggs et al., [111] and is probably the most commonly used fluorochrome for IF and fluorescent immunoassay procedures.

Fluorescein conjugates show an absorption maximum at 495 nm and have a strong fluorescence emission which is an apple-green colour. This colour is rarely encountered in mammalian tissues as autofluorescence and it also corresponds to a region of high retinal sensitivity, in the eye. However, on the debit side, FITC has a small Stokes shift (about 25 nm), with the emission maximum occurring at about 520 nm. Hence, light scattering causes considerable interference. Fluorescein is also subject to severe concentration quenching when several molecules are assembled in close proximity. [112] It is thought that this phenomenon is due to resonance energy transfer among the fluorophores caused by overlap of the fluorescence excitation and emission spectra. The advantage of the initial brilliant fluorescence is marred by rapid fading with continued exposure to exciting radiation. This has been attributed to oxidative and reductive photodegradation processes. [107] The fluorescence intensity of FITC conjugates varies appreciably with pH, with

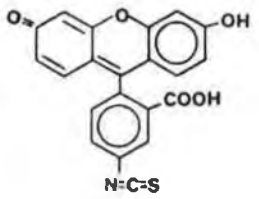

FITC
Fluorescein
isothiocyanate

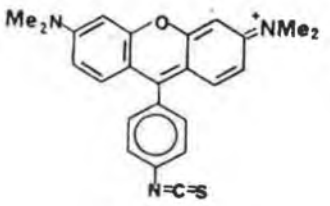

TMRITC
Tetramethyl rhodamine
isothiocyanate

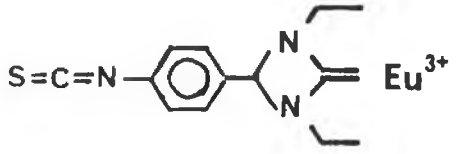

isothiocyanate phenyl-EDTA-Eu

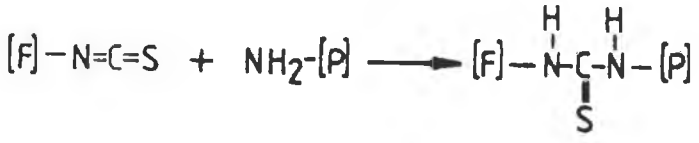

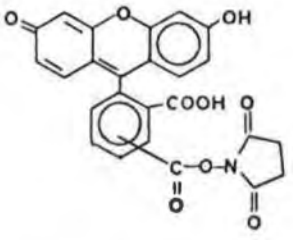

Carboxyfluorescein succinimidyl ester

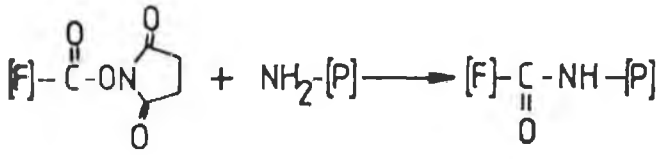

Figure 1.18 Some fluorochromes that bind to protein molecules via amino groups, together with the appropriate conjugation reaction.

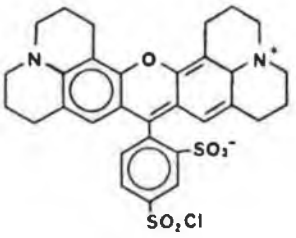

Texas Red

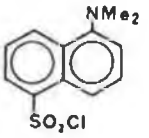

DANS

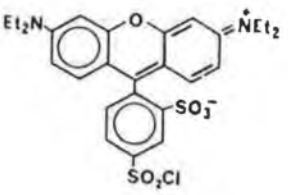

RB200SC

$$[F]\text{-}SO_2Cl + NH_2\text{-}[P] \longrightarrow [F]\text{-}SO_2NH\text{-}[P]$$

Figure 1.18 Some fluorochromes that bind to protein molecules via amino groups, together with the appropriate conjugation reaction.

a maximum around pH 8.0, however, this is not usually a problem since immunoreactions are normally conducted in buffered alkaline aqueous solution.

The principal alternatives to FITC are the rhodamines (tetramethylrhodamine isothiocyanate, TMRITC and rhodamine-B-isothiocyanate, XRITC). Conjugates of these dyes exhibit an orange fluorescence at longer wavelengths than the FITC conjugates, but the fluorescence is not as intense. The rhodamines have lower pH sensitivity of both absorption and emission than fluoresceins, and are more stable to photobleaching (fading). Rhodamine conjugates are widely employed in dual fluorescent studies with FITC as the second fluorophore. [105]

The fluorescent lanthanide chelates form a relatively unique group of fluorophores because of their much

extended fluorescence decay lifetimes. One of these chelates has been presented in Figure 1.18. The strong fluorescence exhibited by these chelates is due to the high absorption of the excitation radiation by the ligand and to the energy transfer from the triplet state of the ligand as a non-radiative transition to the central atom, which then produces a long wavelength, narrow emission typical of the rare earth metal. As far as their fluorescence is concerned, chelates of rare earth metals especially those of europium (Eu) are particularly suitable as probes. The prolonged fluorescence lifetime essentially stems from the delays incurred in the initial transfer processes. A second useful characteristic of the lanthanide chelates is their large Stokes shift. For example, Eu emits fluorescence in a narrow band around 613 nm; maximum excitation of the chelate occurs using incident light of a wavelength of 340 nm, implying a Stokes shift of about 270 nm. The combination of a large Stokes shift and an extended fluorescence decay time provides the basis for their use in time-resolved fluorometry. [113]

Succinimidyl esters are excellent reagents for amine modification since the amide products formed are very stable. [108] Both fluorescein and rhodamine succinimidyl esters are available.

The use of the esterified derivative of $[Ru(bpy)_2(COOHbpy)]^{2+}$, Figure 1.19, to conjugate bovine serum albumin and anti-rabbit immunoglobulin has been described. [114]. The retention of immunological activity after conjugation to the antibody was demonstrated by

immunofluorescence. The complex has also been employed in a time-resolved fluorescence immunoassay. [104]

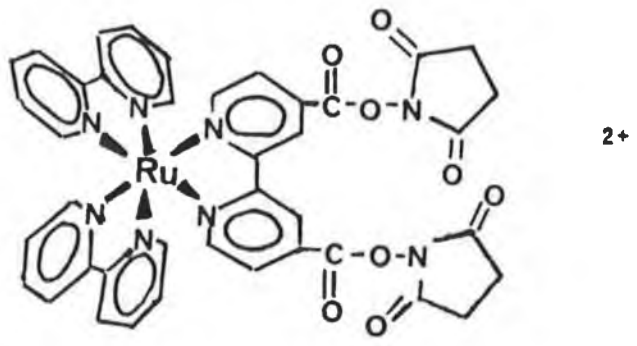

Figure 1.19 Succinimidyl ester of the compound $[Ru(bpy)_2-(COOHbpy)]^{2+}$, where bpy = 2,2'-bipyridyl and COOHbpy = 4,4'-dicarboxylic acid-2,2'-bipyridyl.

The succinimidyl esters of some bathophenanthroline ruthenium (II) complexes (Figure 1.20), have been conjugated to oligonucleotides and the emission measured by time-resolved fluorescence techniques. Decay lifetimes of the order of μsec have been reported. [80] The complexes are thermodynamically very stable, they are chemically very inert and show strong and long lasting fluorescence after excitation by light pulses of short duration which allows their detection by time-resolved measurement methods.

Sulphonyl halides form extremely stable sulphonamides with amines. Texas Red (Figure 1.18), is the sulphonyl chloride derived from sulphorhodamine and exhibits orange / red fluorescence. The compound has a small Stokes

shift with a λ max. of absorption of 595 nm and an emission maximum of 615 nm. In dual labelling techniques Texas Red provides more efficient spectral separation from FITC excitation than TMRITC can. [115]

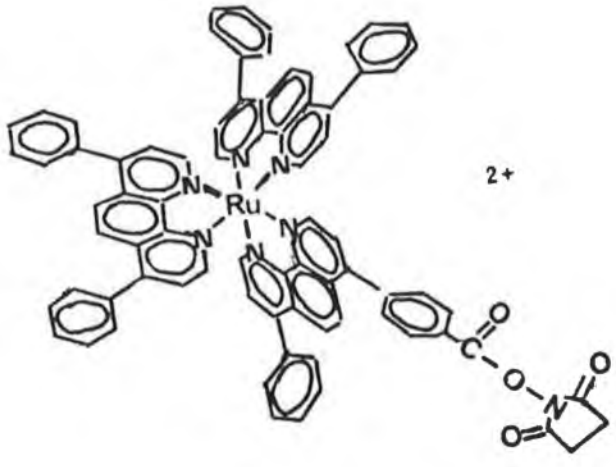

Figure 1.20 Succinimidyl ester of a bathophenanthroline ruthenium(II) complex.

Other sulphonyl chlorides include Dansyl Chloride (DANS) and lissamine Rhodamine B 200 sulphonyl chloride (RB200SC). Spectra of the RB200SC conjugates are very similar to the XRITC conjugates but have higher chemical stability. Conjugates of RB200SC have two emissions, one in the yellow at 595 nm which is excited by any shorter wavelength and the second in the far red at 710 nm which is excited by shortwave radiation below 350 nm. The second longer wavelength fluorescence occurs after conjugation to proteins and is not exhibited by the free dye. [103]

Dansyl chloride is also used in immunological

systems although its fluorescence is weaker. Its greatest drawback is that its excitation and emission wavelengths fall in the same region as those of serum, which leads to interference by the serum's own fluorescence. DANS conjugates have a green fluorescence but less brilliant than FITC and are more subject to photobleaching than FITC. [103] Structural isomers are available. The dye (isomer A),is valuable as a probe of amine terminus analysis of proteins and peptides. Isomer A has one of the largest Stokes shifts known (λmax. ex. 340 nm and λ max. em. 578 nm), and the other isomers B and C (Figure 1.21), have shorter Stokes shifts. Isomer B absorbs maximally at 373 nm and emits at 470 nm, while isomer C absorbs maximally at 359 nm and emits at 435 nm. Isomer B and C have longer emission decay times than isomer A and are employed as protein markers in fluorescence polarisation studies. [108]

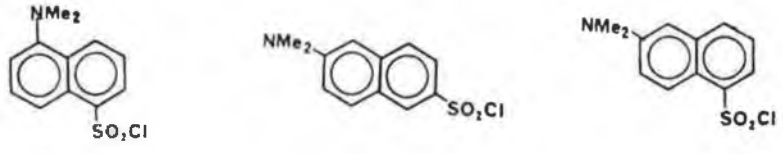

(A) (B) (C)

Figure 1.21 Isomers of DANS.

Dansyl chlorides have longer emission lifetimes (>14ns), than most of the fluorochromes described already, apart from the lanthanide chelates and the ruthenium (II)complexes.

The ruthenium polypyridyl sulphonyl chloride (Figure 1.22), has been prepared and conjugated to human IgG. [104]

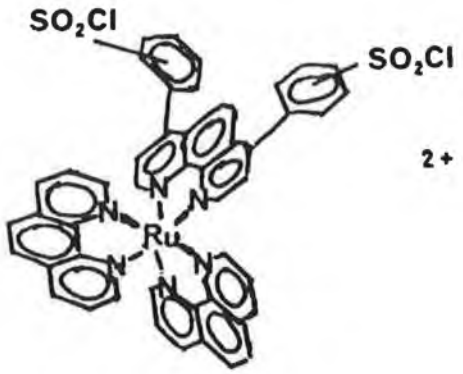

Figure 1.22 Bis(phenanthroline) Ru(II) (4,7-diphenyl-phenanthroline) sulphonyl chloride.

The complex $[Ru(bpy)_2((CONCS)_2bpy)]^{2+}$ has also been synthesised and has been conjugated to antibodies via lysine residues. [104]

Fluorochromes which bind to the amino groups of proteins principally bind to the ε-amino terminal group of the lysine residues (Figure 1.23), or to the α-amino terminal group on a protein.

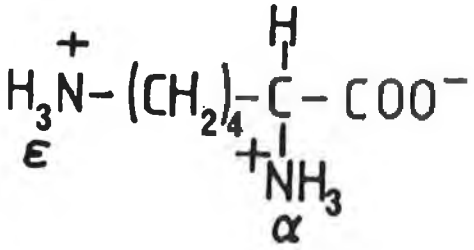

Figure 1.23 Lysine at pH 6.0.

1.4.1.2 Conjugation reactions via modification of the sulphydryl groups of protein molecules.

The sulphydryl group of cysteine residues may also be modified, (Figure 1.24).

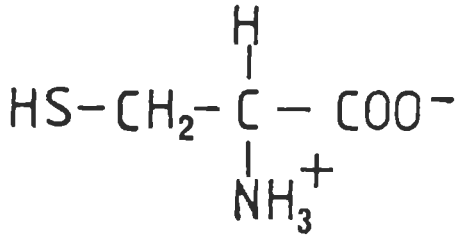

Figure 1.24 Cysteine.

The fluorochromes which target the sulphydryl groups of proteins include the maleimides and haloacetyls, principally the iodacetamides. Some maleimide and iodacetamide fluorochromes are presented in Figure 1.25.

Maleimides are useful reagents for thiol selective modification. They are probably among the most specific protein reagents, reacting under mild conditions and with the minimum of side reactions. Characteristic changes in the ultraviolet absorbance, associated with the reaction of maleimide derivatives with sulphydryl groups provide a convenient method for monitoring the conjugation reaction. [116,117]

Pyrene maleimide is essentially non-fluorescent until reacted with protein, when it exhibits quite long lived fluorescence. The fluorescence shows excimer formation with a

new longer wavelength emission if two fluorophores are in close proximity. The absorbance λ max. occurs at 340 nm and emits at 392 nm and 375 nm. [108] Pyrene maleimides have quite long emission lifetimes of about 100 ns which renders these probes as useful reagents in time-resolved fluorescence techniques.

In the absence of cysteine residues, haloacetyls may react with methionines, histidines or tyrosine residues on protein molecules. Iodacetamides are intrinsically unstable in light and especially in solution. However the tetramethylrhodamine iodacetamide is relatively photostable. [108]

Other sulphydryl reagents include the phycobiliprotein conjugates such as the phycoerythrins, C-phycocyanins and allophycocyanin. The phycobiliproteins are proteins from the light collecting apparatus of algae. Their biological role as light collectors has led to maximal absorption and fluorescence without susceptibility to either internal or external fluorescence quenching. Their fluorescence yield is equivalent to about 30 molecules of fluorescein or 100 rhodamine molecules at comparable wavelengths. [108] These phycobiliprotein conjugates were introduced to provide an alternative fluorescent colour to fluorescein for use in single laser fluorescence activated analysis. Phycoerthryins exhibit orange fluorescence on excitation by light of similar wavelength to fluorescein. However, since the fluorescence spectrum of fluorescein extends into the red region, the use of phycoerythrin in

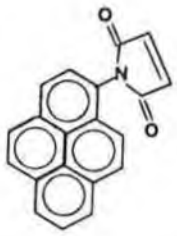

Pyrene maleimide

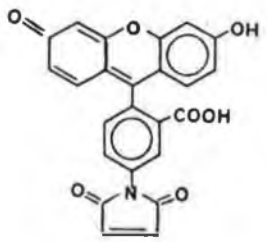

Fluorescein maleimide

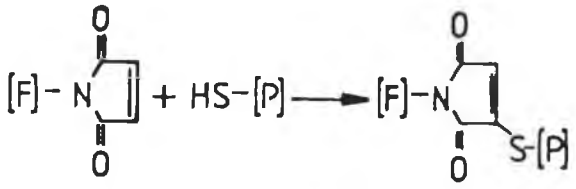

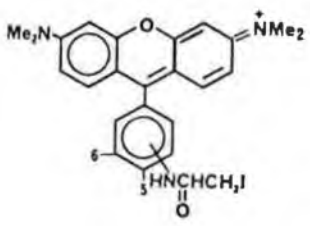

Tetramethylrhodamine
5 (and 6) iodacetamide

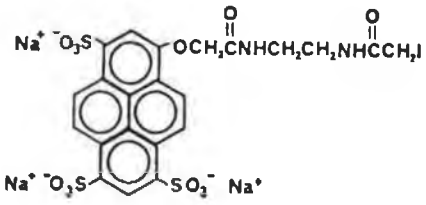

Cascade blue aminoethyl
iodacetamide trisodium salt

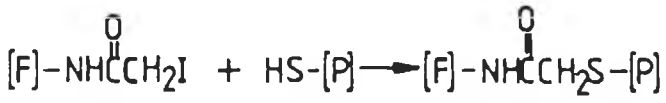

Figure 1.25 Some maleimide and iodacetamide fluorochromes, together with the appropriate conjugation reaction.

discriminatory double fluorescence analysis should be considered carefully.

Recently, attention has been drawn to a previously unrecognised hazard when R-phycoerythrin is employed in dual fluorescence analysis with fluorescein as the second probe. This arises due to energy transfer caused by spectral overlap of the absorbance curve of phycoerythrin and the emission curve of fluorescein, which may lead to an appreciable loss of the fluorescein signal in the presence of high intensity phycoerythrin staining. See Figure 1.26. Control tests in which phycoerythrin is omitted are essential in order to avoid misinterpretation of results particularly in the analysis of subpopulations by single fluorescence activated cell sorting. [107,118].

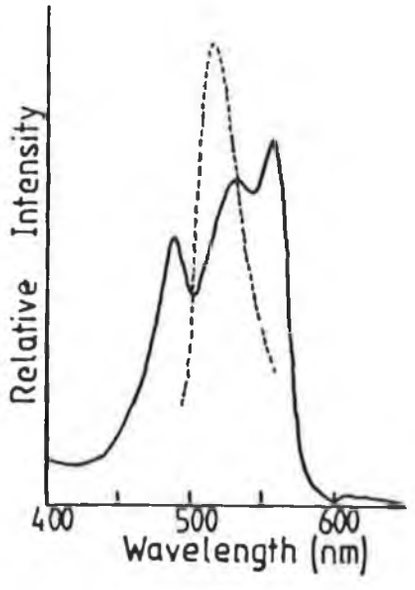

Figure 1.26 Absorption spectra of FITC and R-phycoerythrin demonstrating spectral overlap. [118]

Phycoerythrins and other phycobiliprotein conjugates may be obtained as streptavidin conjugates, which may be linked to the protein via biotinylation of the protein. Streptavidin can bind four biotin ligands per mole with high affinity and low reversibility. By use of this system, increased sensitivity in immunostaining techniques is achieved. [108]

1.4.1.3 Aldehyde and ketone reactive probes.

Aldehydes and ketones are not common in proteins or nucleic acids. The deficiency of aldehydes can be advantageous for site selective modifications in that aldehydes can be introduced into certain biomolecules by periodate oxidation of glycols, including the terminal residue of RNA and carbohydrate sites such as sialic acids of immunoglobulins and glycoproteins, [106,108], Figure 1.27, shows the reactions involved.

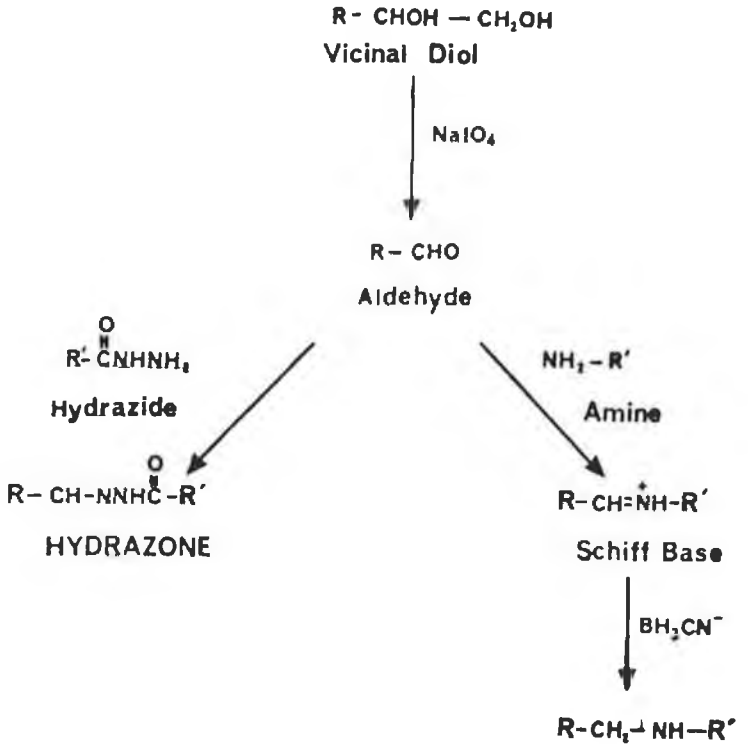

R = antibody molecule; R' = reporter molecule.

Figure 1.27 Chemistry involved in the site-specific modification or conjugation of the oligosaccharide moieties of glycoproteins. [106]

Some reagents which react with the aldehyde groups are shown in Figure 1.28.

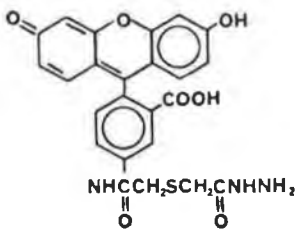

5(((2-(carbohydrazino)methyl)thio) acetyl)amino fluorescein

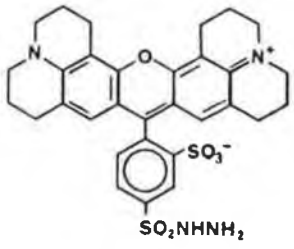

Texas red hydrazide

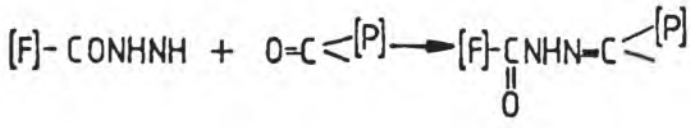

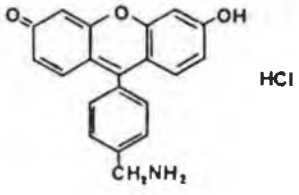

5(aminomethyl)fluorescein hydrochloride

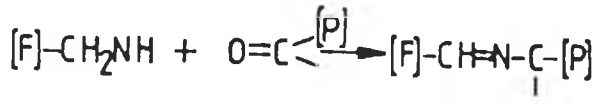

Figure 1.28 Some probes that react with aldehydes and ketones, together with the appropriate conjugation reaction involved.

1.4.1.4 Carboxylic acid reactive probes.

The chemical reactivity of carboxylic acids in aqueous solution is very low and precludes the use of carboxylic reactive probes with biomolecules. However, some probes can modify carboxylic acids of synthetic polymers. So, prior to conjugation the carboxylic acid is usually derivatised by a water soluble carbodiimide followed by reaction with a hydrazine or amine. In some cases, the carbodiimide may have the fluorochrome within its structure (Figure 1.29) and then the fluorophore is specifically incorporated into the protein. [108]

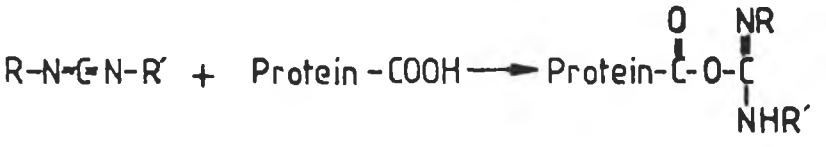

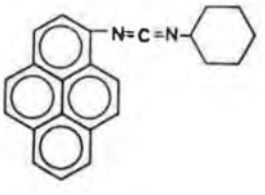

N-cyclohexyl-N'(1-pyrenyl) carbodiimide

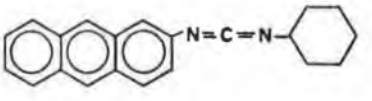

N-(2-anthracenyl)-N' -cyclocarbodiimide

Figure 1.29 Carboxylic acid reactive probes, together with the appropriate conjugation reaction.

1.4.1.5 Diazonium compounds as labels for proteins.

Another labelling technique involves the use of diazonium compounds. When a suitable aromatic amino derivative of a fluorochrome is available, it may be diazotised and the resulting diazonium compound conjugated to a protein to give the azo-protein. The diazonium salts have been shown to couple to the phenolic moiety of tyrosine and to the imidazole group of histidine. [103]

This coupling method has been used to conjugate indium to bifunctional analogues of EDTA resulting in a radioactive probe. [119] The method was modified by Hemmila et al., to couple europium-EDTA-diazophenyl to antibodies and was subsequently employed in time-resolved immunofluorometric assays. [120]

1.4.2 Fading effects in fluorescence microscopy.

One of the drawbacks of immunofluorescence is the fading of fluorescence during microscopy. FITC, RB200 and DANS are all subject to this phenomenon. It has been shown that FITC is susceptible to fading in the presence and absence of oxygen. [121] Later, studies showed that FITC was susceptible to fading in the presence of organic peroxides, hydroperoxides and oxyradicals. [122] Various reagents have been proposed to reduce this effect. [123] In 1981, the use of p-phenylenediamine was reported, however, the dye itself

undergoes rapid photo-oxidation which may be retarded by the incorporation of a reductant which regenerates the diamine from its oxidised form. [107] DABCO (1,4,-diazobicyclo-octane) is extremely stable and is useful in the retardation of fluorescence bleaching. [123] Glutathione in the presence of glutathione peroxidase has also been found to be successful in inhibiting the oxidation processes which are involved in the photobleaching effects. [122]

1.4.3 Fluorescence immunoassay methods.

There are a number of immunoassay techniques (apart from microscopic methods), which employ fluorescent probes. These can be divided into fluoroimmunoassay (FIA), in which the antigen is fluorescently labelled and immunofluorimetric assay (IFMA) in which the antibody is labelled. These can be further divided into assays where (a) the unbound fluorescent probes and endogenous fluorochromes are separated from the bound fluorescent species and (b) separation of the unbound and endogenous fluorophores is not necessary.

In systems where separation is required, the antibody is bound to a suitable solid material such as plastic or glass beads, plastic test-tubes, Sephadex particles or magnetisable particles. The fluorescently labelled antigen binds to the antibody and unbound labelled antigen or other non-specific substances can be separated by rinsing or by centrifuging and washing steps. [102]

Magnetisable particles which have the antibody-antigen fluorescent label complex attached are subjected to a brief magnetic field, while the supernatant containing the potentially interfering compounds may be aspirated to waste. [105] After separation the fluorescence of the antibody-antigen complex may be directly measured.

The formation of an antigen-antibody complex can be studied by fluorescence methods without the necessity of separating the unbound labelled antigen from the bound labelled antigen. A number of techniques are available including fluorescence polarisation, fluorescence quenching, fluorescence enhancement and fluorescence excitation transfer immunoassays.

1.4.3.1 Fluorescence polarisation immunoassay.

In the fluorescence polarisation method, depicted schematically in Figure 1.30, a labelled sample is excited with polarised light and the degree of polarisation of the emission is measured. The extent of polarisation of the emitted light will depend on the extent of random Brownian motion of the molecules that occurs during their excited state lifetimes. The smaller the labelled antigen, the faster will be its random rotation. As the labelled antigen binds to the antibody, its rotation slows down and the degree of polarisation increases. The method requires a fluorescent probe with a relatively long emission lifetime so that rotation can be measured.

The use of FITC-labelled rabbit anti-human placental lactogen for monitoring levels of human placental lactogen by fluorescence polarisation methods has been reported. [112]

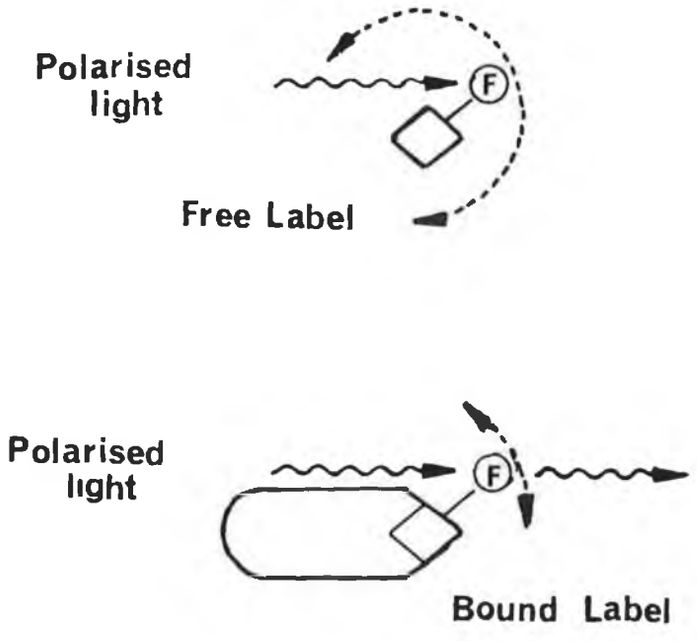

Figure 1.30 Polarisation fluoroimmunoassay.
A fluorophore (F), excited by plane polarised light, can emit polarised fluorescence. However, the rapid movement of a small fluorescent-labelled antigen (Ag) reduces or eliminates the emission of plane polarised fluorescence. Following binding to the much larger antibody, movement is restricted, allowing for emission of plane polarised fluorescence. This can be used as a basis for a simple homogenous immunoassay. [101]

When the FITC-labelled antigen is bound by the large antibody molecule it undergoes an effective increase in size and a decrease in its rotational relaxational rate leading to an increase in polarisation.

1.4.3.2 Enhancement and quenching fluoroimmunoassays.

Fluorophores in labelled antigens can give reduced (quenched) or increased (enhanced) fluorescence when bound by antibodies. Enhancement fluoroimmunoassays are not common but the method has been used for the thyroid hormone, thyroxine. The fluorescein labelled hormone has a low quantum efficiency which is thought to be caused by intramolecular quenching by the iodine in the molecule. The quantum efficiency increases four-fold when the fluorophore is bound by the antibody, presumably by inhibiting the quenching effect. The principle behind the assay is schematically illustrated in Figure 1.31. This effect has been used as the basis of an enhancement FIA for thyroxine in aqueous buffer samples. [105]

Free - impaired fluorescence Bound - enhanced fluorescence

Figure 1.31 Enhancement fluoroimmunoassay. A fluorophore when coupled to an antigen can show impaired fluorescence. The quenching effect of the antigen on the fluorophore can be removed by binding to antibody. [101]

Quenching immunoassays are more common than enhancement assays. Quenching methods are used to measure the quenching of the fluorescence of the antigen-labelled probe when bound to the antibody. The fluorescence may decrease as the small molecule labelled hapten such as FITC-labelled gentamicin binds to the antibody because of the effect of a chemical quencher present in the antibody. Direct quenching methods are used to assay small molecules only, such as haptens, because large molecules, such as proteins, enable unimpaired emission from the fluorophore because of the distances between the sites of antibody binding and of label attachment. Indirect quenching methods are suitable for the assay of large molecules, such as proteins, because the presence of the antibodies in the bound fraction sterically

hinders the binding of the label by the anti-fluorophore immunoglobulins. See Figure 1.32.

The indirect method which is also known as the fluorescence protection immunoassay, has made it possible to apply quenching principles to the measurement of large molecules. Indirect quenching employs a second antibody directed to the fluorophore. In this approach, sample, labelled antigen and anti-serum are incubated until equilibrium is reached when an excess of anti-fluorophore serum is added. This immediately binds to and quenches the fluorescence of any unbound labelled antigen, but because of steric hindrance by the first antibody, is unable to bind the fluorophore groups in the bound fraction, which continue to fluoresce. The method has been used for human albumin in serum, urine and cerebrospinal fluid and for human immunoglobulin G and placental lactogen. [105] The indirect method is not usually applicable to molecules with molecular weight < 20,000.

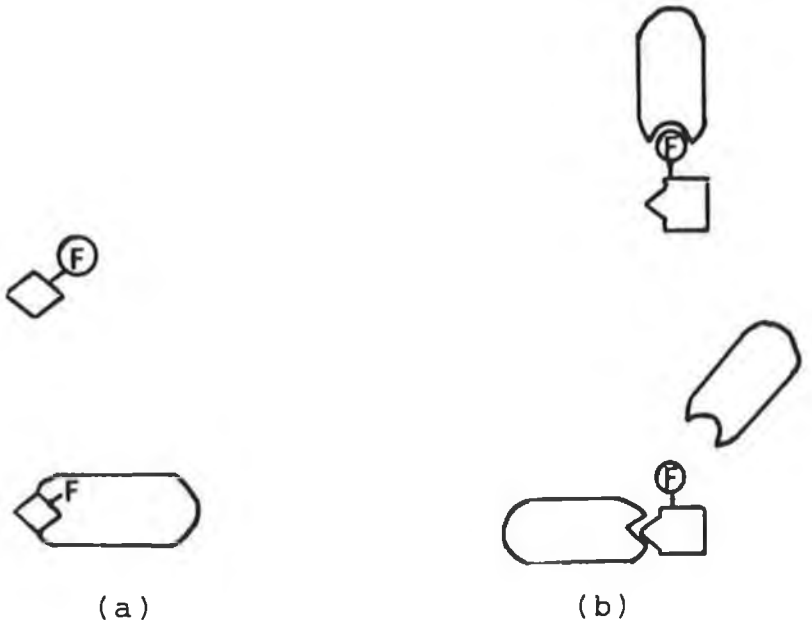

Figure 1.32 Schematic diagram of quenching fluoroimmunoassays. (a) direct quenching fluoroimmunoassay; most fluorophores when coupled to antigens show no reduction in fluorescence. However, in some cases, the binding of antibody may reduce or quench the fluorophore. (b) indirect quenching fluoroimmunoassay; the binding of a fluorophore by a specific anti-fluorophore antibody leads to quenching of the fluorescence. When the antigen fluorophore conjugate is bound by the primary antibody, steric hindrance may prevent the anti-fluorophore antibody from quenching the fluorescence. Increasing concentrations of antigen leads to a greater proportion of labelled antigen in the free fraction and hence to increased quenching. [101]

Antibodies that directly quench the fluorophore of a fluorescent labelled hapten are not common. An assay termed the alternative binding immunoassay allows indirect quenching principles to be applied to the assay of haptens and small molecules. See Figure 1.33. The principle of this immunoassay is that the labelled hapten can bind to only one antibody and if this is directed against the hapten, the fluorescence is unimpaired. Unlabelled hapten competes only for anti-hapten binding sites, so that its addition results in more of the label molecule becoming bound to anti-fluorescein, with a decrease in its signal.

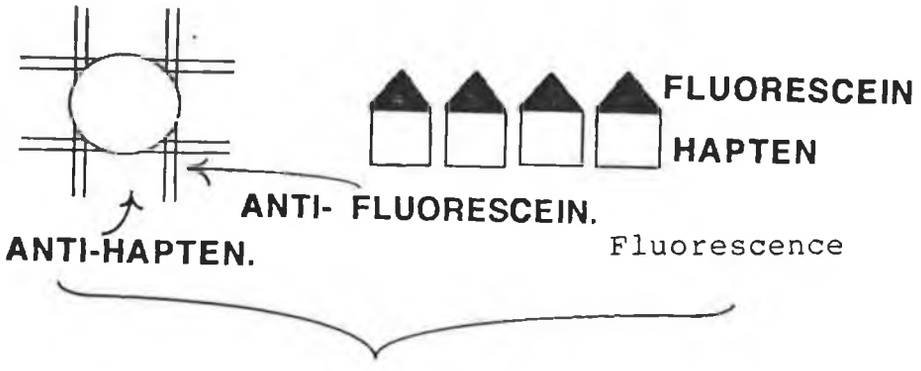

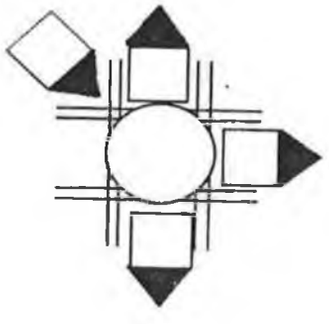

Figure 1.33 Alternative binding immunoassay. A complex of primary antibody and anti-fluorophore will bind an antigen-fluorophore conjugate at either end, yielding some fluorescence. With increasing concentrations of antigen, more conjugate will be bound at the fluorophore end, leading to some quenching. [101]

1.4.3.3 Fluorescence excitation transfer immunoassay.

Fluorescent excitation transfer immunoassays exploit the phenomenon of non-radiative resonance energy transfer between a fluorophore (donor) and an acceptor chromophore. The efficiency of the process depends on the degree of overlap between the emission spectrum of the donor and the absorption spectrum of the acceptor. Fluorescein and rhodamine are the labels most used as the donor-acceptor pair and binding of fluorescein labelled antigen by rhodamine labelled antibody brings the two reagents within energy transfer range, with a consequent reduction in fluorescein fluorescence, up to 70% fluorescence quenching. This is really equivalent to a direct quenching immunoassay and has been used for the determination of haptens and proteins. [105] Other donor-acceptor pairs such as fluorescamine and fluorescein have been reported with better stability than the fluorescein-rhodamine conjugates. [124]

1.4.3.4 Release immunoassay.

Another immunoassay technique (release immunoassay or substrate labelled immunoassay), involves the use of a labelled antigen reagent which is non-fluorescent but releases a fluorophore when split by an enzyme. The enzyme uses the non-fluorescent reagent as a substrate and enzymically liberates a fluorescent species. These

substrates include the umbelliferones. The antigen is usually labelled with a galactosyl-umbelliferone conjugate which is a substrate for a bacterial beta-galactosidase. [105]

1.4.3.5 Time-resolved fluorescence immunoassay.

Background fluorescence is one of the main problems associated with the use of fluorescence immunoassays. This is one of the main reasons for limited sensitivity of the fluorescent labels and is associated with endogenous fluorophores and light scattering effects. In Table 1.3, the fluorescence decay time of some proteins and labels are listed.

Table 1.3 Fluorescence decay time of some fluorophores and proteins.

Substance	Fluorescence decay time (ns)
Non-specific background	10
FITC	4.5
Dansyl chloride	14
N-3-pyrene maleimide	100
Europium chelates	10^3-10^6
Human serum albumin	4.1
Haemoglobin	3.5
Cytochrome C	3.0
RB200SC	1.0

Another problem mentioned already is the bleaching effect derived from continuous exposure of the fluorophore to high intensity light. Some of these problems can be solved by the use of pulsed light time resolved techniques. The basic concept behind this technique may be summarised as follows. When a fluorophore is excited by pulsed radiation, fluorescence is emitted following each pulse, with an intensity which decreases exponentially with time in a characteristic manner. An electronically gated detection system may be used to accumulate photons over any selected time interval immediately following extinction of the incident light source. Such a system may in principal be employed to identify the fluorescent signals emitted by fluorophores characterised by different decay times. The simplest situation for this technique exists when a sample contains two fluorophores, one of which displays a fluorescent decay time very much longer than the other. In this situation, it is possible to measure the signal originating from the fluorophore displaying the longer decay time by permitting the more rapidly decaying fluorescence to die away to an insignificant level before commencing photon measurement. Clearly, this technique may be exploited to reduce or effectively eliminate background fluorescence, if this is characterised by a much shorter lifetime than that of the fluorophore of interest. [113] The basic principal of the measurement is shown in Figure 1.34.

In time-resolved measurements the sample is excited with a short light pulse (about 1 ns), measurement of the fluorescence is started after a certain time (delay time t_o), has elapsed, during which time the short decay time background is reduced to almost zero. The fluorescence of a probe with a long lifetime is measured at certain intervals (t, counting time), starting from t_o.

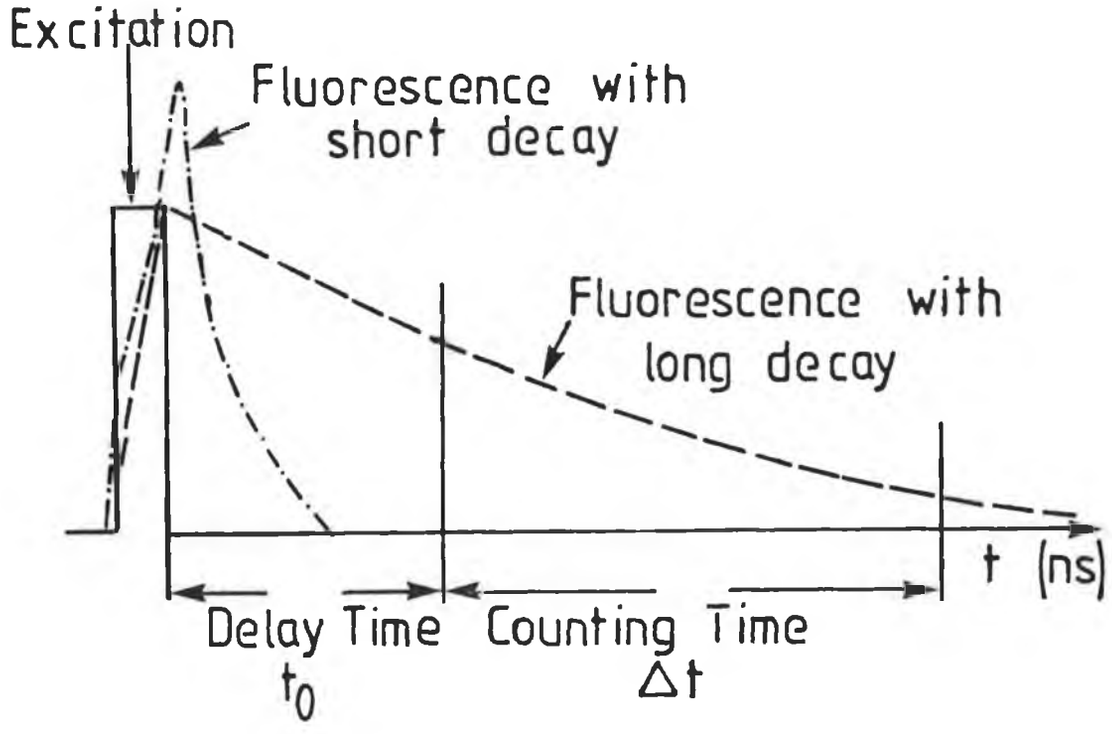

Figure 1.34 Diagram of time-resolved fluorometric measurements.

Clearly, from Table 1.3, the method can not readily be exploited to distinguish between background fluorescence and that characterising many of the fluorophores such as FITC or Dansyl Chloride. Also, depending on the gating system, the use of the relatively long lived pyrene maleimide fluorophore

may not be feasible. However, the lanthanide chelates (europium and terbium) and ruthenium (II) polypyridyl complexes have fluorescence lifetimes which are much longer than that of conventional labels. Thus, the emission from these compounds can be distinguished from the background fluorescence with a short decay time by using a time resolved fluorimeter with appropriately selected delay, counting and cycle times.

A second useful parameter of the lanthanide and ruthenium polypyridyl compounds is that they both possess a large Stokes shift. For the europium chelates, maximum emission occurs at about 613 nm and maximum absorption at 340 nm, so the Stokes shift is about 270 nm. The ruthenium(II) compounds of interest in this work absorb at around 450 nm and emit at about 600 nm, thus the Stokes shift is approximately 150 nm. The combination of the large Stokes shifts and the long emission decay times provides the basis for the application of these compounds in time-resolved techniques where high signal : noise ratios may be achieved.

The model for the fluorescence of a europium chelate consists of a series of four steps, (i) excitation of the organic ligand, (ii) intersystem crossing from the singlet excited state to the triplet excited state of the ligand, (iii) intramolecular energy transfer (energy is transferred from the triplet excited state of the ligand to the resonance levels of the europium ion) and (iv) light emission from the europium ion. [113]

The decay time and intensity of Eu fluorescence is

very much dependent on the structure of the organic ligands which chelate europium. Different β-diketones chelate europium ions. The chelates show typical emission maxima characteristic of europium, although the excitation maxima are dependent on the organic ligand. The fluorescence intensity depends largely on the ligand and solvent effects. Fluorinated β-diketones have been found to give the highest fluorescence. [113]

In aqueous solutions, quenching due to loss of energy as heat from the excited complex to the surrounding water molecules occurs. Since immunoassays are carried out in aqueous buffered solutions, a measuring solution in which the europium ion would be protected from quenching by water molecules was developed. Triton X-100, a non-ionic detergent was found to dissolve the sparingly soluble β-diketone in the micellar phase and excludes the quenching water molecules. Insulation from the solvent has been further optimised by the addition of a synergistic agent, trioctylphosphine oxide to the europium chelate solution. [113] A schematic picture of the hypothetical micellar structure into which the fluorescent europium chelate consisting of the europium β-diketone and the trioctylphosphine oxide molecules is solubilised is shown in Figure 1.35.

In order to use the europium ion as a label in immunoassays, the ion has to be bound strongly to one of the immunoreactive components. Although europium could be measured with high sensitvity as a β-diketone chelate, the

binding is not strong enough for the coupling of europium to antibodies. This may be circumvented by binding the antibody to the europium label in a more or less non-fluorescent form.

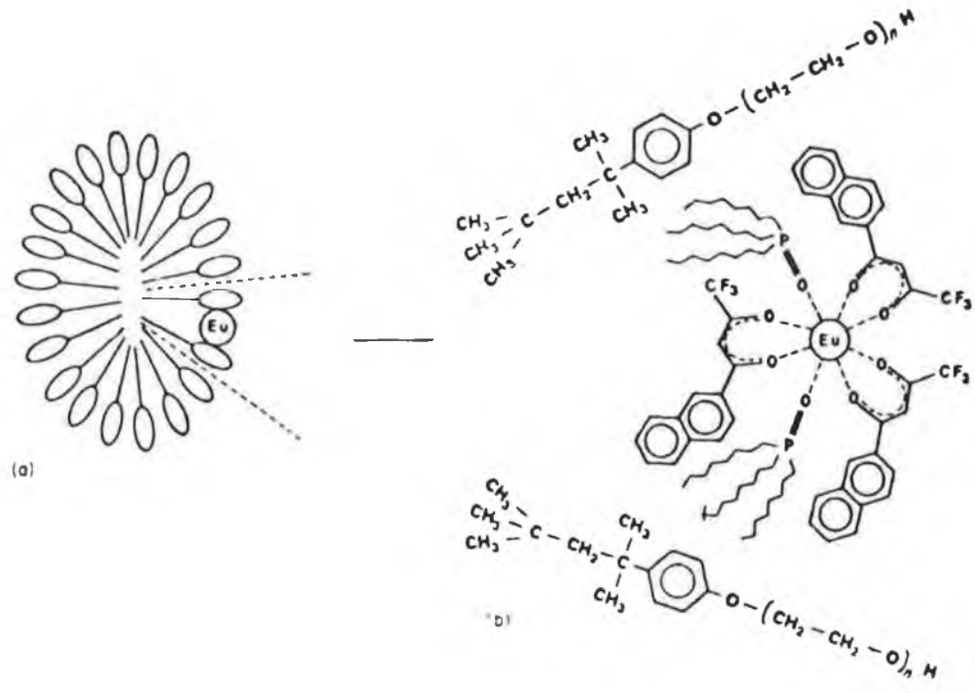

Figure 1.35 (a) A micelle consisting of Triton X-100 molecules with an association number of about 140, in which a fluorescent europium chelate is solubilised. (b) A hypothesised form of the europium chelate, consisting of an europium ion, three 2-napthoyltrifluoroacetone and two tri(n-octyl) phosphine oxide molecules as solubilised in between Triton X-100 structures. [113]

This was achieved by the use of two EDTA derivatives, diazophenyl-EDTA-europium or isothiocyanatophenyl-EDTA-europium. [120,125] EDTA and other polycarboxyl acids bind strongly to europium. By variation of pH, the strength of

binding to EDTA changes and at low pH, the europium is readily dissociated from the complex. This property is utilised when the pH change is caused by the addition of the enhancement solution containing β-diketone, trioctyl-phosphine oxide and Triton X-100 at pH 3.2. A highly fluorescent chelate solubilised in the micelle is formed. Once the EDTA based complexes are bound to the europium label in a non-fluorescent form to the immunoreactive component, the europium may be dissociated from the immunoreactive component into the fluorescent enhancement solution and the fluorescence measured by time-resolved techniques. The presence of diazophenyl and isothiocyanatophenyl moieties allow the conjugation of the EDTA-Eu chelate to the protein or antibody. The diazophenyl moiety reacts with the tyrosine residues and the isothiocyanatophenyl moiety reacts with the lysine residues and free terminal amino groups on proteins. [120] A schematic representation of the immunoassay is depicted in Figure 1.36.

The europium chelate labels have been applied to immunometric assays of the hormones, hTSH, (thyroid stimulating hormone); hCG, (human chorionic gonadotropin) using labelled monoclonal antibodies. In both assays a high sensitivity coupled with a wide linear range and excellent precision was obtained. The labels have been employed in both competitive and in immunometric assays. The europium chelate labels have also been used to measure a number of viral antigens using different immunoassay procedures. [113]

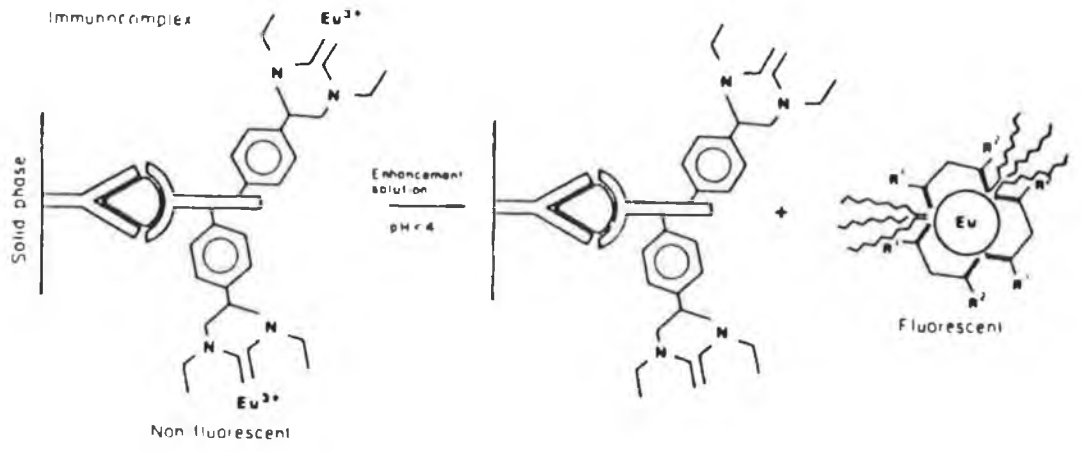

Figure 1.36 Principle for the europium release after the immunometric assay has been completed.
As a final step before fluorescence measurement, an enhancement solution is added. The europium ion dissociates from the labelled protein and forms a fluorescent chelate in solution. [113]

The synthesis of caged lanthanide complexes (cryptands / cryptates) in which the metal is surrounded by a "cage" of ligands such as those depicted in Figure 1.37, greatly improves their capacity and the cryptat described by Alpha et al., [126] (b) in Figure 1.37, has the ability to convert about 1% of the incident uv photons into emitted visible photons which is of interest in labelling of biological materials. [127]

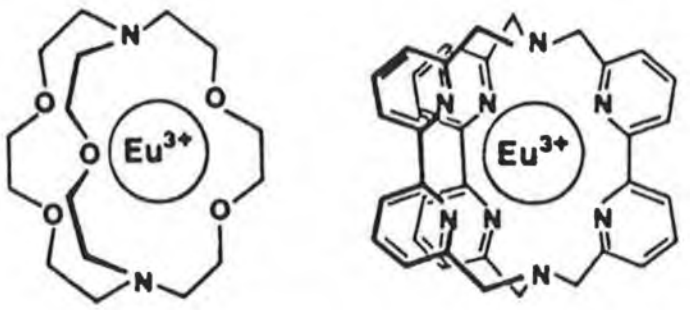

(a) (b)

Figure 1.37 Schematic representation of the [Eu 2.2.1]$^{3+}$ (a) and [Eu bpy.bpy.bpy.]$^{3+}$ cryptates. 2.2.1 stands for 4,7,13,16,21-pentaoxo-1,10-diazabicyclo-[8.8.5]-tricosane and bpy.bpy.bpy. for 6,6',6'',6''',6'''',6'''''-bis [nitrilotri (methylene)]tris(2,2'-bipyridine). [126]

1.4.4 The use of ruthenium polypyridyl complexes as labels for biomolecules.

It is appropriate to complete this section with a discussion on the use of ruthenium polypyridyl compounds in labelling procedures. Various ruthenium complexes have been prepared and coupled to albumins, antibodies and oligonucleotides. The literature describes the use of $[Ru(bpy)_2(COOH\text{-}bpy)]^{2+}$ [78,79,80,104,114,128], and the coupling procedure

involves the esterification of the complex with N-hydroxysuccinimide, followed by coupling to the amino groups on the albumin or antibody or to the primary amino group at the 5' end of oligonucleotides. The coupling reaction has been previously given in Figure 1.18.

The use of $[Ru(bpy)_2(4,4'\text{-dichloromethylbpy})]^{2+}$ has also been described, Figure 1.38, and has been conjugated to sheep and rabbit anti-mouse IgG. The complex reacts with a free amino group which attacks the chloromethyl group and displaces the chloride. [114]

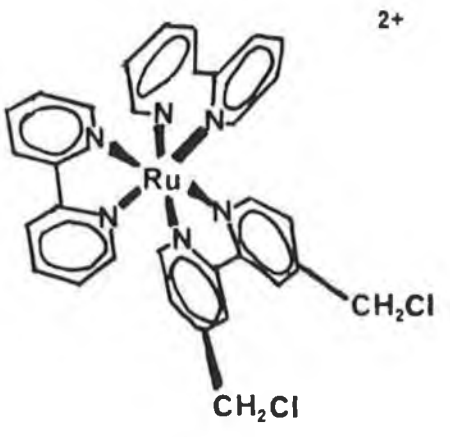

$$[F]\text{-}CH_2Cl + NH_2\text{-}[P] \longrightarrow [F]\text{-}CH_2NH\text{-}[P]$$

Figure 1.38 Structure of the complex $[Ru(bpy)_2(4,4'\text{-dichloromethylbpy})]^{2+}$ together with the conjugation reaction with amino groups of protein molecules.

The active ester of the dicarboxylic acid complex has been conjugated to bovine serum albumin, human IgG,

rabbit anti-salmonella antibody and goat anti-rabbit immunoglobulin. Immunofluorescence studies were conducted using a direct method, where the rabbit anti-salmonella antibody was reacted directly with salmonella cells and bright red/orange emission was observed using a fluorescence optical microscope. [114]

A second indirect assay was conducted using the goat anti-rabbit IgG labelled with the succinimidyl ester derivative of $[Ru(bpy)_2(4,4'\text{-}COOHbpy)]^{2+}$. After incubation with the primary and secondary antibodies and after various washing steps to remove unbound material, bright red/orange emission was viewed under the microscope. These two assays demonstrated that immunological activity was retained after conjugation of the ruthenium complex to the antibodies. [114]

An esterified ruthenium(II) dicarboxylic acid complex conjugated to bovine serum albumin was detected using electrochemiluminescent techniques. Light intensity measurements were carried out by applying a potential of -2.0 V (vs Ag wire) and detecting the emitted light with a Hamamatsu 928 photomultiplier followed by integration of the signal. Ruthenium concentrations of $1x10^{-11}$ M were detected using this method.

The dichloromethyl complex was conjugated to rabbit and sheep anti-IgG and retention of immunological reactivity was demonstrated by fluorometric analysis. The excitation wavelength used was 455 nm and emission was monitored at 623 nm. This experiment involved incubating a

suspension of Legionella pneumophilia with a primary mouse monoclonal IgG antibody. A preparation of pooled rabbit/sheep anti-IgG antibody labelled with the ruthenium dichloromethyl complex was then added. After appropriate incubation and centrifugation steps, the Legionella pneumophilia cells were resuspended in buffer and transferred to a polystyrene cuvette for fluorimetric analysis at 623 nm. Fluorescence was observed, demonstrating retention of immunological activity. [114]

Weber has described the use of some ruthenium complexes in photoelectrochemical immunoassays which bind to the amino groups on the analyte through a thiourea linkage using $[Ru(bpy)_2(4,4'\text{-isothiocyanato-}2,2'\text{-bipyridine})]^{2+}$ and also reports the use of the ester of 3-O-morphinyl ester of $[Ru(bpy)_2(4,4'COOHbpy)]^{2+}$ as a label for the determination of morphine. [128] In the photoelectrochemical immunoassay, the label transfers an electron to a quencher upon photoexcitation and the oxidised molecule is subsequently reduced with an electron from an electrode of the flow cell which is held at a suitable potential. This electron is measured as photocurrent. The amount of free labelled analyte is determined by the photocurrent signal.

The use of ruthenium bathophenanthroline complexes to label oligonucleotides has been described. The complexes have been linked to oligonucleotides via an amino group or via a phosphodiester linkage. The compounds of the type presented in Figure 1.39, which are bound to the

synthetically prepared 5'NH_2-modified fragments of DNA via the amino group, are firstly converted to the esterified derivative before coupling. [80]

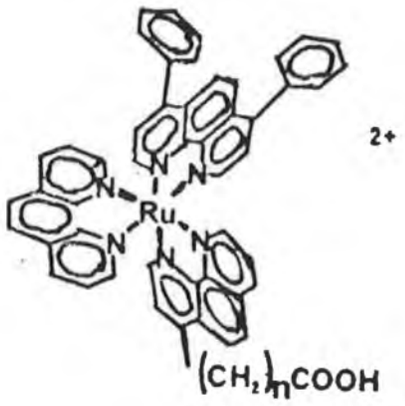

Figure 1.39 Bathophenanthroline Ru (II) complexes which are converted to the hydroxysuccinimide ester before conjugation to oligonucleotides.

The coupling products exhibit the characteristic MLCT absorption band of ruthenium polypyridyl complexes at about 450 nm and the maximum wavelength of emission is approximately 616 nm, when measured in phosphate buffer saline. The conjugates were measured by time-resolved fluorescence and the detection limit was below 10^{-14} M. The decay lifetimes were monitored in the presence of additives such as detergents, salts and reducing agents and longer lifetimes were observed. Increased lifetimes of the order of up to 7.5 μsec were reported, compared to a lifetime of about 2.0 μsec in the absence of any additive. [80]

Ruthenium bathophenanthroline compounds have been used as non-radioactivelabels for dideoxy DNA sequencing. [78] The ruthenium bathophenanthroline complex shown in Figure 1.39 has been coupled to nucleotides directly in the course of their synthesis via a phosphodiester linkage. [79] This approach offers a number of advantages over the previous method for coupling the bathophenanthroline complexes to synthetic DNA fragments, including that functionalisation of the DNA with a primary amino group is not necessary, making the coupling procedure easier and more rapid to perform.

The use of hydroxysuccinimide esters, chloroformate, isothiocyanate and sulphonyl chloride derivatives of ruthenium polypyridyl complexes has been reported. [104] These complexes were conjugated to anti-TSH (thyroid stimulating hormone) and human IgG, and may be employed in time-resolved immunoassay techniques.

The use of ruthenium polypyridyl complexes has one major advantage over the use of the lanthanide EDTA chelates. In contrast to the lanthanide chelates where prior to fluorimetric analysis, the chelates must be destroyed and the lanthanide ion has to be embedded into liposomes in order to be detected. Fluorescence measurements may be carried out directly using the ruthenium(II) polypyridyl complexes.

This thesis describes the synthesis of various ruthenium polypyridyl complexes which were coupled covalently to albumins, antibodies and poly-L-lysine. Various binding methods have been employed to couple the reporter complex to the proteins: (a) via the ε-amino group of lysine residues

using ruthenium complexes containing an isothiocyanate group and via the active ester of a dicarboxylic acid complex; (b) via the carbohydrate moieties of glycoproteins by reaction with a ruthenium polypyridyl amino complex after periodate oxidation of the carbohydrate moieties of the proteins and (c) via tyrosine and possibly histidine residues of proteins by reaction with the diazotised derivative of the amino ruthenium complex.

The effect of binding on the immunological activity, where relevant, the absorption and emission spectra and on the emission lifetimes of the conjugates is investigated.

The compounds have been characterised using various techniques including NMR, electrochemistry and absorption / emission spectroscopy. The emission decay lifetimes of the unbound complexes were also measured and are compared to those of the protein bound ruthenium complexes.

1.5 References.

[1] B.E. Buchanan, Ph.D Thesis, Dublin City University, Dublin, 1989.

[2] R. Hage, R. Prins, J.G. Haasnoot, J. Reedijk and J.G. Vos, J. Chem. Soc., Dalton Trans., 1987, 1389.

[3] A. Juris, V. Balzani, F. Barigelletti, S. Campagna, P, Belser and A. von Zelewsky, Coord. Chem. Rev., 1988, 84, 85 and references therein.

[4] K. Kalyanasundaram, Coord. Chem. Rev., 1982, 46, 159.

[5] K.R. Seddon, Coord. Chem. Rev., 1982, 41, 79.

[6] E.A. Seddon and K.R. Seddon, The Chemistry of Ruthenium, Monograph 19, Elsevier, 1984 and references therein.

[7] R.J. Watts, J. Chem. Ed., 1983, 60, 834.

[8] E.M. Kober and T.J. Meyer, Inorg. Chem., 1982, 21, 3967.

[9] E.M. Kober and T.J. Meyer, Inorg. Chem., 1983, 22, 1614.

[10] E.M. Kober and T.J. Meyer, Inorg. Chem., 1984, 23, 3877.

[11] J.V. Casper and T.J. Meyer, Inorg. Chem., 1983, 22, 2444.

[12] R.J. Crutchley and A.B.P. Lever, Inorg. Chem., 1982, 21, 2276.

[13] K. Kalyanasundaram, M. Gratzel, E. Pelizzetti, Coord. Chem. Rev., 1986, 69, 57.

[14] F. Barigelletti, L. de Cola, V. Balzani, P. Belser, A. von Zelewsky, F. Vogtle, F. Ebmeyer, S. Grammenudi, J. Am. Chem. Soc., 1989, 111, 4662.

[15] L. de Cola, F. Barigelletti, V. Balzani, P. Belser, A. von Zelewsky, F. Vogtle, F. Ebmeyer, S. Grammenudi, J. Am. Chem. Soc., 1989, 110, 7210.

[16] P. Belser, L. de Cola, A. von Zelewsky, J. Am. Chem. Soc. Commun., 1988, 1057.

[17] J.N. Demas, G.A. Crosby, J. Am. Chem. Soc., 1971, 93, 2841.

[18] J.N. Demas and D.G. Taylor, Inorg. Chem., 1979, 18, 3177.

[19] K.W. Hipps and G.A. Crosby, J. Am. Chem. Soc., 1975, 97, 7042.

[20] R.W. Harrigan and G.A. Crosby, J. Chem. Phys., 1973, 59, 3468.

[21] R.H. Harrigan, G.D. Hagen and G.A. Crosby, Chem. Phys. Lett., 1973, 21, 487.

[22] G.A. Heath, L.J. Yellowless and P.S. Braterman, Chem. Phys. Lett., 1982, 92, 646.

[23] P.S. Braterman, A. Harriman, G.A. Heath and L.J. Yellowless, J. Chem. Soc., Dalton Trans., 1983, 1801.

[24] W.M. Wacholtz, R.A. Auerbach, R.H. Schmehl, M. Ollino and W.R. Cherry, Inorg. Chem., 1985, 24, 1785.

[25] W.J. Vining, J.V. Casper and T.J. Meyer, J. Phys. Chem., 1985, 89, 1095.

[26] A. Juris, F. Barigelletti, V. Balzani, P. Belser and A. von Zelewsky, Inorg. Chem., 1985, 24, 202.

[27] J. van Houten and R.J. Watts, J. Am. Chem. Soc., 1976, 98, 4853.

[28] J. van Houten and R.J. Watts, Inorg. Chem., 1978, 17, 3381.

[29] B. Durham, J.V. Casper, J.K. Nagle and T.J. Meyer, J. Am. Chem. Soc., 1982, 104, 4803.

[30] J.V. Casper and T.J. Meyer, J. Am. Chem. Soc., 1983, 105, 5583.

[31] F. Barigelletti, P. Belser, A. von Zelewsky, A. Juris and V. Balzani, J. Phys. Chem., 1985, 89, 3680.

[32] W.R. Cherry and L.J. Henderson, Inorg.Chem., 1984, 23, 983.

[33] F. Barigelletti, A. Juris, V. Balzani, P. Belser and A. von Zelewsky, J. Phys. Chem., 1986, 90, 5190.

[34] A. Juris, M.F. Manfrin, M. Maestri and N. Serpone, Inorg. Chem., 1978, 17, 2258.

[35] F. Bolleta, M. Maestri, L. Moggi and V. Balzani, J. Chem. Soc. Commun., 1975, 901.

[36] C. Creutz and N. Sutin, J. Am. Chem. Soc., 1976, 98, 6384.

[37] C. Creutz, Inorg. Chem., 1978, 17, 1046.

[38] G.P. Porter, J. Chem. Ed., 1983, 60, 785.

[39] C-T. Lin, W. Bottcher, M. Chou, C. Creutz and N. Sutin, J. Am. Chem. Soc., 1976, 98, 6536.

[40] C-T. Lin and N. Sutin, J. Phys. Chem., 1976, 80, 97.

[41] N. Lasser and J. Feitelson, J. Phys. Chem., 1973, 77, 1011.

[42] D.E. Morris, Y. Ohsawa, D.P. Segers, M.K. De Armond and K.W. Kanck, Inorg. Chem., 1984, 23, 3010.

[43] P.J. Giordano, C.R. Bock and M.S. Wrighton, J. Am. Chem. Soc., 1978, 100, 6960.

[44] T. Schmidzu, T. Iyodo and K. Izaki, J. Phys. Chem., 1985, 89, 642.

[45] P. Ford, D.F.P. Rudd, R. Gaugner and H. Taube, J. Am. Chem. Soc., 1968, 90, 1187.

[46] T.J. Meyer, Pure. Appl. Chem., 1986, 57, 1193.

[47] M. Haga, Inorg. Chim. Acta, 1983, 75, 29.

[48] A.M. Bond and M. Haga, Inorg. Chem., 1986, 25, 4507.

[49] C.R. Johnson, W.W Henderson and R.E. Shephard, Inorg. Chem., 1984, 23, 2754.

[50] M.G. Elliot and R.E. Shephard, Inorg. Chem., 1987, 26, 2067.

[51] R.J. Sundberg and R.B. Martin, Chem. Rev., 1974, 74, 471.

[52] B.P. Sullivan, D.J. Salmon, T.J. Meyer and J. Peedin, Inorg. Chem., 1978, 18, 3369.

[53] C.R. Johnson, R.E. Shephard, B.Marr, S. O'Donnell and W. Dressick, J. Am. Chem. Soc., 1980, 102, 6227.

[54] C. Long and J.G. Vos, Inorg. Chim. Acta, 1984, 89, 125.

[55] P.J. Giordano, C.R. Bock, M.S. Wrighton, L.V. Interrante and R.F.X. Williams, J. Am. Chem. Soc., 1977, 99, 3187.

[56] Md.K. Nazeeruddin and K. Kalyanasundaram, Inorg. Chem., 1989, 28, 4251.

[57] J. Ferguson, A.W.H. Mau and W.H.F. Sasse, Chem. Phys. Lett., 1979, 68, 21.

[58] P.A. Lay and W.H.F. Sasse, Inorg. Chem., 1984, 23, 4125.

[59] K. Shinozaki, Y. Kaiza, H. Hirai and H. Kobayashi, Inorg. Chem., 1989, 28, 3675.

[60] R.J. Crutchley, N. Kress and A.B.P. Lever, J. Am. Chem. Soc., 1983, 105, 1170.

[61] A. Kisrch-de Mesmaeker, L. Jacquet and J. Nalsielski, Inorg. Chem., 1988, 27, 4451.

[62] J.F. Ireland and P.A.H. Whyatt, Adv. Phys. Org. Chem., 1976, 12, 131.

[63] J.K. Barton, J. Biomol. Struct. Dyn., 1983, 1, 621.

[64] J.K. Barton, L.A. Basile, A.T. Danishefsky and A. Alexandrescu, Proc. Natl. Acad. Sci. USA., 1984, 81, 1961.

[65] J.K. Barton, A.T. Danishefsky and J.M. Goldberg, J. Am. Soc., 1984, 106, 2172.

[66] H. Gorner, A.B. Tossi, C. Stradowski and D. Schulte-Frohlinde, J. Photochem. Photobiol. B, 1988, 2, 67.

[67] J.M. Kelly, A.B. Tossi, D.J. McConnell and C. OhUigin, Nuc. Acids Res., 1985, 13, 6017.

[68] J.M. Kelly, D.J. McConnell, C. OhUigin, A.B. Tossi, A. Kirsch-de Mesmaeker, A. Masschelein and J. Nasielski, J. Chem. Soc. Chem. Commun., 1987, 1821.

[69] C.V. Kumar, J.K. Barton and N.J. Turro, J. Am. Chem. Soc., 1985, 107, 5518.

[70] H-Y. Mei, J.K. Barton, Proc. Natl. Acad. Sci. USA, 1988, 85, 1339.

[71] A.B. Tossi and J.M. Kelly, Photochem. Photobiol., 1989, 49, 545.

[72] C.V. Kumar, A.L. Raphael and J.K. Barton, 1986, Biomolecular Stereodynamics III, Proceedings of the Fourth Conversation in the Discipline Biomolecular Stereodynamics. R.H. Sarma and M.H. Sarma Eds., Adenine Press, New York.

[73] J.K. Barton, Comments Inorg. Chem., 1985, 3, 321.

[74] A. Kirsch-de Mesmaeker, G. Orellana, J.K. Barton and N.J. Turro, Photochem. Photobiol., 1990, 52, 461.

[75] (a) B. Rosenberg, L. van Camp, J.E. Trosko, V.H. Mansour, Nature (London), 1969, 222, 385. (b) B. Rosenberg and L. Van Camp, Cancer Res, 1970, 30, 1979.

[76] J.K. Barton and E. Lolis, J. Am. Chem. Soc., 1985, 107, 108.

[77] J. Telser, K.A. Cruickshank, K.S. Schanze and T.L. Netzel, J. Am. Chem. Soc., 1989, 111, 7221.

[78] W. Bannwarth, Anal. Biochem., 1989, 181, 216.

[79] W. Bannwarth and D. Schmidt, Tetrahedron Lett., 1989, 30, 1513.

[80] W. Bannwarth, D. Schmidt, R.L. Stallard, C. Hornung, R. Knorr and F. Muller, Helv. Chim. Acta, 1988, 71, 2085.

[81] J.D. Watson and F.H. Crick, (a) Nature, 1952, 171, 737. (b) Proc. Royal. Soc., 1954, 2234, 80.

[82] J.K. Barton, C and En, 1988, 30.

[83] (a) S.J. Lippard, Acc. Chem. Res., 1978, 11, 211. (b) K.W. Jennette, S.J. Lippard, G.A. Vassiliades and W.R. Bower, Proc. Natl. Acad. Sci. USA, 1974, 71, 3839.

[84] C. Hiort, B. Norden, A. Rodger, J. Am. Chem. Soc., 1990, 112, 1971.

[85] H-Y. Mei and J.K. Barton, J. Am. Chem. Soc., 1986, 108, 7414.

[86] A.M. Pyle, J.P. Rehmann, R. Meshoyrer, C.V. Kumar, N.J. Turro and J.K. Barton, J. Am. Chem. Soc., 1989, 111, 3051.

[87] E.C. Long and J.K. Barton, Acc. Chem. Res., 1990, 23, 271.

[88] J.K. Barton, Science, 1986, 233, 727.

[89] J.K. Barton, J.M. Goldberg, C.V. Kumar, N.J. Turro, J. Am. Chem. Soc., 1986, 108, 2081.

[90] J.K. Barton, C.V. Kumar and N.J. Turro, J. Am. Chem. Soc., 1986, 108, 6291.

[91] C. Stradowski, H. Gorner, L.J. Currell and D. Schulte-Frohlinde, Biopolymers, 1987, 26, 189.

[92] H. Gorner, A.B. Tossi, C. Stradowski, D. Schulte-Frohlinde, J. Photochem. Photobiol. B: Biology, 1988, 2, 67.

[93] L. Kittler, G. Lober, F.A. Gollmick, H. Berg, J. Electroanal. Chem., 1980, 116, 503.

[94] A.E. Friedman, J.C. Chambron, J-P. Sauvage, N.J. Turro and J.K. Barton, J. Am. Chem. Soc., 1990, 112, 4960.

[95] J.K. Barton, Pure and Applied Chem., 1989, 61, 563.

[96] M.B. Fleisher, K. Waterman, N.J. Turro and J.K. Barton, Inorg. Chem., 1986, 25, 3549.

[97] J.M. Kelly, M.M. Feeney, A.B. Tossi, J-P. Lecomte and A. Kirsch-de Mesmaeker, Anti-Cancer Drug Design, 1990, 5, 69.

[98] C.S. Chow and J.K. Barton, J. Am. Chem. Soc., 1990, 112, 2839.

[99] L.A. Basile and J.K. Barton, J. Am. Chem. Soc., 1987, 109, 7548.

[100] L.A. Basile and J.K. Barton, J. Am. Chem. Soc., 1987, 109, 7550.

[101] R. Edwards, Immunoassay : An Introduction, William Heinemann Medical Books, London, 1985.

[102] E. Soini and I. Hemmila, Clin. Chem., 1979, 25, 353.

[103] R.C. Nairn, Fluorescent Protein Tracing, 4th edition, Churchill Livingstone, London, 1976.

[104] R.S. Davidson, Transition Metal Complexes and Method for Time-Resolved Luminescence Binding Assay, 1986, British Patent Application No. 8601646; 1987, International Patent Application No. 8704523.

[105] D.S. Smith, M.H.H. Al-Hakiem and J. Landon, Ann. Clin. Biochem, 1981, 18, 253.

[106] D.J. O'Shannessy and R.H. Quarles, J. Immunol. Meth., 1987, 99, 153.

[107] R.S. Davidson and M.M. Hilchenbach, Photochem. Photobiol., 1990, 52, 431.

[108] R.P. Haughland, Handbook of Fluorescent Probes and Research Chemicals, Molecular Probes Inc., Oregon 97402, USA, 1989.

[109] J. March, Advanced Organic Chemistry, 3rd. edition, John Wiley and Sons, New York, 1985.

[110] A.H. Coons, H.J. Creech, R.N. Jones and E. Berliner, J. Immunol., 1942, 45, 159.

[111] J.L. Riggs, R.J. Seiwald, J.H. Burckhalter, C.M. Downs and T.G. Metcalf, Amer. J. Path., 1958, 34, 1081.

[112] D.S. Smith, M. Hassan and R.D. Nargessi, Principles and Practice of Fluorimmunoassay Procedures in Modern Fluorescence Spectroscopy 3, E.L. Wehry, Plenum Press, New York, 1981.

[113] (a) E.P. Ekins, Current concepts and future developments and (b) T. Lovgren, I. Hemmila, K. Pettersson and P. Halonen, Time-resolved fluorometry in Alternative Immunoassays, W.P. Collins, Ed., John Wiley and Sons Ltd., New York, 1985.

[114] A.J. Bard, Luminescent Metal Chelate Labels and Means for Detection, 1986, International Application No., PCT/US85/02153.

[115] J.A. Titus, R.P. Haughland, S.O. Sharrow, D.M. Segal, J. Immunol. Methods, 1982, 50, 193.

[116] H.J. Tae, Bifunctional reagents in Methods in Enzymology, Vol. 91, Ed. C.H.W. Hirs and S.N. Timasheff, Academic Press, New York, 1983.

[117] F. Wold, Bifunctional reagents in Methods in Enzymology, Vol. XXV, Ed. C.H.W. Hirs and S.N. Timasheff, Academic Press, New York, 1972.

[118] M.R. Chapple, G.D. Johnson, R.S. Davidson, J. Immunol. Meth., 1988, 111, 209.

[119] M.W. Sundberg, C.F. Meares, D.A. Goodwin, C.I. Diamenti, J. Med. Chem., 1974, 17, 1304.

[120] I. Hemmila, S. Dakubu, V.M. Mukkala, H. Siitari and T. Lovgren, Anal. Biochem., 1984, 137, 335.

[121] G.D. Johnson, R.S. Davidson, K.C. McNamee, G. Russell, D. Goodwin and E.J. Holborrow, J. Immunol. Meth., 1982, 55, 231.

[122] R.S. Davidson and J.E. Pratt, J. Photochem. Photobiol. B: biology, 1988, 1, 361.

[123] G.D. Johnson and G.M. de C. Nogeuira Araujo, J. Immunol. Meth., 1981, 43, 349.

[124] J.N. Miller, C.S. Lim and J.W. Bridges, Analyst, 1980, 105, 91.

[125] T. Lovgren, I. Hemmila, K. Pettersson, J.U. Eskola and E. Bertoft, Talanta, 1984, 31, 909.

[126] B. Alpha, V. Balzani, J.M. Lehn, L. Perathoner and N. Sabbatini, Angew. Chem. Int. Ed. Engl., 1987, 26, 1266.

[127] V. Balzani and R. Ballardini, Photochem. Photobiol, 1990, 52, 409.

[128] S.G. Weber, Photoelectrochemical Immunoassays, 1981, U.S. Patent US 4,293,310.

CHAPTER 2

MATERIALS and METHODS

2.1 Synthesis.

2.1.1 Preparation of the complexes cis- $[Ru(L\text{-}L)_2(NH_2py)_2]^{2+}$, $[Ru(L\text{-}L)_2(NH_2phen)]^{2+}$ and $[Ru(L\text{-}L)_2(COOHbpy)]^{2+}$.

where L-L = 1,10-phenanthroline (phen) or 2,2'-bipyridine (bpy), NH_2phen = 5-amino-1,10-phenanthroline, NH_2py = 4-amino-pyridine and COOHbpy = 4,4'-dicarboxylic acid -2,2'-bipyridine.

The complexes were prepared according to literature methods. [1]

2.1.1.1 $[Ru(bpy)_2(NH_2py)_2](PF_6)_2.CH_3COCH_3$. (1)

Yield 680 mg (72%). Found C,41.66; H,3.62; N,11.76. Calculated C,41.72; H,3.58; N, 11.80%.

^1H NMR; $[(CD_3)_2CO]$: 2,2'-bipyridine ligand, 8.57-8.68 ($H^3/H^{3'}$); 7.98-8.04, 8.22-8.28 ($H^4/H^{4'}$); 7.43-7.48, 7.90-7.95 ($H^5/H^{5'}$); 8.15-8.17, 9.24-9.26 ($H^6/H^{6'}$). 4-amino-pyridine ligand, 7.89-7.92 (H^2); 6.58-6.60 (H^3); 6.26 (NH_2).

2.1.1.2 $[Ru(bpy)_2(NH_2phen)](PF_6)_2 . 1/2 CH_3COCH_3$. (2)

Yield 700mg (75%). Found C,43.40; H, 3.04; N, 10.37. Calculated C, 43.36; H, 3.02; N, 10.57%.
^1H NMR; $[(CD_3)_2CO]$: 2,2'-bipyridine ligand, 8.80-8.86, (H^3); 8.12-8.28 (H^4); 7.40-7.48, 7.59-7.68 ($H^5/H^{5'}$; 7.87-7.93, 8.12-8.20, ($H^6/H^{6'}$).
5-amino-1,10-phenanthroline ligand, 7.96 (H^2); 7.66 (H^3); 8.35 (H^4); 7.31 (H^6); 8.95 (H^7); 7.88 (H^8); 8.39 (H^9); 6.43 (NH_2).

2.1.1.3 $[Ru(phen)_2(NH_2phen)](PF_6)_2$. (3)

Yield 650 mg (69%). Found C, 45.16; H, 2.67; N, 10.28. Calculated C, 45.66; H, 2.63; N, 10.36%.
^1H NMR; $[(CD_3)_2CO]$: 1,10-phenanthroline ligand, 7.84-7.88, 8.35-8.44 (H^2/H^9); 7.77-7.89 (H^3/H^8); 8.76-8.82 (H^4/H^7); 8.42 (H^5/H^6).
5-amino-1,10-phenanthroline ligand, 7.92 (H^2); 7.53 (H^3); 8.32 (H^4); 7.31 (H^6); 8.93 (H^7); 7.75 (H^8); 8.36 (H^9); 6.43 (NH_2).

2.1.1.4 $[Ru(bpy)_2(bdd)](PF_6)_2$. (4)

This complex was kindly donated by Joe Bolger, Dublin City

University. The ligand bdd = 2,3-butanedionedihydrazone.

2.1.1.5 Preparation of the isothiocyanate derivatives of (1) to (4).

The amino complex (0.2 mmol) in 10 ml distilled water was stirred in the presence of an anion exchange resin (Amberlite exchange resin Cl^-, which had been treated with 2 M NaOH, washed thoroughly and then treated with 2 M HCl and washed thoroughly again) to exchange the PF_6^- anion for Cl^- ions until the compound became soluble in the aqueous solution. The solution was filtered, to remove the resin. The dichloride compound was then reacted with thiophosgene, 0.01 mol in acetone (10 ml), which was added dropwise to the aqueous solution over 30 mins. During this time the reaction vessels were kept in an ice-bath, to inhibit the evaporation of the thiophosgene.

After addition was complete, the reaction was allowed to proceed at room temperature overnight in a covered vessel. The complex $[Ru(phen)_2(NCSphen)]^{2+}$ which precipitated, was isolated by filtration and dried under vacuum. The other complexes remained in solution and were isolated by evaporation of the excess thiophosgene under reduced pressure, followed by precipitation using a saturated aqueous solution of NH_4PF_6. The compounds were dried under vacuum. All procedures were carried out with care due to the toxicity of thiophosgene. Gloves were worn and due to

the volatility of the thiophosgene, each stage was carried out in a fume-hood.

2.1.1.6 Diazotisation of compounds (2) and (3).

These amino complexes were diazotised according to the method described by Sundberg *et al.* [2]

The amine complexes (0.1 mmol) were dissolved in 1:1 H_2O : acetone (2 ml); 0.5 ml conc. HCl was added and the mixture cooled to 0^oC in an ice bath. Cold 0.5 M $NaNO_2$ (0.25 ml, 0.125 mmol) was added dropwise with stirring at 0^oC and the reaction allowed to proceed for 1 hour at 0^oC. Urea (3 mg, 0.05 mmol) was added to destroy excess $NaNO_2$ and the mixture was filtered. The filtrate was neutralised by the addition of solid $NaHCO_3$ to pH 7.5. The solution was made up to 5 ml with cold distilled H_2O.

2.1.1.7 $[Ru(bpy)_2(COOHbpy)](PF_6)_2$.

The ligand 4,4'-dicarboxylic acid-2,2'bipyridine was prepared from 4,4'-dimethyl-2,2'bipyridine according to literature methods. [3]. Synthesis of the ruthenium complex (a) and its conversion to the active ester (b) were carried out according to Bard. [4]

(a) Sodium bicarbonate (6 mmol), $[Ru(bpy)_2Cl_2].\ 2H_2O$ (1 mmol), and 4,4'-dicarboxylic acid-2,2'bipyridine (1.2 mmol)

were heated at reflux in methanol (80 ml) / H_2O (20 ml) for 9 hours. The solution was then cooled in an ice bath, treated with 5 drops conc. H_2SO_4 and allowed to stand at ice bath temperature for 1.5 hours. A precipitate formed which was separated by filtration and washed with methanol (10 ml).

The filtrate and wash solution were combined and were treated with a saturated aqueous solution of NH_4PF_6. The resulting solution was cooled in an ice bath and the precipitate was collected. Yield 620 mg, (65%)

(b) Dicyclohexylcarbodiimide (DCC, 0.046g) and N-hydroxysuccinimide (0.034g) were dissolved in dimethylformamide (DMF), 2 ml, with stirring and cooled in an ice bath. A solution of $[Ru(bpy)_2(COOHbpy)](PF_6)_2$ (0.10g, 0.1 mmol) in 1 ml DMF was then added and the mixture stirred for 5 hours, at ice bath temperature. Any precipitate which formed was removed by centrifugation. The supernatant was retained for conjugation procedures.

2.1.2 Ligand preparation.

The following four ligands were obtained from and prepared by Ronald Hage, [5], according to literature methods.

2.1.2.1 3-(pyridin-2-yl)-1H-1,2,4-triazole. (Hptr)

M.P.; 158-160°C. (lit.[6] 164-165°C.). ^{1}H N.m.r.; [$(CD_3)_2SO$], 14.62 (N-H), 8.70 (H^6), 8.27 ($H^{5'}$), 8.09 (H^3), 7.98 (H^4) and 7,51 (H^5). ^{13}C; [$CDCl_3$], 154.8 ($C^{3'}$), 151.8 ($C^{5'}$), 146.6 (C^2), 137.8 (C^4), 125.0 (C^5) and 121.9 (C^3) p.p.m..

2.1.2.2 4-Methyl-3-(pyridin-2-yl)-4H-1,2,4-triazole. (4Mptr)

M.P.; 96-99°C. (lit.[7] 104-105°C.). ^{1}H N.m.r.; [$(CD_3)_2SO$], 8.66 (H^6), 8.62 (H^5), 8.11 (H^3), 7.95 (H^4), 7.47 (H^5) and 3.99 (CH_3). ^{13}C; [$CDCl_3$], 33.4 (CH_3), 122.8 (C^3), 124.2 (C^5), 137.4 (C^4), 147.2 ($C^{5'}$), 147.5 (C^2), 149.0 (C^6) and 151.1 ($C^{3'}$) p.p.m..

2.1.2.3 3-Methyl-5-(pyridin-2-yl)-1H-1,2,4-triazole. (H3Mptr)

M.P.; 163-165°C.(lit.[8] 165-166°C). ^{1}H N.m.r.; [$(CD_3)_2SO$], 14.2 (N-H), 8.83 (H^6), 8.02 (H^3), 7.90 (H^4), 7.43 (H^5) and 2.36 (CH_3). ^{13}C; ($CDCl_3$), 13.0 (CH_3), 121.6 (C^3), 124.3 (C^5), 137.3 (C^4), 147.5 (C^2), 149.2 (C^6), 156.5 ($C^{3'}$) and 158.5 ($C^{5'}$) p.p.m..

2.1.2.4 1-Methyl-3-(pyridin-2-yl)-1,2,4-triazole. (1Mptr)

M.P.; 51-54^{0}C.(lit.[9] 47-48^{o}C.) ^{1}H N.m.r.; [$(CD_3)_2SO$], 8.66 (H^6), 8.61 (H^5), 8.16 (H^3), 7.91 (H^4), 7.43 (H^5) and 3.97 (CH_3). ^{13}C; ($CDCl_3$), 36.1 (CH_3), 121.4 (C^3), 123.8 (C^5), 136.9 (C^4), 145.8 ($C^{5'}$), 149.5 (C^6), 149.7 (C^2) and 161.2 ($C^{3'}$) p.p.m..

2.1.3 Preparation of complexes of the type cis-$[Ru(L\text{-}L)_2\text{-}(L\text{-}L')]^{2+}$.

(L-L) = 4,4'-dimethyl-2-2'bipyridine, (dmbpy) or 1,10-phenanthroline, (phen). (L-L') = Hptr, H3Mptr, 1Mptr, or 4Mptr.

Hydrated ruthenium trichloride was obtained as a loan from Johnson Matthey and used without further purification. The complexes cis-$[Ru(dmbpy)_2Cl_2].2H_2O$ and cis-$[Ru(phen)_2Cl_2].2H_2O$ were prepared according to literature methods. [10,11]

2.1.3.1 $[Ru(dmbpy)_2(Hptr)](PF_6)_2.H_2O$. (1)

The complex cis-$[Ru(dmbpy)_2Cl_2.2H_2O$ (1 mM) was heated at reflux in water - ethanol (1:1) in the presence of excess pyridyl triazole ligand (1.2 mM) for four hours. In order to ensure complete protonation of the bound ligand, 1-2 drops conc. HCl were added. The solvent was removed by rotary evaporation and the remaining residue was dissolved in 5 ml water and added dropwise to an aqueous solution of NH_4PF_6. The resulting precipitate was filtered and purified by recrystallisation from acidic (HCl) mixtures of acetone - water. Yield 730 mg (79%). Found C,40.28; H,3.64; N,11.76. Calculated C,40.3; H,3.46; N,12.13%.
Isomers were separated using semi-preparative HPLC (Section 2.2.5) and amounts up to 100 mg were isolated.
^1H N.m.r.; $[(CD_3)_2CO]$ acidified with one drop conc. DCl. Isomer 1: Pyridyltriazole ligand, 8.38 ($H^{5'}$), 8.26 (H^3), 7.94 (H^4), 7.30 (H^5), 7.62 (H^6).
4,4'-dimethyl-2,2'-bipyridine ligand, 2.38-2.41 (CH_3), 8.29-8.31 (H^3), 7.08-7.22 (H^5), 7.55-7.77 (H^6).
Isomer 2: Pyridyltriazole ligand, 8.66 ($H^{5'}$), 8.22 (H^3), 7.98 (H^4), 7.32 (H^5), 7.69 (H^6). 4,4'-dimethyl-2,2'-bipyridine ligand, 2.38-2.40 (CH_3), 8.27-8.32 (H^3), 7.09-7.21 (H^5), 7.52-7.64 (H^6).
^1H N.m.r.; $[(CD_3)_2CO]$ with one drop conc. NaOD.
Isomer 1: Pyridyltriazole ligand, 7.47 ($H^{5'}$), 8.20 (H^3), 7.91 (H^4), 7.19 (H^5), 7.53 (H^6).
4,4'-dimethyl-2,2'-bipyridine ligand, 2.45-2.55 (CH_3),

8.37-8.41 (H^3), 7.15-7.28 (H^5), 7.57-7.73 (H^6).
Isomer 2: Pyridyltriazole ligand, 7.97 ($H^{5'}$), 7.98 (H^3), 7.82 (H^4), 7.12 (H^5), 7.53 (H^6). 4,4'-dimethyl-2,2' -bipyridine ligand, 2.37-2.39 (CH_3), 8.21-8.28 (H^3), 7.04-7.16 (H^5), 7.36-7.60 (H^6).

2.1.3.2 $[Ru(dmbpy)_2(H3Mptr)](PF_6)_2.2H_2O$. (2)

This compound was prepared as for (1). Yield 633 mg (64%). Found C,39.41; H,3.58; N,11.55. Calculated C,40.21; H,3.77; N,11.73%.
Isomers were separated as for (1) in mg quantities. ^1H N.m.r.; [$(CD_3)_2CO$] acidified with one drop conc. DCl.
Isomer 1: Pyridyltriazole ligand, 1.62 (CH_3), 8.16 (H^3), 7.89, (H^4), 7.23 (H^5), 7.83 (H^6). 4,4'-dimethyl-2,2- bipyridine ligand, 2.37-2.42 (CH_3), 8.27-8.31 (H^3), 7.10-7.18 (H^5), 7.49-7.63 (H^6).
Isomer 2: Pyridyltriazole ligand, 2.44 (CH_3), 8.14 (H^3), 7.97 (H^4), 7.31 (H^5), 7.55 (H^6). 4,4'-dimethyl-2,2' -bipyridine ligand, 2.40-2.42 (CH_3), 8.28-8.33 (H^3), 7.10-7.24 (H^5), 7.51-7.71 (H^6).
^1H N.m.r.; [$(CD_3)_2CO$] with one drop conc. NaOD.
Isomer 1: Pyridyltriazole ligand, 1.37 (CH_3), 8.00 (H^3), 7.78 (H^4), 7.07 (H^5), 7.43 (H^6). 4,4'-dimethyl-2,2' -bipyridine ligand, 2.37-2.40 (CH_3), 8.24-8.28 (H^3), 7.09-7.18 (H^5), 7.51-7.61 (H^6).
Isomer 2: Pyridyltriazole ligand, 7.91 (H^3), 7.81 (H^4),

7.09 (H^5), 7.50 (H^6). 4,4'-dimethyl-2,2'-bipyridine ligand, 2.37-2.39 (CH_3), 8.21-8.30 (H^3), 7.09-7.19 (H^5), 7.44-7.57 (H^6).

2.1.3.3 $[Ru(dmbpy)_2(lMptr)](PF_6)_2.2H_2O$. (3)

This compound was prepared as described for (1), without the addition of conc. HCl whilst heating at reflux, since the complex does not undergo protonation / deprotonation processes. Yield 680 mg (69%). Found C,40.35; H, 3.63; N, 11.37. Calculated C, 40.21; H, 3.77; N, 11.73%
Isomers were separated as for 1. in mg quantities.
Isomer 1: ^1H N.m.r., $[(CD_3)_2CO]$: Pyridyltriazole ligand, 8.69 ($H^{5'}$), 4.08 (CH_3), 8.40 (H^3), 8.16 (H^4), 7.53 (H^5), 7.89 (H^6). 4,4'-dimethyl-2,2'-bipyridine ligand, 2.55-2.58 (CH_3), 8.62-8.69 (H^3), 7.31-7.42 (H^5), 7.81-7.96 (H^6).
Isomer 2: ^1H N.m.r., $[(CD_3)_2CO]$: Pyridyltriazole ligand, 8.78 ($H^{5'}$), 3.44 (CH_3), 8.45 (H^3), 8.20 (H^4), 7.54 (H^5), 7.89 (H^6). 4,4'-dimethyl-2,2'-bipyridine ligand, 2.55-2.59 (CH_3), 8.62-8.78 (H^3), 7.40-7.45 (H^5), 7.75-8.02 (H^6).

2.1.3.4 $[Ru(dmbpy)_2(4Mptr)](PF_6)_2$. (4)

This compound was prepared as for (3). Yield 700 mg (76%). Found C, 41.48; H, 3.57; N, 11.91. Calculated C, 41.78; H, 3.48; N, 12.19%

^1H N.m.r., $[(CD_3)_2CO]$; Pyridyltriazole ligand, 8.75 ($H^{5'}$), 4.39 (CH_3), 8.60 (H^3), 8.20 (H^4), 7.57 (H^5), 8.09 (H^6). 4,4'-dimethyl-2,2'-bipyridine ligand, 2.56-2.58 (CH_3), 8.58-8.68 (H^3), 7.31-7.43 (H^5), 7.75-7.94 (H^6).

2.1.3.5 $[Ru(phen)_2(Hptr)](PF_6)_2$. (5)

This compound was prepared as for (1). except that cis-$[Ru(phen)_2Cl_2].2H_2O$ was used instead of cis-$[Ru(dmbpy)_2Cl_2].2H_2O$. Yield 694 mg (77%). Found C, 41.74; H, 2.80; N, 12.08. Calculated C, 41.56; H, 2.46; N, 12.51%. Isomers were separated as for 1. in amounts up to 100 mg.

^1H N.m.r., $[(CD_3)_2CO]$ with one drop conc. DCl.

Isomer 1: Pyridyltriazole ligand, 8.37 ($H^{5'}$), 8.34 (H^3), 8.01 (H^4), 7.24 (H^5), 7.61 (H^6). Phenanthroline ligand, 7.46-7.85 (H^3), 7.96-8.36 (H^2), 8.44-8.65 (H^4), 8.15-8.20 (H^5).

Isomer 2: Pyridyltriazole ligand, 8.65 ($H^{5'}$), 8.31 (H^3), 8.01 (H^4), 7.26 (H^5), 7.77 (H^6). Phenanthroline ligand, 7.93-8.38 (H^2), 7.47-7.85 (H^3), 8.45-8.65 (H^4), 8.15-8.19 (H^5).

^{1}H N.m.r., [$(CD_3)_2CO$] with one drop conc.NaOD.

Isomer 1: Pyridyltriazole ligand, 7.43 ($H^{5'}$), 8.18 (H^3), 7.87 (H^4), 7.06 (H^5), 7.51 (H^6). Phenanthroline ligand, 7.95-8.38 (H^2), 7.45-7.82 (H^3), 8.42-8.60 (H^4), 8.13-8.17 (H^5).

Isomer 2: Pyridyltriazole ligand, 7.95 ($H^{5'}$), 8.07 (H^3), 7.86 (H^4), 7.05 (H^5), 7.54 (H^6). Phenanthroline ligand, 7.90-8.32 (H^2), 7.43-7.81 (H^3), 8.39-8.57 (H^4), 8.11-8.16 (H^5).

2.1.3.6 $[Ru(phen)_2(H3Mptr)](PF_6)_2.2H_2O$. (6)

This compound was prepared as for (5). Yield 760 mg (81%). Found C, 40.56; H, 3.01; N, 11.35. Calculated C, 40.54; H, 2.96; N, 11.82%.

Isomers were separated as for (1) in mg quantities.

^{1}H N.m.r., [$(CD_3)_2CO$] with one drop conc. DCl.

Isomer 1: Pyridyltriazole ligand, 1.37 (CH_3), 8.25 (H^3), 7.93 (H^4), 7.18 (H^5), 7.53 (H^6). Phenanthroline ligand, 7.98-8.48 (H^2), 7.44-7.84 (H^3), 8.56-8.63 (H^4), 8.14-8.20 (H^5).

Isomer 2: Pyridyltriazole ligand, 2.35 (CH_3), 8.20 (H^3), 8.00 (H^4), 7.24 (H^5), 7.68 (H^6). Phenanthroline ligand, 7.92-8.45 (H^2), 7.47-7.86 (H^3), 8.45-8.65 (H^4), 8.16-8.20 (H^5).

^{1}H N.m.r., [$(CD_3)_2CO$] with one drop conc. NaOD.

Isomer 1: Pyridyltriazole ligand, 1.10 (CH_3), 8.10 (H^3), 7.82 (H^4), 7.01 (H^5), 7.42 (H^6). Phenanthroline ligand, 7.42-7.82 (H^3), 8.39-8.58 (H^4), 8.12-8.16 (H^5).
Isomer 2: Pyridyltriazole ligand, 2.15 (CH_3), 8.00 (H^3), 7.84 (H^4), 7.02 (H^5). 7.51 (H^6). Phenanthroline ligand, 7.89-8.30 (H^2), 7.43-7.82 (H^3), 8.38-8.57 (H^4), 8.09-8.15 (H^5).

2.1.3.7 $[Ru(phen)_2(lMptr)](PF_6)_2$. (7)

This compound was prepared as for (3) except that cis-[Ru $(phen)_2Cl_2].2H_2O$ was used instead of cis-$[Ru(dmbpy)_2Cl_2].2H_2O$. Yield 715 mg (78%). Found C, 42.14; H, 2.80; N, 11.99. Calculated C, 42.15; H. 2.63; N, 12.29%.
Isomers were separated as for (1) in mg quantities.
Isomer 1: ^1H N.m.r., $[(CD_3)_2CO]$. Pyridyltriazole ligand, 8.64 ($H^{5'}$), 4.03 (CH_3), 8.46 (H^3), 8.17 (H^4), 7.42 (H^5), 7.87 (H^6). Phenanthroline ligand, 8.24-8.70 (H^2), 7.66-8.04 (H^3), 8.71-8.91 (H^4), 8.37-8.41 (H^5).
Isomer 2: ^1H N.m.r., $[(CD_3)_2CO]$. Pyridyltriazole ligand, 8.77 ($H^{5'}$), 3.25 (CH_3), 8.58 (H^3), 8.20 (H^4), 7.43 (H^5), 7.86 (H^6). Phenanthroline ligand, 8.19-8.59 (H^2), 7.73-8.07 (H^3), 8.66-8.93 (H^4), 8.39-8.45 (H^5).

2.1.3.8 $[Ru(phen)_2(4Mptr)](PF_6)_2$ (8)

This compound was prepared as for (7). Yield 698mg (77%). Found C, 42.19; H, 2.76; N, 12.09. Calculated C, 42.15; H, 2.63; N, 12.29%.

^1H N.m.r., $[(CD_3)_2CO]$. Pyridyltriazole ligand, 8.69 ($H^{5'}$), 4.39 (CH_3), 8.64 (H^3), 8.20 (H^4), 7.46 (H^5), 8.09 (H^6). Phenanthroline ligand, 8.10-8.60 (H^2), 7.67-8.09 (H^3), 8.67-8.85 (H^4), 8.35-8.41 (H^5).

2.2 Instrumentation.

2.2.1 Absorption and emission measurements.

UV/vis spectra or set wavelength measurements were obtained using either a Shimadzu UV 24 instrument or a Hewlett Packard 8452A Diode Array spectrometer. Absorption coefficients are accurate to 5%. Emission spectra were obtained on a Perkin-Elmer LS-5 luminescence spectrometer equipped with a red sensitive Hamamatsu R 928 photomultiplier tube. An emission slit width of 10 nm was used at room temperature and 2.5/5 nm at 77 K and the results were not corrected for photomultiplier response.

2.2.2 pK_a and pK_a^* measurements.

Sample measurements were carried out in Britton-Robinson buffer (0.04 M boric acid, 0.04 M acetic acid and 0.04 M phosphoric acid). The pH of the solutions was adjusted using a 2 M NaOH solution. Luminescence titrations were carried out using an appropriate isosbestic point as the excitation wavelength. To facilitate dissolution of samples in aqueous solutions a minimal volume of acetone (<2 ml), was added. Measurements were carried out at room temperature.

Absorption and emission intensities were monitored as a function of pH. The pK_a values (from absorption titration data) and pH_i (from inflection point on the

emission titration curve) values were determined using a program developed by Boris Fennema and Renyi Wang at DCU for a BBC microcomputer. The pK_a^* (excited state pK_a) values, were then determined using the equations given in Chapter 5.

2.2.3 Electrochemical measurements.

Cyclic voltammetry (CV) and differential pulse voltammetry (DPV) were carried out with an EG&G Par 174A polarographic analyser and an EG&G Par 175 universal programmer. A saturated calomel electrode was used as the reference electrode. Measurements were carried out in spectroscopic HPLC grade CH_3CN dried over molecular sieves and with 0.01 M TEAP (tetraethylammoniumperchlorate) or TBAP (tetra-butylammoniumperchlorate) as supporting electrolyte. A glassy carbon was used as the working electrode and a platinum electrode as the auxillary electrode. The electrochemical cell was a conventional three compartment cell. The solutions were degassed with nitrogen for measurements conducted below 0.0 V. The scan rate was 100 mV/s for the CV mode and 5 mV/s for the DPV mode. The pulse height in DPV measurements was 25 mV. Measurements were carried out at room temperature.

2.2.4 High Performance Liquid Chromatography (HPLC).

A Waters 990 Photodiode array HPLC system was employed, in conjunction with a NEC APC111 computer, a Waters pump model 6000 or 501, a 20 μlitre injector loop and a μPartisil SCX radial PAK cartridge. The mobile phases used were (a) CH_3CN : H_2O (80 : 20) containing 0.08 M $LiClO_4$ (about pH 6-7); (b) mobile phase (a) adjusted to pH 2-3 with $HClO_4$. The flow rate was 2.5 ml/min.

2.2.5 Semi-preparative HPLC.

An Applied Chromatography Services pump (model RR/066), detector (model 750/11 uv/vis), a 1 ml injection loop and a Magnum 9 Partisil cation exchange column (10 mm/25 cm) was used. The mobile phase was CH_3CN : H_2O (80:20) containing 0.08 M $LiClO_4$. The flow rate used ranged from 4.0-6.0 ml/min.

2.2.6 Infra-red spectra.

Infra-red spectra were recorded on a Perkin-Elmer 983G Infrared Spectrometer using pressed KBr discs. This technique was used to check for the presence of the isothiocyanate group in the complexes which were subsequently used for conjugations to biomolecules. [12]

2.2.7 NMR spectroscopy.

^1H NMR spectra were recorded on a Jeol JNM-FX 200 NMR spectrometer. The measurements have been carried out in $(CD_3)_2CO$. The peak positions are relative to TMS. For the COSY experiments 256 FID's of eight scans each, consisting of 1K data points were accumulated. After digital filtering (sine bell squared), the FID was zero filled to 512 W in the F_1 dimension. Acquisition parameters were F_1 = +/- 500 Hz and $t_{1/2}$ = 0.001 sec; the cycle time was 1.5 s.

These measurements were carried out at Leiden University, The Netherlands.

2.2.8 Lifetime measurements.

The lifetimes of the complexes employed in conjugation procedures were measured using the time correlated single photon counting technique and were carried out at the University of Dublin, Trinity College, Dublin. These lifetimes were measured on an Edinburgh Instruments Fl 900 fluorescence spectrophotometer. Instrumental conditions : ns flash lamp, N_2 filled to 0.3 bar, electrode gap 1.5 mm, applied voltage 0.5 kV, frequency (pulse rate) 30,000 Hz. The N_2 emission line at 337 nm was used to excite the complexes. The measurements were carried out in 0.1 M carbonate buffer, pH 9.6, at 23^{o}C. The analysis was performed with non-linear programs and the quality of the fit was assessed by the chi squared value (χ^2) close to unity and

by regular distribution of the residuals along the time axis. [13,14]

The lifetimes of the pyridyltriazole complexes described in Chapter 5 were measured by Renyi Wang in Tulane University, New Orleans, USA. The long lifetime components were measured using a Laser Photoionics LN 1000 MegaPlus Nitrogen Laser (excitation wavelength 337 nm, pulse width 600 picoseconds). The short lifetime components were measured using the time correlated single photon counting system employing a mode locked, cavity dumped Ar^+ laser for excitation (doubled dye output at 295 nm).

The ruthenium pyridyltriazole complexes were measured at room temperature, in Britton-Robinson buffer and the pH was adjusted using either conc. NaOH or conc. H_2SO_4 and were degassed prior to measurement.

2.2.9 Elemental analyses.

Elemental analyses on C,H and N were carried out at the Microanalytical Laboratory at University College Dublin, Dublin.

2.3 Biological procedures.

2.3.1 Buffers.

The buffers used were (a) 0.1 M carbonate buffer, pH 9.6, prepared from 0.1 M sodium carbonate / 0.1 M sodium hydrogen carbonate in distilled water; (b) 0.1 M phosphate buffer, pH 7.4, prepared from 0.1 M sodium dihydrogen phosphate / 0.1 M disodium hydrogen phosphate in distilled water; (c) 0.1 M citrate buffer, pH 4.3, prepared from 0.1 M citric acid / 0.1 M sodium citrate in distilled water and (d) 0.1 M acetate buffer, pH 5.5, prepared from 0.1 M glacial acetic acid / 0.1 M sodium acetate in distilled water.

2.3.2 Conjugation Procedures.

2.3.2.1 Conjugation of $[Ru(L\text{-}L)_2(NH_2phen)]^{2+}$ to albumins.

This involves firstly the periodate oxidation of the albumin which is followed by conjugation to the amino complex. BSA (bovine serum albumin), HSA (human serum albumin) or OVA (ovalbumin), 10-25 mg, was dissolved in 0.1 M $NaHCO_3$ (1-2 ml) and treated with 2.5 ml of 16 mmol $NaIO_4$ for two hours at $4^{o}C$ in the dark. [15] The label solution was then added (50 molar excess) dropwise to the protein solution. The ruthenium complex was dissolved in the minimum volume of

dimethylformamide (DMF) and 0.1 M carbonate buffer, pH 9.6, the total reaction volume was kept to a minimum. The conjugation reaction was allowed to proceed overnight at $4^{o}C$, in the dark, with minimal agitation. Unbound ruthenium compound was then removed by extensive dialysis against 0.1 M carbonate buffer, pH 9.6, (at least 4 changes of buffer). The oxidation of the protein results in the formation of a Schiffs base which was then stabilised by the addition of 4 volumes of $NaBH_4$ (5 mg/ml) and reacted for one hour at $4^{o}C$, in the dark. [15] Finally, the conjugate was dialysed against two changes of carbonate buffer.

2.3.2.2 Conjugation of $[Ru(bpy)_2(NH_2phen)]^{2+}$ to goat anti-mouse IgG.

The conjugation procedure is similar to that described in Section 2.3.2.1. 1-2 mg of pure goat anti-mouse IgG was used per conjugation which was dissolved in 0.1 M acetate buffer, pH 5.5. The anti-IgG was oxidised using 1 ml of 10 mmol $NaIO_4$. [16]

2.3.2.3 Conjugation of the active ester of $[Ru(bpy)_2(COOHbpy)]^{2+}$ to albumins and poly-L-lysine (PLL).

20 mg albumin / PLL was dissolved in 1-2 ml 0.1 M carbonate buffer, pH 9.6. The active ester solution (Section 2.1.1.7),

was added dropwise in amounts which were equivalent to a 50 molar excess of the ester to the albumin or PLL. The conjugation reaction was allowed to proceed overnight at $4^{o}C$, in the dark, with minimal agitation. The conjugate was extensively dialysed against 0.1 M carbonate buffer, pH 9.6.

2.3.2.4 Conjugation of $[Ru(L\text{-}L)_2(NCSphen)]^{2+}$ and $[Ru(L\text{-}L)_2(NCSpy)_2]^{2+}$ to albumins, immunoglobulins and PLL.

Albumin / PLL (10-25 mg), pure goat anti-mouse IgG (1-2 mg), or 5 mg of the crude preparations of anti-mouse IgG and anti-BSA were dissolved in 1-2 ml 0.1 M carbonate buffer, pH 9.6. The ruthenium complex (50 molar excess) was dissolved in the minimum volume of DMF / 0.1 M carbonate buffer, pH 9.6 (<2 ml) and added dropwise to the protein / PLL solution. The conjugation reaction was allowed to proceed overnight at $4^{o}C$, in the dark, with minimal agitation. The resultant solution was extensively dialysed against 0.1 M carbonate buffer, pH 9.6, to remove unbound label.

The above describes the standard procedure used in conjugations. In Section 4.2.3, Chapter 4, where BSA was labelled with $[Ru(bpy)_2(NCSphen)]^{2+}$ and $[Ru(bpy)_2(NCSpy)]^{2+}$, conjugations were carried out at three different pHs and also using varying ratios of initial ruthenium : protein. The unbound label complex may also be

removed by gel filtration chromatography using Sephadex G-25 (bead size 50-150 μm, column size 1x25 cm^3) and phosphate buffered saline (PBS), pH 7.4 as eluent. The flow rate was adjusted to 1-2 ml/min.

2.3.2.5 Conjugation of the diazotised complexes of $[Ru(bpy)_2(NH_2phen)]^{2+}$ and $[Ru(phen)_2(NH_2phen)]^{2+}$ to albumins.

The diazotised material prepared according to Sundberg [2], and described in Section 2.1.3.6, (50 molar excess) was added dropwise to solutions of BSA, OVA, HSA or PLL (10-25 mg) in carbonate buffer, pH 9.6, (1-2 ml), overnight at $4^{o}C$, in the dark, with minimal agitation. Unbound label was removed by extensive dialysis against 0.1 M carbonate buffer, pH 9.6.

2.3.3 Estimation of the conjugation ratio.

The amount of ruthenium complex present was determined by its absorption at λ max. (approx 450 nm). The extinction coefficients of the unbound labels were previously measured in 0.1 M carbonate buffer, pH 9.6. No allowance was made for a change in the extinction coefficient upon binding to biomolecules. The protein concentration was determined using two methods described in Section 2.3.4. The conjugation ratio was estimated according to Nairn, [17] given by:

$$\text{moles F/moles P} = x.A/Cp$$

where x = molecular weight of the protein / extinction coefficient of the label at λ max.; A = absorbance of the label at λ max.; Cp = protein concentration in mg/ml; F = fluorochrome and P = protein.

2.3.4 Determination of the protein concentration.

Two methods were used, the (a) Folin-Lowry method [18] and the (b) Bradford method [19]. A standard curve for each albumin, immunoglobulin and PLL (unconjugated) was prepared.

2.3.4.1 The Folin-Lowry method of protein determination.

Procedure:

Materials:

(1) Alkaline sodium carbonate solution (20 g/l Na_2CO_3 in 0.1 M NaOH.

(2) Copper sulphate-sodium potassium tartrate solution (5 g/l $CuSO_4.5H_2O$ in 10 g/l Na,K tartrate). Prepare fresh by mixing stock solutions.

(3) "Alkaline solution". Prepare on day of assay mixing, 50 ml of (1) with 1 ml of (2).

(4) Folin-Ciocalteu reagent. Dilute the commercial reagent

with an equal volume of water on the day of use. This is a solution of sodium tungstate and sodium molybdate in phosphoric and hydrochloric acid.

(5) Standard protein solution (for albumins and immunoglobulins use 0.2 mg/ml; for PLL use 0.2 mg/ml).

Method:

Prepare a set of tubes at least in duplicate as follows:

Tube No.	Protein	Water	Alkaline solution	Folin-Ciocalteu
	ml	ml	ml	ml
1	----	1.00	5.00	0.50
2	1.00	----	5.00	0.50
3	0.75	0.25	5.00	0.50
4	0.50	0.50	5.00	0.50
5	0.25	0.75	5.00	0.50
6	A suitable dilution of unknown.	----	5.00	0.50

After addition of "alkaline solution", allow the solution to stand at room temperature for 10 min. Add 0.5 ml of the diluted Folin-Ciocalteu reagent rapidly with immediate

mixing. After 30 min, read the absorbance at 750 nm using tube 1 as the blank. Prepare a standard curve and estimate the protein concentration in the unknown sample.

2.3.4.2 The Bradford method of protein determination.

Procedure:

Materials:

(1) Bradford reagent obtained from Bio-Rad as a 5x concentrate. Dilute 1 in 5 (200 ml dye plus 800 ml distilled water). Filter through Whatman No. 1 paper, store at room temperature for up to two weeks.

(2) Protein standard solutions in the range 0 to 140 μg/ml in either PBS or 0.1 M carbonate buffer, pH 9.6. Use 0, 20, 35, 70, 100 and 140 μg/ml for the albumins. PLL requires a higher concentration range.

Method:

(1) Place 0.10ml of each sample or standard in a labelled test tube.

(2) Add 2.5ml of the diluted Bradford dye reagent.

(3) Vortex (avoid foaming) or mix by gentle inversion.

(4) Read absorbance at 595 nm after 5 and before 60 minutes.

(5) Plot standard curve and estimate unknown.

2.3.5 Enzyme-linked immunosorbent assay (ELISA).

This assay was conducted to determine whether the immunological activity of the immunoglobulins was retained after conjugation to the ruthenium complexes.
The wells of a 96 well Nunc maxisorb microtitre plate (obtained from Intermed Nunc, Denmark.) were coated overnight at 4°C with 100 µl mouse IgG, 10 µg/ml, for checking anti-IgG conjugates or BSA, 10 µg/ml, for checking anti-BSA conjugates in phosphate buffered saline PBS, pH 7.4 . The plate was emptied by inversion and washed x3 with Tween-20/PBS (0.05% v/v) for 3 min. at room temperature. Blocking of free adsorption sites was achieved by the addition of 100 µl lysine (1 mg/ml in Tween-20/PBS, 0.05% v/v) for 2 hours at 37°C. The plate was emptied and washed as before. Dilutions of samples and standards (positive controls) were prepared in PBS, (the samples used were the ruthenium labelled anti-IgG or anti-BSA conjugates and the standards were unconjugated anti-IgG or anti-BSA), 100 µl of blank (PBS), sample or standard was added and incubated at 37°C for 1 hour. The plates were emptied and washed as before. 100 µl of 1/750 dilution of rabbit anti-goat IgG (the ruthenium labelled anti-IgG and anti-BSA were raised in a goat) conjugated to horse radish peroxidase (HRP) was added to the wells and incubated for two hours at room temperature. The plates were emptied and washed. The HRP substrate was freshly prepared and consisted of 10 mg ortho-phenylenediamine (OPD) in 0.5 M Na_2HPO_4 and 0.1 M

citric acid, pH 5.0. 5 µl H_2O_2 was added to the substrate solution just prior to addition to the microtitre plate. The plate was incubated for 30 min at room temperature. 50 µl H_2SO_4 (20% v/v) was added to each well to stop the reaction. The absorbance was read at 414 nm using an ELISA reader, (Titertek twinreader plus). [15]

2.4 References.

[1] C.D. Ellis, L.D. Margerum, R.W. Murray and T.J. Meyer, Inorg. Chem., 1983, 22, 1283.

[2] M.W. Sundberg, C.F. Meares, D.A. Goodwin and C.I. Diamenti, J. Med. Chem., 1974, 17, 1304.

[3] G. Sprintschnik, H.W. Sprintschnik, P.P. Kirsch nad D.G. Whitten, J. Amer. Chem. Soc., 1977, 99, 4947.

[4] A.J. Bard, Luminescent Metal Chelate Labels and Means for Detection, U.S. Patent Application Number, PCT / US85 / 02153, 1986.

[5] R. Hage, Ph.D Thesis, Leiden University, Leiden, The Netherlands, 1991.

[6] M. Uda, G. Hisazumi, K. Sato and S. Kubota, Chem. Pharm. Bull., 1976, 24, 3103.

[7] S. Kubota, M. Uda and M. Ohtsuku, Chem. Pharm. Bull., 1971, 19, 2331.

[8] R. Hage, R. Prins, J.G. Haasnoot, J. Reedijk and J.G. Vos, J. Chem. Soc., Dalton Trans., 1987, 1389.

[9] S. Kubota, M. Uda, T. Nakagawa, J. Heterocycl. Chem., 1975, 12, 855.

[10] C.F. Liu, N.C. Liu and J.C. Bailar,Jr., Inorg. Chem., 1964, 3, 1197.

[11] D.F. Mahoney and T.J. Beattie, Inorg. Chem., 1973, 12, 2561.

[12] R.M. McKinney, J.T. Spillane and G.W. Pearce, Anal. Chem., 1964, 7, 74.

[13] J.N. Demas, Excited State Lifetime Measurements, Academic press, London, 1983.

[14] D.V. O'Connor and D. Phillips, Time Correlated Single Photon Counting, Academic Press, London, 1984.

[15] P. Tijssen, Practice and Theory of Enzyme Immunoassays, Elsevier, New York, 1985.

[16] D.J. O'Shannessy and R.H. Quarles, J. Appl. Biochem., 1985, 7, 347.

[17] R.C. Nairn, Fluorescent Protein Tracing, 4th edition, Churchill Livingstone, London, 1976.

[18] G.L. Peterson, Anal. Biochem., 1979, 100, 201.

[19] M.M. Bradford, Anal. Biochem., 1976, 72, 248.

CHAPTER 3

SYNTHESIS AND CHARACTERISATION OF RUTHENIUM POLYPYRIDYL AMINO AND ISOTHIOCYANATE COMPLEXES.

3.1 Introduction.

In this chapter, the synthesis and characterisation of some ruthenium polypyridyl amino and isothiocyanate compounds which were used in conjugations to biomolecules are described. These compounds are $[Ru(bpy)_2(NH_2py)_2]^{2+}$, $[Ru(bpy)_2(NCSpy)_2]^{2+}$, $[Ru(bpy)_2(NH_2phen)]^{2+}$, $[Ru(bpy)_2(NCSphen)]^{2+}$, $[Ru(phen)_2(NH_2phen)]^{2+}$ and $[Ru(phen)_2(NCSphen)]^{2+}$. (See Figure 3.1 for ligand abbreviations).

The compounds have been characterised using HPLC, NMR, UV/vis spectroscopy, electrochemistry and emission spectroscopy.

3.2 Preparation of compounds of the type $[Ru(L\text{-}L)_2(NH_2py)_2)]^{2+}$ and $[Ru(L\text{-}L)_2(NH_2phen)]^{2+}$.

L-L = 2-2'bipyridyl(bpy) or 1,10-phenanthroline (phen); NH_2py = 4-aminopyridine and NH_2phen = 5-amino-1,10-phenanthroline. The compounds were prepared based on literature methods [1]. Reaction of cis-$[Ru(bpy)_2Cl_2].2H_2O$ [2], with a 10-fold molar excess of NH_2py yielded the compound $[Ru(bpy)_2(NH_2py)_2]^{2+}$. Reaction of cis-$[Ru(L\text{-}L)_2Cl_2].2H_2O$ [3,4], with equimolar amounts of NH_2phen yielded the compound $[Ru(L\text{-}L)_2(NH_2phen)]^{2+}$. The compounds were isolated as the divalent cations with PF_6^- as the counter ion.

For the compound $[Ru(bpy)_2(NH_2py)_2](PF_6)_2$, two of the NH_2py ligands are coordinated to the ruthenium via the nitrogen on the pyridine rings. For the complexes $[Ru(bpy)_2(NH_2phen)](PF_6)_2$ and $[Ru(phen)_2(NH_2$-phen)$](PF_6)_2$, only one NH_2phen ligand is coordinated to the ruthenium, via the N^1 and N^{10} positions of the NH_2phen ligand.

The isothiocyanate derivatives of these three compounds were prepared by reaction with thiophosgene, (See Section 2.1.1.5, Chapter 2). The $[Ru(bpy)_2(NCSpy)_2]^{2+}$ and $[Ru(bpy)_2(NCSphen)]^{2+}$ compounds were isolated as the divalent cations with PF_6^- as the counter ion. $[Ru(phen)_2(NCSphen)]^{2+}$ was isolated as the dichloride salt.

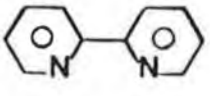

2-2'-bipyridyl

(bpy)

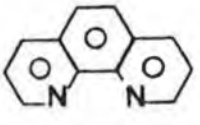

1,10-phenanthroline

(phen)

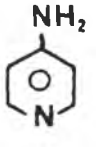

4-aminopyridine

(NH_2py)

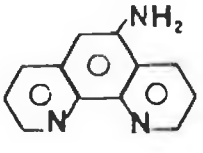

5-amino-1,10-phenanthroline

(NH_2phen)

Figure 3.1 Structures and abbreviations of the bipyridyl, phenanthroline and pyridine ligands.

3.3 High Performance Liquid Chromatography (HPLC).

The purity of the amino and isothiocyanate compounds was analysed using the HPLC method described in Section 2.2.4, Chapter 2. The retention time of each compound is listed in Table 3.1.

Table 3.1: **Retention times for the ruthenium polypyridyl amino and isothiocyanate compounds.**

Compound	Retention Time (min)
$[Ru(bpy)_2(NH_2py)_2](PF_6)_2$	2.72
$[Ru(bpy)_2(NCSpy)_2](PF_6)_2$	2.34
$[Ru(bpy)_2(NH_2phen)](PF_6)_2$	4.10
$[Ru(bpy)_2(NCSphen)](PF_6)_2$	3.38
$[Ru(phen)_2(NH_2phen)](PF_6)_2$	3.14
$[Ru(phen)_2(NCSphen)]Cl_2$	2.52

Retention times of the compounds as listed above after separation in 80:20, $CH_3CN:H_2O$, with 0.08 M $LiClO_4$ as mobile phase. The flow rate was 2.5 ml/min.

The amino compounds were found to be pure by HPLC.

Figures 3.2 and 3.3 depict representative chromatograms and the associated absorption spectra of the amino and isothiocyanate compounds in this case $[Ru(bpy)_2(NH_2phen)](PF_6)_2$ and $[Ru(bpy)_2(NCS-phen)](PF_6)_2$. The HPLC analysis of the isothiocyanate compound after separation by HPLC clearly shows the presence of a second component (< 10%). The absorption spectrum of this second compound is similar to the amino compound and has been assumed to be the amino compound.

The isothiocyanate compounds were not recrystallised due to their instability in aqueous solution [5,6], and were used in the unrecrystallised form for characterisation and conjugation procedures.

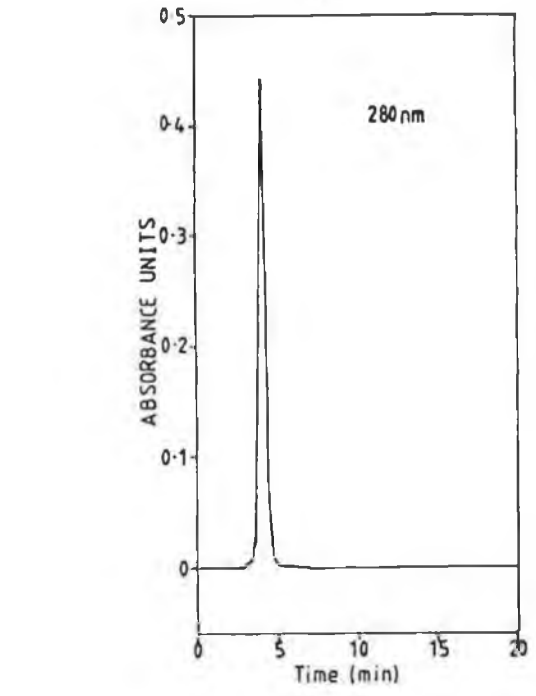

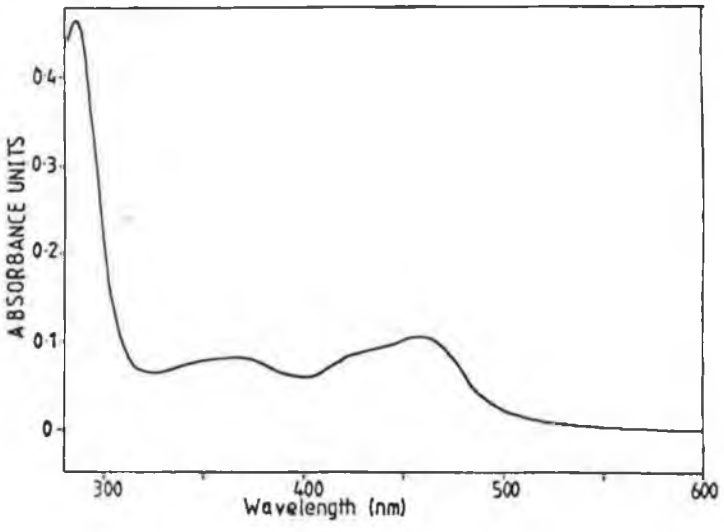

Figure 3.2 Chromatogram and the absorption spectrum of $[Ru(bpy)_2(NH_2phen)](PF_6)_2$ after separation in 80:20, $CH_3CN:H_2O$ with 0.08 M $LiClO_4$. The flow rate was 2.5 ml/min.

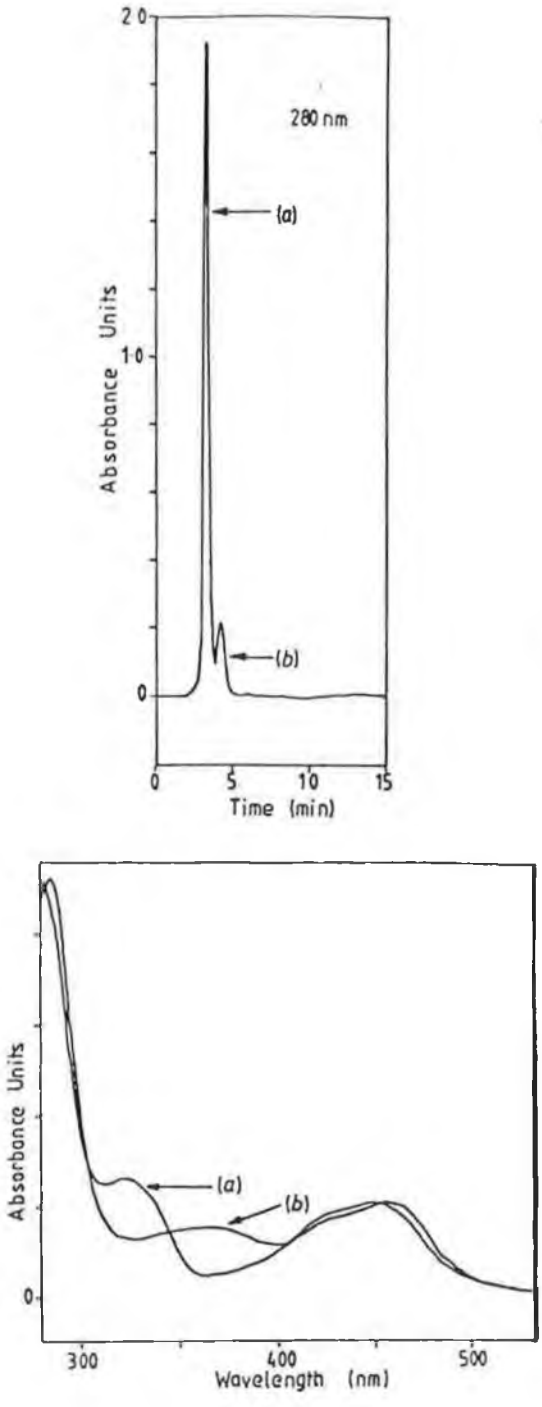

Figure 3.3 Chromatogram and the absorption spectra of (a) $[Ru(bpy)_2(NCSphen)](PF_6)_2$ and (b) a second component after separation in 80:20, CH_3CN : H_2O with 0.08 M $LiClO_4$. The flow rate was 2.5 ml/min.

3.4 Infra-red spectroscopy.

Infra-red spectra were examined in a purely qualitative manner to assess the success of the derivatisation reaction of the amino compound to the isothiocyanate compound. The presence of the isothiocyanate group was confirmed by the presence of an infra-red band at about 2050 cm^{-1} which is characteristic of isothiocyanate compounds [7]. The infra-red spectra of the various compounds were compared to that of fluorescein isothiocyanate (FITC) where the absorption band due to the isothiocyanate group occurs at 2036 cm^{-1}.

The infra-red spectra of $[Ru(bpy)_2(NH_2\text{-}phen)](PF_6)_2$ and $[Ru(bpy)_2(NCSphen)](PF_6)_2$ which are typical of these compounds are presented in Figures 3.4 and 3.5. Table 3.2 lists the frequency at which the absorption band due to the isothiocyanate moiety occurs for the various compounds.

Table 3.2 The infra-red stretching frequency of the NCS moiety in the isothiocyanate compounds.

Compound	Frequency (cm^{-1}) ν
$[Ru(bpy)_2(NCSpy)_2](PF_6)_2$	2031
$[Ru(bpy)_2(NCSphen)](PF_6)_2$	2056
$[Ru(phen)_2(NCSphen)]Cl_2$	2051
FITC	2036

The infra-red spectra were obtained using KBr discs.

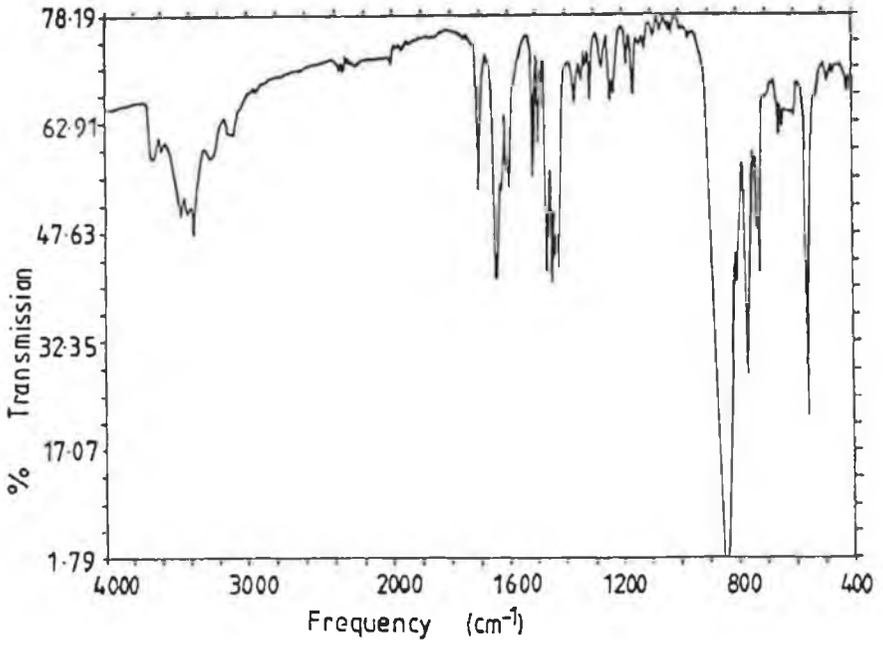

Figure 3.4 Infra-red spectrum of $[Ru(bpy)_2(NH_2\text{-phen})](PF_6)^2$ obtained as a KBr disc.

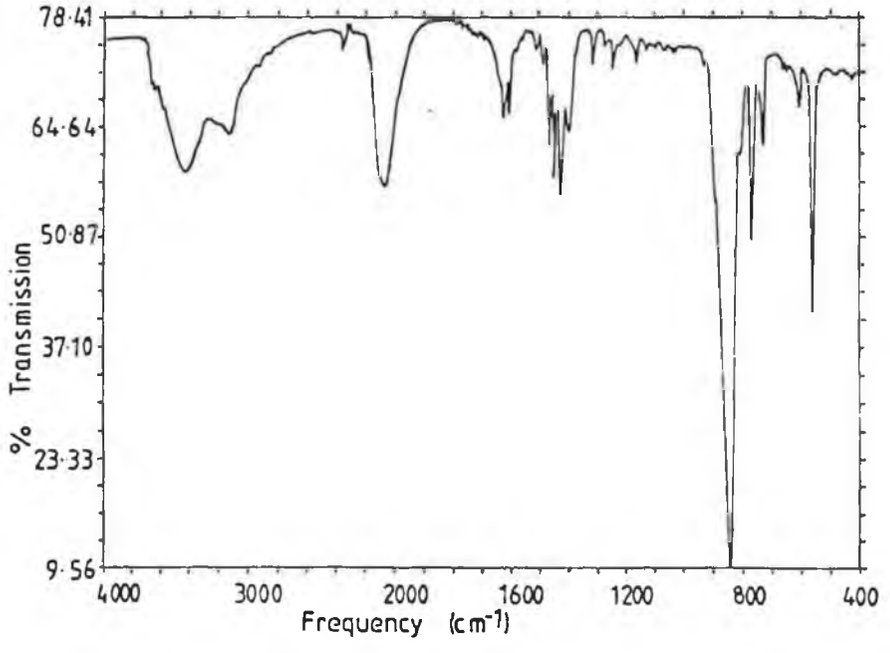

Figure 3.5 Infra-red spectrum of $[Ru(bpy)_2(NCS\text{-phen})](PF_6)_2$ obtained as a KBr disc.

3.5 Proton nuclear magnetic resonance spectroscopy.

The proton resonance signals obtained for the different compounds have been attributed to the different protons by comparison with literature data for similar compounds [8,9,10,11], and also by comparison with the bis(2,2'-bipyridyl) ruthenium [12,13] and bis(1,10-phenan-throline) ruthenium compounds containing pyridyltriazole ligands (Chapter 5). 2D COSY techniques also facilitated in the assignment of the various resonances. The proton NMR spectra clearly confirm the expected cis geometry for all the compounds [8,14].

The main difference between the ^{1}H NMR spectra of the uncoordinated 2,2'-bipyridyl and phenanthroline ligands and the ruthenium coordinated ligands is that the $H^{6}/H^{6'}$ protons of the pyridine rings of the bpy ligand and the H^{2}/H^{9} protons of the phen ligands experience a large upfield shift of about 1 ppm upon coordination to the ruthenium atom. This is because these protons are located just above a pyridine ring of an adjacent polypyridyl ligand and as such are located within the shielding cones of these ligands [15,16]. This diamagnetic anisotropic effect has previously been observed for the bis(2,2'-bipyridyl) ruthenium compounds containing pyridyltriazole ligands [12,13]. In Figure 3.6, the 2D COSY NMR spectrum for $[Ru(bpy)_2(NH_2phen)](PF_6)_2$ is presented.

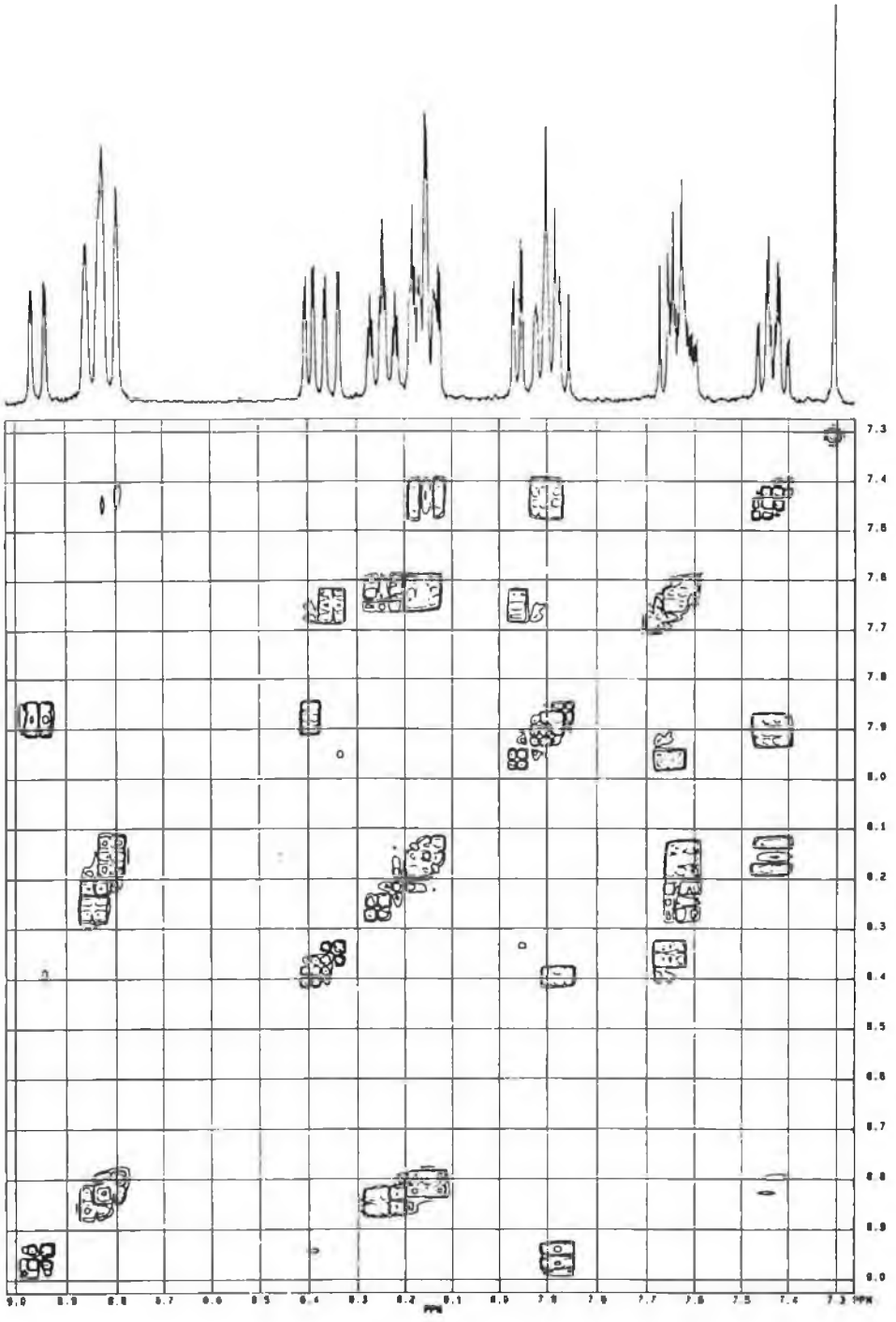

Figure 3.6 2D COSY NMR spectrum of $[Ru(bpy)_2(NH_2\text{-}phen)](PF_6)_2$ measured in $(CD_3)_2CO$.

The NMR spectra of the isothiocyanate compounds were not assigned due to impurities of the amino compounds. Table 3.3 lists the relevant NMR data for the coordinated NH_2py and NH_2phen ligands. The proton resonances of the coordinated bpy and phen ligands are given in Section 2.1.1, Chapter 2. The ^1H NMR spectrum of $[Ru(bpy)_2(NH_2py)_2](PF_6)_2$ is presented in Figure 3.7.

The proton resonance signals of the compound $[Ru(bpy)_2(NH_2py)_2](PF_6)_2$ were assigned by comparison with the NMR data on the $[Ru(bpy)_2(py)_2]^{2+}$ compound [17].

For this compound one of the H6/H6' protons of the bipyridine ligand lies trans to another bipyridine and experiences a downfield shift (at 9.25 ppm) and the other proton lies trans to the aminopyridine ligand and experiences an upfield shift (8.15 ppm). The proton which lies at lowest field is that due to the proton which is located trans to the bipyridine ligand.

The reason this proton resonates at much lower field compared to the H6/H6' protons of $[Ru(bpy)_3]^{2+}$ is that the proton is not rigidly located above the plane of an aromatic ring. This has been confirmed by the crystal structure of $[Ru(bpy)_2(py)_2]^{2+}$, which shows that the pyridine is free to rotate around the Ru-N bond [17].

Table 3.3 ^{1}H NMR resonances of the coordinated ligands.

$[Ru(L\text{-}L)_2(L')]^{2+}$	Chemical shift(δ) L'
$[Ru(bpy)_2(NH_2py)_2]^{2+}$	H2 7.89-7.92; H3 6.58-6.60; NH_2 6.26.
$[Ru(bpy)_2(NH_2phen)]^{2+}$	H2 7.96; H3 7.66; H4 8.35; H6 7.31; H7 8.95; H8 7.88; H9 8.39; NH_2 6.43.
$[Ru(bpy)_2(bpy)]^{2+}$ (a)	H3 8.90; H4 8.12; H5 7.53; H6 7.71.
$[Ru(phen)_2(NH_2phen)]^{2+}$	H2 7.92; H3 7.53; H4 8.32; H6 7.31; H7 8.93; H8 7.75; H9 8.36; NH_2 6.43.
$[Ru(phen)_2(phen)]^{2+}$ (b)	H2/H9 8.09; H3/H8 7.60; H4/H7 8.57; H5/H6 8.16.

^{1}H NMR data for the amino compounds measured in d^6 acetone.
(a) Ref. 18 measured in $[CD_3)_2CO]$; (b) Refs. 4 and 19, measured in D_2O.

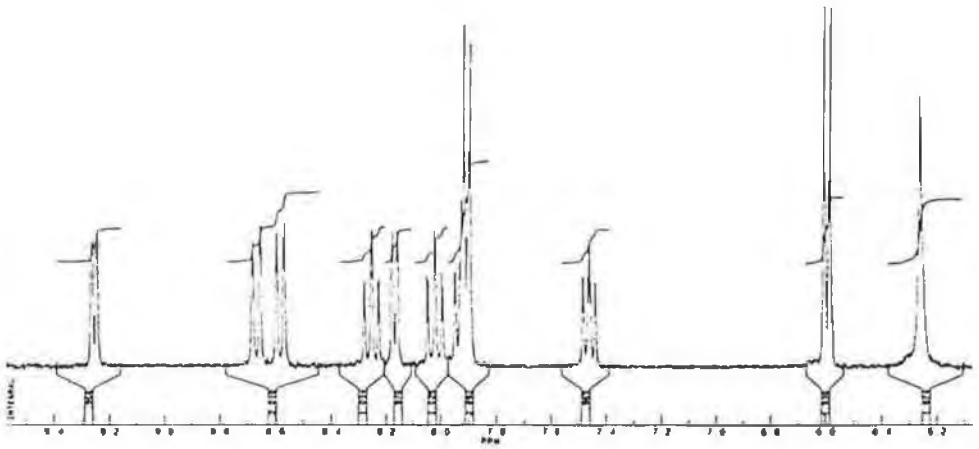

Figure 3.7 ^{1}H NMR spectrum of the compound $[Ru(bpy)_2-(NH_2py)_2]^{2+}$. The spectrum was measured in $(CD_3)_2CO$.

Generally, for all the protons of the bipyridine, phenanthroline and aminophenanthroline ligands, a slight downfield shift is observed upon coordination to ruthenium, probably due to the decrease in electron density caused by the σ-donation effect of the metal. This deshielding effect means that a lower value of the applied magnetic field is required to bring the protons to resonance.

For the H3/H3' protons of the bipyridine ligand this shift is quite significant (about 0.3 ppm) and is due to the steric crowding of these protons giving rise to strong Van der Waals interactions [16].

3.6 Electronic spectra and redox properties.

The data obtained from electronic and electrochemical measurements on the ruthenium polypyridyl compounds are presented in Table 3.4. The intense absorption bands around 450 nm have been assigned to $d\pi - \pi^*$ metal-to-ligand-charge transfer bands [20]. The position of this band is determined by σ-donor and π-acceptor properties of the ligands.

For all the compounds with the exception of $[Ru(bpy)_2(NH_2py)_2]^{2+}$, the maximum wavelength of absorption occurs at about 450 nm. The λ max. of absorption for the aminopyridine compound occurs at 491 nm which indicates that this compound is a weaker π-acceptor than the other compounds. As a result the metal $d\pi$ orbitals are destabilised by the increase in the effective charge on the ruthenium.

Interestingly, upon conversion to the isothiocyanate derivative the λ max. of absorption (and emission) shifts to higher energy (Figures 3.8 and 3.9), higher even than the max. abs. for $[Ru(bpy)_2(py)_2]^{2+}$. [21]

The absorption and emission spectra for some of the bis-bipyridyl and bis-phenanthroline compounds containing the NH_2phen and NCSphen ligands are presented in Figures 3.10-3.12.

Table 3.4 Electronic and electrochemical data for the ruthenium polypyridyl compounds with the aminophen/aminopy and isothiocyanate phen/isothiocyanate py ligands.

Compound	Absorption nm (log ε) (a)	Emission 303 K nm (b)	77 K	Redox properties (V vs SCE.) (c)
$[Ru(bpy)_2(NH_2py)_2]^{2+}$	491(3.95)	648	623	1.00 -1.45, -1.68
$[Ru(bpy)_2(NCSpy_2]^{2+}$	440(4.02)(h)	638	605	1.15 -1.42 -1.68
				1.32
$[Ru(bpy)_2(NH_2phen)]^{2+}$	457(4.15)(h)	615	576	1.20 -1.37, -1.56, -1.82
				1.34
$[Ru(bpy)_2(NCSphen)]^{2+}$	449(4.18)(h)	618	583	1.26 -1.38, -1.59, -1.86
$[Ru(bpy)_3]^{2+}$ (d)	452(4.11)	608	582	1.22 -1.36, -1.53, -1.80
$[Ru(phen)_2(NH_2phen)]^{2+}$	456(4.24)(h)	600	570	1.18 -1.38, -1.53, -1.96
				1.34
$[Ru(phen)_2(NCSphen)]^{2+}$	445(4.16)(h)	613	576	1.09 -1.36, -1.60, -1.93
				1.28
$[Ru(phen)_3]^{2+}$ (e)	442(4.27)	604	568	1.27 -1.35
$[Ru(bpy)_2(py)_2]^{2+}$ (f)	455(3.91)	606		1.30 -1.32, -1.56
$[Ru(bpy)_2(phen)]^{2+}$ (g)	447(4.18)	610		1.26 -1.36

(a) Absorption spectra were measured in CH_3CN, (log ε) was measured in CH_3CN, $M^{-1}cm^{-1}$.

(b) Emission spectra were measured in CH_3CN at 303 K and in EtOH at 77 K. Emission slit at 303 K was 10 nm; at 77 K, 5 nm.

(c) Redox values obtained from differential pulse traces measured in CH_3CN/0.1 M Tetrabutylammoniumperchlorate (TBAP). Volts vs SCE.

(d) ref [18]. (e) ref [20]. (f) ref [21]. (g) ref [23].

(h) Extinction coefficients were measured in 0.1 M carbonate buffer, pH 9.6. Units are $M^{-1}cm^{-1}$.

All compounds were found to emit at room temperature. A well defined vibrational progression was observed when emission spectra were measured at 77 K. For all compounds emission at low temperature is stronger than that at room temperature because thermal population of the deactivating d-d orbital is possible at room temperature resulting in a decrease in emission intensity, [23,24,25].

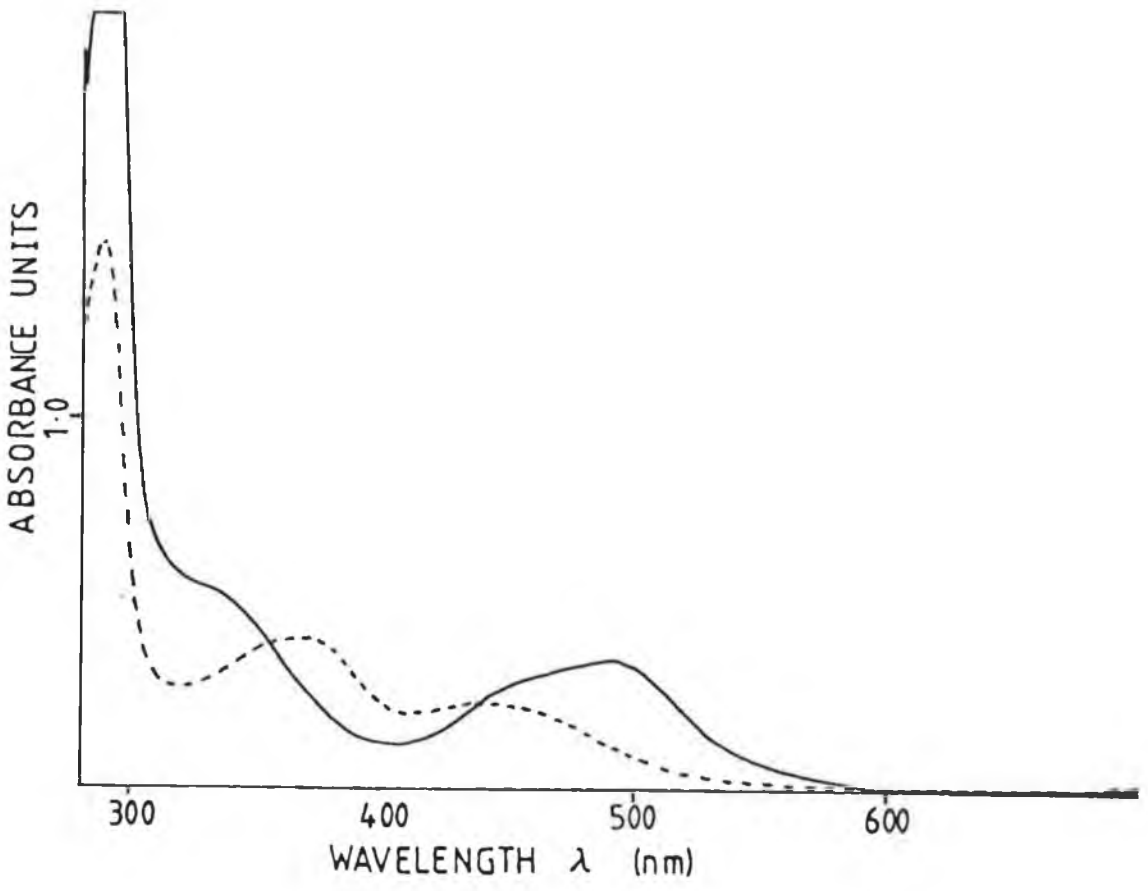

Figure 3.8 Absorption spectra of $[Ru(bpy)_2(NH_2\text{-}py)_2]^{2+}$ $2x10^{-5}$ M, (——) and $[Ru(bpy)_2(NCSpy)_2]^{2+}$ $3x10^{-5}$ M, (-----) in CH_3CN.

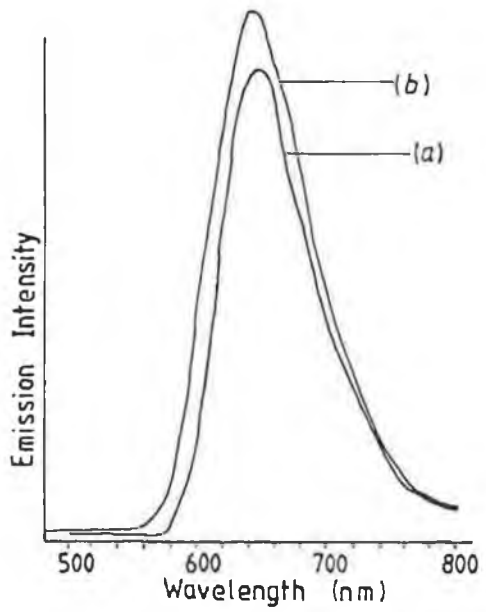

Figure 3.9 Emission spectra of (a) $[Ru(bpy)_2(NH_2\text{-}py)_2]^{2+}$ and (b) $[Ru(bpy)_2(NCSpy)_2]^{2+}$ in EtOH at 303 K.

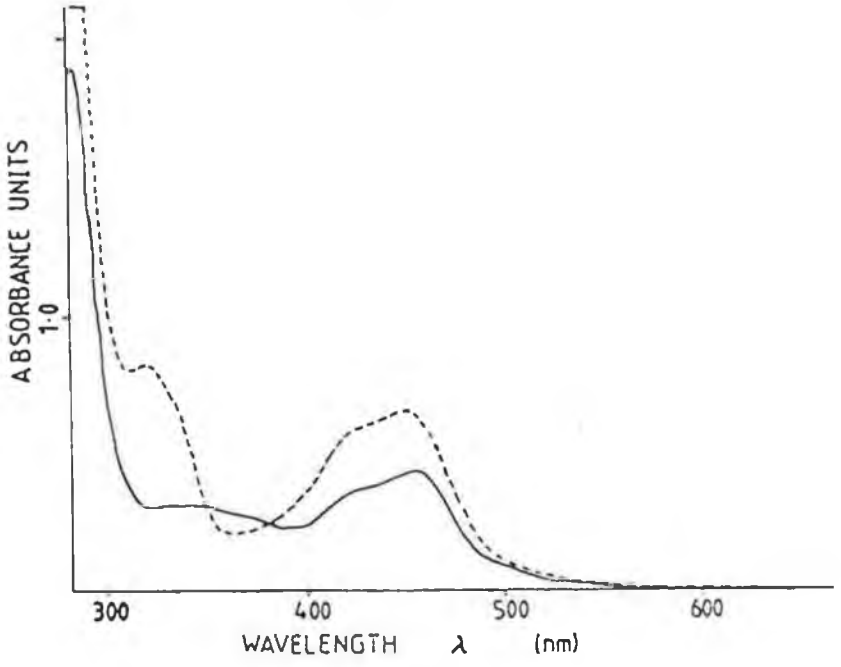

Figure 3.10 Absorption spectra of $[Ru(bpy)_2(NH_2\text{-}phen)]^{2+}$, 1.5×10^{-5} M (——) and $[Ru(bpy)_2(NCSphen)]^{2+}$, 2×10^{-5} M (-----) in CH_3CN.

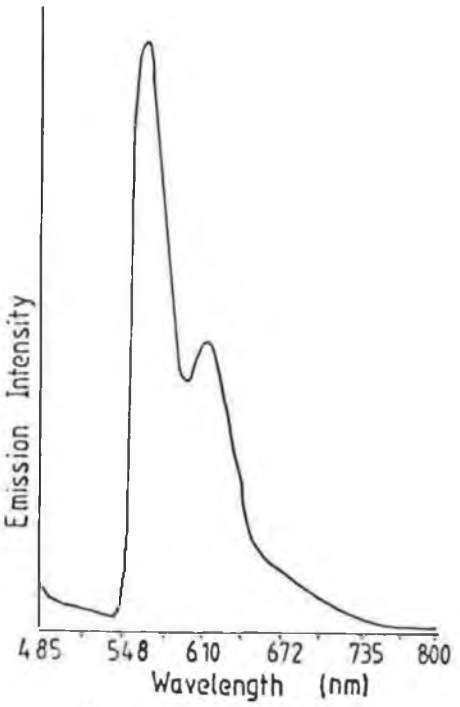

Figure 3.11 Emission spectrum of $[Ru(bpy)_2(NH_2\text{-}phen)]^{2+}$ in EtOH at 77 K.

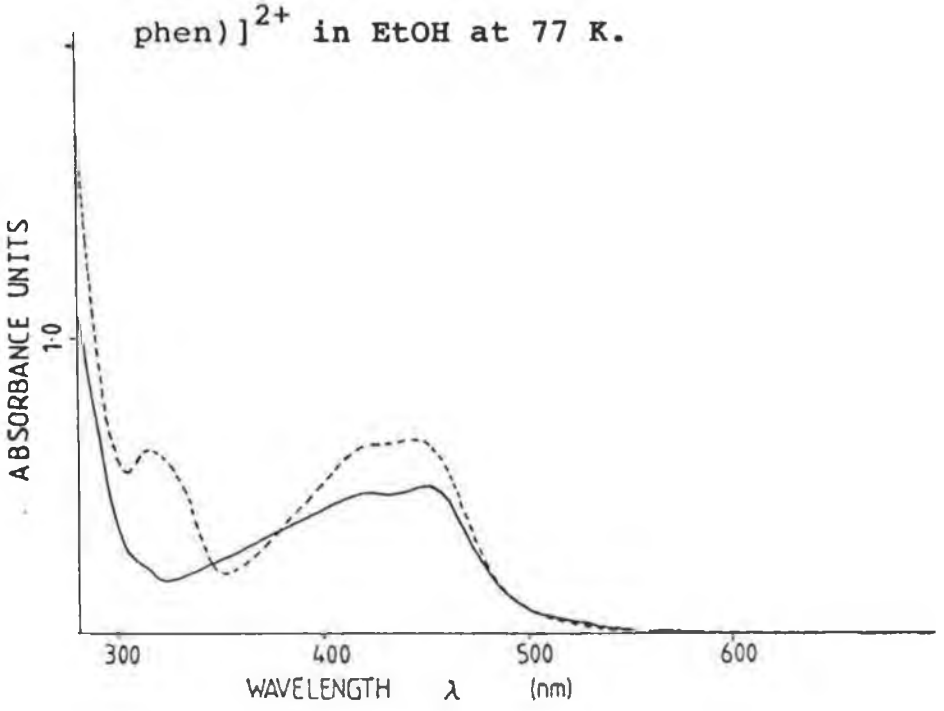

Figure 3.12 Absorption spectra of $[Ru(phen)_2(NH_2\text{-}phen)]^{2+}$, $1x10^{-5}$ M (———) and $[Ru(phen)_2(NCSphen)]^{2+}$, $2.5x10^{-5}$ M (-----) in CH_3CN.

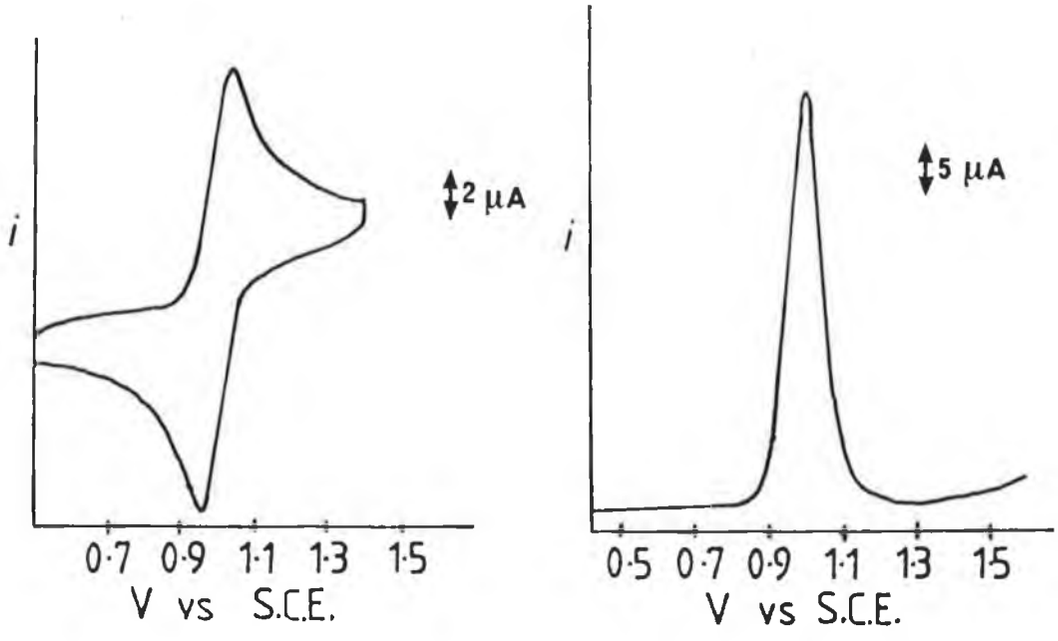

Figure 3.13 Cyclic voltammogram and differential pulse voltammogram of the oxidation of $[Ru(bpy)_2(NH_2py)_2]^{2+}$ in 0.1 M TBAP/CH_3CN.

The first reduction potential for each compound is quite similar to those of $[Ru(bpy)_3]^{2+}$ or $[Ru(phen)_3]^{2+}$ as appropriate. This indicates that most likely a bpy/phen based reduction is observed. The first reduction potentials are all at least as negative or more negative than that of the tris compounds suggesting that the amino and isothiocyanate ligands may be harder to reduce and are therefore, weaker π-acceptors than their bpy or phen counterparts. The results suggest that the bpy or phen

ligands may act as the emitting ligands and the amino and isothiocyanate ligands are the spectator ligands. This is corroborated to some degree by the trace presented in Figure 3.14, of the reduction of $[Ru(phen)_2(NH_2phen)]^{2+}$. The third reduction process occurs at about -1.96 V, the shape of this peak is somewhat different to those obtained for the first two reductions and may indicate that this third reduction is due to the reduction of the aminophenanthroline ligand, which may not be as straight forward as the reduction of an unsubstituted bpy or phen ligand.

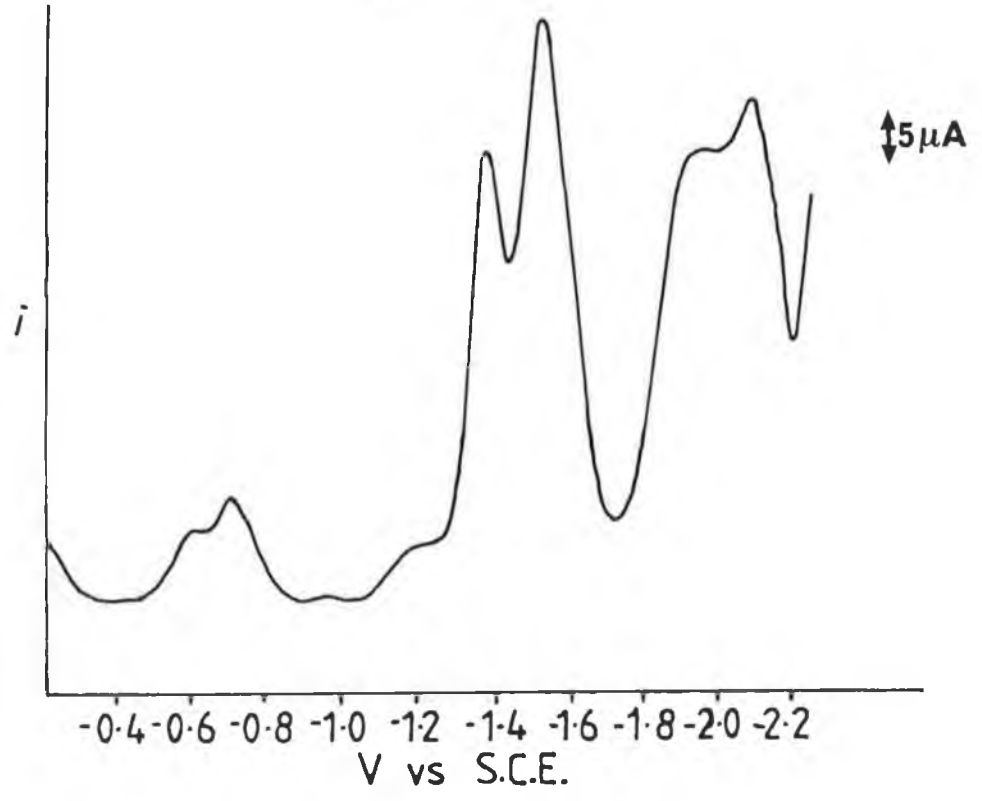

Figure 3.14 Differential pulse voltammogram of the reduction of $[Ru(phen)_2(NH_2phen)]^{2+}$ in 0.1 M TBAP / CH_3CN.

The electrochemical results also indicate that the emission and absorption processes most likely arise from the bpy or phen ligands. This is demonstrated in Figure 3.15, which shows a linear relationship exists between the energy of the lowest MLCT band and $\Delta E_{1/2}$ (the difference between the Ru^{III}- Ru^{II} oxidation potential and the first reduction potential of the complex E_{ox}-E_{red}), and between $\Delta E_{1/2}$ and the emission energy. [25,26].

In an MLCT absorption process, an electron is removed from the filled d metal orbital to an empty orbital of the ligand (π^*). Oxidation is also removal of an electron from the d-orbitals and by reduction, an electron is transferred to the lowest unoccupied molecular orbital of the complex. For these complexes the lowest unoccupied orbital is the π^* orbital of bpy or phen. A similar explanation holds for the emission processes.

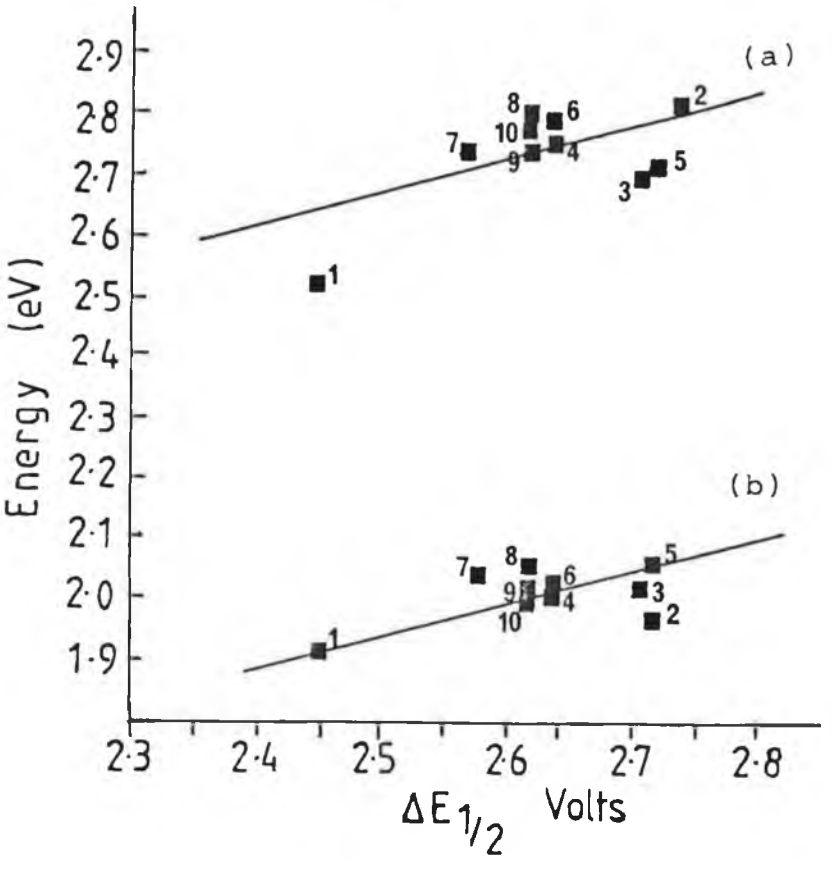

Figure 3.15 Plots of $\Delta E_{1/2}$ vs Absoption (a) and Emission (b) energies for compounds 1-10. Emission spectra, absorption spectra and values for $\Delta E_{1/2}$ were obtained at room temperature in CH_3CN.

These are:

1. $[Ru(bpy)_2(NH_2py)_2]^{2+}$.
2. $[Ru(bpy)_2(NCSpy)_2]^{2+}$.
3. $[Ru(bpy)_2(NH_2phen)]^{2+}$.
4. $[Ru(bpy)_2(NCSphen)]^{2+}$.
5. $[Ru(phen)_2(NH_2phen)]^{2+}$.
6. $[Ru(phen)_2(NCSphen)]2+$.
7. $[Ru(bpy)_3]^{2+}$. [Ref. 18]
8. $[Ru(phen)_3]^{2+}$. [Ref. 20]
9. $[Ru(bpy)_2(py)_2]^{2+}$. [Ref. 21]
10. $[Ru(bpy)_2(phen)]^{2+}$. [Ref. 23]

All measurements were conducted at room temperature.

3.7 Conclusion.

In this chapter, the characterisation and synthesis of a number of ruthenium polypyridyl amino and isothiocyanate compounds has been described. The compounds have been characterised using various techniques. HPLC is useful in determining the purity of the compounds. The amino compounds were all HPLC pure. The isothiocyanate compounds however, show some impurities by HPLC analysis. The NCS compounds were not recrystallised due to their instability in solution. The closeness of the retention times for the amino compounds and their isothiocyanate derivatives suggest that it may have been difficult to achieve pure isothiocyanate preparations anyway.

Infra-red spectra were used in a purely qualitative manner to assess the success of the derivatisation procedure, although these spectra may be used for the quantitative determination also. [27,28).

The various proton resonances of the amino compounds were assigned using NMR and 2D COSY NMR techniques. NMR spectra were taken of the isothiocyanate compounds but were too complex to analyse due to the presence of the amino impurities.

Generally the electronic and electrochemical data of the amino-phenanthroline and isothiocyanate - phenanthroline compounds are quite similar indicating that the properties do not change significantly upon conversion of the amino to the NCS derivatives, unlike those of the

aminopyridine complex when converted to the NCS derivative.

The fact that the first reduction potentials of all the compounds are at least as negative or more negative than the $[Ru(bpy)_3]^{2+}$ or $[Ru(phen)_3]^{2+}$ analogues may indicate that the lowest π^* orbital is located on the bpy or phen ligands. The third reduction potential observed for $[Ru(bpy)_2(NH_2phen)]^{2+}$ and $[Ru(bpy)_2(NCSphen)]^{2+}$ is more negative than the third reduction potential measured for $[Ru(bpy)_3]^{2+}$, which suggests that this potential is probably located at the NCSphen/NH_2phen ligand and that these ligands are weaker π-acceptors then bpy.

However, this is not possible to state unambigously. For the compounds containing the NH_2py or NCSpy ligands, the first reduction potential is more negative than the first reduction potential of $[Ru(bpy)_3]^{2+}$ indicating that the first reduction potential for these compounds is indeed bpy based.

The correlation between the absorption/emission energies and Δ E1/2 shows that the spectroscopic and electrochemical processes involve the same orbitals. Thus the bpy/phen ligands are most likely the emitting ligands whilst the NH_2phen and NCSphen ligands and definitely NH_2py and NCSpy act as the spectator ligands.

The questionable purity of the isothiocyanate compounds really renders it difficult to discuss the properties of these compounds in a definitive manner. Therefore throughout the previous discussion the possibility of amino impurities in the NCS preparations must be

considered. The difficulties arising with impurities in the discussion of the characteristics of these compounds are not significant when these compounds are conjugated to biological molecules. The unbound molecules together with any impurities are removed by extensive dialysis leaving only a high molecular weight ruthenium bound biomolecule.

The emission lifetimes of some of the compounds were measured and are included in the chapter discussing the lifetimes of the various conjugates, Chapter 4.

3.8 References

[1] E.D. Ellis, L.D. Margerum, R.W. Murray and T.J. Meyer, Inorg. Chem., 1983, 22, 1283.

[2] B.P. Sullivan, D.J. Salmon and T.J. Meyer. Inorg. Chem., 1978, 17, 3334.

[3] C.F. Liu, N.C. Liu and J.C. Bailar,Jr., Inorg. Chem.,1964, 3, 1197.

[4] D.F. Mahoney and T.J. Beattie, Inorg. Chem., 1973, 12, 2561.

[5] R.C. Nairn, Fluorescent Protein Tracing, Livingstone, Edinburgh, 4th Edition, 1976.

[6] R.G. Haughland, Handbook of Fluorescent Probes and Research Chemicals, Molecular Probes Inc., Oregon. U.S.A., 1989.

[7] R.M. McKinney, J.T. Spillane and G.W. Pearce, Anal. Chem., 1964, 7, 74.

[8] J.M. Kelly, C. Long, C.M. O'Connell, J.G. Vos and A.H.A. Tinnemans, Inorg. Chem., 1983, 22, 2818.

[9] P.J. Steel, F. Lahousse, D. Lerner and C. Marzin, Inorg. Chem., 1983, 22, 1488.

[10] P. Belser and A. von Zelewsky, Helv. Chim. Acta, 1980, 63, 1675.

[11] J.L. Walsh and B. Durham, Inorg. Chem., 1982, 21, 329.

[12] B.E. Buchanan, Ph.D thesis, Dublin City University, Dublin, Ireland, 1989.

[13] R. Hage, Ph.D thesis, Leiden University, Leiden, The Netherlands, 1991.

[14] L.J. Fitzpatrick, H.A. Goodwin, A. Launikonis, A.W.H. Mau and W.H.F. Sasse, Aust. J. Chem., 1983, 36, 2169.

[15] P. Belser and A. von Zelewsky, Helv. Chim. Acta, 1980, 63, 1675.

[16] E.C. Constable and J. Lewis, Inorg. Chim. Acta, 1983, 70, 251.

[17] P.B. Hitchcock, K.R. Seddon, J.E. Turp, Y.S. Yousif, J.A. Zora, E.C. Constable and O. Wernberg, J. Chem. Soc., Dalton Trans., 1988, 1837.

[18] R. Hage, R. Prins, J.G. Haasnoot, J. Reedijk and J.G. Vos, J. Chem. Soc., Dalton Trans., 1987, 1389.

[19] J.D. Miller and R.H. Prince, J. Chem. Soc., 1965, 3185.

[20] A. Juris, V. Balzani, F. Barigelletti, S. Campagna, P. Belser and A. von Zelewsky, Coord. Chem. Rev., 1988, 84, 85.

[21] B.P. Sullivan, D.J. Salmon, T.J. Meyer and J. Peedin, Inorg. Chem., 1979, 18, 3369.

[22] B.P. Sullivan, D. Conrad and T.J. Meyer, Inorg. Chem., 1985, 24, 3640.

[23] K. Kalyanasundaram, Coord. Chem. Rev., 1982, 46, 159.

[24] A. Juris, F. Barigelletti, V. Balzani, P. Belser and A. von Zelewsky, Inorg. Chem., 1985, 24, 202.

[25] J.V. Casper and T.J. Meyer, Inorg. Chem., 1983, 22, 2444.

[26] E.S. Dodsworth and A.P.B. Lever, Chem. Phys. Lett., 1986, 124, 152.

[27] R.M. McKinney and J.T. Spillane, Ann. New York. Acad. Sci., 1975, 254, 55.

[28] A. Jobbagy and G.M. Jobbagy, J. Immunol. Meth., 1972, 2, 169.

CHAPTER 4

THE CONJUGATION OF RUTHENIUM POLYPYRIDYL COMPLEXES TO BIOMOLECULES.

4.1 Introduction

In this chapter the conjugation of some ruthenium (II) polypyridyl complexes to albumins, immunoglobulins and poly-L-lysine is described. The complexes were bound at different sites on the biomolecules, using different binding methods.

Initial investigations were conducted on the conjugation of $[Ru(bpy)_2(NCSphen)]^{2+}$ and $[Ru(bpy)_2(NCSpy)_2]^{2+}$ to bovine serum albumin (BSA). The pH and initial fluorochrome to protein ratio (F/P), was varied and the effect of these parameters on the binding efficiency was examined. From these experiments the reaction pH and initial fluorochrome to protein ratio was selected and used in further studies using the NCS-type label molecules.

Two other compounds $[Ru(phen)_2(NCSphen)]^{2+}$ and $[Ru(bpy)_2(COOHbpy)]^{2+}$ were then synthesised, and conjugated to albumins, immunoglobulins and poly-L-lysine (PLL), together with the $[Ru(bpy)_2(NCSphen)]^{2+}$ complex. Those compounds containing the NCS moiety bind to the ε-amino groups of lysine residues directly via a thiourea linkage, the dicarboxylic acid compound upon conversion to the succinimidyl ester also binds to these ε-amino groups.

Methods for attaching a label to a protein molecule which involve modification of the amino acid side chains are not specific, in that the label molecule can not be directed to a particular site on the protein and this results in heterologous labelling. Where immunoglobulin

(antibody) labelling is concerned, modification of the amino acid side chains may also lead to a decrease in the affinity of the antibody for the antigen, since these moieties are situated in or in close proximity to the antigen-binding site. [1]

In contrast to modification of the amino acid side chains, the carbohydrate moieties of immunoglobulins are not involved in the antigen binding site so that modification of these groups should not directly affect antigen binding. [1] So, in addition to modification of the amino acid side chains of proteins and antibodies, modification of the carbohydrate moieties of glycoproteins was also examined.

Immunoglobulins may be classed as glycoproteins with a carbohydrate content ranging from 4 to 18% depending on the immunoglobulin. In this work immunoglobulin G (IgG) and ovalbumin (OVA), were modified through periodate oxidation of the carbohydrate moiety (IgG has about 4% [1] and ovalbumin has about 1% carbohydrate [2]). This was followed by conjugation to an amino ruthenium complex, either $[Ru(bpy)_2(NH_2phen)]^{2+}$ or $[Ru(phen)_2(NH_2phen)]^{2+}$. Periodate oxidation of BSA and human serum albumin (HSA), although not usually treated as glycoproteins, followed by conjugation to the ruthenium (II) amino compounds was also successful.

A third method of attaching a label molecule to a biomolecule was used. This involved diazotisation of the ruthenium (II) polypyridyl amino compounds by the method described by Sundberg et al..[3] Diazotised reporter

molecules have been shown to bind via the tyrosine or histidine residues of a protein molecule. [4]

Where immunoglobulins were conjugated to ruthenium compounds, the retention of immunological activity after conjugation was monitored by employing an enzyme-linked immunosorbent assay (ELISA).

The effects of conjugation on the absorption and emission spectra of the ruthenium compounds and the effect of conjugation on the emission decay lifetimes of some of the free and biomolecule-bound ruthenium complexes was investigated.

4.2 Results and Discussion.

The visible region in the absorption spectrum of the ruthenium complexes is unaffected by the absorbances due to the protein molecules since these occur in the ultraviolet region. Therefore, any changes in the ^{3}MLCT band reflects changes in the spectroscopic properties of the ruthenium complexes upon conjugaton to proteins.

The absorption and emission data on the unbound ruthenium complexes which have been used in these investigations are presented in Table 4.1.

Table 4.1 Spectroscopic data for the ruthenium polypyridyl complexes which were used in conjugations involving biomolecules.

Compound	Absorption λ max.(nm) (log ε)	Emission (303 K) λ max.(nm)
$[Ru(bpy)_2(NH_2py)_2]^{2+}$	488 (----)	645
$[Ru(bpy)_2(NCSpy)_2]^{2+}$	449 (4.02)	631
$[Ru(bpy)_2(NH_2phen)]^{2+}$	454 (4.14)	609
$[Ru(phen)_2(NH_2phen)]^{2+}$	452 (4.24)	604
$[Ru(bpy)_2(NCSphen)]^{2+}$	453 (4.17)	610
$[Ru(phen)_2(NCSphen)]^{2+}$	447 (4.16)	608
$[Ru(bpy)_2(COOHbpy)]^{2+}$	460 (4.19)	642
$[Ru(bpy)_2(esterbpy)]^{2+}$	458	639

The absorption and emission spectra were measured in 0.1 M carbonate buffer, pH 9.6, at room temperature. Extinction coefficients (log ε) were measured in 0.1 M carbonate buffer, pH 9.6; units are $M^{-1}cm^{-1}$.

4.2.1 Optimisation of conjugation conditions.

The conjugation procedure involved reacting BSA and a range of ruthenium label concentrations at three different pHs; (a) pH 4.3 in 0.1 M citrate buffer, (b) pH 7.4 in 0.1 M phosphate buffer and (c) pH 9.6 in 0.1 M carbonate buffer. The initial label : protein ratios used were 5:1, 10:1, 20:1, 30:1, 50:1, and 90:1. The ruthenium labels used were $[Ru(bpy)_2(NCS\text{-}py)_2]^{2+}$ and $[Ru(bpy)_2(NCSphen)]^{2+}$ and were dissolved in the minimum volume of dimethylformamide (DMF). The reaction was allowed to proceed for 18 hours, in the dark at $4^{o}C$, with minimal agitation. The free and BSA bound ruthenium complexes were separated by gel-filtration chromatography using Sephadex G-25 and phosphate buffered saline (pH 7.4) as eluent. Using gel-filtration chromatography, two coloured fractions are obtained. The first fraction is the BSA-bound ruthenium complex (protein was monitored qualitatively by using the Bradford reagent for protein determination [5]). The second coloured fraction was the unbound label and does not contain any protein. The absorption and emission spectra of these fractions, for both labels are shown in Figures 4.1 and 4.2.

From the absorption spectrum presented in Figure 4.1, it can be seen that the λ max. of absorption of the free unbound $[Ru(bpy)_2(NCSpy)_2]^{2+}$ species is about 485 nm. However, a freshly prepared solution of the complex has a λ max. of absorption at 449 nm. Also, the emission maximum of this gel filtration fraction is about 650 nm, whilst that

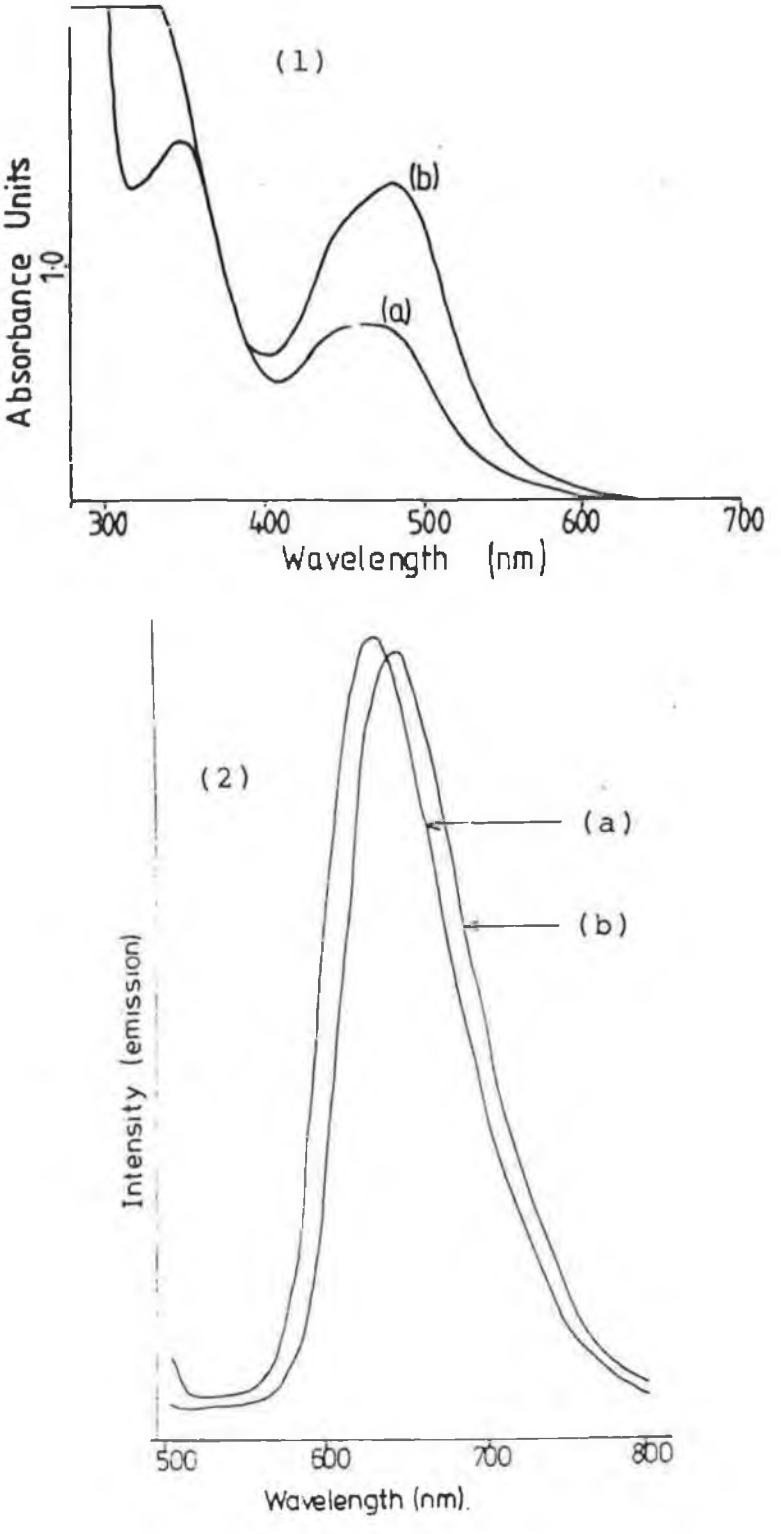

Figure 4.1 Absorption (1) and emission (2) spectra of the two fractions obtained after gel-filtration chromatography of the $[Ru(bpy)_2(NCSpy)_2]^{2+}$: BSA conjugate. Fraction (a) is the conjugate and fraction (b) is the unbound species.

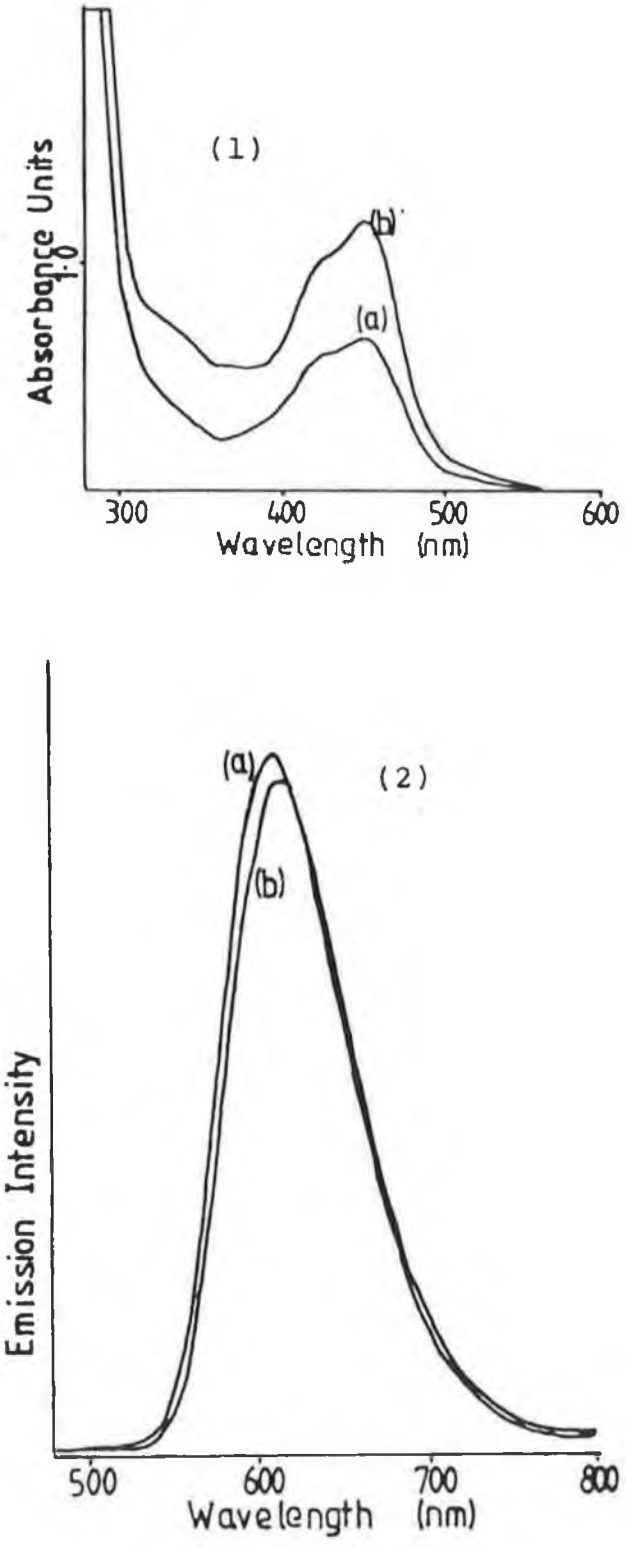

Figure 4.2 Absorption (1) and emission (2) spectra of the two fractions obtained after gel-filtration chromatography of the $[Ru(bpy)_2(NCSphen)]^{2+}$: BSA conjugate. Fraction (a) is the conjugate and fraction (b) is the unbound species.

of the fresh solution is 631 nm. Upon comparison with the absorption and emission λ max. of $[Ru(bpy)_2(NH_2\text{-}py)_2]^{2+}$, the absorption and emission data for this complex are more similar to that of the unbound fraction than that of the isothiocyanate analogue which suggests that the unbound complex converts back to the amino complex. This indicates the limited stability of the isothiocyanate complexes in aqueous solution. It is easier to arrive at this conclusion for the pyridine-containing complex, since the absorption and emission data are quite different for each complex. It is difficult to say whether the same occurs for the complex $[Ru(bpy)_2(NCSphen)]^{2+}$, since the absorption and emission data for both the isothiocyanate and amino complex are quite similar. However, it may be observed that upon conversion of the NH_2phen complex to its NCS derivative, an absorption band appears at about 320 nm, which disappears upon conjugation and is probably related to the reordering of the energy levels of the ligand orbitals. This band is not present in the unbound fraction obtained after gel filtration which could indicate that the unbound $[Ru(bpy)_2(NCSphen)]^{2+}$ also converts back to $[Ru(bpy)_2(NH_2phen)]^{2+}$.

The conjugation ratio was estimated according to Nairn. [4] This method is described in detail in Chapter 2. It was assumed that the extinction coefficient of the bound label complex is the same as that of the free complex. Protein concentration was assayed using two methods, (a) the Bradford method [5] and (b) the Folin-Lowry method.[6]

The results obtained at various pHs, using a range of initial fluorochrome : protein (F/P) ratios, are presented graphically in Figures 4.3 and 4.4.

Some discrepancies were noted between the F/P ratios estimated using the Bradford method and the Folin-Lowry method. However, at this stage these discrepancies were not thought to be significant since the method of determining F/P is really only an estimate. In later investigations, the Folin-Lowry method was employed as the more accurate method for protein determination in certain conjugation reactions. The reason why this assay was chosen over the Bradford assay will be discussed in Section 4.2.2.

The following discussion on the calculated F/P ratios deals with those ratios estimated by using the protein concentration (C_p, mg/ml), determined by the Folin-Lowry assay [6]. At maximum initial F/P ratios, approximately 12 molecules of $[Ru(bpy)_2(NCSpyr)_2]^{2+}$ and about 14 molecules of $[Ru(bpy)_2(NCSphen)]^{2+}$ were bound per molecule of BSA, at pH 7.4 and pH 9.6, with a slightly higher F/P at pH 9.6. At pH 4.3, conjugation did not occur. At this pH, the first fraction obtained after gel-filtration chromatography which contained BSA, was uncoloured and absorptions arising from the ruthenium complexes were absent. This is significant because this indicates that the label molecules are probably reacting with the ε-amino group of the lysine residues according to :

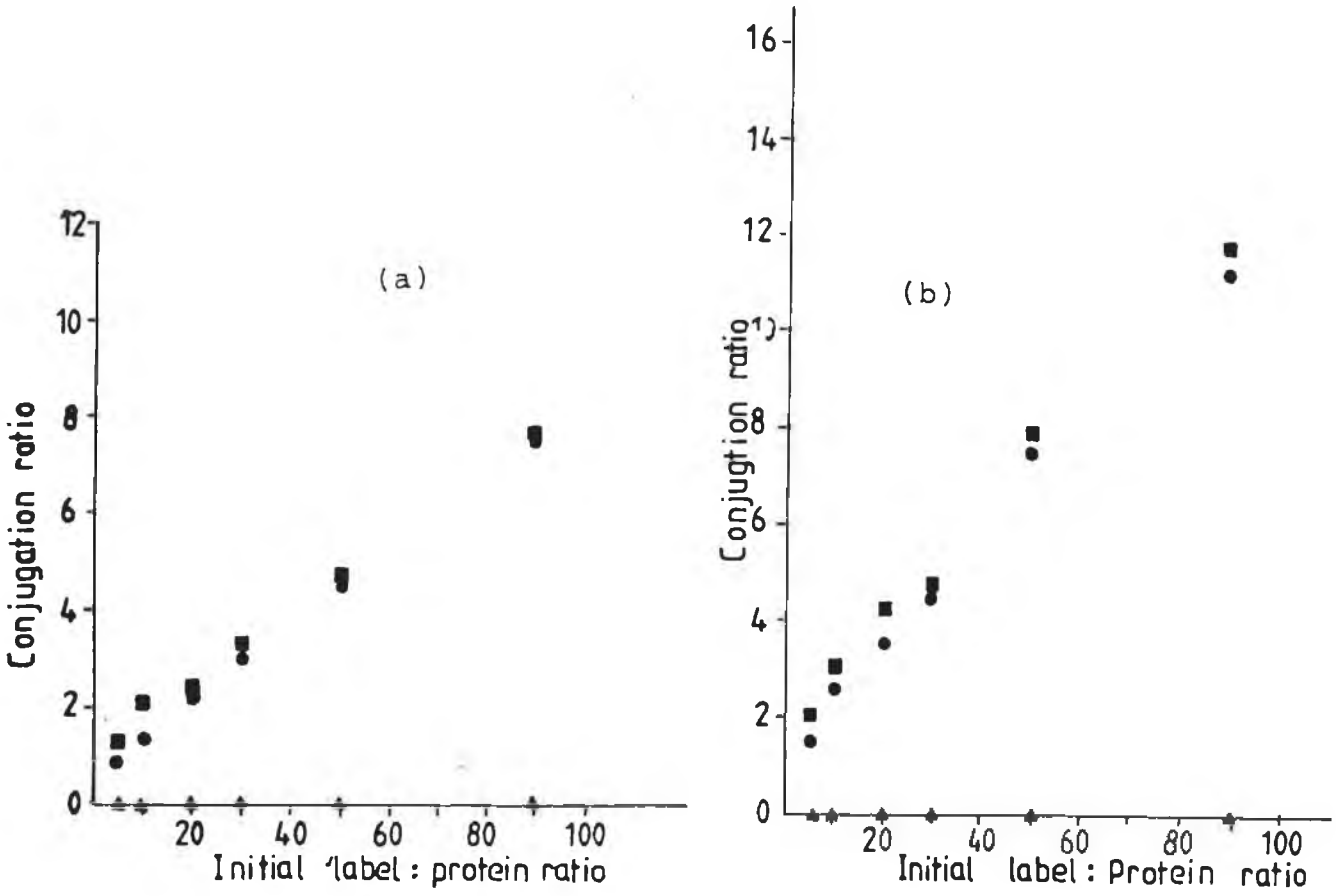

Figure 4.3 Graph showing the fluorochrome / protein ratios (F/P), obtained at various initial F/P ratios, at (1) pH 9.6, in 0.1 M carbonate buffer, ■, (2) pH 7.4, in 0.1 M phosphate buffer, ●, and (3) pH 4.3, in 0.1 M citrate buffer, ▲. The protein concentration was determined using (a) the Bradford method [5] and (b) the Folin-Lowry method [6]. The label is $[Ru(bpy)_2(NCSpy)_2]^{2+}$ and the protein is BSA.

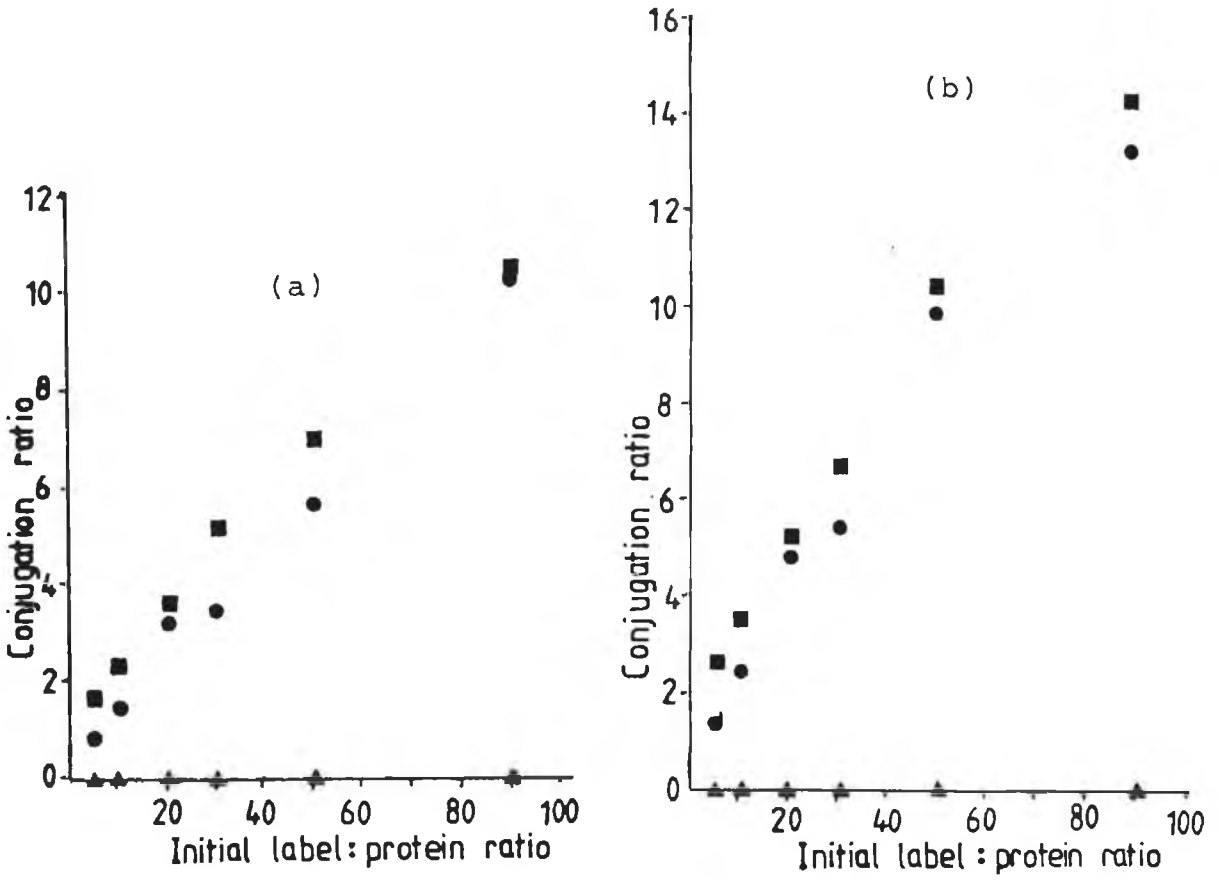

Figure 4.4 Graph showing the fluorochrome / protein ratios (F/P), obtained at various initial F/P ratios, at (1) pH 9.6, in 0.1 M carbonate buffer, ■, (2) pH 7.4, in 0.1 M phosphate buffer, ●, and (3) pH 4.3, in 0.1 M citrate buffer, ▲. The protein concentration was determined using (a) the Bradford method [5] and (b) the Folin-Lowry method [6]. The label is $[Ru(bpy)_2-(NCSphen)]^{2+}$ and the protein is BSA.

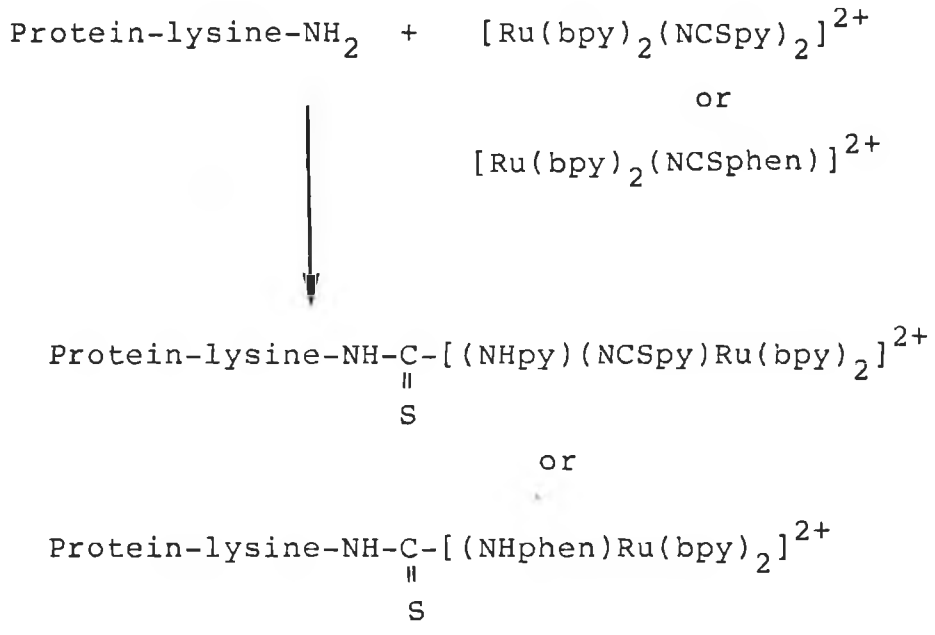

The increase in F/P ratios as a function of pH is most likely due to the greater deprotonation of the ε-amino group of the lysines at higher pH values, providing additional sites for reaction with the isothiocyanate group. [7]

BSA has 57 lysine residues [8], and F/P ratios of 12 and 14 label molecules per molecule of BSA represents about 21% labelling efficiency using $[Ru(bpy)_2(NCSpy)_2]^{2+}$ and 25% labelling efficiency using $[Ru(bpy)_2(NCSphen)]^{2+}$, based on the total number of lysine residues. These labelling efficiencies indicate that there may only be limited access of the label to the lysine moieties, most likely due to the structural conformation of the albumin. Steric hindrance due to the size and shape of the label molecule, as well as the proximity of the lysine residues to each other also plays a role in determining how much label may be attached to the albumin. In fact, Canfi et al. [9], have reported that there

are only about 15 lysine residues available for reaction in albumins, (referring to BSA and HSA molecules rather than ovalbumin (OVA)), so the labelling efficiencies observed in these investigations could be estimated at 80% and 93%, instead of 21% and 25% for the NCSpy and NCSphen complexes bound to BSA respectively, based on the availability of 15 lysine residues for binding.

It is unlikely that the label $[Ru(bpy)_2(NCSpy)_2]^{2+}$, could bind to two lysine residues since these residues are for the most part well separated along the albumin molecule. Thus, only one NCS group / label molecule would be available for binding to the lysine residues. It would be expected then, that similar F/P ratios to those of the $[Ru(bpy)_2(NCSphen)]^{2+}$ conjugate would be obtained and this is indeed observed.

For all further conjugations, the initial F/P ratio chosen was a 50 molar excess of label to protein, and reactions were conducted in 0.1 M carbonate buffer pH 9.6. Even though higher F/P ratios were attained when the initial F/P ratio was 90:1, it was found that increased dye concentrations required increased volumes of DMF for dissolution which could denature the protein and also that protein was lost by precipitation with increasing dye concentrations. This observation of increasing loss of protein due to precipitation with increasing F/P ratios has been reported previously for tetramethyl rhodamine isothiocyanate labelling of rabbit immunoglobulin. [10] However, the precipitate may be removed by centrifugation.

4.2.2 Conjugation of $[Ru(bpy)_2(NCSphen)]^{2+}$, $[Ru(phen)_2(NCSphen)]^{2+}$ and the succinimidyl ester of $[Ru(bpy)_2(COOHbpy)]^{2+}$ to some albumins and poly-L-lysine.

The synthesis and characterisation of the isothiocyanate complexes has already been described in Chapter 3.

Synthesis of the complex $[Ru(bpy)_2(COOH\text{-}bpy)]^{2+}(PF_6)_2$ and its conversion to the succinimidyl ester were carried out according to Bard. [11] The purity of the dicarboxylic acid complex was checked by HPLC and the chromatogram is shown in Figure 4.5. The absorption spectrum of the complex, together with that of the ester derivative are presented in Figure 4.6.

Using the optimised conditions described in Section 4.2.1, the complexes were bound to BSA, human serum albumin (HSA), Ovalbumin (OVA) and poly-L-lysine (PLL). In this study and in the remaining conjugation procedures, the unbound complexes were separated from the conjugates by extensive dialysis against 0.1 M carbonate buffer, pH 9.6.

The conjugation ratios were estimated and the absorption and emission spectra were measured. The results obtained are presented in Table 4.2.

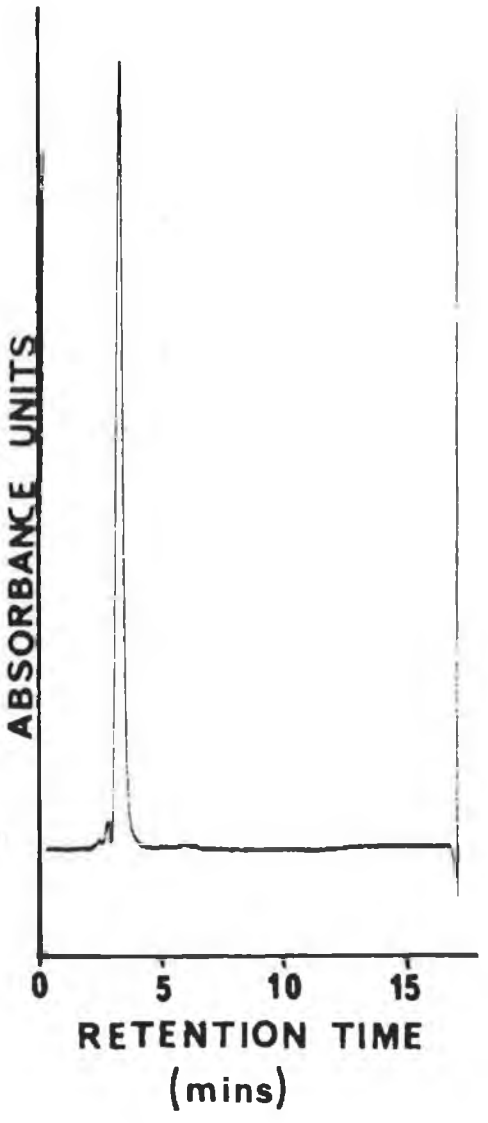

Figure 4.5 The HPLC chromatogram of $[Ru(bpy)_2(COOHbpy)]^{2+}$. The mobile phase used was 80:20, $CH_3CN:H_2O$ with 0.08 M $LiClO_4$. The HPLC system used is described in Chapter 2, Section 2.2.4.

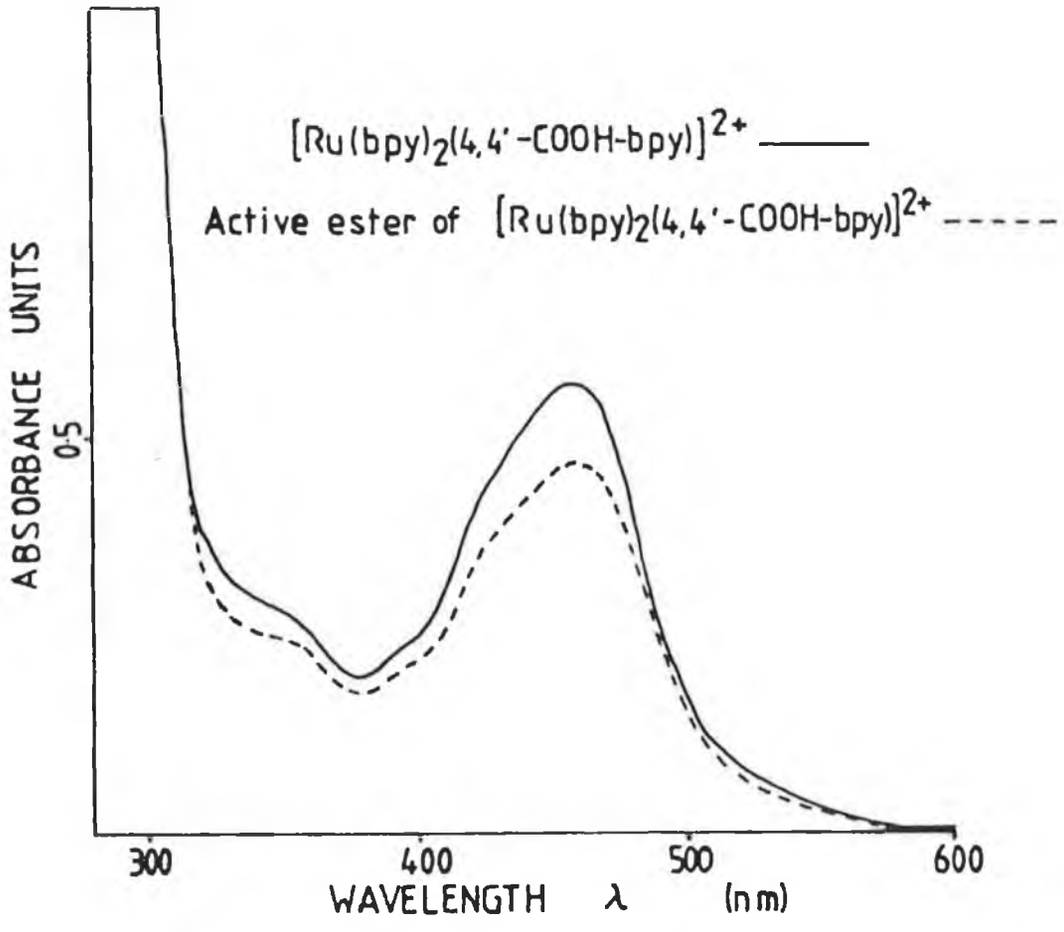

Figure 4.6 The absorption spectra of $[Ru(bpy)_2(COOH\text{-}bpy)]^{2+}$ (———) and its active succinimidyl ester derivative (-----), measured in 0.1 M carbonate buffer, pH 9.6.

Table 4.2 Assessment of the extent of conjugation of $[Ru(L\text{-}L)_2(NCSphen)]^{2+}$ and the ester derivative of $[Ru(L\text{-}L)_2(COOHbpy)]^{2+}$ to BSA, HSA, OVA, and PLL.

Conjugate	F/P (1) (a)	F/P (1) (b)	% labelling efficiency (2)	Abs. λ max. (3)	Em. λ max. (3)
BSA: $[Ru(bpy)_2(NCSphen)]^{2+}$	20	15	35	455	606
HSA: $[Ru(bpy)_2(NCSphen)]^{2+}$	20	13	35	454	608
OVA: $[Ru(bpy)_2(NCSphen)]^{2+}$	9	9	44	454	607
PLL: $[Ru(bpy)_2(NCSphen)]^{2+}$	22	15	3 (5)	454	608
BSA: $[Ru(phen)_2(NCSphen)]^{2+}$	16	13	29	450	600
HSA: $[Ru(phen)_2(NCSphen)]^{2+}$	13	10	22	450	600
OVA: $[Ru(phen)_2(NCSphen)]^{2+}$	6	8	33	449	601
PLL: $[Ru(phen)_2(NCSphen)]^{2+}$	31	11	4 (5)	451	604
BSA: $[Ru(bpy)_2(COOHbpy)]^{2+}$	14	12	24 (4)	467	657
HSA: $[Ru(bpy)_2(COOHbpy)]^{2+}$	15	10	26 (4)	467	657
OVA: $[Ru(bpy)_2(COOHbpy)]^{2+}$	5	6	30 (4)	465	655
PLL: $[Ru(bpy)_2(COOHbpy)]^{2+}$	32	10	4 (4)(5)	465	660

(1). Fluorochrome to Protein (F/P) ratios were determined according to Nairn [4], using C_p (protein conc.in mg/ml) calculated using (a) the Folin-Lowry protein assay [6] and (b) the Bradford protein assay [5]. The assays were performed in duplicate.

(2). The % labelling efficiencies were calculated using the total number of lysine residues: BSA, 57; HSA, 58; and OVA, 18. The results were obtained using F/P ratios, derived using the Folin-Lowry assay to determine C_p.

(3). Absorption / Emission spectra were measured in 0.1 M carbonate buffer, pH 9.6, at room temperature; λ max. in nm.

(4). This compound was converted to the active ester before conjugation to the biomolecules.

(5). See text.

The labelling efficiencies have been calculated on the basis of the total number of lysine residues rather than on the number available, which as described already in Section 4.1 increases the labelling efficiency significantly. As in Section 4.1, the protein concentration was assayed using both the Bradford and Folin-Lowry assays. Again the Bradford assay results in F/P conjugation ratios that are lower than those obtained using the Folin-Lowry assay, especially for the PLL conjugates.

This can be explained in terms of where the reagents actually bind on the protein molecule. The mechanism of dye-binding for the Bradford assay has been investigated. The dye used in this assay is Coomassie Brilliant Blue G. Slightly conflicting reports have been published, in one report it has been suggested that the dye binds to protein by electrostatic attractions of the sulphonic groups of the dye with protonated primary amino groups of proteins such as lysine and N-terminal groups. [12] A second report suggests that interaction is primarily with the arginine residues rather than with primary amino groups, but lysine gives a slight response. [13] The results obtained in this work would suggest that the dye does indeed interact quite significantly with lysine residues. Therefore, any possibility of dye binding through interaction with the lysine residues casts uncertainty on results obtained by this method, since both the Bradford reagent and the ruthenium complexes interact with the same groups on the protein or PLL molecule.

The Folin-Lowry method combines the well known biuret reaction where proteins react with Cu^{2+} in an alkaline medium to produce Cu^{2+}, with the detection of phenolic groups of tyrosine residues and to a lesser extent tryptophan residues, by the use of the Folin-Ciocalteu reagent, the main constituents of which are phosphotungstic and phosphomolybdic acids. The cupric ions form a coordination complex with the four nucleophilic -NH groups provided by the peptide bonds, of the protein or PLL molecule. A Cu-protein (or PLL) complex produced using a dilute version of the biuret reagent, causes the reduction of the phosphotungstic and phosphomolybdic acids to tungsten blue and molybdenum blue. Approximately 75% of the reduction which occurs is due to the copper protein complex, while tyrosine (and to a lesser extent tryptophan) residues are responsible for the remainder. [14] In this method, therefore, the lysine residues are not involved in the protein binding process, so more accurate protein determinations, leading to more accurate estimates of conjugation ratios should be achieved.

For the reasons just outlined, the results are discussed based on F/P ratios derived using the Folin-Lowry method of protein determination. The conjugation ratios achieved for the PLL conjugates suggest that there is quite a substantial interaction between the Bradford reagent and the lysine groups which is in agreement with the observations reported by Fazekas de St. Groth *et al.*. [12] The differences between the Bradford and Folin-Lowry methods are not as significant for the albumins.

Quite a noticeable difference in conjugation ratio is observed between the HSA or BSA conjugates and the OVA conjugates. This is expected since both BSA and HSA contain about 13% lysine with 57 and 58 lysine residues, respectively [8], while OVA contains only 6.3% lysine [15] or about 18 lysine residues based on a molecular weight of 43,000 for OVA. The conjugation ratios for the OVA conjugates are approximately half those obtained for the BSA and HSA conjugates. However, the labelling efficiencies for the OVA conjugates are actually higher than for the HSA or BSA conjugates which may reflect differing degrees of accessibility of the labels for the lysine residues depending on the albumin. The fact that an initial F/P ratio of 50:1, which is in excess of the total number of lysines in ovalbumin, but is really only about 1:1 for HSA and BSA must also be considered.

Samuel et al. [16]] in their assessment of the extent of conjugation of FITC to BSA and OVA, have reported for initial reaction F/P ratios of 5:1, that approximately 4 molecules of FITC bound per molecule of BSA and 2 molecules of FITC per molecule of OVA, or 80% and 40% labelling efficiencies for the FITC/BSA and FITC/OVA conjugates, respectively. If the labelling efficiencies are calculated, based on total lysines rather than on the available lysines, this results in a significant underestimation of the labelling efficiency, then the labelling efficiencies are 7% and 12% for the FITC/BSA and FITC/OVA conjugates, respectively. In that report, as in the work presented here,

the molar extinction coefficient of the conjugated fluorochrome, in this case FITC, was assumed to be the same as unbound FITC.

As mentioned in Section 4.2.1, the conformational structure of the albumins, which are globular proteins with compact folded peptide chains, plays an important role in determining how many lysine residues are accessible to the ruthenium compounds.

The conjugation ratios are higher for the PLL conjugates than for the albumins. This is expected since there are nearly 750 lysine molecules in the poly-L-lysine molecule used in this work. The labelling efficiencies as defined in Table 4.2, are much lower but based on the initial F/P ratio of 50:1, the maximum labelling efficiency possible would be about 6%, (a possible 50 lysines out of a total of 750 lysines), so the ratios obtained here (about 3-4%), are high given the initial amount of label added. The fact that 6% labelling efficiencies were not achieved may reflect (a) a limited accessibility of the label to the polymer depending on the conformational structure at the pH used in this study or (b) limitations based on measurements used to calculate F/P or perhaps (c) steric hindrance due to the size of the ruthenium complex.

On average, about 28 molecules of ruthenium complex were conjugated to each PLL molecule. Based on an initial ratio of 50:1 (F/P), this represents about 56% labelling efficiency for ruthenium labelling. This concept of labelling efficiencies can be quite confusing, since there

are a number of ways in which the labelling efficiencies can be interpreted. Labelling efficiencies can be determined based on (a) the amount of label complex that is added, (b) the total number of amino acid residues (in this case, lysine) that can react with the label complex and (c) the available number of amino acid residues with which the label molecule can react. The latter will be dependent on the accessibility of the label to the protein or polymer, the conformational structure of the protein or polymer, the pH at which conjugation occurs and on the structure of the label molecule itself.

For the three ruthenium complexes examined, the F/P ratios are quite similar for a given albumin or PLL. The succinimidyl ester complex may potentially react with two lysine residues, depending on whether both carboxylic acid groups were converted to ester moieties. However, it is unlikely that the complex could bind two lysine residues for the same reason that the complex $[Ru(bpy)_2(NCSpy)_2]^{2+}$, probably does not bind two lysine residues, which is that the lysine residues are probably too well separated along the peptide chain.

The absorption spectra of the various unbound labels, together with the spectra of their albumin and PLL conjugates, are presented in Figures 4.7 - 4.9. The label and conjugate solutions were diluted in 0.1 M carbonate buffer, pH 9.6, in order to present all the spectra on the same absorbance scale.

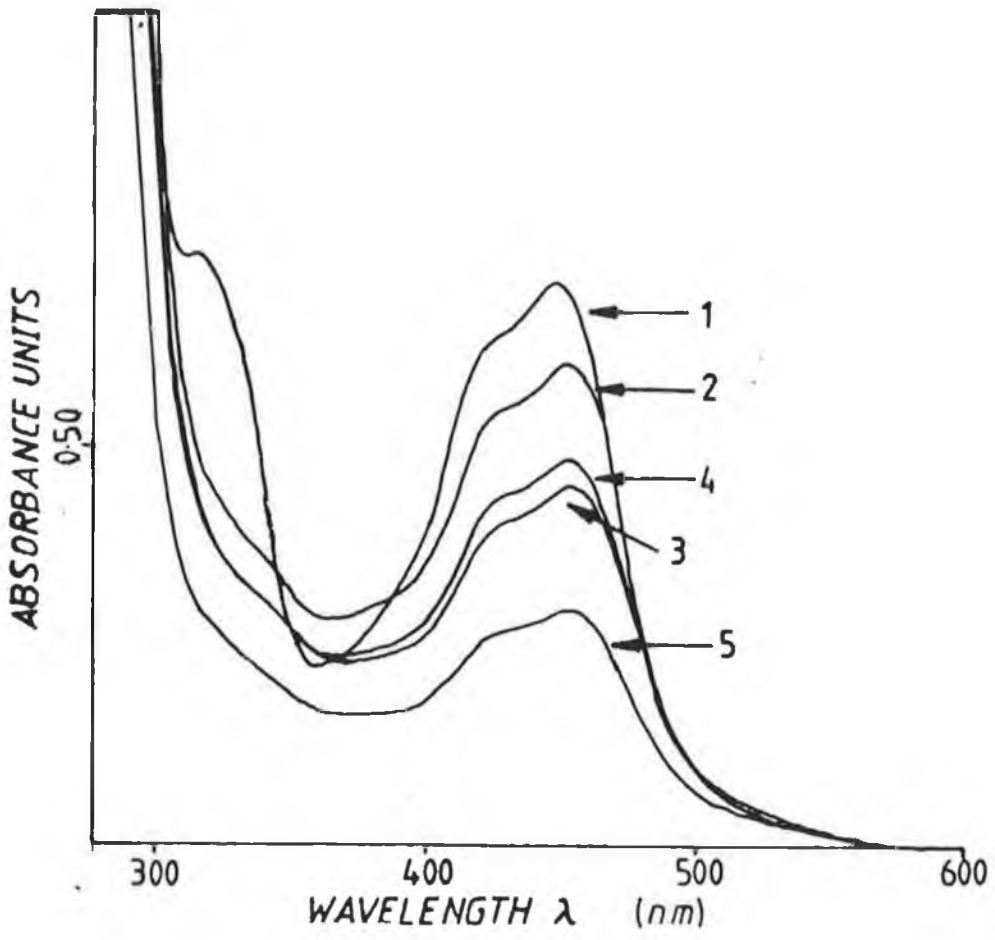

Figure 4.7 Absorption spectra of (1) free $[Ru(bpy)_2-(NCSphen)]^{2+}$ and bound to (2) PLL, (3) BSA, (4) HSA and (5) OVA, measured in 0.1 M carbonate buffer, pH 9.6. Ruthenium complex concentrations are in the range 2-4 x 10^{-5} M.

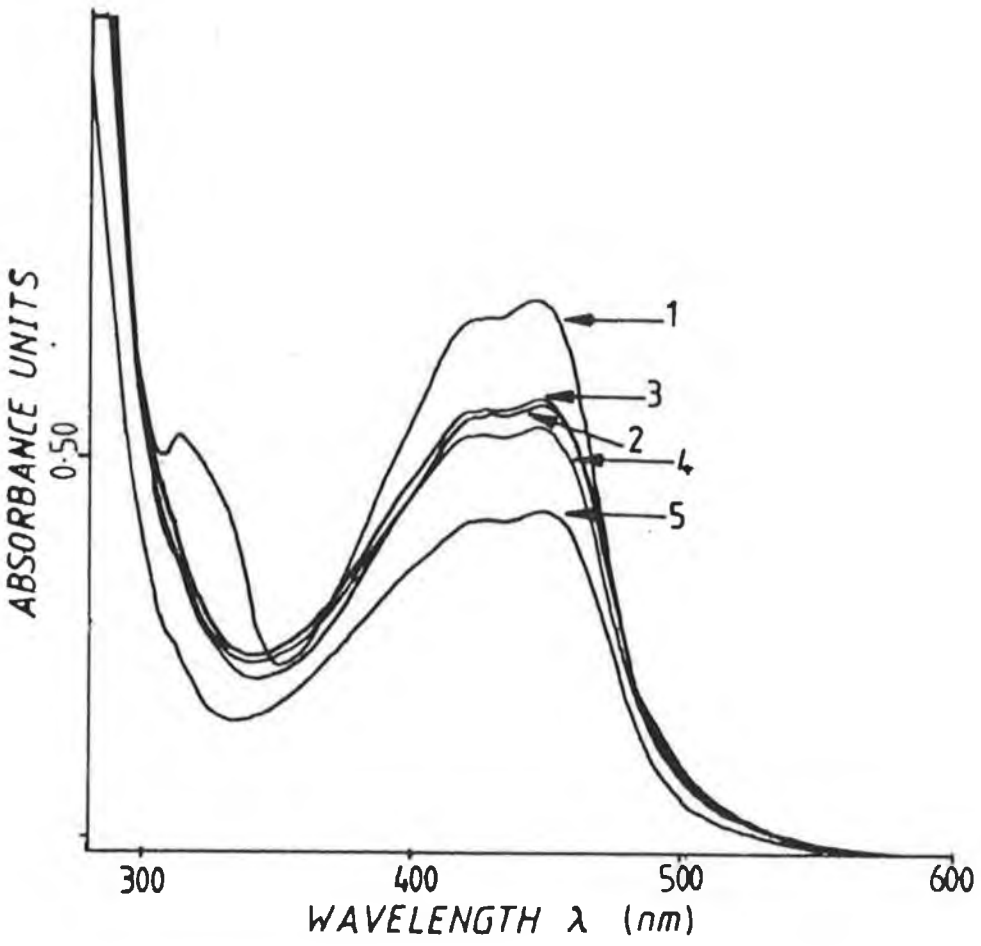

Figure 4.8 Absorption spectra of (1) free $[Ru(phen)_2-(NCSphen)]^{2+}$ and bound to (2) OVA, (3) BSA, (4) HSA and (5) PLL, measured in 0.1 M carbonate buffer, pH 9.6. Ruthenium complex concentrations are in the range 3-5 x 10^{-5} M.

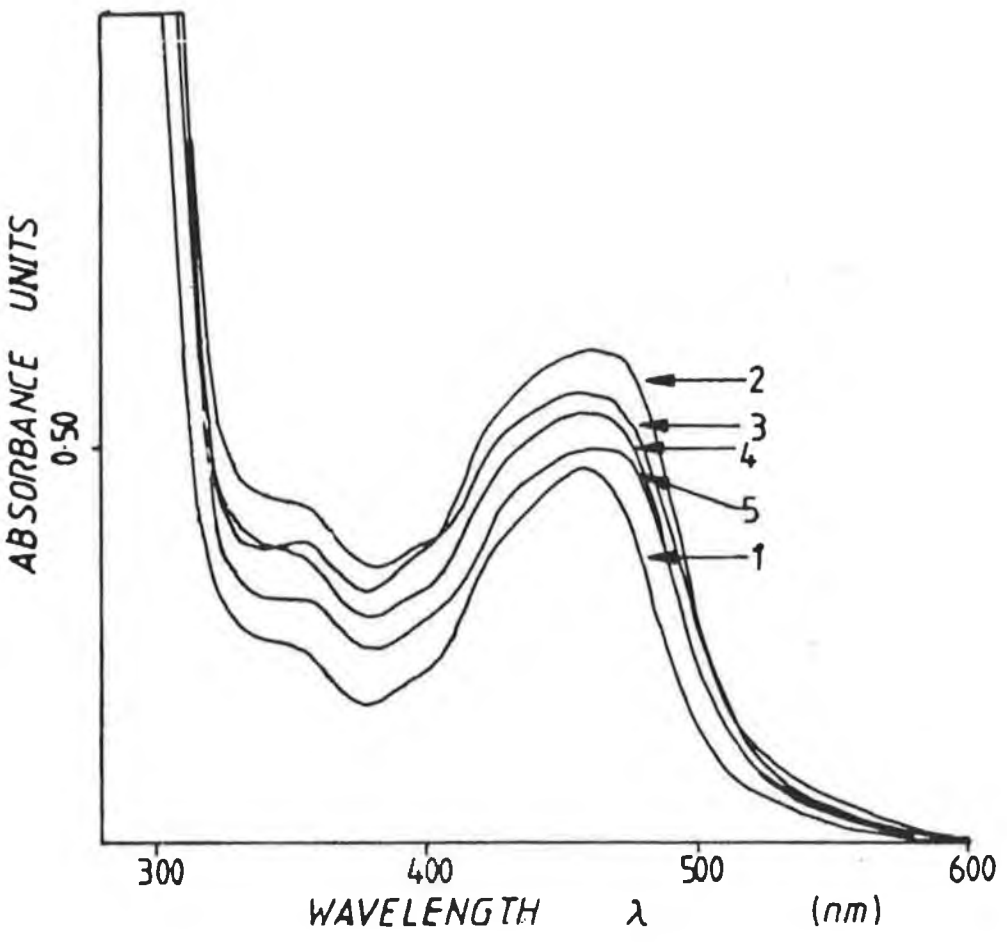

Figure 4.9 Absorption spectra of (1) the free succinimidyl ester of $[Ru(bpy)_2(COOHbpy)]^{2+}$ and bound to (2) PLL, (3) BSA, (4) OVA and (5) HSA, measured in 0.1 M carbonate buffer, pH 9.6. Ruthenium complex concentrations are in the range 3-4 x 10^{-5} M.

The absorption spectra of the bound $[Ru(bpy)_2(NCSphen)]^{2+}$ and $[Ru(phen)_2(NCSphen)]^{2+}$ are quite similar to their unbound spectra. For $[Ru(bpy)_2(NCSphen)]^{2+}$ conjugates, the absorption intensity of the peak at λ max. appears to have decreased slightly, with perhaps some broadening of the ^{3}MLCT band to lower wavelength. The general shape of the ^{3}MLCT band has changed. The same effects are observed for the $[Ru(phen)_2(NCSphen)]^{2+}$ conjugates. The ^{3}MLCT bands seem to experience a slight red shift of the order of 1-4 nm, but it is difficult to confirm this since these shifts are so small that some are within instrumental error.

Similar changes in the absorption spectrum of the succinimidyl ester of $[Ru(bpy)_2(COOHbpy)]^{2+}$ upon binding to the albumins and PLL are observed. The ^{3}MLCT band is quite clearly broadened and the λ max. is red shifted by about 7-9 nm.

These changes in the general shape of the ^{3}MLCT band upon conjugation to the albumins and PLL are to be expected. Quite similar effects have been described for ruthenium polypyridyls which interact with DNA, the extent of which seems to depend on the type of binding (whether intercalative or electrostatic) [17].

For both $[Ru(bpy)_2(NCSphen)]^{2+}$ and $[Ru(phen)_2(NCSphen)]^{2+}$ conjugates, the emission λ max. appear to be blue shifted slightly, about 2-4 nm for the bpy conjugates and about 4-8 nm for the phen conjugates. This is difficult to evaluate accurately, since these variations are

probably within instrumental error. The emission λ max. of the $[Ru(bpy)_2(COOHbpy)]^{2+}$ complexes which were esterified before conjugations, have blue shifted considerably (about 20 nm), upon conjugation. However, this may not be as a consequence of conjugation, since the literature reports two different λ max. of emission at pH > 7, 638 nm and 659 nm for the complex $[Ru(bpy)_2(COOHbpy)]^{2+}$. Also depending on pH, the emission λ max. shifts from 638 nm to 670 nm at low pH. [18]

Generally, it is difficult to obtain much information from the slight changes occurring in the emission spectra of the complexes, when conjugated to the albumins and PLL. More information would be available from monitoring the changes in emission intensity which occur upon conjugation.

Indeed, this has been reported for ruthenium polypyridyl interactions with DNA, where the emission intensity and quantum yields were found to increase in the presence of DNA. These observations were substantiated from measurements of the emission decay lifetimes of the unbound and DNA bound ruthenium complexes. [17] The necessity of separating bound from unbound ruthenium complexes in this work renders it more difficult to monitor changes in emission intensity upon conjugation. In the DNA studies just mentioned, changes in the emission intensity from the ruthenium complexes have been monitored in the presence of DNA, and as with the absorption spectra measurements for these complexes, separation of any unbound from bound ruthenium is not required since the amount of DNA used is in

excess of the amount of ruthenium complex, so that it is assumed that all of the added ruthenium complex becomes DNA bound.

The changes in the spectroscopic properties of the complexes described here may perhaps be indicative of the type, or indeed the site of binding which may make these complexes useful probes of protein structure especially in terms of their emission decay characteristics which will be discussed in Section 4.2.7.

The size and structural conformation of the biomolecule to which the ruthenium complex is bound does not appear to significantly affect the shape of the absorption or emission spectra. The actual binding mechanism leads to changes in the spectra but the size and conformational characteristics do not. The biomolecules studied in this work range in molecular weights of 43,000 (OVA), 67,000 (HSA) and 68,000 (BSA) to 109,000 for PLL, yet the absorption and emission spectra of a particular ruthenium complex bound to different biomolecules are all quite similar.

The structural conformation of the albumins and PLL are quite different. Albumins are globular proteins and exhibit (a) compact folding with little or no internal space for water molecules, (b) internal location of at least 50% of the hydrophobic R groups on the amino acid side chains and (c) external location of nearly all the hydrophilic R groups. The tertiary structure of globular proteins is stabilised by hydrophobic interactions between the non-polar R groups. [2]

PLL can exist in an irregular random form at pH 7.0, or as an α -helix at pH 12.0, depending on whether or not the ε -amino groups of all the lysine residues are charged. (See Figure 4.10.) At pH 7.0, these groups are charged and repel each other so strongly that the tendency for intrachain hydrogen bonding is overcome. At pH 12.0, the ε -amino groups are uncharged and the polymer adopts an α -helical conformation. [2] At the pH used in these studies (pH 9.6), it is expected that the polymer may exhibit a somewhat intermediatory conformation with quite a number of uncharged ε -amino groups.

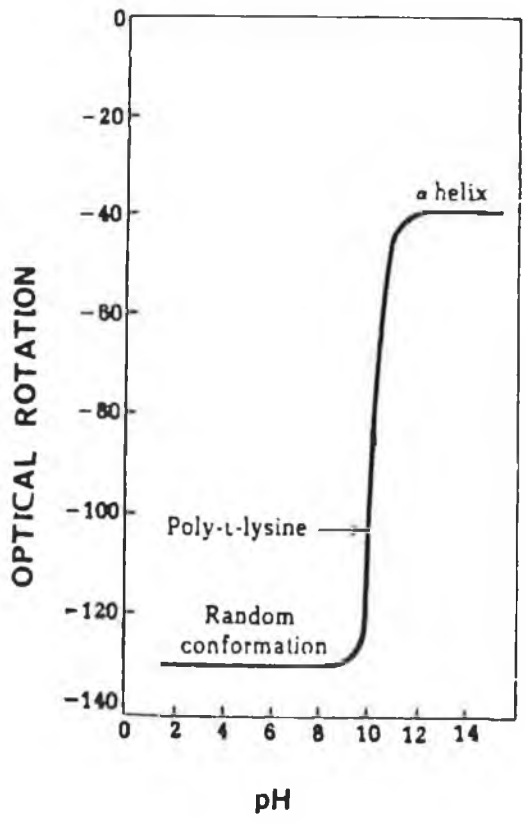

Figure 4.10 The effect of pH on the transition between the random conformation and the α -helical forms of poly-L-lysine. [2]

Any changes observed in the absorption and emission spectra of the ruthenium complexes upon binding to biomolecules are difficult to quantify, in terms of the investigations carried out in this work. However, differences between binding to albumins and PLL are demonstrated from the emission lifetime decay measurements. (Section 4.2.7) As already discussed, it would be easier to monitor changes in absorption or emission properties if the separation step to remove any unbound label molecule was not required, as with the DNA studies mentioned earlier. In future investigations, it would be interesting to monitor changes in the absorption and emission spectra (and intensities) upon conjugation by ensuring that the protein or polymer concentration is in excess of the ruthenium complex concentration, so that all of the ruthenium complex would be bound. This would mean that the separation step to remove unbound label would not be necessary, and changes in absorption or emission properties would be easier to follow.

4.2.3 Conjugation of $[Ru(bpy)_2(NH_2phen)]^{2+}$ and $[Ru(phen)_2(NH_2phen)]^{2+}$ to BSA, HSA and OVA.

The conjugation procedure is detailed in the experimental chapter (Chapter 2), and essentially involves the periodate oxidation of the carbohydrate moieties of the proteins which results in the generation of aldehyde groups which can then be condensed specifically with the nucleophilic amine group

of the ruthenium compounds. This reaction of an amine and an aldehyde results in the formation of a Schiff base which is stabilised by the addition of sodiumborohydride. The reaction sequence is shown below. Mild periodate oxidation results in the generation of aldehyde groups which can then be condensed specifically with a nucleophile such as an amine. [1]

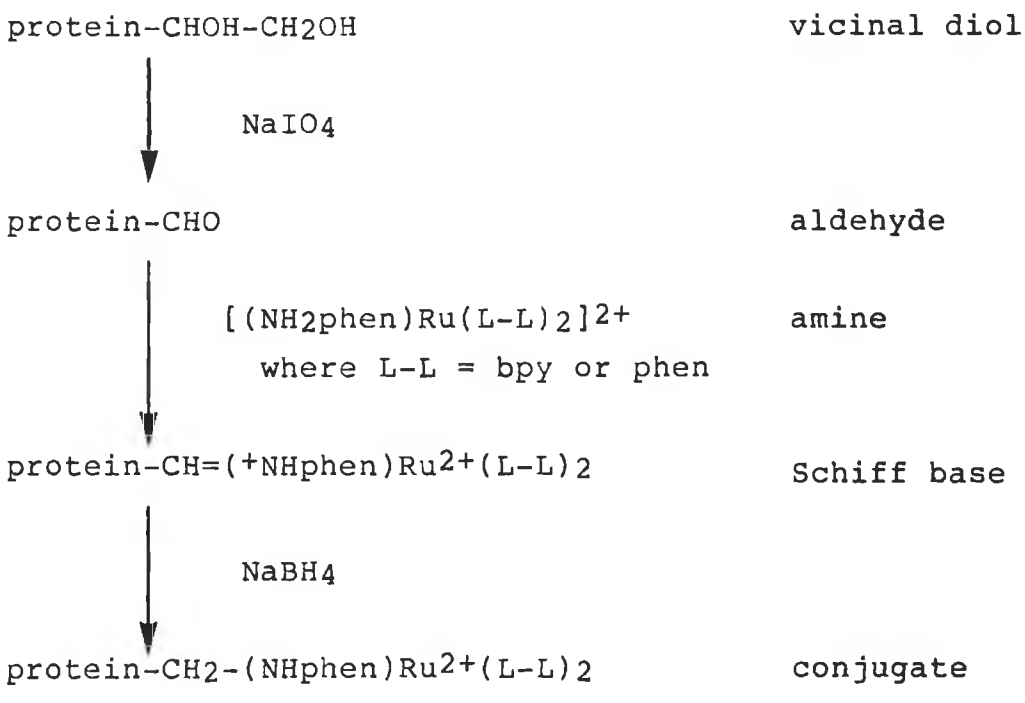

The conjugation ratios were again estimated using both the Bradford and Folin-Lowry assays to determine protein concentration. The results obtained are presented in Table 4.3.

Table 4.3 Assessment of the extent of conjugation of $[Ru(L\text{-}L)_2(NH_2phen)]^{2+}$ to OVA, BSA and HSA.

Conjugate	F/P[1] (a)	F/P[1] (b)	Absorption[2] λ max.	Emission[2] λ max.
BSA:$[Ru(bpy)_2(NH_2phen)]^{2+}$	4	4	454	609
HSA:$[Ru(bpy)_2(NH_2phen)]^{2+}$	3	3	454	610
OVA:$[Ru(bpy)_2(NH_2phen)]^{2+}$	2	3	454	608
BSA:$[Ru(phen)_2(NH_2phen)]^{2+}$	4	4	450	606
HSA:$[Ru(phen)_2(NH_2phen)]^{2+}$	4	4	448	610
OVA:$[Ru(phen)_2(NH_2phen)]^{2+}$	2	3	449	609

(1). Fluorochrome to Protein (F/P) ratios were determined according to Nairn [4], using C_p (protein conc. in mg/ml) calculated from (a) the Folin-Lowry protein assay and (b) the Bradford protein assay. The assays were performed in duplicate.

(2). Absorption / Emission spectra were measured in 0.1 M carbonate buffer, pH 9.6, at room temperature, λ max. in nm.

The importance of considering which protein assay to use has already been highlighted in Section 4.2.2. In these investigations, the carbohydrate moieties have been modified. Since the carbohydrate moieties are not involved in the binding mechanism of either the Bradford reagent or the reagents employed in the Folin-Lowry assay, both assays may be used to determine the protein concentration. Good correlation between both assays was achieved.

The proteins in this study have been treated as glycoproteins. Ovalbumin is a well recognised glycoprotein, with approximately 1% by weight of carbohydrate. The oligosaccharide groups of most glycoproteins are covalently attached to the R groups of specific amino acid residues in the polypeptide chain. In ovalbumin, as shown below and immunoglobulins, the oligosaccharide moiety is attached via a glycosylamine linkage between N-acetyl-D-glucosamine of the oligosaccharide to the amide nitrogen of an asparagine residue in the polypeptide chain. [2,19]

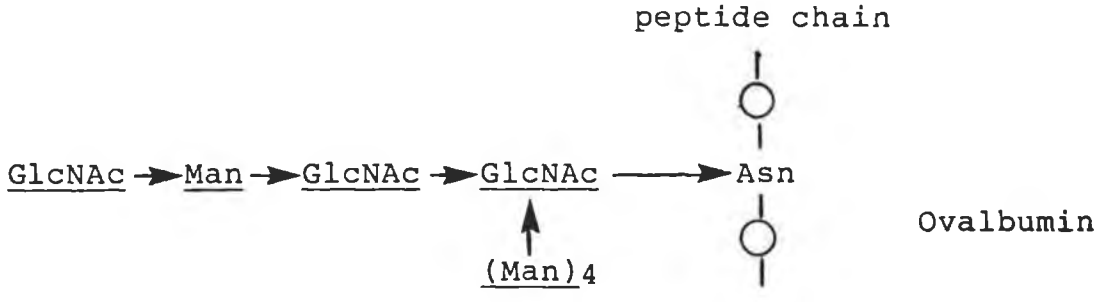

GlcNAc = N-acetylglucosamine, Man = mannose, Asn = asparagine
The oligosaccharide side chains are underlined.

Both BSA and HSA have been treated as glycoproteins although they are not usually regarded as such.

The much lower proportion of carbohydrate moieties compared to lysine residues on the protein molecules is clearly reflected in the conjugation ratios, with slightly higher ratios achieved for the higher molecular weight

albumins.

This method of binding via the carbohydrate moieties is not of particularimportance in terms of albumins because the lysine residues can be readily conjugated to label molecules. Binding via the carbohydrate moieties on immunoglobulins is of more importance because not only does it generate specificity in the labelling but it may minimise the effect on the affinity of the antibody for the antigen, a decrease in which has often been ascribed to the modification of the amino acids in or in close proximity to the antigen binding site. This will be discussed in more detail in Section 4.2.5.

Modification of the carbohydrate moieties of albumins demonstrates the feasibility of the technique. Albumins are relatively inexpensive in comparison to immunoglobulins. This means that reasonable amounts of albumins (10-30 mg) were available per conjugation whilst for immunoglobulin conjugations only 1-2 mg per conjugation were available.

The absorption spectra of the free and bound $[Ru(phen)_2(NH_2(phen)]^{2+}$ and $[Ru(bpy)_2(NH_2phen)]^{2+}$ are presented in Figures 4.11 and 4.12.

The λ max. of absorption of the conjugated labels does not appear to have shifted appreciably. However, the changes in the shape of the absorption spectra are somewhat similar to those of the conjugates described earlier. The ^{3}MLCT band becomes much less resolved and is broadened considerably upon conjugation. Again, the size of the

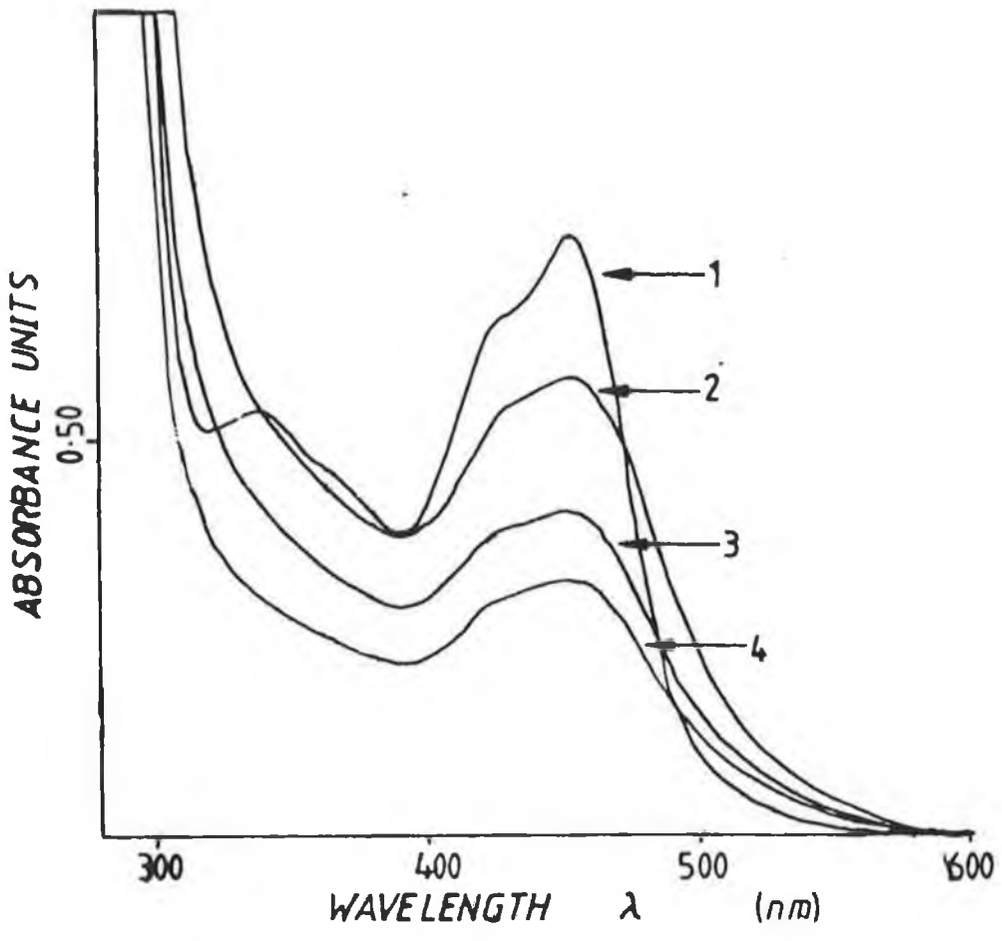

Figure 4.11 Absorption spectra of (1) free $[Ru(bpy)_2-(NH_2phen)]^{2+}$ and bound to (2) BSA, (3) OVA and (4) HSA. The spectra were measured in 0.1 M carbonate buffer, pH 9.6. Ruthenium complex concentrations are in the range 2-5 x 10^{-5} M.

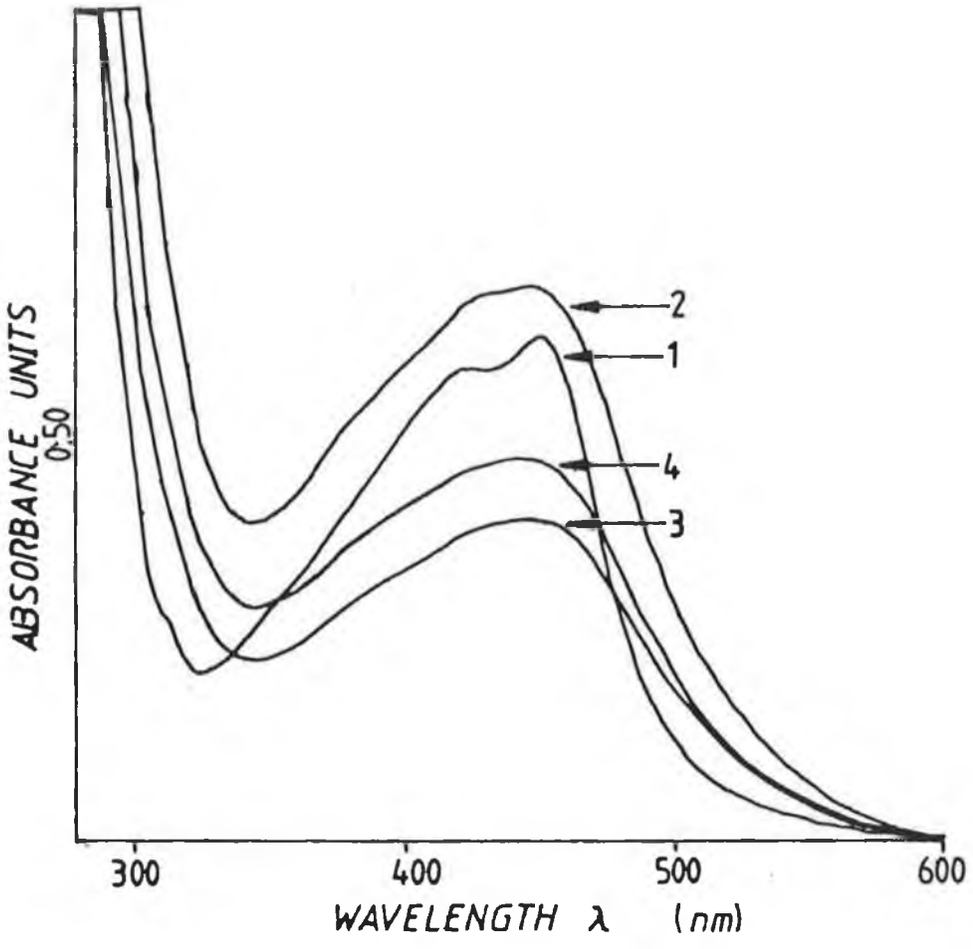

Figure 4.12 Absorption spectra of (1) free $[Ru(phen)_2-(NH_2phen)]^{2+}$ and bound to (2) BSA, (3) HSA and (4) OVA. The spectra were measured in 0.1 M carbonate buffer, pH 9.6. Ruthenium complex concentrations are in the range 2-4 x 10^{-5} M.

protein does not seem to affect the shape of the spectra. The ^{3}MLCT band for these conjugates appears broader and less well resolved than the ^{3}MLCT band of the ruthenium isothiocyanate conjugates. This may be associated with the difference in binding sites, where one complex binds via the lysine residues and another via the carbohydrate moieties or, it may simply reflect differences between the labels.

As with the other conjugates, the emission λ max. has not changed significantly upon binding to the albumins. The λ max. may be slightly red shifted, whereas for the other conjugates described in Section 4.2.2, where the lysine residues are modified, the λ max. was blue shifted slightly. However, nothing conclusive may be stated, since once again the shifts are within instrumental error.

4.2.4. Conjugation of diazotised $[Ru(bpy)_2(NH_2phen)]^{2+}$ and $[Ru(phen)_2(NH_2phen)]^{2+}$ to BSA, HSA and OVA.

Preliminary experiments were carried out on conjugating diazotised ruthenium complexes to albumins, which under mildly alkaline conditions bind through the tyrosine residues of albumins. The amino complexes were diazotised according to the method described by Sundberg *et al.* [3]. The diazotised material was not isolated and the protein was added to the diazotised material as soon as it was prepared. The conjugation reaction was allowed to proceed as normal, at

$4^{o}C$, in the dark, with minimal agitation.

During the diazotisation reaction of $[Ru(phen)_2(NH_2phen)]^{2+}$, much of the complex precipitated out of solution. The conjugation was still attempted using this complex, but very little of the complex was found to bind to the albumins. The F/P ratio for all three albumins was <1.

More success was attained with the diazotisation of $[Ru(bpy)_2(NH_2phen)]^{2+}$. The complex remained in solution and a 50:1 molar excess of this diazo solution was reacted with the albumins. After conjugation the unbound ruthenium complex was removed by dialysis against 0.1M carbonate buffer, pH 9.6. In this instance, the protein content was estimated by using the Bradford assay since the Folin-Lowry assay involves reaction with the tyrosine residues. The Folin-Ciocalteu reagent used in the assay reacts with the phenolic moieties of tyrosines, the same groups which are targeted by the diazo compound. The results are presented in Table 4.4.

Table 4.4 Assessment of the extent of conjugation of diazotised $[Ru(L\text{-}L)_2(NH_2phen)]^{2+}$ to BSA, HSA, and OVA.

Conjugate	F/P ratio (1)	% labelling efficiency (2)	Abs. λ max. (3)	Em. λ max. (3)
$[Ru(bpy)_2(^+N_2phen)]^{2+}$	-	--	454	619
BSA:$[Ru(bpy)_2(^+N_2phen)]^{2+}$	3	18	455	617
HSA:$[Ru(bpy)_2(^+N_2phen)]^{2+}$	2	11	455	620
OVA:$[Ru(bpy)_2(^+N_2phen)]^{2+}$	2	22	455	619
PLL:$[Ru(bpy)_2(^+N_2phen)]^{2+}$	1	--	455	622
$[Ru(phen)_2(^+N_2phen)]^{2+}$	-	--	446	603
BSA:$[Ru(phen)_2(^+N_2phen)]^{2+}$	<1	<6	445	605
HSA:$[Ru(phen)_2(^+N_2phen)]^{2+}$	<1	<6	445	605
OVA:$[Ru(phen)_2(^+N_2phen)]^{2+}$	<1	<11	445	604
PLL:$[Ru(phen)_2(^+N_2phen)]^{2+}$	-	--	445	605

(1) Fluorochrome to Protein (F/P) ratios were determined using the Bradford assay to determine protein conc. F/P was calculated according to Nairn. [4]

(2) The % labelling efficiencies have been determined based on the total number of tyrosines, BSA, 17; HSA, 18; and OVA, 9. [8,15]

(3) The absorption / emission spectra were measured in 0.1 M carbonate buffer, pH 9.6, at room temperature, λ max. in nm.

The labelling efficiencies have been calculated on the basis of total tyrosines rather than available tyrosines so the labelling efficiencies could actually be higher.

In mildly alkaline conditions, diazonium salts are thought to react preferentially with phenols. Whilst in mildly acidic solution, the salts react preferentially with amines. [20] By using alkaline conditions in these experiments, it has been assumed that only tyrosine residues were modified. However, the diazonium salt was found to react with PLL (although not to any great extent), which does not have any tyrosines, suggesting that the diazonium complex does react with the lysine residues of the PLL molecule. Diazonium salts have previously been reported to couple with histidine and lysine residues [4,21], the efficiency of which presumably depends on the pH.

The choice of which assay to employ to determine the protein concentration should be considered. In these experiments, the total volume remaining after dialysis was noted for each conjugate and the protein content determined by dividing the total amount of protein used in mg by the total volume after dialysis. The results were very similar to those obtained using the Bradford assay. This simple method of monitoring protein concentration may be just as accurate as some of the other assays. Some protein is probably lost, through transfer and removal of the conjugate solution to and from the dialysis tubing, some protein could adhere to the reaction vessel and also to the dialysis tubing itself, but use of the Bradford and Folin-Lowry assays can

also lead to an underestimate of the protein concentration.

Another method of measuring protein concentration is by measuring the absorption of the protein in the UV region. The ruthenium complexes also absorb about 280 nm, so this leads to difficulties in measuring the protein in the UV, especially if the extinction coefficient of the complex or indeed, the protein varies upon conjugation.

It is not necessary to discuss at length the advantages and disadvantages of the various methods of measuring protein concentration, since F/P ratios are only an estimate and not a precise quantity. However, the choice of method should be given some consideration, in order to minimise gross inaccuracies.

The coupling of diazonium salts represents just a preliminary investigation. Further tests will have to be conducted (a) to ensure the successful diazotisation of the ruthenium complexes and (b) to determine which residues are being targeted by the diazonium salts. This could be investigated by monitoring reactions with simple amino acids or poly amino acids in mildly alkaline and acidic solutions.

The absorption spectra of the diazotised ruthenium complex together with its conjugate to the albumins and PLL are presented in Figure 4.13. As with other conjugates the absorption band in the visible is subject to band-broadening effects. The ^{3}MLCT band is also less well resolved than in the free diazonium salt.

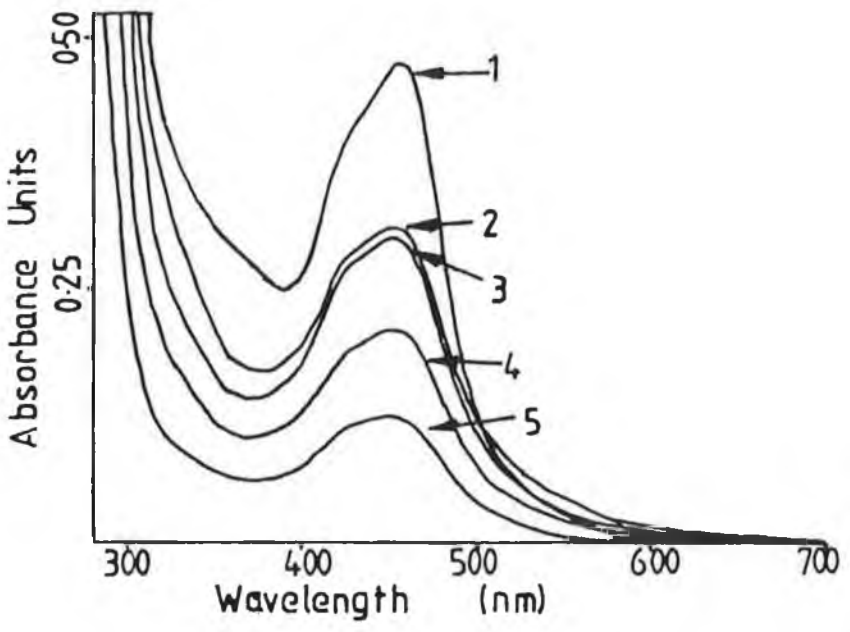

Figure 4.13 Absorption spectra of the free and bound diazotised $[Ru(bpy)_2(NH_2phen)]^{2+}$. The spectra were measured in 0.1 M carbonate buffer, pH 9.6. (1) free label; (2) bound to OVA; (3) bound to BSA; (4) bound to HSA and (5) bound to PLL. Ruthenium complex concentrations are in the range 1-4 x 10^{-5} M.

The emission spectrum of the freshly prepared diazonium complexes were measured prior to conjugation in order to measure the wavelength of maximum emission of the unbound complex for comparison with the bound complexes. As may be seen from Table 4.4, the shifts in the λ max. are very small and are within instrumental error.

4.2.5 Conjugation of ruthenium complexes to immunoglobulins.

Preliminary studies employed the use of crude preparations of anti-BSA and anti-mouse IgG. These preparations were impure in that they contained other proteins, which made the estimation of the F/P ratios impossible. Also it is difficult to specify initial molar F/P ratios as 50:1, since the protein preparation is impure. But as a starting point the initial ratios were prepared assuming that the preparation was pure. The conjugation reaction was allowed to proceed for 18 hours, at $4^{o}C$ with minimal agitation in 0.1 M carbonate buffer, pH 9.6. The immunoglobulins were conjugated to $[Ru(bpy)_2(NCSphen)]^{2+}$ and $[Ru(phen)_2(NCSphen)]^{2+}$, thus modifying the lysine residues on these immunoglobulins. After conjugation, the unbound and bound ruthenium complexes were separated by gel-filtration chromatography on Sephadex G-25, using phosphate buffered saline, (PBS), pH 7.4 as eluent. The column volume was about 10 times the volume of the reaction solution. Two coloured

fractions were collected. The first fraction to elute is the high molecular weight conjugate and the second is the unbound label (or as discussed earlier the amino precursor complex).

Table 4.5 Spectroscopic data on the immunoglobulin conjugates of $[Ru(bpy)_2(NCSphen)]^{2+}$ and $[Ru(phen)_2(NCSphen)]^{2+}$.

Conjugate	Absorption λ max. (nm)	Emission λ max. (nm)
anti-mouse IgG : $[Ru(bpy)_2(NCSphen)]^{2+}$	451	606
anti-BSA : $[Ru(bpy)_2(NCSphen)]^{2+}$	450	606
anti-mouse IgG : $[Ru(phen)_2(NCSphen)]^{2+}$	448	598
anti-BSA : $[Ru(phen)_2(NCSphen)]^{2+}$	445	599

The absorption / emission spectra were measured in phosphate buffered saline, pH 7.4.

The absorption spectra presented in Figure 4.14 show the spectra of the bound and unbound ruthenium complex ($[(Ru(bpy)_2(NCSphen)]^{2+}$ which is conjugated to anti-BSA), fraction 1 and 2 from the gel filtration column respectively. The observed changes in the spectra are similar to those already described for other conjugates. It is not possible, using the absorption spectra, to distinguish between conjugates of albumins, PLL and immunoglobulins, once again indicating that it is the fact that the ruthenium complex binds to a biomolecule rather than the size of the biomolecule which dictates the observed changes in the spectra. As for the other conjugates only slight changes in the emission λ max, were observed.

Retention of immunological activity was demonstrated by ELISA (enzyme-linked immunosorbent assay) assays, as described in Chapter 2. For anti-BSA conjugates, the microtitre plate was initially coated with BSA, so that only the anti-BSA conjugates should bind. Similarly, for the anti-mouse IgG conjugates the microtitre plate was initially coated with mouse IgG. The specificity of the antigen-antibody reaction is such that any non-specific protein in the conjugate preparation should be removed by the various washing steps in the assay procedure. The positive result visualised when the antibody conjugated enzyme label reacts with the substrate resulting in a coloured product indicates that the immunological activity was retained.

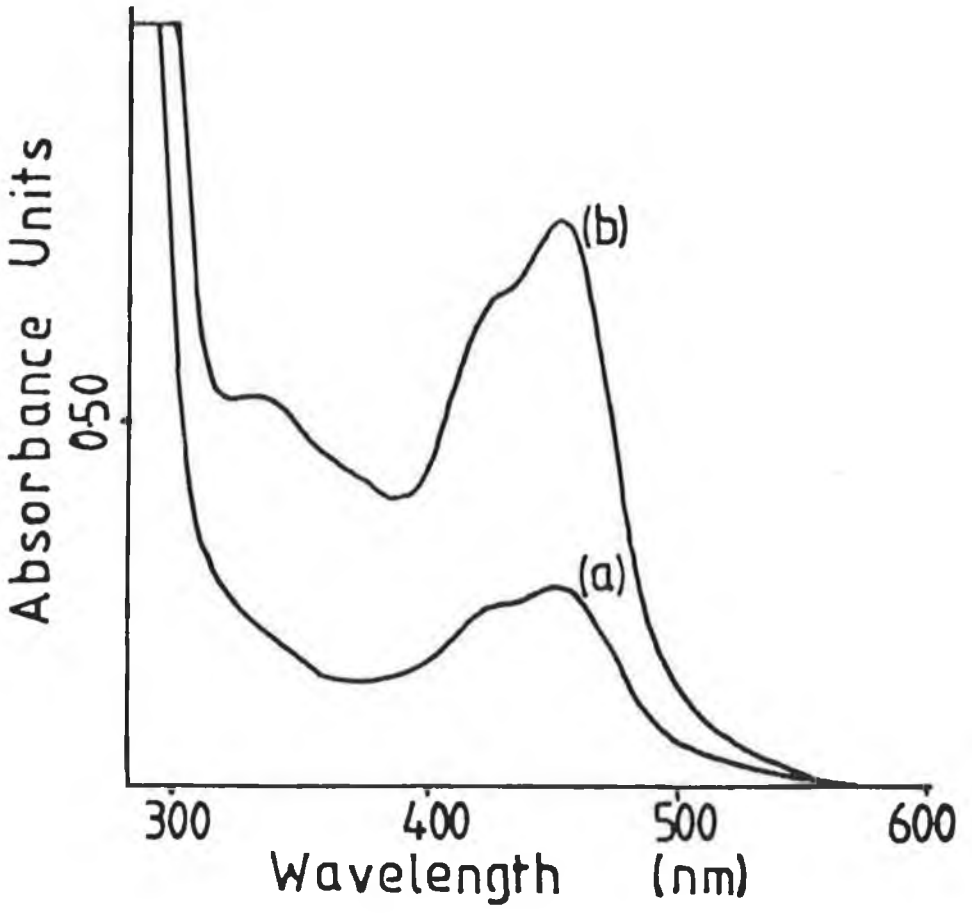

Figure 4.14 The absorption spectra of the unbound and anti-BSA bound $[Ru(bpy)_2(NCSphen)]^{2+}$, after gel filtration chromatography using Sephadex G-25 and phosphate buffered saline, pH 7.4, as eluent.

Pure anti-IgG was labelled with $[Ru(bpy)_2(NCSphen)]^{2+}$ and $[Ru(bpy)_2(NH_2phen)]^{2+}$. $[Ru(bpy)_2(NCSphen)]^{2+}$ binds to the anti-IgG molecule via the lysine residues and $[Ru(bpy)_2(NH_2phen)]^{2+}$ binds via the carbohydrate moieties. The methods used to conjugate the complexes to the anti-IgG molecule are given in Chapter 2. The anti-mouse IgG was reacted with a 50 molar excess of the appropriate ruthenium complex. Unbound complex was removed by extensive dialysis against 0.1 M carbonate buffer, pH 9.6. The conjugation ratios were estimated to be about 3, for conjugation via the lysine residues and about 1 for conjugation via the carbohydrate moieties. Protein was determined using the Folin-Lowry assay. Initial F/P ratios of 100:1 and 200:1 were also used, in an effort to increase the conjugation ratio for the conjugates bound via the lysine residues but the final conjugation ratios after dialysis were the same as those calculated for initial F/P ratios of 50:1.

ELISA assays were conducted on all the conjugates involving the pure anti-IgG and immunological activity was found to be retained in all cases.

An attempt was made to confirm retention of immunological activity using immunofluorescence microscopy. Solutions of $[Ru(bpy)_2(NCSphen)]^{2+}$ conjugates of BSA were initially examined under the microscope and it was observed that a solution of at least 10^{-3} M $[Ru(bpy)_2(NCSphen)]^{2+}$ was required in order to view red fluorescence under the microscope. Therefore, after reaction of the $Ru(bpy)_2(NCSphen)]^{2+}$: anti-IgG conjugate with isolated

mouse spleen cells, with which the anti-IgG molecule should bind specifically, quite a large concentration of the ruthenium label would have to bind to the spleen cells in order to visualise the red fluorescence. Mouse spleen cells were incubated with the anti-IgG conjugate at various dilutions of the conjugate but after the appropriate incubation and washing steps, no red fluorescence was observed. In some respects this was not surprising, considering that quite a large concentration of the ruthenium complex was required to view fluorescence in the first place and after the various incubation and washing steps the solutions were totally colourless.

Bard [11], has described the use of the active ester of $[Ru(bpy)_2(COOHbpy)]^{2+}$ bound to rabbit anti-salmonlla antibody in immunofluorescence studies, but specific details on the conjugation ratio were not given. The initial F/P ratio was in the order of 20:1.

Further studies were hindered due to the lack of sufficient quantities of anti-mouse IgG, but obviously further investigations are necessary. The fluorescence microscope was set up for the routine examination of FITC labelled preparations and the filters used in this system were also used to examine the ruthenium conjugates. Perhaps the use of filters should be investigated further, but since the red fluorescence of the BSA conjugates was observed using this system it was assumed that these filters were suitable for all the ruthenium complexes. The filters used in the Nikon fluorescence microscope were Nikon B filter blocks. The

excitation filter allows the sample to be excited in the range 450 - 490 nm, and the barrier filter operates at about 520 nm, cutting excitation light not absorbed by the specimen which can obstruct fluorescence observation and transmits fluorescence of wavelength > 520 nm. The difficulties associated with using small quantities of anti-IgG for conjugation resulted in conjugates in which the IgG concentration was low and consequently, also low in ruthenium content. So unlike preparing conjugates of, for example BSA where the resultant conjugates were highly coloured, the conjugates of anti-IgG were not very coloured. In order to conduct in depth studies on conjugation to immunological molecules, a sufficient quantity of the anti-IgG is essential. Another aspect which should also be examined is the suitability of the use of mouse spleen cells in these immunofluorescence investigations. Other cell types may possess better binding sites for the immunoglobulin.

The conjugation ratios obtained for the ruthenium conjugates linked to the ε-amino groups of lysine residues are quite similar to those usually reported for FITC preparations. Generally for immunological conjugation 1-4 molecules of FITC per molecule of IgG is recommended for tissue staining procedures and higher ratios could lead to loss of immunological activity and also non-specific staining.

It has been reported that there are approximately 50 lysines available for reaction in IgGs [9], obviously labelling with this number would probably lead to

inactivation of the biomolecule. Most of the literature suggests conjugation ratios much lower than this. In fact, most fluorochrome / protein ratios reported are less than 10 molecules of fluorochrome per molecule of protein (where lysines are modified). Usual initial FITC / IgG ratios are of the order of about 20:1 and result in conjugation ratios of about 4:1, which may indicate that there is limited accessibility of the label to the protein. This would seem to be substantiated in these studies, since use of 100:1 and 200:1 molar excesses of ruthenium complex to IgG did not lead to higher conjugation ratios.

Two small points are worth consideration; (a) any inaccuracies in protein estimation could lead to substantial errors in estimation of the conjugation ratios especially where anti-IgG conjugation is concerned, since the protein concentration is quite low initially and (b) at higher initial molar ratios such as those described, there is a greater chance of inactivation of the immunoglobulin because higher volumes of DMF were required to dissolve the ruthenium complexes and indeed, some precipitation was observed.

Periodate oxidation of the goat anti-mouse IgG and subsequent conjugation to $[Ru(bpy)_2(NH_2phen)]^{2+}$ yielded an F/P ratio of about 1. The average carbohydrate content of IgGs is about 4% consisting of two oligosaccharide chains, so a low conjugation ratio is not surprising. The emission spectrum of this conjugate after extensive dialysis is presented in Figure 4.15 and shows that even at low conjugation ratios emission may still be detected, (assuming

all the unbound label has been removed).

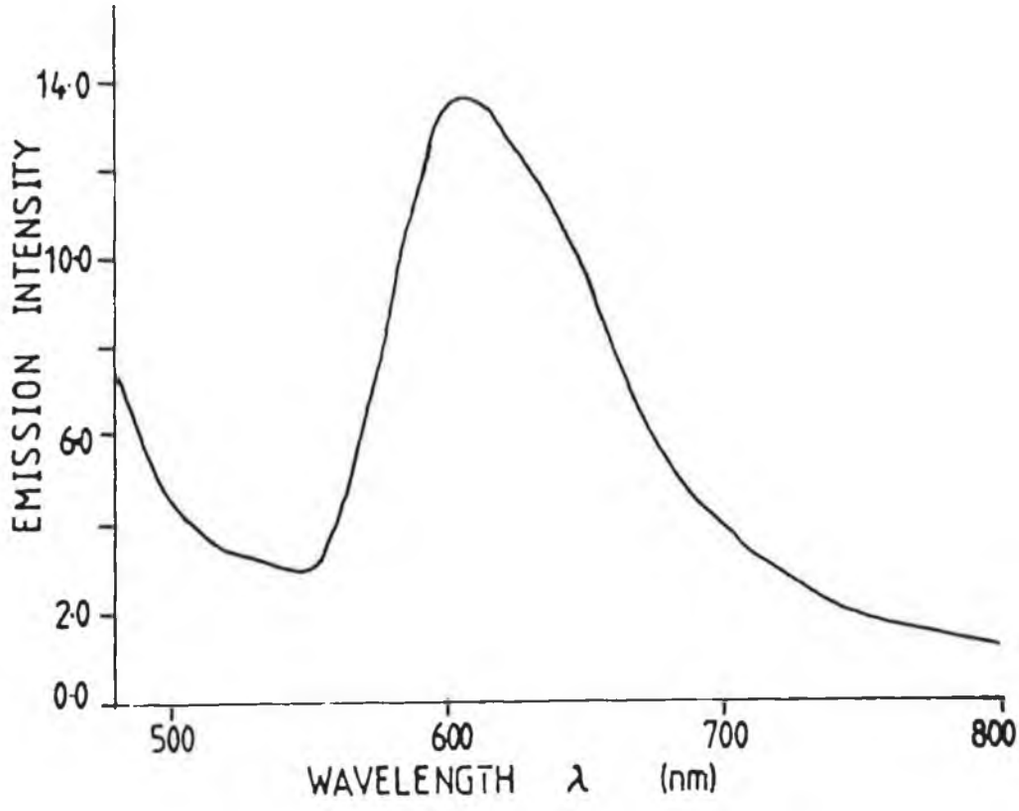

Figure 4.15 Emission spectrum of $[Ru(bpy)_2(NCSphen)]^{2+}$ bound to anti-IgG (pure preparation), measured in 0.1 M carbonate buffer, pH 9.6.

The commonly employed chemical reagents for immunoglobulin conjugations include succinimidyl esters and isothiocyanates which react predominately with the ε-amino groups of lysine residues. This method often leads to poor recovery of the antibody and significant loss of immunological activity.

This has been suggested to be due to modification of lysine residues in or in close proximity to the antigen binding site. Since the carbohydrate moieties of immunoglobulins are not involved in the process of antigen binding and are most often situated on the heavy chain in the F_c portion of the molecule far removed from the antigen binding F_{ab} region, modification of these carbohydrate moieties should not cause a loss of immunological activity, a phenomenon which is more common with monoclonal antibodies rather than with polyclonal preparations.

The oxidation of carbohydrates with sodium periodate is dependent on a number of variables including the concentration of oxidant, pH, temperature and time. [1] Under the suitably mild conditions employed in these studies, the oxidation is made specific for the generation of aldehydes at the exocyclic C7 atom of the sialic acid residues. Sialic acids serve as the terminal residues of the oligosaccharide side chains of glycoproteins and are derived from glucosamine. Under harsher conditions the amino acids serine and threonine may be oxidised, if they occur as terminal residues, and this may lead to a reduction in the specificity of the site of modification. [1]

Inherent in the modification of carbohydrate moieties is the fact that F/P ratios achieved by modification of lysine residues may be higher than those achieved through modification of the carbohydrate sites. The sensitivity of the method of detecting a conjugated reporter molecule whether the reporter molecule is a fluorescent species, an

enzyme or a radioactive species etc. must be considered. Modification of carbohydrate moieties is quite a useful method when the loss of immunological activity is being avoided, but only a small number of reporter molecules can be covalently linked to the oligosaccharide moieties of an immunoglobulin, so the method of detecting the reporter molecules must be sensitive enough to detect the lower number of reporter molecules.

Nairn [4], reports that labelling of immunoglobulins with fluorochromes is not evenly distributed, some molecules are heavily labelled, others optimally and others not at all. This possibility must be taken into account when assessing the results from the ELISA assays. The positive results obtained may originate from the binding of an unlabelled anti-IgG molecule to IgG coated on the microtitre plates rather than from binding of a ruthenium labelled anti-IgG molecule to IgG as depicted below.

]-IgG - goat-anti-mouse IgG - rabbit-anti-goat-Enz*

instead of :

]-IgG - goat-mouse IgG-Ru* - rabbit-anti-goat-Enz*

Immunofluorescence microscopy or fluorescent immunoassay methods would be more definitive in assessing the retention of immunological activity after labelling with the ruthenium fluorochromes, although non-specific staining must also be considered.

Based on the results obtained, it is probably reasonable to assume that if the anti-IgG molecule is not over labelled with reporter molecule, the immunological activity will be retained.

4.2.6 Conjugation of $[Ru(bpy)_2(2,3\text{-butanedione-dihydrazone})](PF_6)_2$ and its isothiocyanate derivative to BSA.

This section describes the use of $[Ru(bpy)_2(2,3\text{-butanedionedihydrazone})](PF_6)_2$ and its isothiocyanate derivative in conjugation procedures. Although these complexes do not emit, presumably because of some deactivation process associated with the 2,3-butanedione-dihydrazone (bdd) ligand, it was hoped that emission from the conjugate would be observed. The idea to attempt this arose from a report regarding the complex $[Ru(bpy)_2(dppz)]^{2+}$, where dppz = phenazine, (Figure 1.13, Chapter 1), which has been reported to be a "molecular" light switch for DNA. [22] The free complex does not emit in aqueous solution, but upon intercalation into DNA, emission is observed. It has been suggested that the unbound complex does not emit because the

nitrogen atoms on the phenazine ring become protonated in the excited state, thus leading to deactivation of the emission process. However, it is unclear whether it is the electronic characteristics of the DNA bases and their overlap with the dppz ring, the accessibility of the dppz ring to protonation or some mixture thereof, that is responsible for the emission of the DNA bound complex. [22]

The complex $[Ru(bpy)_2(2,3\text{-butanedionedihydrazone})](PF_6)_2$ was synthesised and obtained from Joe Bolger at Dublin City University. The ligand 2,3-butanedionedihydrazone is shown in Figure 4.16.

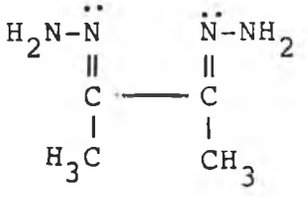

Figure 4.16 Structure of 2,3-butanedionedihydrazone, (bdd).

The isothiocyanate derivative was prepared by reaction with thiophosgene as described in Chapter 2. The absorption spectra of the bdd complex and its isothiocyanate derivative are presented in Figure 4.17.

For conjugation to $[Ru(bpy)_2(bdd)]^{2+}$, BSA was as usual, first oxidised with sodium periodate. The albumin was reacted with a 50 molar excess of the ruthenium complex

and conjugation was allowed to proceed in the usual manner. After the conjugation reaction was completed, the unbound label was removed by dialysis and the Schiff base was stabilised by reduction with sodium borohydride.

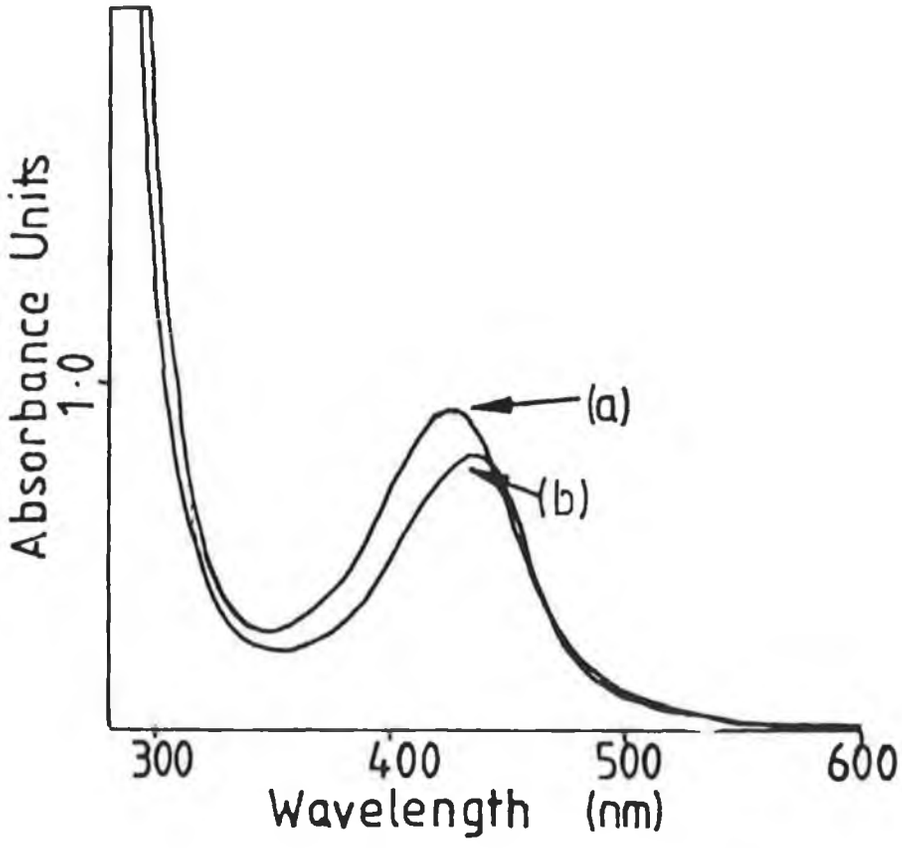

Figure 4.17 Absorption spectra of (a) $[Ru(bpy)_2(bdd)]^{2+}$ and (b) $[Ru(bpy)_2(NCSbdd)]^{2+}$, in 0.1 M carbonate buffer, pH 9.6. Ruthenium complex concentrations in the range 7.5×10^{-4} to 1×10^{-5} M.

The isothiocyanate derivative was reacted with BSA also and the unreacted label was removed by dialysis. The absorption spectra of the two conjugates are presented in Figure 4.18. The protein concentration was determined using the Folin-Lowry method. The absorption data pertaining to the bound and free complexes are presented in Table 4.6.

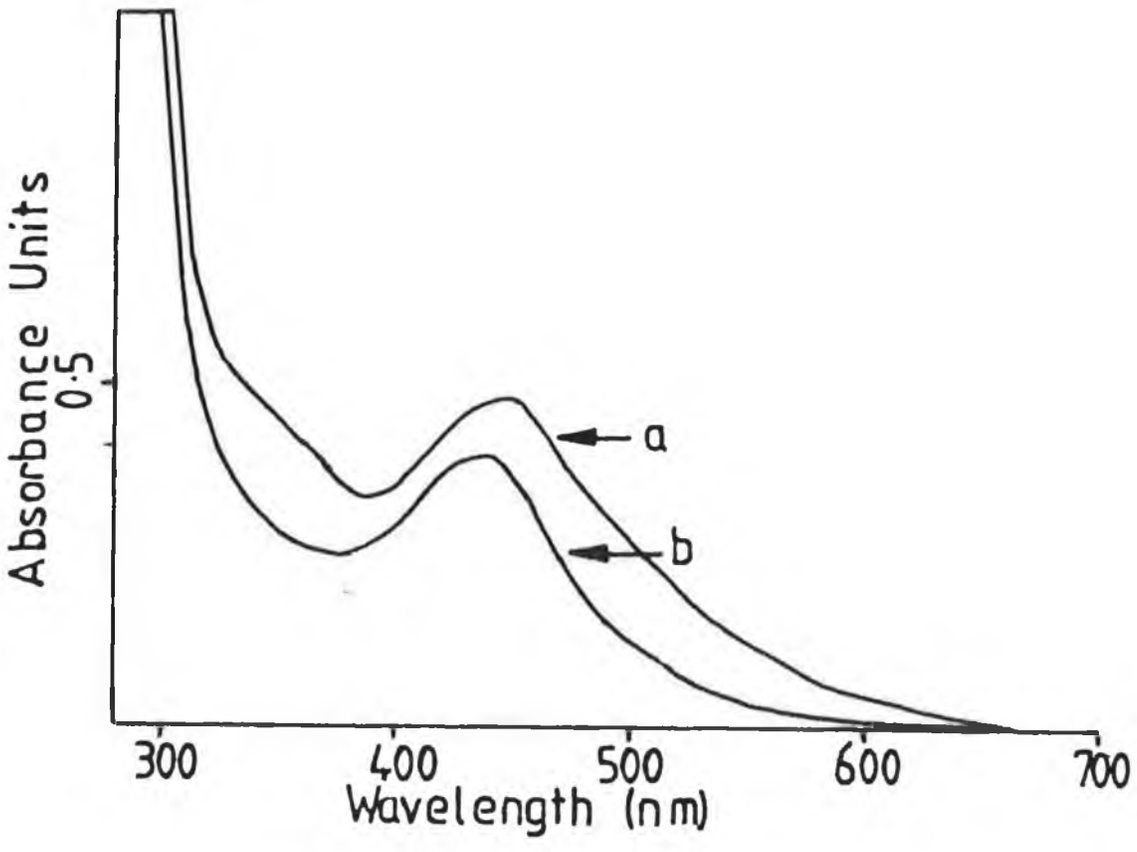

Figure 4.18 Absorption spectra of the complexes (a) $[Ru(bpy)_2(bdd)]^{2+}$ (3×10^{-5} M) and (b) $[Ru(bpy)_2(NCSbdd)]^{2+}$ (6×10^{-5} M), conjugated to BSA, measured in 0.1 M carbonate buffer, pH 9.6.

As expected the F/P ratio for the complex bound via the carbohydrate moiety is considerably lower than that for conjugation via the lysine residues. It seems probable that only one of the NCS groups (if the two NH_2 groups were both converted to NCS groups), would bind per lysine molecule. The F/P ratio for conjugation to the isothiocyanate is somewhat lower than those obtained for the other conjugates of BSA modified at the lysine residues. However, the structural nature of the ligand may prevent the complex from coming into close contact with the protein molecule, unlike the NCSphen or NCSpy ligands where the NCS moiety can quite easily come into close contact with the protein molecule.

As can be seen from the absorption spectra for both of the conjugated complexes, the ^{3}MLCT band is red shifted and broadened considerably upon conjugation to BSA. Similar effects have already been described for the other BSA-bound ruthenium conjugates.

The use of these complexes as fluorescent probes is not possible since both the bound and free complexes do not emit, presumably the 2,3 butanedionedihydrazone ligand and its isothiocyantae derivative contribute to the deactivation of the emission process. However, conjugation of these complexes to BSA demonstrates the flexibility of using amino and isothiocyanate ruthenium polypyridyls for binding to proteins.

Table 4.6 **Absorption data and F/P ratios achieved using the ruthenium complexes incorporating the bdd and NCSbdd ligands.**

Complex / Conjugate	Absorption λ max. (nm) (1)	F/P ratio (2)
$[Ru(bpy)_2(NCSbdd)]^{2+}$	425 (3.93)	-
$[Ru(bpy)_2(NCSbdd)]^{2+}$: BSA	438	8
$[Ru(bpy)_2(bdd)]^{2+}$	435 (4.12)	-
$[Ru(bpy)_2(bdd)]^{2+}$: BSA	445	3

(1) Absorption spectra were measured in 0.1 M carbonate buffer pH 9.6. Extinction coefficients measured in 0.1 M carbonate buffer, pH 9.6, are in parentheses, units are M^{-1} cm^{-1}, log ε .

(2) Protein conc. was measured using the Folin-Lowry method. The F/P ratios were determined according to Nairn. [4]

4.2.7 Emission lifetime measurements of selected ruthenium complexes and their conjugates of BSA and PLL.

The emission lifetimes of selected BSA and PLL conjugates, together with the unbound complexes, were measured using the time correlated single photon counting technique (TCSPC). The measurements were carried out in aerated, oxygenated and degassed solutions in 0.1 M carbonate buffer, pH 9.6, at 23^{o}C. Upon binding of BSA and PLL, the complexes display essentially double exponential decay behaviour, with a component which is substantially longer than the unbound and a second component which is short-lived with a lifetime about the same or shorter than the unbound complexes. This behaviour was exhibited in aerated, degassed and oxygenated solutions.

The results have been presented in Table 4.7. The emission decay lifetimes of $[Ru(bpy)_3]^2$ and $[Ru(phen)_3]^{2+}$ measured in aqueous solutions are also included. [23]

The lifetimes of the excited states of the protein bound ruthenium complexes were compared to those of the free complexes. The excited state decay of both $[Ru(bpy)_2(NH_2phen)]^{2+}$ and $[Ru(phen)_2(NH_2phen)]^{2+}$ can be fitted well by single exponential kinetics. (Figures 4.19 and 4.20). The excited states of both complexes are efficiently quenched by oxygen.

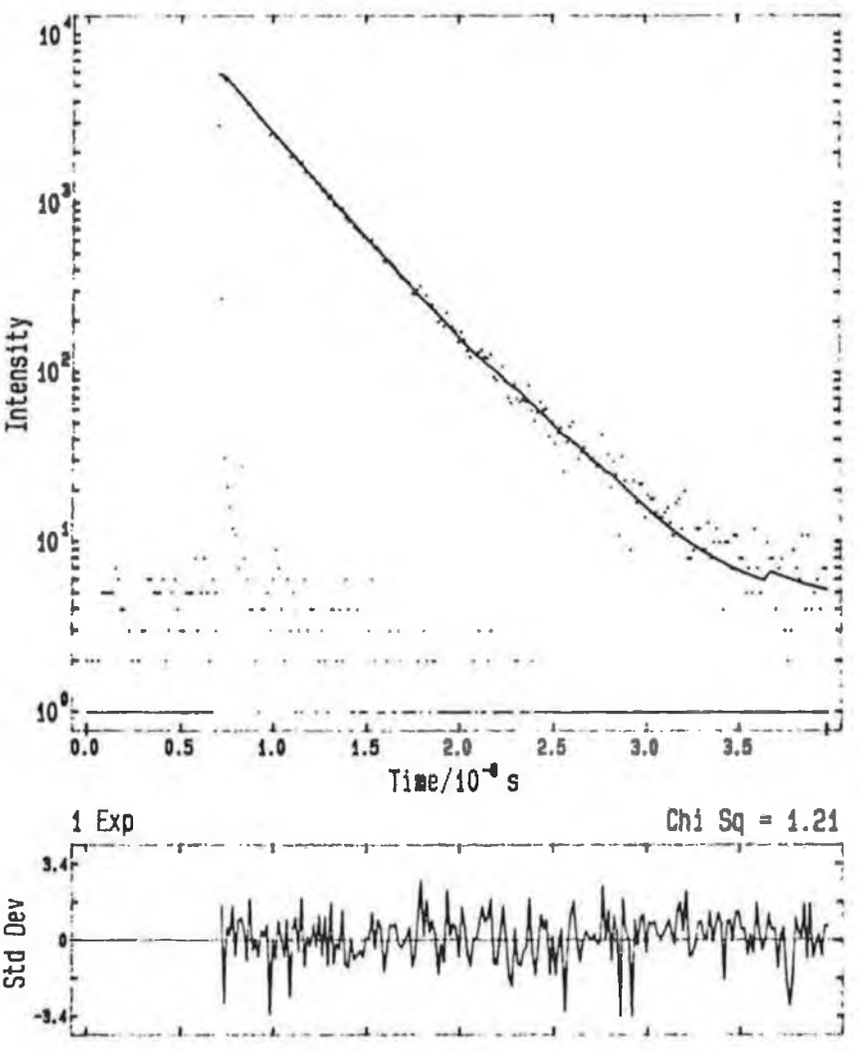

Figure 4.19 Emission decay profile of $[Ru(bpy)_2(NH_2phen)]^{2+}$ in an aerated solution of 0.1 M carbonate buffer, pH 9.6.

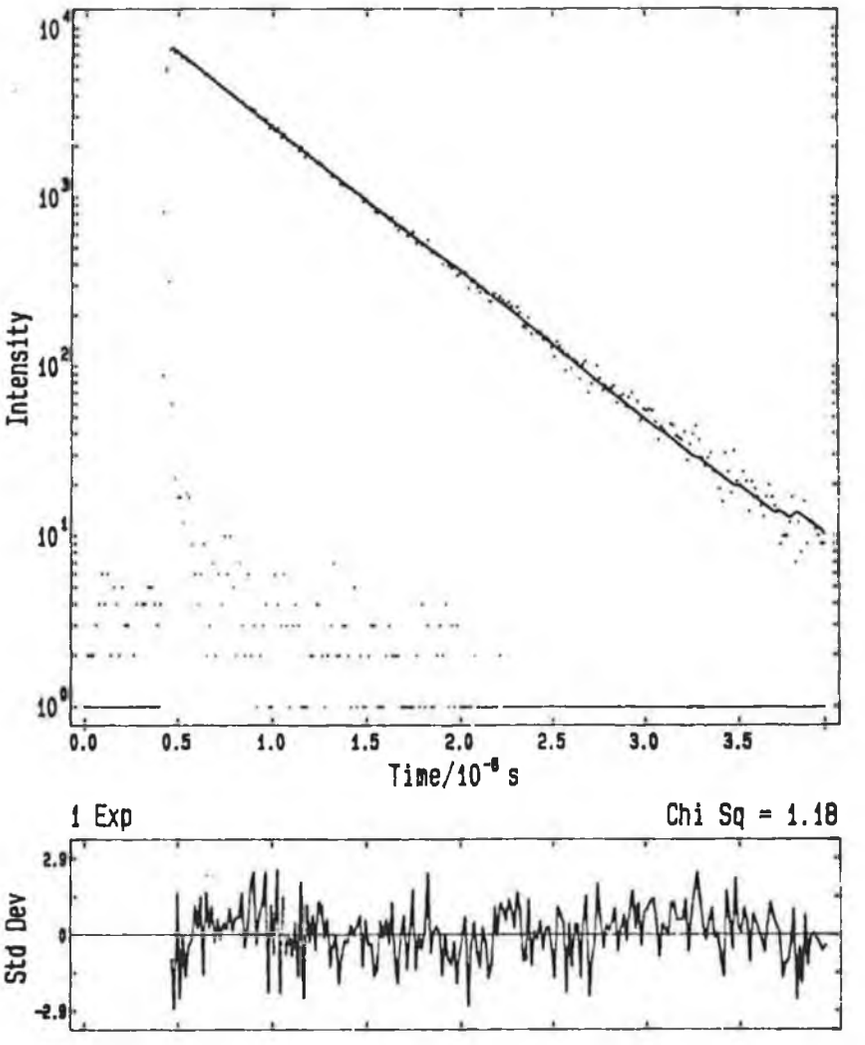

Figure 4.20 Emission decay profile of $[Ru(phen)_2(NH_2phen)]^{2+}$ in an aerated solution of 0.1 M carbonate buffer, pH 9.6.

Lifetime measurements were also carried out with the $[Ru(phen)_2(NCSphen)]^{2+}$ and $[Ru(bpy)_2(NCSphen)]^{2+}$ complexes but the fits were less good for single exponential kinetics, (possibly as a consequence of impurities or of the instability of these complexes). Interestingly, the measured lifetimes of the isothiocyanate derivatives are substantially longer than those recorded for the corresponding $[Ru(bpy)_2(NH_2phen)]^{2+}$ and $[Ru(phen)_2(NH_2phen)^{2+}$ and indeed for the $[Ru(bpy)_3]^{2+}$ and $[Ru(phen)_3]^{2+}$ complexes, which may be indicative of an increase in the energy gap between the emitting state and the metal centered deactivating state.

As stated earlier, none of the lifetimes of the excited states of the conjugates could be fitted to single exponential kinetics. In some cases triple exponential analysis gave better fits, but still indicated the dominance of two exponential decays. Even in the case of poly-L-lysine conjugates where only one type of amino acid is present, double exponential analyses were required to obtain an acceptable fit. Figures 4.21 and 4.22 show emission decay profiles for $[Ru(bpy)_2(NCSphen)]^{2+}$ bound to PLL, fitted to a single exponential decay (Figure 4.21) and to a double exponential decay (Figure 4.22). Further investigations are ongoing to determine whether these decays (for both BSA and PLL conjugates) are truly double exponential or if triple exponential kinetics fit the experimental data better.

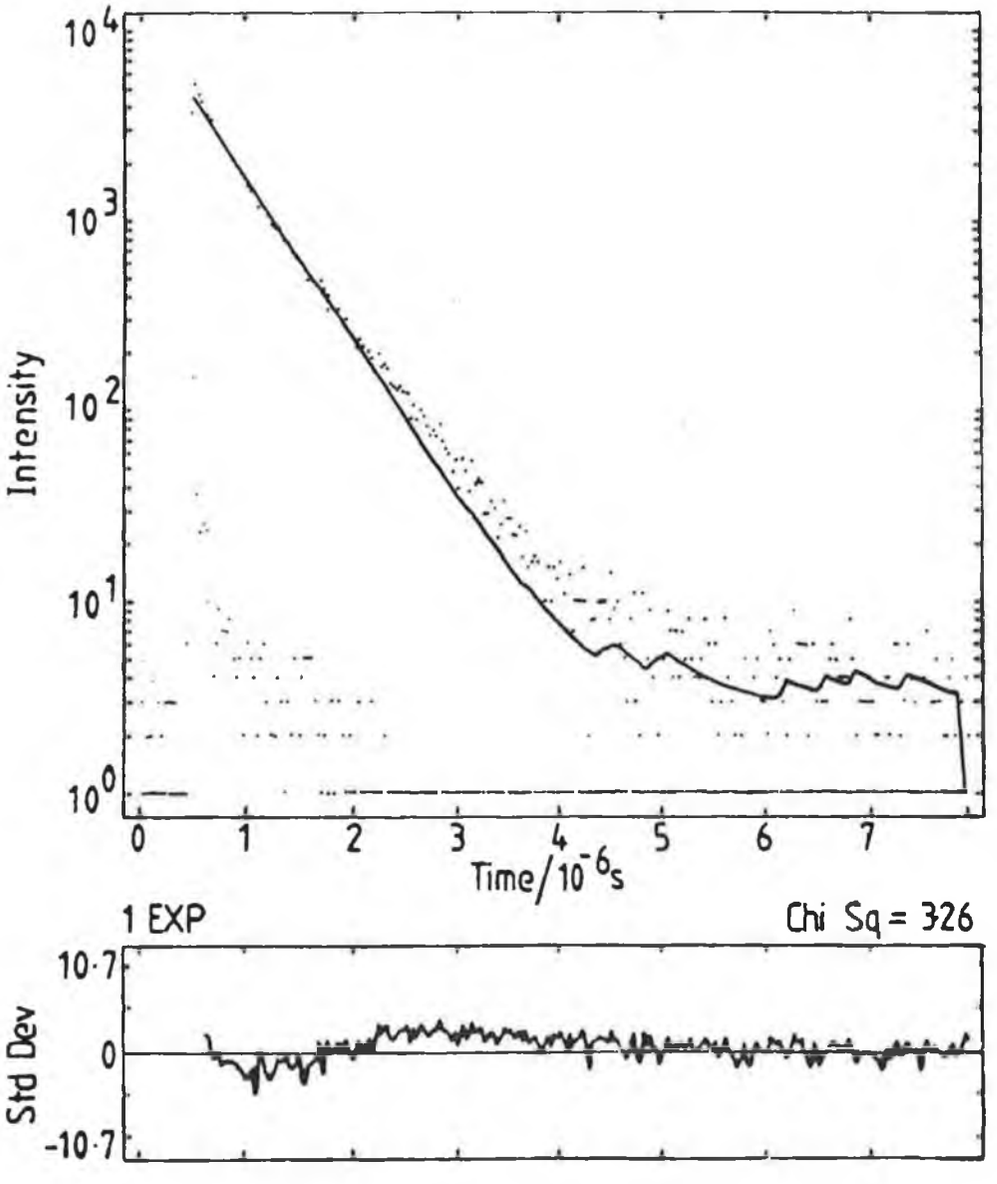

Figure 4.21 Emission decay profile for $[Ru(bpy)_2(NCSphen)]^{2+}$ conjugated to PLL fitted to single exponential decay kinetics, measured in an aerated solution of 0.1 M carbonate buffer, pH 9.6.

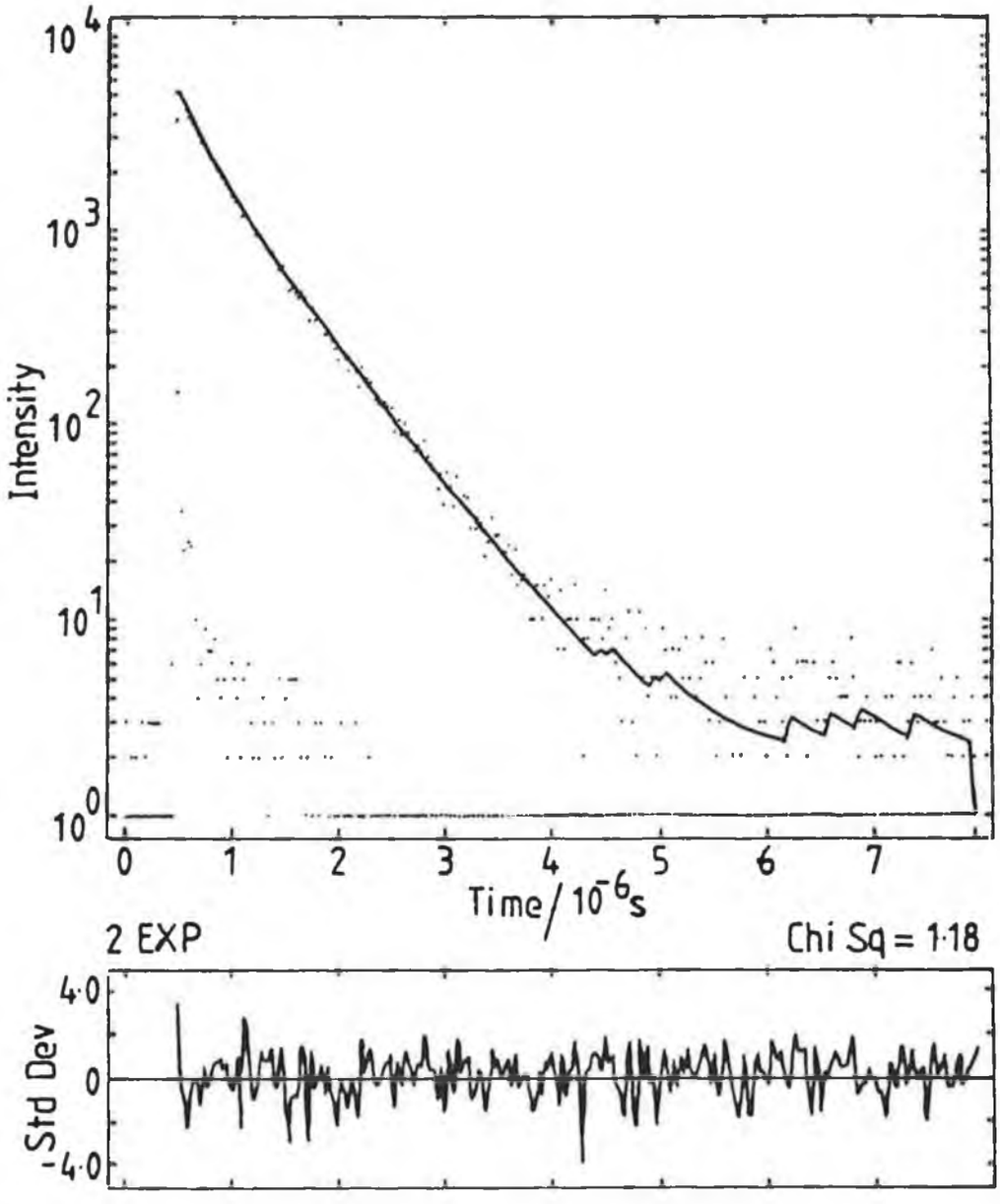

Figure 4.22 Emission decay profile for $[Ru(bpy)_2(NCSphen)]^{2+}$ conjugated to PLL fitted to double exponential decay kinetics, measured in an aerated solution of 0.1 M carbonate buffer, pH 9.6.

Table 4.7 Emission decay lifetimes for the bound and unbound complexes measured in 0.1M carbonate buffer, pH 9.6.

Complex / Conjugate	Lifetime(ns) Oxygenated (1)	Aerated (2)	Degassed (3)
$[Ru(bpy)_2(NH_2phen)]^{2+}$	177 (1.05)	330 (1.18)	610(1.23)
$[Ru(bpy)_2(NH_2phen)]^{2+}$ / BSA	299 [77]	320 [63]	376 [60]
	808 [23]	931 [37]	1111 [40]
	(1.10)	(1.17)	(1.16)
$[Ru(phen)_2(NH_2phen)]^{2+}$	156 (1.30)	470 (1.18)	658(1.08)
$[Ru(phen)_2(NH_2phen)]^{2+}$ / BSA	253 [76]	305 [74]	280 [60]
	761 [34]	1018 [26]	1206 [40]
	(1.47)	(1.28)	(1.43)
$[Ru(bpy)_2(NCSphen)]^{2+}$	178 (1.54)	425 (1.23)	780(1.12)
$[Ru(bpy)_2(NCSphen)]^{2+}$ / BSA	363 (88)	460 (65)	525 (56)
	810 (12)	909 (35)	1092 (44)
	(1.74)	(1.34)	(1.11)
$[Ru(bpy)_2(NCSphen)]^{2+}$ / PLL	186 [80]	256 [52]	178 [48]
	431 [20]	593 [48]	550 [52]
	(1.25)	(1.18)	(1.30)
$[Ru(bpy)_2(NCSphen)]^{2+}$ /anti-Ig	--	616 [68]	--
	--	1097 [32]	--
		(1.20)	
$[Ru(phen)_2(NCSphen)]^{2+}$	169(1.34)	640(1.20)	1201(1.76)(4)
$[Ru(phen)_2(NCSphen)]^{2+}$ / BSA	314 [73]	447 [57]	519 [59]
	762 [27]	1210 [43]	1380 [41]
	(1.44)	(1.15)	(1.14)
$[Ru(phen)_2(NCSphen)]^{2+}$ / PLL	147 [65]	237 [39]	278 [55]
	384 [35]	601 [61]	880 [45]
	(1.37)	(1.09)	(1.75)
$[Ru(bpy)_3]^{2+}$ (5)	150	370	580
$[Ru(phen)_3]^{2+}$ (5)	150	470	960

Samples were measured in (1) 0.1 M carbonate buffer pH 9.6, which was oxygenated for 30 mins, then about 0.2 ml of sample was added and further oxygenated for 15 mins; (2) aerated solution of 0.1 M carbonate buffer, pH 9.6; (3) 0.1 M carbonate buffer, pH 9.6 was degassed with argon for 30 mins, then about 0.2 ml sample was added and further degassed for 15 mins.
(4) A double exponential fit was also obtained, 915 ns [56] and 1530 ns [44], (1.38). (5) Ref. 23.
Figures in [ ] represents the proportion of each species.
Figure in ( ) are the chi. sq. values.

The use of mixed ligand complexes might lead to complications in analysing the double exponential behaviour of the conjugates, since there is the possibility (although not very likely, based on the electrochemical results), of two types of ligand participating in the emission process. However, it has been shown for $[Ru(bpy)_2(phen)]^{2+}$ [24], and indeed for the complexes investigated here, that these exhibit single exponential behaviour in the free form. For mixed ligand complex interactions with DNA, it has been assumed generally that only one type of ligand is involved in the emission process from the DNA bound complexes. This assumption has been carried through in this work.

Both of the recorded lifetimes of the BSA and anti-IgG conjugates are longer than those of the PLL conjugates suggesting that the PLL molecule may be more accessible to the oxygen quencher.

As a first approximation, it may be assumed that decays are double exponential, consisting of a long-lived bound species and short-lived unbound / quenched bound species. On closer examination of the short-lived component, it seems unlikely that this species is the unbound form, since the lifetime of the free form in degassed solution is much longer than the lifetime of the short-lived species in degassed conjugate solutions. Also, all unbound material should be removed after dialysis, which removes the unbound label. Therefore, this component could be the bound form, which appears to be considerably quenched even in the absence of oxygen. In the absence of oxygen, other deactivation

mechanisms must also play a role otherwise no change in emission on binding would be observed in degassed solution. Bound excited complexes may be quenched by triplet-triplet annhilation (collision of two excited complexes) or by self-quenching (collision of excited and ground state).

Triplet-triplet annhilation has been proposed to cause quenching of DNA bound $[Ru(bpy)_3]^{2+}$, but in that case, high laser excitation intensities were employed [25], unlike in these studies where a low intensity lamp was used. So triplet-triplet annhilation most likely is not significant. Self-quenching is another possibility but this is not likely to be of much significance either since the lysine residues on the albumins are well separated from each other and for the PLL conjugates the Ru/PLL ratio is about 1:30, implying that the ruthenium molecules may not come into contact with each other for this process to occur. However, it is difficult to dismiss these possibilities entirely and further detailed investigations are required.

This phenomenon of a long-lived component and a short-lived component also occurs for ruthenium polypyridyl interactions with DNA. The reason for the short-lived component has not really been elucidated. It is thought that this component may be due to an unbound or bound quenched species most probably the latter since in degassed solution as in this work the short-lived component was still considerably shorter in comparison to the free complex, where the emission decay lifetime is considerably longer in degassed solutions.

It is worth pointing out that the long-lived species can be a composite of several decays from complexes bound to the same chemical site but at different locations along the albumin or PLL molecules.

In the absence of quenching, various factors may result in the enhancement of the emission lifetime, (a) protection from quenching in the sheltered environment of the protein molecule, (b) changes in the solvent environment, (c) a decrease in the vibrational activity of the complex as it is held in a more rigid environment and (d) an increase in the energy gap between the emitting state and the metal centered deactivating state.

It seems likely that (b) and (c) do not play very significant roles in explaining why enhancement of the emission lifetimes of the ruthenium conjugates occurs here. The free and bound complexes have been measured in the same solvent so obviously it is not just the solvent which contributes to the enhancement of emission lifetime, although changes from solvent to solvent would be expected.

The decrease in vibrational activity of the complex would be expected to be of more relevance for intercalation of the ruthenium complexes into DNA. Here, the ruthenium complex is probably not held much more rigidly than it is in the free form, although this would depend to a certain degree on the conformation of the protein molecule and the extent to which the complex is surrounded by protein.

The two main factors governing the enhancement of the emission decay lifetimes are probably (a) and to a

certain extent (d). From the results it can be seen that binding to the large protein and PLL molecules affords considerable protection from quenching effects. Also it has been shown in preliminary studies on the interaction of $[Ru(phen)_3]^{2+}$ with DNA, that enhancement of emission is partly due to a reduction in thermal deactivation. This requires an increase in the energy gap between the emitting state and the higher lying metal centered state which is responsible for thermal deactivation. [23] It is possible that similar effects for the conjugates discussed here could in part be responsible for the increased emission lifetimes.

Consideration of all the parameters involved in the interaction of ruthenium polypyridyls with protein molecules leads to the conclusion that the excited state decay behaviour of the conjugates could be quite complicated. It is unlikely that from these studies, a clear understanding of what is involved will be obtained, but these investigations will hopefully point the way towards unravelling the processes involved in the emission decays of the albumin / PLL bound ruthenium complexes.

The presence of two components (if not more) is consistent with the complexes occupying a number of different sites on the albumin / PLL molecules.

The effect of triplet oxygen on quenching was estimated by calculating K_q, the quenching rate constant using the Stern-Volmer equation:

$$1 / \tau = 1 / \tau_o + K_q [Q]$$

where τ = quenched lifetime in aerated or oxygenated solutions, τ_o = unquenched lifetime in degassed solution, K_q = quenching rate constant and [Q] = concentration of quencher, in aerated solutions $[O_2]$ = 0.265 mM and in oxygenated solution $[O_2]$ = 1.33 mM. [23] The results have been tabulated in Table 4.8.

The oxygen quenching rate constants are markedly reduced for the long components of the BSA and PLL conjugates, which shows that the excited states of the bound complexes are protected from quenching by oxygen.

Substantial differences between the PLL and BSA conjugates may be observed, with both of the recorded lifetimes being longer for the BSA conjugates than for the PLL conjugates. This is reflected in the calculated quenching rate constants which are lower for the BSA conjugates than for the PLL conjugates indicating that the PLL molecule may be more accessible to oxygen than BSA. The values shown in Table 4.8 are only indicative as one representative emission decay profile was chosen to calculate K_q. No attempt has been made to quantify errors in this calculation since to do so would be misleading inferring accuracy in the measurements. Also, the levels of oxygen

present in the aerated and oxygenated solutions used in this work were assumed to be the same as those reported in the literature, [23] and deviations from these values for the solutions used in this work would lead to inaccuracies in the calculated K_q values.

The two recorded lifetimes of the $[Ru(bpy)_2(NCSphen)]^{2+}$ / anti-IgG conjugates are longer than those of either the BSA or PLL conjugates to the same ruthenium complex. The lifetime of the long-lived species is just slightly longer than that of the long-lived species of $[Ru(bpy)_2(NCSphen)]^{2+}$ / BSA, but the lifetime of the shorter component is significantly longer than that of the BSA conjugate indicating that perhaps this second bound component is not as susceptible to quenching and deactivation effects, as the short lived species of the BSA or particularly, the PLL conjugates appear to be.

The long lifetimes of the complexes bound via the carbohydrate moieties on the BSA molecule are quite similar to those measured for the complexes bound via the lysine residues. However, the shorter-lived component is significantly shorter than those of the complexes bound via the lysine residues. This requires further investigation because the actual linkage of each complex to the protein is quite similar, as depicted in Figure 4.23.

Figure 4.8 The triplet oxygen quenching rates for the free and bound ruthenium complexes in aerated and oxygenated solutions.

Emitting species	10^{-9} K_q M^{-1} sec^{-1} aerated	oxygenated
$[Ru(bpy)_2(NH_2phen)]^{2+}$	5.3	3.0
$[Ru(bpy)_2(NH_2phen)]^{2+}$ / BSA	1.8 (s)	0.5 (s)
	0.7 (l)	0.3 (l)
$[Ru(phen)_2(NH_2phen)]^{2+}$	2.3	3.6
$[Ru(phen)_2(NH_2phen)]^{2+}$ / BSA	4.2 (s) *	1.3 (s) *
	1.0 (l) *	0.4 (l) *
$[Ru(bpy)_2(NCSphen)]^{2+}$	4.0	3.3
$[Ru(bpy)_2(NCSphen)]^{2+}$ / BSA	1.0 (s)	0.6 (s)
	0.7 (l)	0.2 (l)
$[Ru(bpy)_2(NCSphen)]^{2+}$ / PLL	3.0 (s) **	1.7 (s) **
	1.2 (l) **	0.7 (l) **
$[Ru(phen)_2(NCSphen)]^{2+}$	2.8	3.8
$[Ru(phen)_2(NCSphen)]^{2+}$ / BSA	1.2 (s)	1.0 (s)
	0.4 (l)	0.4 (l)
$[Ru(phen)_2(NCSphen)]^{2+}$ / PLL	2.4 (s)	2.4 (s)
	2.0 (l)	1.10 (l)

Those figures denoted with asterisks indicate that triplet exponential fits were used to calculate K_q, for the appropriate degassed solution, because the double exponential lifetime fits were less than the aerated or oxygenated values. The third decaying component which is of the order of about 40 - 90 ns not has been taken into account. * 462 ns,1383 ns; ** 319 ns,724ns. (s) denotes short-lived species and (l) denotes long-lived species.

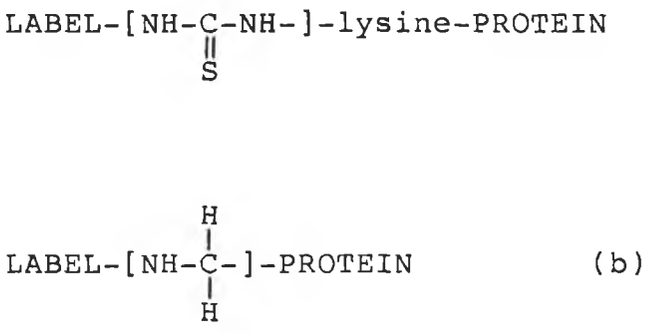

Figure 4.23 Linkage of protein to ruthenium (a) NCS complexes via lysine residues; (b) NH_2 complexes via carbohydrate moieties.

It seems unlikely that the presence of the C=S group in the linkage group from the ruthenium to albumin would account for the longer lifetime of the isothiocyanate complexes. A possible explanation which would be of relevance in immunoglobulin conjugates is that the carbohydrate moieties are located at a specific site on the protein molecule which may lead to self-quenching effects. Since, BSA and HSA are not generally treated as glycoproteins and references to this effect could not be found in the literature, it is difficult to speculate on the location of the carbohydrate moieties. However, it may be reasonable to assume that the carbohydrate moieties are attached to the albumin in a similar manner as they are attached to ovalbumin, which is via the aspargine residues. The asparagine residues are few in number and are

well spaced out on the BSA molecule so self-quenching effects may not in fact be of relevance here. What may be significant is that asparagine is an uncharged polar amino acid whilst in contrast lysine is a non-polar amino acid. So the orientation of the asparagine residues on the albumin molecule may be significant.

The emission lifetime results and indeed K_q values should be taken as being indicative rather than precise values. These measurements were preliminary investigations and changes in lifetime values were found depending on the starting channel of analysis from which the estimation of the fit was calculated. The stop channel was the same throughout but the start channel could be varied and depending on where this channel was chosen differences in lifetimes were observed. If the analysis was started at the lowest possible channel, the fits were less good, probably because of the inclusion of the lamp profile. However, when the analysis was started at the channel with the greatest number of counts or the next channel up, good fits were obtained. The results presented in this work are those obtained from fits where the analysis of the fit was started at the channel with the greatest number of counts.

Another factor which should be considered is the possibility of "pile up", which depends on the pulse rate of the flash lamp. The "pile up" effect may occur if the lamp in pulsing at a faster rate than that of the decay of the ruthenium complexes. This was not a problem in these

measurements since the pulse rate of the flash lamp was set at a much slower rate than the decay of the sample.

The effect of purging protein solutions with either oxygen or argon could lead to denaturation of the protein molecules. This was circumvented (it is hoped) by purging the buffer before addition of the sample after which the solution was only purged for a further 15 mins.

Factors such as the number of counts to collect before analysing data and which the time-scale to use should also be considered. In general 5,000-10,000 photons were accumulated in the highest channel, before the measurement was finished. If the TAC (time to amplitude converter) scale is not set appropriately, the full decay profile may not be measured leading to errors in the calculated lifetimes.

Obviously, the effects of all these parameters on the calculated lifetime need to be taken into account. Also, it is of course preferable that the measurements should be made in at least duplicate if not in triplicate.

4.3 Conclusion

In this chapter, the conjugation of a number of ruthenium polypyridyl complexes to albumins, immunoglobulins and poly-L-lysine is described.

The complexes were bound at different sites on the biomolecules, via the lysine residues, the carbohydrate

moieties, and via the tyrosine residues. This demonstrates the chemical flexibility available for using these complexes as reporter molecules. Conjugation via the lysine residues has generally remained the most widely used method of conjugating reporter molecules to proteins, mainly through the use of isothiocyanate moieties or succinimidyl ester moieties on the label molecule. This work has shown that these moieties may be introduced on ruthenium polypyridyl compounds.

The conjugation ratios were estimated and the importance of considering which protein assay to employ depending on where the reporter molecule binds, in order to determine the protein concentration was highlighted..

The effect of conjugation on the spectroscopic properties of the complexes has been examined. The absorption spectra were found to exhibit changes in the ^{3}MLCT band, with the absorption wavelength maximum experiencing slight red shifts together with general band broadening effects. These effects have also been found for ruthenium polypyridyls upon interaction with DNA, with an additional effect of hypochromicity of the band maximum. It is possible this also arises in this work but the nature of the conjugation procedure (i.e. the necessity of having to separate the unbound label), precludes the possibility of investigating this phenomenon.

The emission spectra were measured, however changes in the spectra upon conjugation are difficult to

monitor since the emission band is broad and only slight changes in the emission λ max. were observed. In addition, these changes are within instrumental error. For future studies it would be useful to monitor the changes in emission intensity upon conjugation.

The emission decay behaviour has also been studied. The unbound complexes were found to exhibit single exponential decay behaviour and the bound complexes exhibited what is essentially double exponential decay behaviour, however, a third decaying component may be present. From the double exponential decay fits, the first short-lived component was deemed to be a quenched bound species whilst the second much longer-lived species probably arises from a bound complex which is considerably protected from the effects of quenching molecules.

The effect of oxygen on quenching was examined. It was found that the short-lived component was more efficiently quenched than the long-lived component which exhibited quite a long lifetime in the presence of oxygen and which suggests that this species is indeed protected from the effects of quenching molecules. It was also found that the two decay components of the PLL conjugates were more effectively quenched by oxygen than those of the BSA conjugates, which is perhaps related to the structural conformation of these molecules. It was also observed that for those complexes bound via the carbohydrate moieties, the short-loved component was significantly shorter than those of the conjugates bound via the lysine residues. It is

difficult to explain this but the effect obviously requires further investigation.

Much of the work described in this chapter represents initial experiments into the use of these ruthenium complexes as reporter molecules in biological systems. The interaction of ruthenium polypyridyls with DNA has received extensive examination by various groups but the use of these complexes as labels for albumins and immunoglobulins has not been as extensively studied, particularly in terms of the effects of conjugation on the spectroscopic properties of the label molecules, but also regarding conjugation ratios and the significance of targeting different sites on the biomolecules. The literature describes the conjugation of ruthenium polypyridyl succinimidyl esters to albumins, immunoglobulins and nucleotides and the subsequent use of these conjugates in time-resolved measurements and in fluorescence microscopy and which have been described in a number of patents. [11,26]

These investigations will hopefully initiate detailed examination of the complexes in two main areas, (a) the study of these complexes in terms of their emission decay behaviour with the possibility of their application as probes of protein structure and (b) the use of these complexes in regard to their potential application as reporter molecules in time-resolved immunoassay techniques.

4.4 References

[1] D.J. O Shannessy and R.H. Quarles, J. Immunol. Meth.. 1987, 99, 153.

[2] A. Lehninger, Biochemistry, Worth Publishers Inc., New York, 1979.

[3] M.W. Sundberg, C.F. Meares, D.A. Goodwin and C.I. Diamenti, J. Med. Chem., 1974, 17, 1304.

[4] R.C. Nairn, Fluorescent Protein Tracing, 4th edition, Churchill Livingstone, London, 1976.

[5] M.M. Bradford, Anal. Biochem., 1976, 72, 248.

[6] G.L. Peterson, Anal. Biochem., 1979, 100, 201.

[7] S. Mirzadeh, M.W. Brechbiel, R.W. Atcher and D.A. Ganson, Bioconjugate Chem., 1990, 1, 59.

[8] G.D. Fasman, (Ed.), Handbook of Biochemistry and Molecular Biology, Proteins, Vol. 3, 3rd edition, CRC Press, Ohio, 1976.

[9] A. Canfi, M.P. Bailey and B.F. Rocks, Analyst, 1989, 114, 1407.

[10] R.M. McKinney and J.T. Spillane, Ann. New York Acad. Sci., 1975, 254, 55.

[11] A.J. Bard, Luminescent Metal Chelate Labels and Means for Detection, U.S. Patent Application, PCT/US85/02153, 1986.

[12] S. Fazekas de St. Groth, R.G. Webster, and A. Datyner, Biochim. Biophys. Acta, 1963, 71, 377.

[13] S.J. Compton and C.G. Jones, Anal. Biochem., 1985, 151, 369.

[14] D.J. Holme and H. Peck, Analytical Biochemistry, Longman, New York, 1983.

[15] C. Long, Biochemist's Handbook, E. and F.N. Spon Ltd., London, 1961.

[16] D. Samuel, R.J. Patt and R.A. Abuknesha, J. Immunol. Meth., 1988, 107, 217.

[17] A.B. Tossi and J.M. Kelly, Photochem. Photobiol., 49, 545, 1989.

[18] Md. K. Nazeeruddin and K. Kalyanasundaram, Inorg. Chem., 1989, 28, 4251.

[19] R.S. Nezlin and Y.K. Sykulev, Molecular Immunol., 1982, 19, 347.

[20] J. March, Advanced Organic Chemistry, John Wiley and Sons, New York, 3rd edition, 1985.

[21] P. Tijssen, Practice and Theory of Enzyme Immunoassays, Elsevier, New York, 1985.

[22] A.E. Friedman, J-C. Chambron, J.P. Sauvage, N.J. Turro and J.K. Barton, J. Amer. Chem. Soc., 1990, 112, 4960.

[23] A.J. Tossi, Ph.D. Thesis, University of Dublin, Trinity College Dublin, 1987.

[24] E.A. Seddon and K.R. Seddon, The Chemistry of Ruthenium, Monograph 19, Elsevier, Amsterdam, 1984.

[25] C. Stradowski, H. Gorner, L.J. Currell and D. Schulte-Frohlinde, Biopolymers, 1987, 26, 189.

[26] R.S. Davidson, Transition Metal Complexes and Method for Time Resolved Luminescence Binding Assay, British Patent App. No. 8601646, 1986; International Patent No. 8704523, 1987.

CHAPTER 5

PREPARATION, CHARACTERISATION AND ACID-BASE PROPERTIES OF RUTHENIUM COMPOUNDS CONTAINING ASYMMETRIC PYRIDYLTRIAZOLE LIGANDS.

5.1 Introduction

In this chapter, the synthesis and properties of some ruthenium (II) complexes ($[Ru(phen)_2(L\text{-}L')]^{2+}$ or $[Ru(dmbpy)_2(L\text{-}L')]^{2+}$), where L-L' are various substituted 3-(pyridin-2-yl)-1,2,4-triazole ligands are described. The 2,2'-bipyridyl (bpy) analogues have already been described. [1,2], and their properties are compared to those of the complexes investigated here. The complexes have been characterised using NMR, UV/Vis absorption spectroscopy, electrochemistry and emission spectroscopy.

For some of the complexes, geometrical isomers were obtained and have been separated using semi-preparative HPLC techniques. These were subsequently analysed using proton NMR spectroscopy.

The acid-base chemistry (both ground state and excited state) has been studied for those compounds where the 3-(pyridin-2-yl)-1,2,4-triazole ligand may undergo protonation/deprotonation processes.

5.2 Preparation of complexes of the type $[Ru(L\text{-}L)_2(L\text{-}L')]^{2+}$.

Reaction of cis-$[Ru(L\text{-}L)_2Cl_2].2H_2O$ where L-L = 1,10-phenanthroline (phen) or 4,4'-dimethyl-2,2'-bipyridyl (dmbpy) with equimolar amounts of ligand (L-L'), where (L-L') = Hptr, H3Mptr, 4Mptr or 1Mptr (See Figure 5.1 for

structures, numbers, names and abbreviations of these ligands), yielded complexes of the type $[Ru(L\text{-}L)_2\text{-}(L\text{-}L')]^{2+}$. The compounds were isolated as the divalent cations with PF_6^- as the counter ion. For the ligands Hptr and H3Mptr, deprotonation occurs easily, therefore to ensure protonation these complexes were recrystallised from acidic acetone / H_2O mixtures. The purity of the complexes was analysed using the HPLC method described in Chapter 2.

For three of the chelating ligands, Hptr, H3Mptr and 1Mptr, different coordination modes are possible. For Hptr and 1Mptr coordination is possible through the $N^{2'}$ and $N^{4'}$ of the triazole ligand. For H3Mptr coordination is possible through the $N^{1'}$ or $N^{4'}$ of the triazole ring. Clearly only one coordination mode is possible for the ligand 4Mptr.

The mode of coordination is anticipated to be affected by the position of the methyl substituent present on the triazole ring. Since the ligand Hptr does not have a methyl substituent on the triazole ring, it is likely that there is an equal possibility of coordination through either the $N^{2'}$ or $N^{4'}$ sites on the triazole ring.

On the other hand, the presence of a methyl substituent on the triazole ring will cause steric hindrance for coordination at the $N^{2'}$ / $N^{1'}$ and $N^{4'}$ sites on the triazole ring for the complexes $[Ru(L\text{-}L)_2(1Mptr)]^{2+}$ and $[Ru\ (L\text{-}L)_2(H3Mptr)]^{2+}$ respectively. Therefore it is likely that coordination will be primarily through the $N^{4'}$ site for $[Ru(L\text{-}L)_2(1Mptr)]^{2+}$ and through the $N^{1'}$ site

for $[Ru(L\text{-}L)_2(H3Mptr)]^{2+}$. This has already been confirmed for $[Ru(bpy)_2(H3Mptr)]^{2+}$, the X-ray crystal structure of which has been determined. [1]

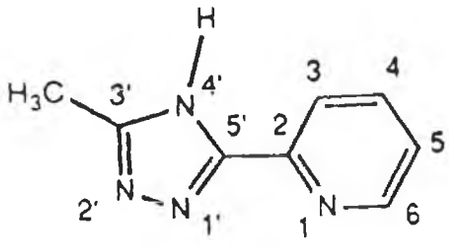

H3Mptr

3-methyl-5-(pyridin-2-yl)-1,2,4-triazole

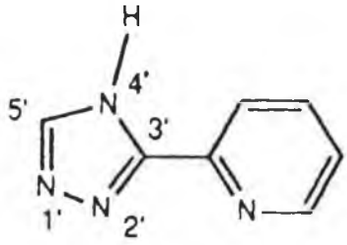

Hptr

3-(pyridin-2-yl)-1,2,4-triazole

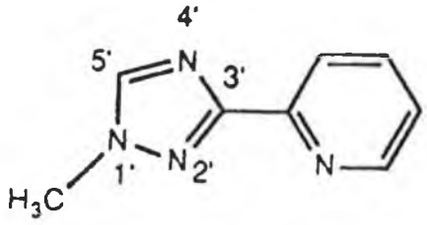

1M3ptr

1-methyl-3-(pyridin-2-yl)-1,2,4-triazole

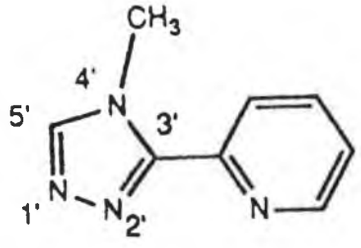

4Mptr

4-methyl-3-(pyridin-2yl)-1,2,4-triazole

Figure 5.1 Structures, names, numbering schemes and abbreviations of the pyridyl-1,2,4-triazole ligands.

5.2.1 HPLC analysis.

The purity and coordination modes of the ruthenium compounds described were analysed using HPLC. The compounds $[Ru(L\text{-}L)_2(Hptr)]^{2+}$ and $[Ru(L\text{-}L)_2(H3Mptr)]^{2+}$ are easily deprotonated and were therefore studied in both a neutral mobile phase (about pH 6-7) and in an acidic mobile phase (about pH 2-3). The compounds $[Ru(L\text{-}L)_2(1Mptr)]^{2+}$ and $[Ru(L\text{-}L)_2(4Mptr)]^{2+}$ were separated using the neutral mobile phase.

The retention time of each complex is listed in Table 5.1. A change in retention time was observed when the Hptr and H3Mptr complexes were separated in both mobile phases. The UV/vis spectrum was obtained for each component. However the different pHs of the two mobile phases did not result in a shift of the wavelength of maximum absorption, which would be consistent with protonation / deprotonation processes occuring. This implies that the compounds remained protonated even in the neutral mobile phase where the pH is about 6-7. This may be due to the fact that the protonated forms were injected onto the HPLC column and possibly stay protonated because the pH of the mainly organic mobile phase may not be high enough to ensure deprotonation. This indicates that the changes in retention time observed in both mobile phases may be caused by a medium effect and not by protonation / deprotonation effects.

5.2.1.1 $[Ru(L\text{-}L)_2(Hptr)]^{2+}$.

These compounds were separated using both mobile phases. Two peaks were obtained which are assigned as the two coordination isomers. The isomers were better separated using the neutral mobile phase (pH about 6-7) in approximately equal ratios, i.e. in this mobile phase there is better peak to peak resolution, (See Figure 5.2).

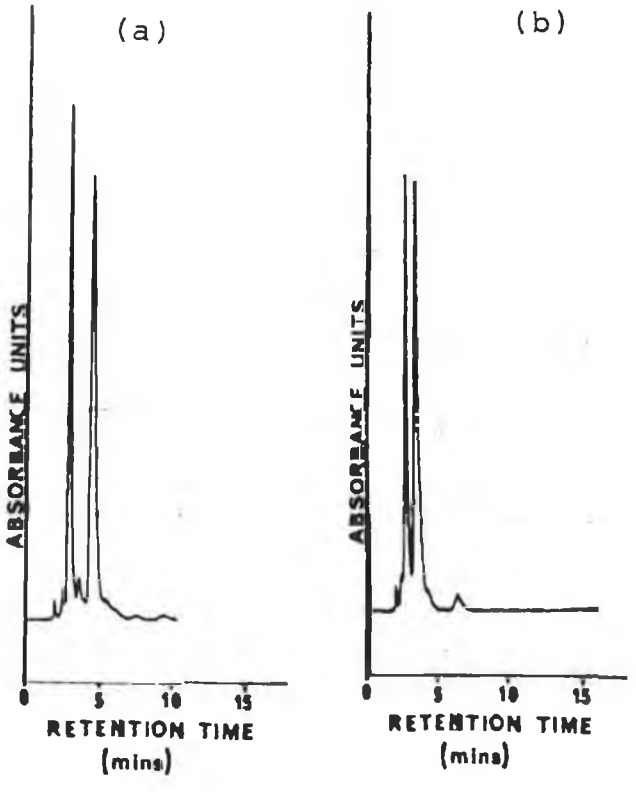

Figure 5.2 Chromatograms of the isomers of $[Ru(dmbpy)_2(Hptr)]^{2+}$ in (a) acetonitrile : water (80:20) with 0.08 M $LiClO_4$ and (b) mobile phase (a) adjusted to pH 2-3 with $HClO_4$. Flow rate = 2.5 ml/min.

Table 5.1 Retention times of the $[Ru(L\text{-}L)_2(L\text{-}L')]^{2+}$ compounds.

Compound		Retention time (min) mobile phase	
		neutral	acidic
$[Ru(dmbpy)_2(Hptr)]^{2+}$	isomer 1	2.67	2.42
"	isomer 2	4.15	3.14
$[Ru(phen)_2(Hptr)]^{2+}$	isomer 1	4.00	3.42
"	isomer 2	6.04	5.20
$[Ru(dmbpy)_2(H3Mptr)]^{2+}$	isomer 1	2.28	2.74
"	isomer 2	2.96	3.62
$[Ru(phen)_2(H3Mptr)]^{2+}$	isomer 1	3.00	3.70
"	isomer 2	4.94	6.08
$[Ru(dmbpy)_2(lMptr)]^{2+}$	isomer 1	2.08	-
"	isomer 2	2.62	-
$[Ru(phen)_2(lMptr)]^{2+}$	isomer 1	2.82	-
"	isomer 2	4.00	-
$[Ru(dmbpy)_2(4Mptr)]^{2+}$		3.14	-
$[Ru(phen)_2(4Mptr)]^{2+}$		5.00	-

The compounds were separated in a neutral (pH about 6-7) mobile phase, acetonitrile : water (80:20) with 0.08 M $LiClO_4$ and in an acidic mobile phase where the neutral mobile phase is adjusted to about pH 2-3 with $HClO_4$. Flow rate = 2.5 ml/min.

These isomers were separated on the semi-preparative HPLC system using the neutral mobile phase, pH 6-7. After separation, the purity of the isomers was checked on the analytical column, (See Figure 5.3).

The coordination isomers of $[Ru(bpy)_2(Hptr)]^{2+}$ have previously been separated using this method. [1]

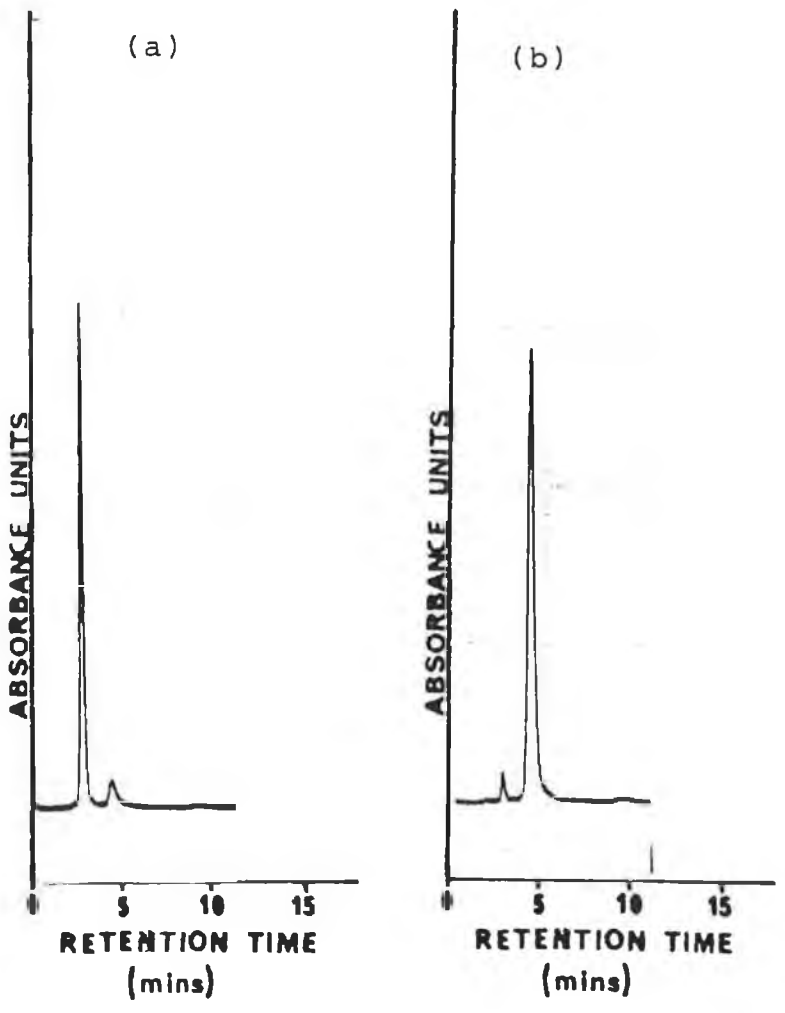

Figure 5.3 Chromatograms of the isomers of $[Ru(dmbpy)_2(Hptr)]^{2+}$ after separation in acetonitrile : water (80:20) with 0.08 M $LiClO_4$. (a) isomer 1 (fraction 1). (b) isomer 2 (fraction 2). Flow rate = 2.5 ml/min.

5.2.1.2 $[Ru(L\text{-}L)_2(H3Mptr)]^{2+}$.

Isomers of these compounds were found to be present after HPLC analysis of the recrystallised products. Although this is not unexpected, only one isomer was observed for the bipyridyl analogues of these compounds. This may be due to solubility factors or to the manner in which the compounds were recrystallised. The ratios of the peaks were approximately 10-20% for isomer 1 (peak 1) and about 80-90% for isomer 2 (peak 2). From these peak ratios, peak 1 is probably due to that isomer where coordination is through the $N^{4'}$ site on the triazole ring which is sterically hindered because of the presence of the methyl substituent, (See Figure 5.4).

The degree of separation was slightly better in the acidic mobile phase. It is possible to achieve separation of the isomers on the semi-preparative HPLC system and isomers were obtained in mg quantities. Their purity was checked as before on the analytical column, (See Figure 5.5).

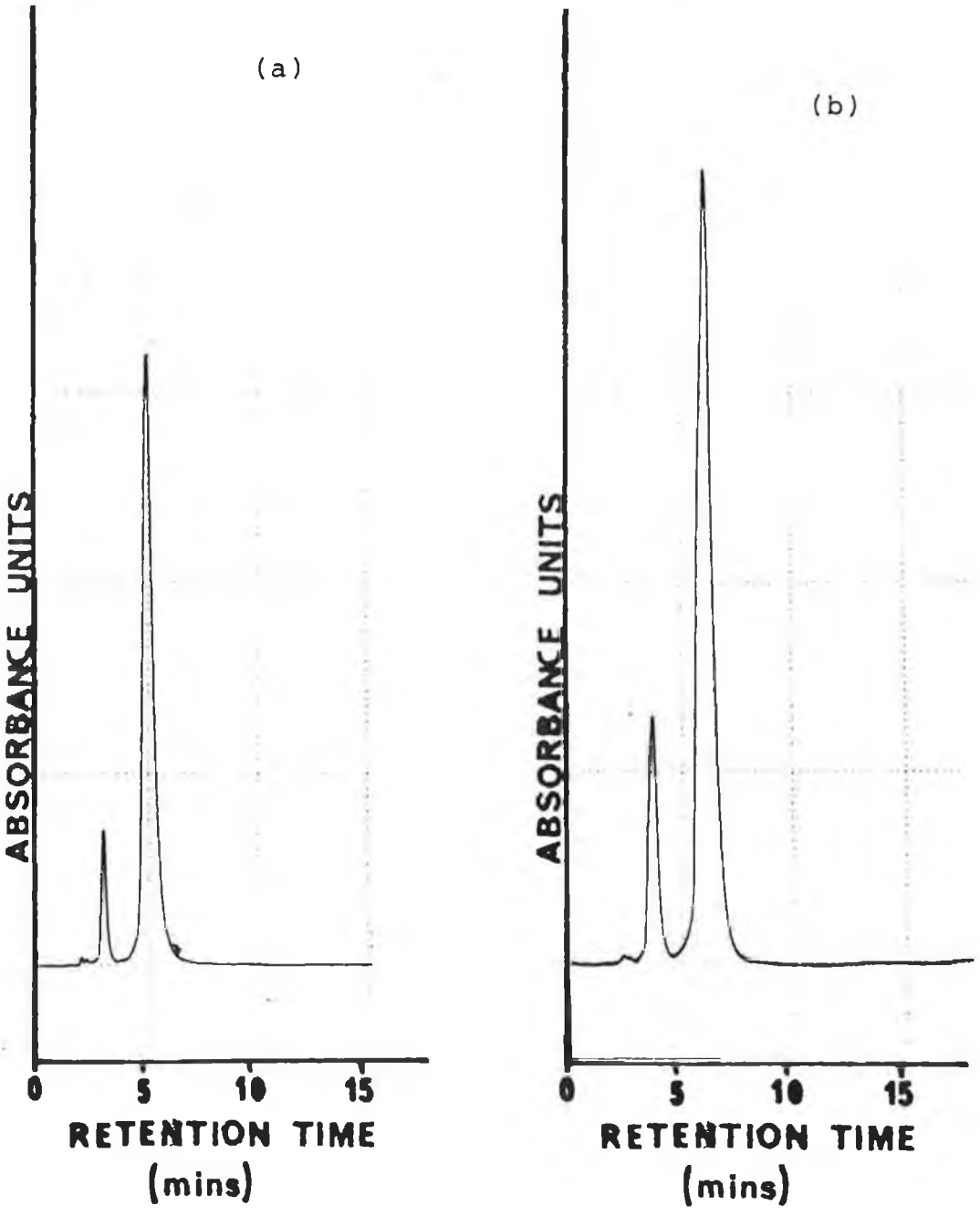

Figure 5.4 Chromatograms of the isomers of $[Ru(phen)_2(H3Mptr)]^{2+}$ in (a) acetonitrile : water (80:20) with 0.08 M $LiClO_4$ and (b) mobile phase (a) adjusted to pH 2-3. Flow rate = 2.5 ml/min.

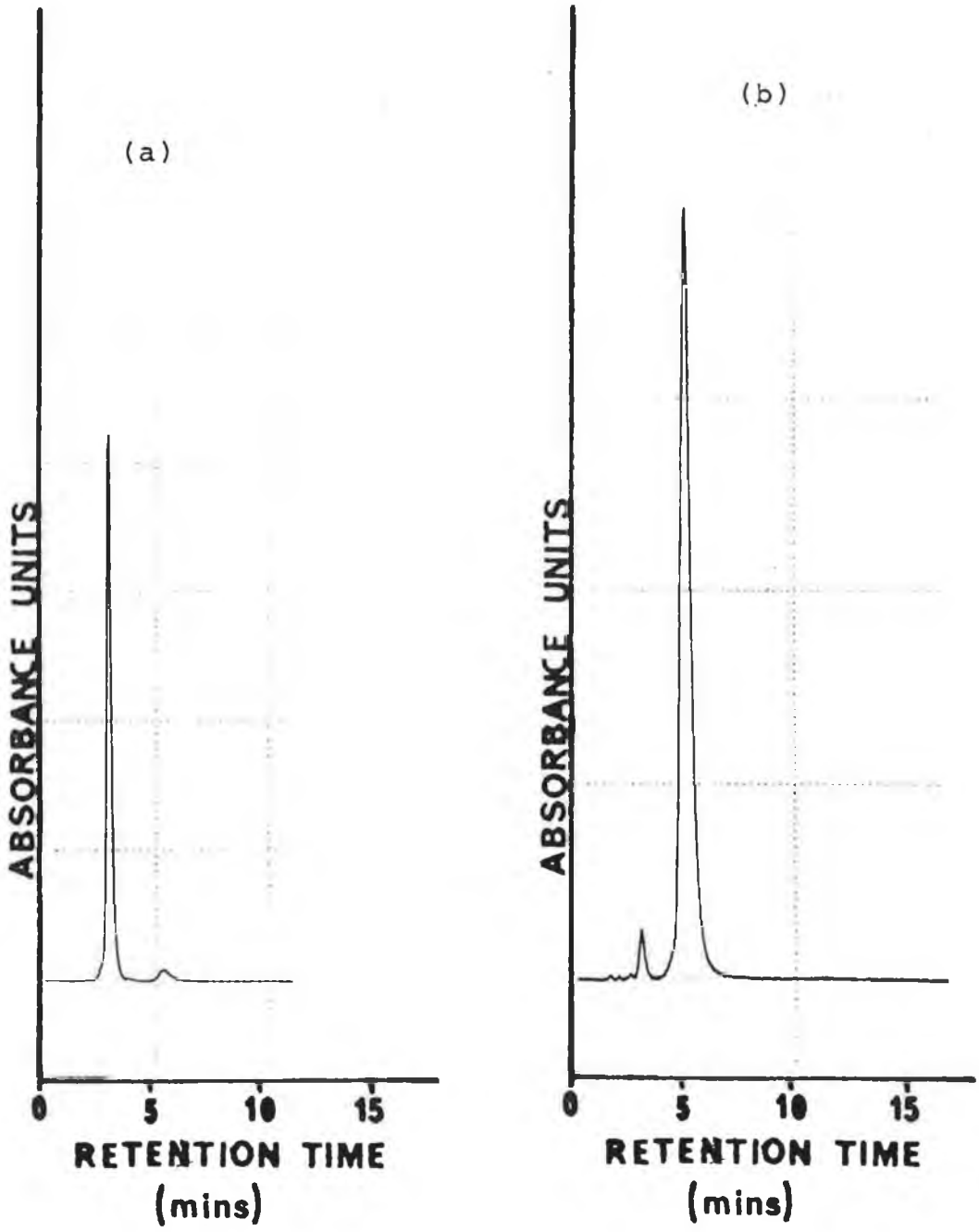

Figure 5.5 Chromatograms of the isomers of $[Ru(phen)_2(H3Mptr)]^{2+}$ after separation in acetonitrile : water (80:20) with 0.08 M $LiClO_4$. (a) isomer 1 (fraction 1), (b) isomer 2 (fraction 2). Flow rate = 2.5 ml/min.

5.2.1.3 $[Ru(L\text{-}L))_2(L\text{-}L')]^{2+}$, where L-L = dmbpy or phen; L-L' = 1Mptr or 4Mptr.

These compounds were separated using the neutral mobile phase, (about pH 6-7). Two peaks were obtained for the compounds incorporating the 1Mptr ligand, (See Figure 5.6).

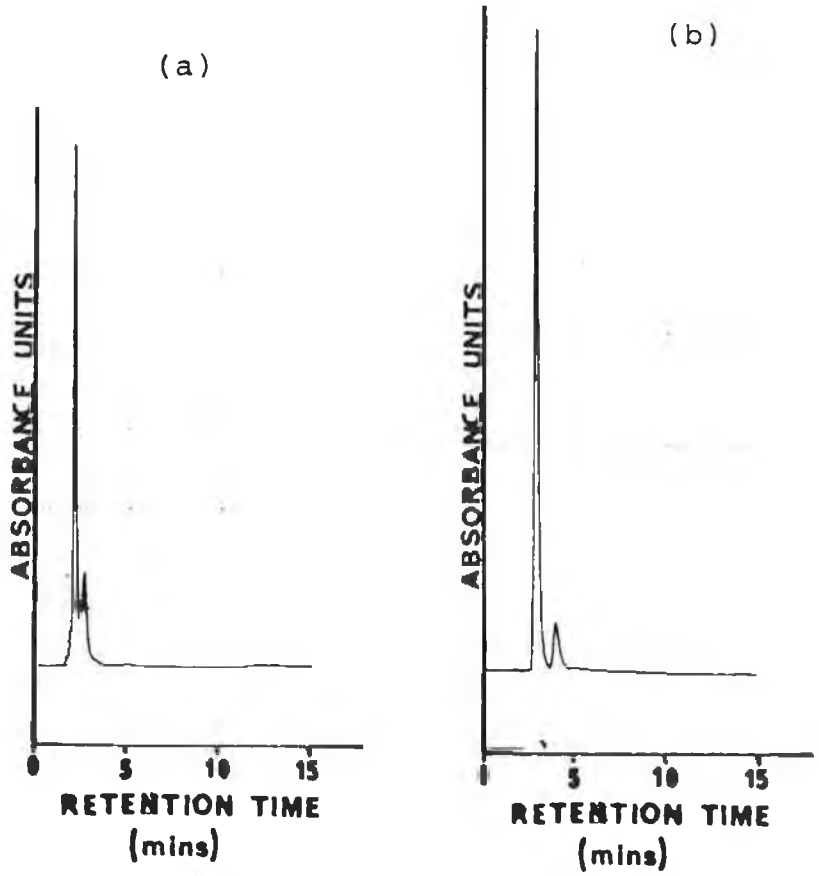

Figure 5.6 Chromatograms of the isomers of (a) $[Ru(dmbpy)_2(1Mptr)]^{2+}$ and (b) $[Ru(phen)_2(1Mptr)]^{2+}$ in acetonitrile : water (80:20) with 0.08 M $LiClO_4$. Flow rate = 2.5 ml/min.

The ratios are reversed compared to the $[Ru(L\text{-}L)_2(H3Mptr)]^{2+}$ isomers with ratios of about 90-95% for peak 1 (isomer 1) and 5-10% for peak 2 (isomer 2). This suggests that isomer 2 is the complex where coordination to the ruthenium is sterically hindered, i.e. through the $N^{2'}$ site on the triazole ring.

The isomers were separated and isolated in mg quantities and purity was checked using the analytical HPLC column. It proved difficult to obtain isomer 2 in pure form as can be seen for example for the dmbpy and phen compounds in Figures 5.7 and 5.8, however about 80% purity was achieved. Isomer 1 was isolated in pure form. Only one peak was observed for the $[Ru(L\text{-}L)_2(4Mptr)]^{2+}$. This was anticipated since only one coordination mode is possible, See Figure 5.9..

5.2.1.4 Comment on HPLC results.

It is interesting to note that even at this early stage in the characterisation of the various ruthenium compounds synthesised, it is possible to tentatively assign the coordination mode based on HPLC data i.e. peak ratios. This provides a good basis for further characterisation. It can be seen that compounds with coordination through the $N^{4'}$ site on the triazole ring elute first with $N^{1'}$ / $N^{2'}$ coordinating compounds eluting second.

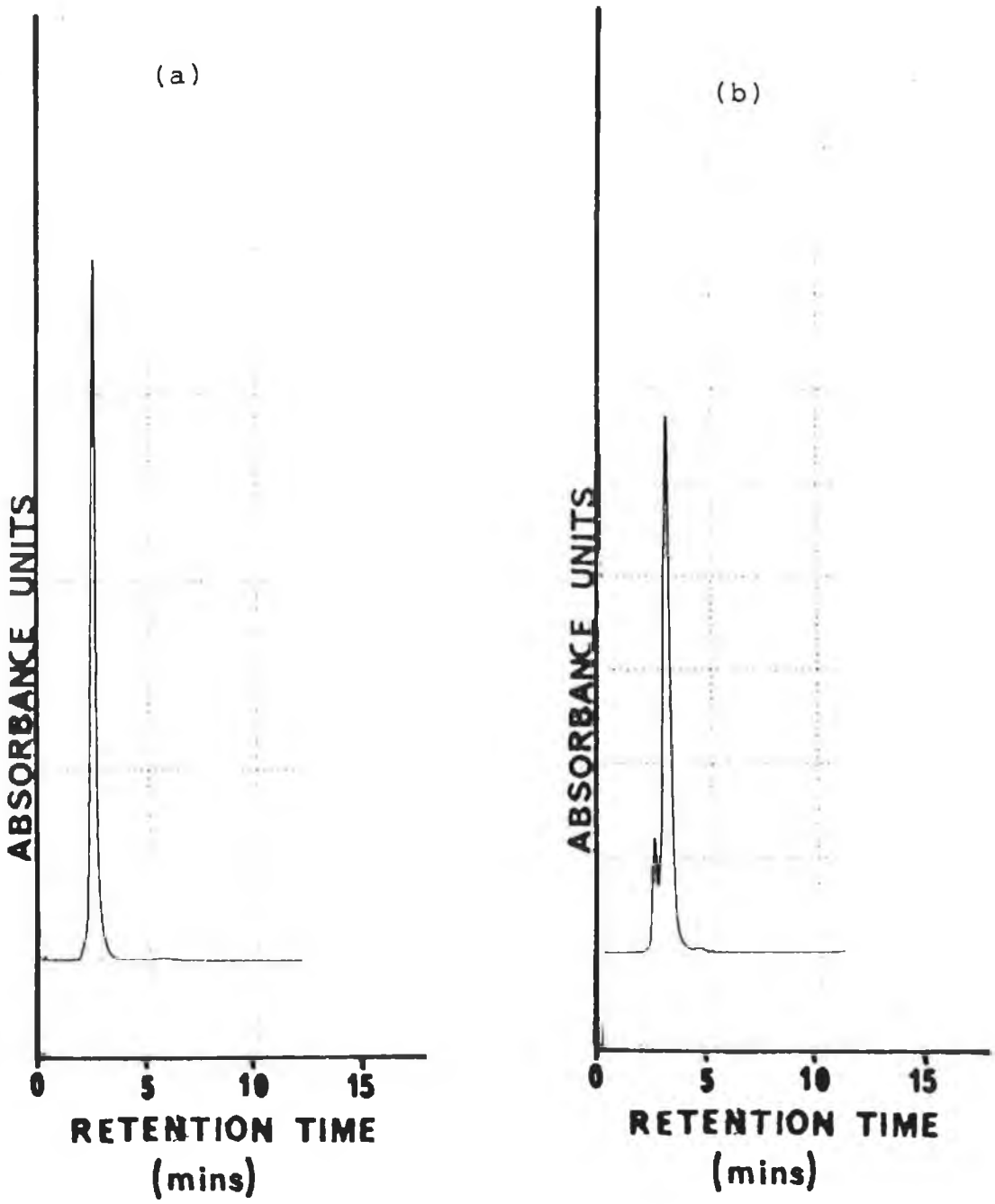

Figure 5.7 Chromatograms of the isomers of $[Ru(dmbpy)_2(lMptr)]^{2+}$ after separation in acetonitrile : water (80:20) with 0.08 M $LiClO_4$. (a) isomer 1 (fraction 1) and (b) isomer 2 (fraction 2). Flow rate = 2.5 ml/min.

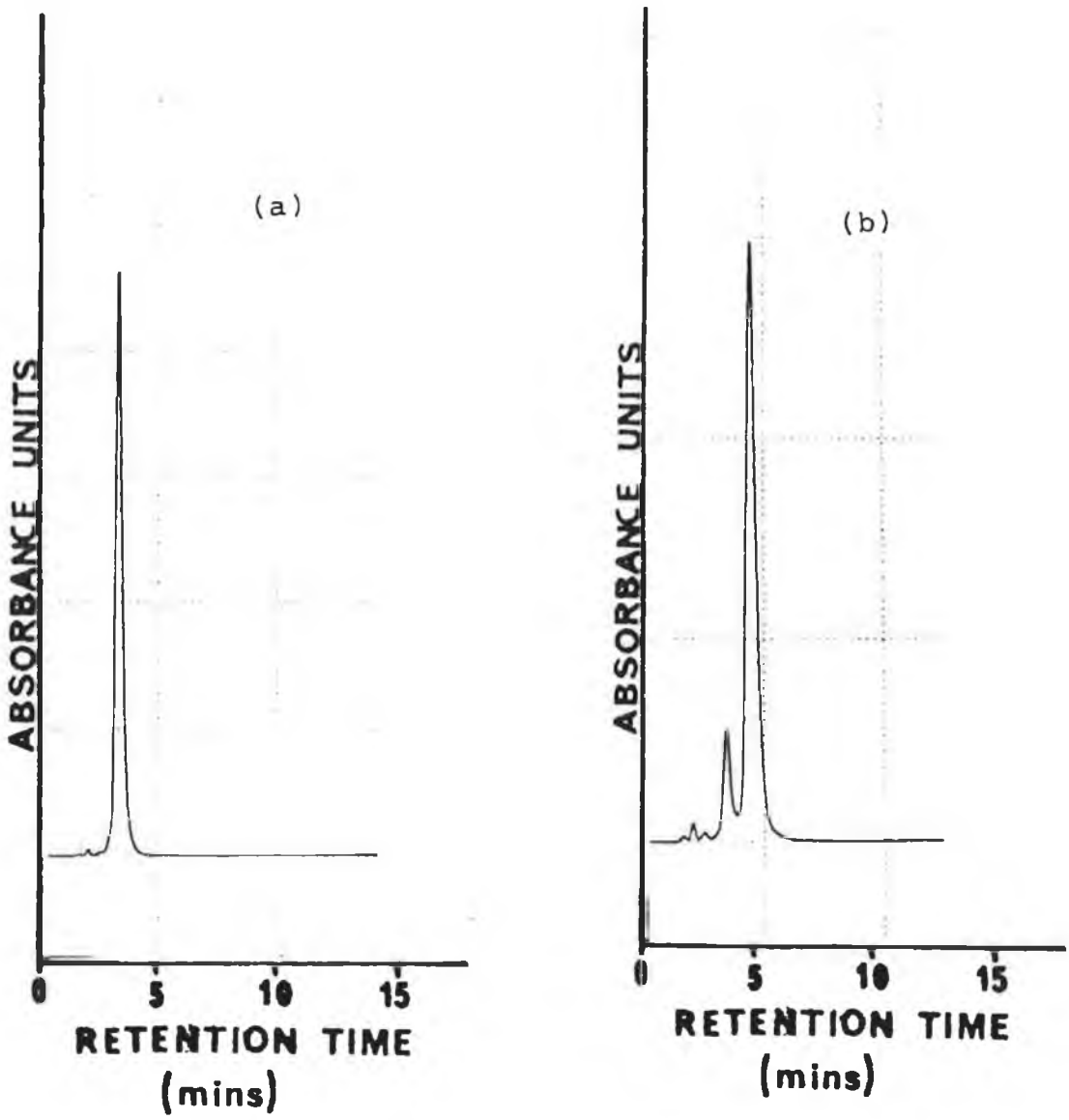

Figure 5.8 Chromatograms of the isomers of $[Ru(phen)_2(lMptr)]^{2+}$ after separation in acetonitrile : water (80:20) with 0.08 M $LiClO_4$. (a) isomer 1 (fraction 1) and (b) isomer 2 (fraction 2). Flow rate = 2.5 ml/min.

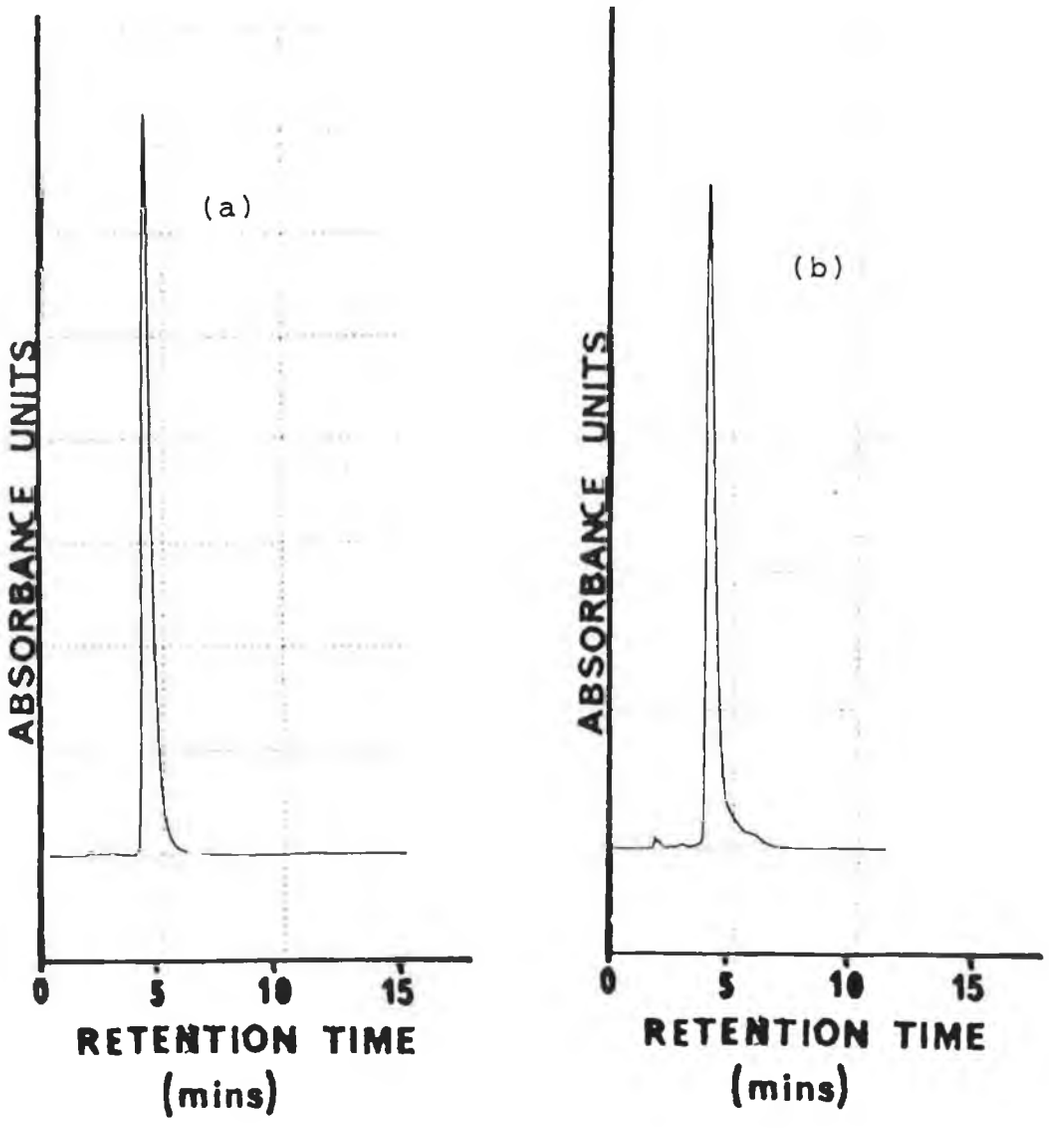

Figure 5.9 Chromatograms of (a) $[Ru(dmbpy)_2(4Mptr)]^{2+}$ and (b) $[Ru(phen)_2(4Mptr)]^{2+}$ in acetonitrile : water (80:20) with 0.08 M $LiClO_4$. Flow rate = 2.5 ml/min.

5.3 NMR spectroscopic characterisation of complexes of the type $[Ru(L\text{-}L)_2(L\text{-}L')]^{2+}$.

The presence of two phenanthroline or two dimethylbipyridyl ligands and one pyridyltriazole renders it difficult to identify the manner in which the triazole is coordinated using UV/vis spectroscopic or electrochemical methods. ^1H NMR techniques were used to unambigously assign the mode of coordination for the pyridyltriazole ligands.

The ^1H NMR data confirm cis-geometry for all the compounds. [3,4] By using 2D COSY techniques and by comparison with assignments made for other similar compounds, [1], a complete assignment of the resonances was made.

2D COSY NMR spectra were obtained for the $[Ru(L\text{-}L)_2(4Mptr)]^{2+}$ complexes where coordination to ruthenium via the triazole ring is only possible through the $N^{2'}$ position. These spectra are presented in Figures 5.10 and 5.11. The methyl / hydrogen resonances of the pyridyltriazole ring are quite distinguishable from those of the dmbpy and phen ligands. These spectra were very useful in assigning the pyridyltriazole resonances of the other complexes. By comparison with these spectra, the proton resonances of the other complexes were assigned.

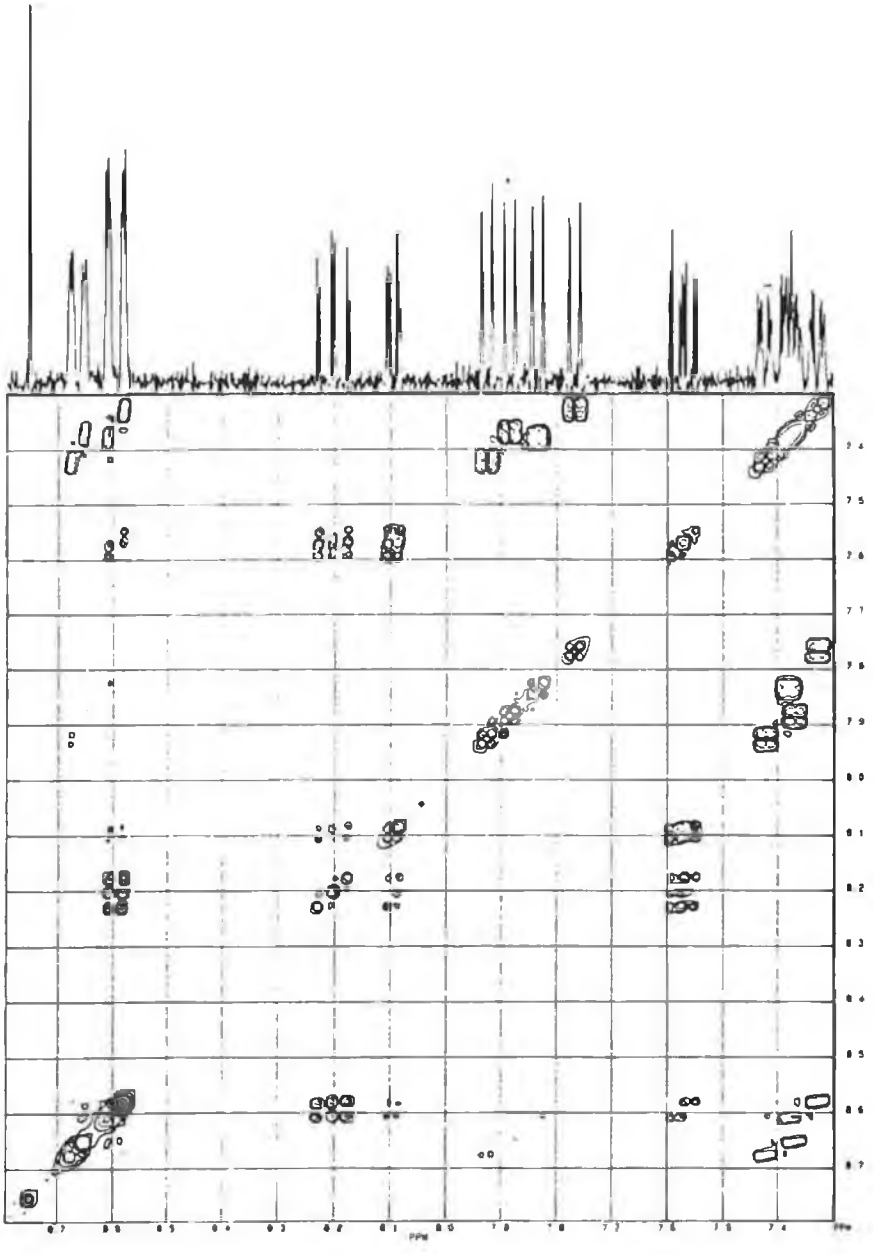

Figure 5.10 COSY NMR spectrum of $[Ru(dmbpy)_2(4Mptr)]^{2+}$ measured in $(CD_3)_2CO$.

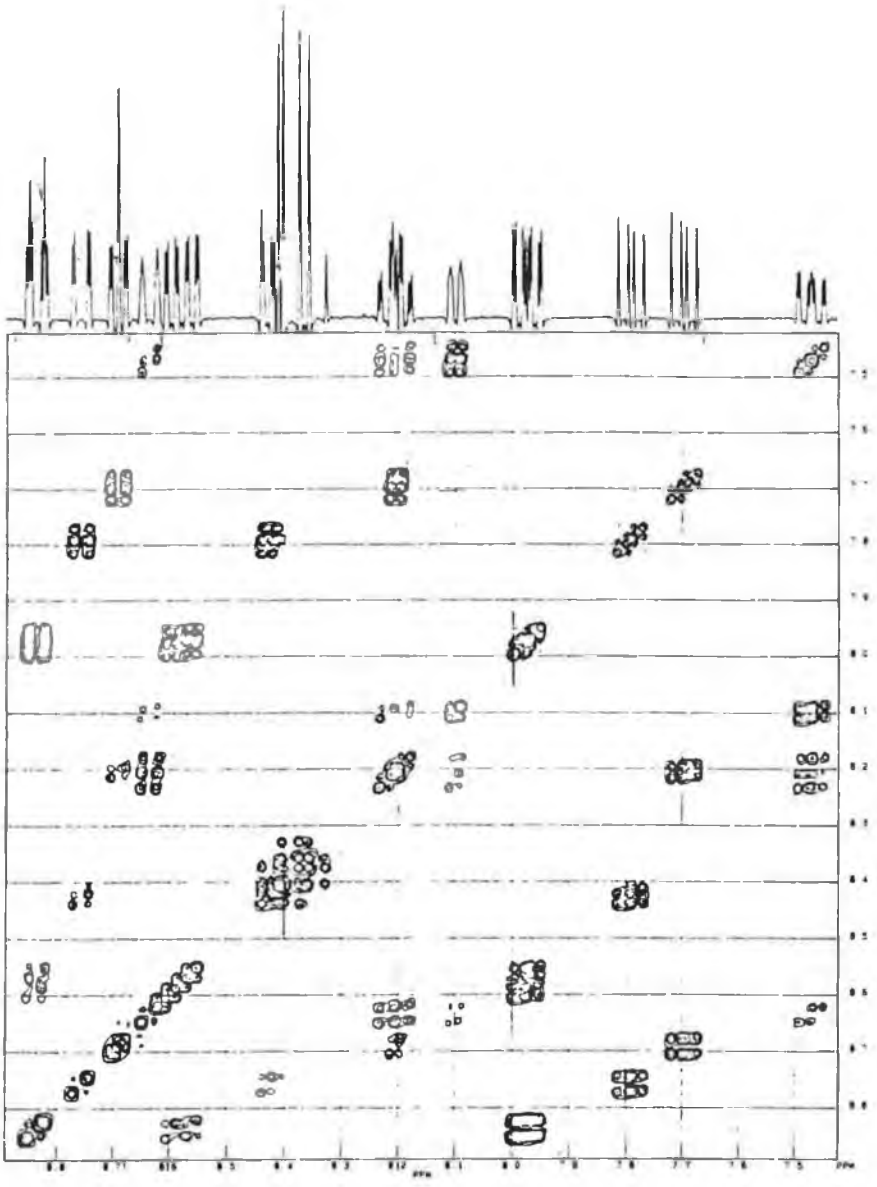

Figure 5.11 COSY NMR spectrum of $[Ru(phen)_2(4Mptr)]^{2+}$ measured in $(CD_3)_2CO$.

The two possible modes of coordination of ruthenium to the Hptr ligand are shown in Figure 5.12.

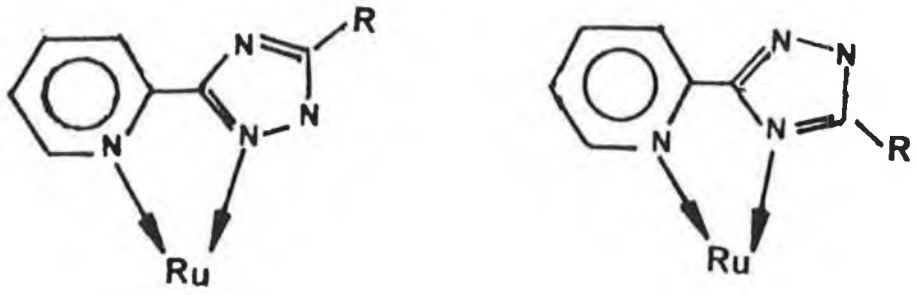

where R = H, ligand = Hptr; R = CH_3, ligand = H3Mptr

Figure 5.12 Possible coordination modes for the two isomers of $[Ru(L\text{-}L)_2(L\text{-}L')]^{2+}$ where L-L' = Hptr or H3Mptr.

For the purposes of this characterisation an analysis of the pyridyltriazole resonances is sufficient. The ^1H NMR data for the coordinated complexes have been tabulated and are presented in Tables 5.2 - 5.4. For each pyridyltriazole ligand an upfield shift of the H^6 proton of the pyridine ring ranging from 0.6 - 1.4 ppm, depending on the compound, resulted upon bidentate coordination to ruthenium. This shift may be explained by diamagnetic anisotrophic interaction of this proton with the ring currents of dmbpy and phen ligands. [2,5,6,7] The other protons have also been shifted somewhat because of the influence of the metal atom.

Table 5.2 ^{1}H NMR data for the $[Ru(dmbpy)_2(L\text{-}L')]^{n+}$ complexes.

Compound	CH_3	H5'	H3	H4	H5	H6
$[Ru(dmbpy)_2(Hptr)]^{2+}$ Isomer 1 N4' (a)	-	8.38 (+0.11)	8.26 (+0.17)	7.94 (-0.04)	7.30 (-0.21)	7.62 (-1.08)
$[Ru(dmbpy)_2(Hptr)]^{2+}$ Isomer 2 N2' (a)	-	8.66 (+0.39)	8.22 (+0.13)	7.98 (+0.00)	7.32 (-0.19)	7.69 (-1.01)
$[Ru(dmbpy)_2(ptr)]^{+}$ Isomer 1 N4' (b)	-	7.47 (-0.80)	8.20 (+0.11)	7.91 (-0.07)	7.19 (-0.32)	7.53 (-1.17)
$[Ru(dmbpy)_2(ptr)]^{+}$ Isomer 2 N2' (b)	-	7.97 (-0.30)	7.98 (-0.11)	7.82 (-0.16)	7.12 (-0.39)	7.53 (-1.17)
$[Ru(dmbpy)_2(H3Mptr)]^{2+}$ Isomer 1 N4' (a)	1.62 (-0.74)	-	8.16 (+0.14)	7.89 (-0.01)	7.23 (-0.20)	7.83 (-1.00)
$[Ru(dmbpy)_2(H3Mptr)]^{2+}$ Isomer 2 N1' (a)	2.44 (+0.08)	-	8.14 (+0.12)	7.97 (+0.07)	7.31 (-0.12)	7.55 (-1.28)
$[Ru(dmbpy)_2(3Mptr)]^{+}$ Isomer 1 N4' (b)	1.37 (-0.99)	-	8.00 (-0.02)	7.78 (-0.12)	7.07 (-0.36)	7.43 (-1.40)
$[Ru(dmbpy)_2(3Mptr)]^{+}$ Isomer 2 N1' (b)	2.35 (-0.01)	-	8.20 (+0.18)	8.00 (+0.10)	7.24 (-0.19)	7.68 (-1.15)
$[Ru(dmbpy)_2(1Mptr)]^{2+}$ Isomer 1 N4'	4.08 (+0.11)	8.69 (+0.08)	8.40 (+0.24)	8.16 (+0.25)	7.53 (+0.10)	7.89 (-0.77
$[Ru(dmbpy)_2(1Mptr)]^{2+}$ Isomer 2 N2'	3.44 (-0.53)	8.78 (+0.17)	8.45 (+0.29)	8.20 (+0.29)	7.54 (+0.11)	7.89 (-0.77
$[Ru(dmbpy)_2(4Mptr)]^{2+}$	4.39 (+0.40)	8.75 (+0.13)	8.60 (+0.49)	8.20 (+0.25)	7.57 (+0.10)	8.09 (-0.57

Complexes denoted (a) or (b) were measured in D_2O with a drop of either conc. DCl or NaOD to ensure protonation or deprotonation respectively. The other compounds were measured in $(CD_3)_2CO$. Figures in parentheses are shifts compared to the free ligands measured in $(CD_3)_2SO$, those to higher field being positive. Only resonances of the pyridyltriazole ligands are included. Resonance positions of the dmbpy ligands are given in Chapter 2.

Table 5.3 ^{1}H NMR data for the [Ru(phen)$_2$(L-L')]n+ complexes.

Compound	CH_3	H5'	H3	H4	H5	H6
$[Ru(phen)_2(Hptr)]^{2+}$ Isomer 1 N4'(a)	-	8.37 (+0.07)	8.34 (+0.25)	8.10 (+0.12)	7.24 (-0.27)	7.61 (-1.09)
$[Ru(phen)_2(Hptr)]^{2+}$ Isomer 2 N2'(a)	-	8.65 (+0.38)	8.31 (+0.22)	8.01 (+0.03)	7.26 (-0.25)	7.77 (-0.93)
$[Ru(phen)_2(ptr)]^{+}$ Isomer 1 N4' (b)	-	7.43 (-0.84)	8.18 (+0.09)	7.87 (-0.11)	7.06 (-0.45)	7.51 (-1.19)
$[Ru(phen)_2(ptr)]^{+}$ Isomer 2 N2' (b)	-	7.95 (-0.32)	8.07 (-0.02)	7.86 (+0.12)	7.05 (-0.46)	7.54 (-1.16)
$[Ru(phen)_2(H3Mptr)]^{2+}$ Isomer 1 N4' (a)	1.37 (-0.99)	-	8.25 (+0.23)	7.93 (+0.03)	7.18 (-0.25)	7.53 (-1.30)
$[Ru(phen)_2(H3Mptr)]^{2+}$ Isomer 2 N1' (a)	2.35 (-0.01)	-	8.20 (+0.18)	8.00 (+0.10)	7.24 (-0.19)	7.68 (-1.15)
$[Ru(phen)_2(3Mptr)]^{+}$ Isomer 1 N4' (b)	1.10 (-1.26)	-	8.10 (+0.08)	7.82 (-0.08)	7.01 (-0.42)	7.42 (-1.41)
$[Ru(phen)_2(3Mptr)]^{+}$ Isomer 2 N1' (b)	2.15 (-0.21)	-	8.00 (-0.02)	7.84 (-0.06)	7.02 (-0.41)	7.51 (-1.32)
$[Ru(phen)_2(1Mptr)]^{2+}$ Isomer 1 N4'	4.03 (+0.06)	8.64 (+0.03)	8.46 (+0.30)	8.17 (+0.26)	7.42 (-0.01)	7.87 (-0.79)
$[Ru(phen)_2(1Mptr)]^{2+}$ Isomer 2 N2'	3.25 (-0.72)	8.77 (+0.16)	8.58 (+0.42)	8.20 (+0.29)	7.43 (+0.00)	7.86 (-0.80)
$[Ru(phen)_2(4Mptr)]^{2+}$	4.39 (+0.40)	8.69 (+0.07)	8.64 (+0.53)	8.20 (+0.25)	7.46 (-0.01)	8.09 (-0.57)

Complexes denoted (a) or (b) were measured in D_2O with either a drop of conc. DCl or NaOD to ensure protonation or deprotonation respectively. The other complexes were measured in $(CD_3)_2CO$. Figures in parenthesis are shifts compared to free ligand measured in $(CD_3)_2SO$, those to higher field being positive. Only resonances for the pyridyltriazole ligand are included. The resonances of the phen ligands are given in Chapter 2.

Table 5.4 ^{1}H NMR data on $[Ru(bpy)_2(L\text{-}L')]^{n+}$ complexes.

Compound	CH_3	H5'	H3	H4	H5	H6
$[Ru(bpy)_2(Hptr)]^{2+}$ Isomer 1 N4'(a)	-	8.38 (+0.11)	8.27 (+0.18)	7.96 (-0.02)	7.36 (-0.15)	7.62 (-1.08)
$[Ru(bpy)_2(Hptr)]^{2+}$ Isomer 2 N2'(a)	-	8.65 (+0.38)	8.23 (+0.14)	8.00 (+0.02)	7.26 (-0.25)	7.70 (-1.00)
$[Ru(bpy)_2(ptr)]^{+}$ Isomer 1 N4'(b)	-	7.54 (-0.73)	8.08 (-0.01)	7.8-7.9 (-0.1/2)	7.10 (-0.41)	7.52 (-1.18)
$[Ru(bpy)_2(ptr)]^{+}$ Isomer 2 N2'(b)	-	7.99 (-0.28)	8.05 (-0.04)	7.8-8.0 (-0.2/0)	7.16 (-0.28)	7.55 (-1.15)
$[Ru(bpy)_2(H3Mptr)]^{2+}$ (a)	2.40 (+0.04)	-	8.24 (+0.22)	8.08 (+0.18)	7.41 (-0.02)	7.63 (-1.00)
$[Ru(bpy)_2(3Mptr)]^{+}$ (b)	2.20 (-0.16)	-	8.02 (+0.00)	7.99 (+0.09)	7.23 (-0.20)	7.67 (-0.96)
$[Ru(bpy)_2(1Mptr)]^{2+}$	3.97 (+0.00)	8.73 (+0.12)	8.36 (+0.24)	8.10 (+0.19)	7.46 (+0.03)	7.58 (-1.00)
$[Ru(bpy)_2(4Mptr)]^{2+}$	4.35 (+0.36)	8.74 (+0.12)	8.59 (+0.48)	8.13 (+0.18)	7.57 (+0.10)	8.05 (-0.61)

Complexes denoted (a) and (b) were measured in D_2O with a drop of either conc. DCl or NaOD to ensure protonation or deprotonation respectively. The other complexes were measured in $(CD3)_2CO$. Figures in parentheses are shifts compared to the free ligands measured in $(CD3)_2SO$, those to higher field being positive. Only data on pyridyltriazole ligand resonances are included.

For the ligands Hptr, H3Mptr and 1Mptr the resonance positions of the hydrogen / methyl substituent on the triazole ring are expected to be influenced by the co-ordination mode of the ligand. If a nitrogen atom is coordinated to ruthenium, the neighbouring group will be affected not only by a change in electron density in the five-membered ring but also by the shielding cone of a dmbpy or phen ring, as has been demonstrated for the bpy analogues [1], leading to upfield shifts of these resonances. These resonance positions are therefore indicative of the manner in which the pyridyltriazole ligand is coordinated to the ruthenium and it is expected that for $N^{4'}$ coordination, the CH_3 on the $C^{3'}$ position of the H3Mptr ligand and the H on the $C^{5'}$ position of the ligand 1Mptr and Hptr are shielded, resulting in a shift of these resonances to a higher field relative to the free ligand.

In the case of coordination at $N^{1'}$, the CH_3 on the $C^{3'}$ position of the H3Mptr ligand will not be shielded and will resonate at lower field. For the ligand 1Mptr, coordination via $N^{2'}$ should result in a shift to higher field for the CH_3 group on the $N^{1'}$ site of the triazole ring, while the H on the $C^{5'}$ position should result in a shift to lower field. This effect has also been shown by Steel et al. [8], for the complex $[Ru(bpy)_2(L\text{-}L')]^{2+}$ where L-L' = 3,5-dimethyl-1-(pyridin-2-yl) pyrazole. Relative to the free ligand, a shift upfield of -0.72 ppm was observed for the methyl moiety on the $C^{3'}$ position close to the coordinating $N^{2'}$, while the methyl group on

the $C^{5'}$ site was shifted downfield by +0.26 ppm.

For isomer 2 of $[Ru(L\text{-}L)_2(1Mptr)]^{2+}$, the methyl resonance has been shifted upfield by -0.53 ppm and -0.72 ppm for (L-L) = dmbpy and phen respectively, relative to the free ligand. This suggests that in this case coordination to the ruthenium atom is through the $N^{2'}$ position of the pyridyltriazole ring. For isomer 1, the methyl resonance occurs at lower field for both the dmbpy and phen compounds relative to the free ligand. The shift is only 0.11 ppm and 0.06 ppm for the dmbpy and phen compounds respectively. This suggests coordination via the $N^{4'}$ on the pyridyltriazole ligand. It is difficult to unambigously assign the coordination mode based on the shifts of the $H^{5'}$ proton as only small shifts were observed. Nonetheless, the $H^{5'}$ resonances occurred at marginally higher field for the $N^{4'}$ coordinated compounds. The effect is much smaller than for the methyl group because of the smaller radius of the protons compared to the radius of the methyl group.

The same effect on the methyl resonance is observed for the $[Ru(L\text{-}L)_2(H3Mptr)]^{2+}$ compounds. For isomer 1 (protonated), the methyl resonance has been shifted upfield by -0.74 ppm for the dmbpy compound and by -0.99 ppm for the phen compound. This indicates that coordination is through the $N^{4'}$ position on the triazole ring. For isomer 2 (protonated), the methyl resonances occur at about the same frequency as the free ligand. This is anticipated for coordination via the $N^{1'}$ position on the pyridyltriazole

ligand.

These assignments are in agreement with those proposed from HPLC data, which suggests that the main fraction for the $[Ru(L\text{-}L)_2(1Mptr)]^{2+}$ compounds is isomer 1 where coordination through $N^{4'}$ is not sterically hindered and the second smaller fraction (isomer 2) is that which would be sterically hindered (via $N^{2'}$ coordination). The reverse is true for the $[Ru(L\text{-}L)_2(H3Mptr)]^{2+}$ compounds where the main fraction (isomer 2) should be the isomer which is coordinated to the ruthenium atom via the $N^{1'}$ position where steric hindrance would not be a problem. The smaller fraction (isomer 1) would be subject to steric hindrance.

Deprotonation of $[Ru(L\text{-}L)_2(H3Mptr)]^{2+}$ causes the methyl resonances of the protons on the pyridyltriazole ligand to shift upfield for both isomers. The shift in the resonance positions of the triazole protons can be explained by the increased electron density in the triazole ring of the pyridyltriazole ligand which probably also affects the electron density in the pyridine ring of the ligand. [2,9]

It is rather more difficult to assign the $[Ru(L\text{-}L)_2(Hptr)]^{2+}$ isomers. The shifts of the methyl resonances where the methyl substituents are shielded, because of the presence of the shielding ring cones of dmbpy and phen are sufficiently different to those where shielding does not occur, to allow distinction between them. However, the shifts of the $H^{5'}$ protons for the protonated isomers of

the $[Ru(L\text{-}L)_2(Hptr)]^{2+}$ compounds are similar. The NMR spectra of these compounds are difficult to interpret because the $H^{5'}$ proton resonance will also depend on the location of the N-H proton. Upon deprotonation there is quite a large difference between the singlet ($H^{5'}$) resonances, 0.50 ppm for $[Ru(dmbpy)_2(ptr)]^{+}$ isomers and 0.52 ppm for the $[Ru(phen)_2(ptr)]^{+}$ isomers. This difference in ppm should facilitate the assignment of the coordination mode. See Figure 5.13, which shows the ^1H NMR spectra for the two deprotonated isomers of $[Ru(dmbpy)_2(Hptr)]^{2+}$. From the data it can be seen that the $H^{5'}$ of isomer 1 is more shielded than isomer 2. This suggests that isomer 1 is that isomer where coordination is through the $N^{4'}$ position of the pyridyltriazole ligand where the $H^{5'}$ proton would be affected to a greater extent by the dmbpy/phen shielding cone. [1]

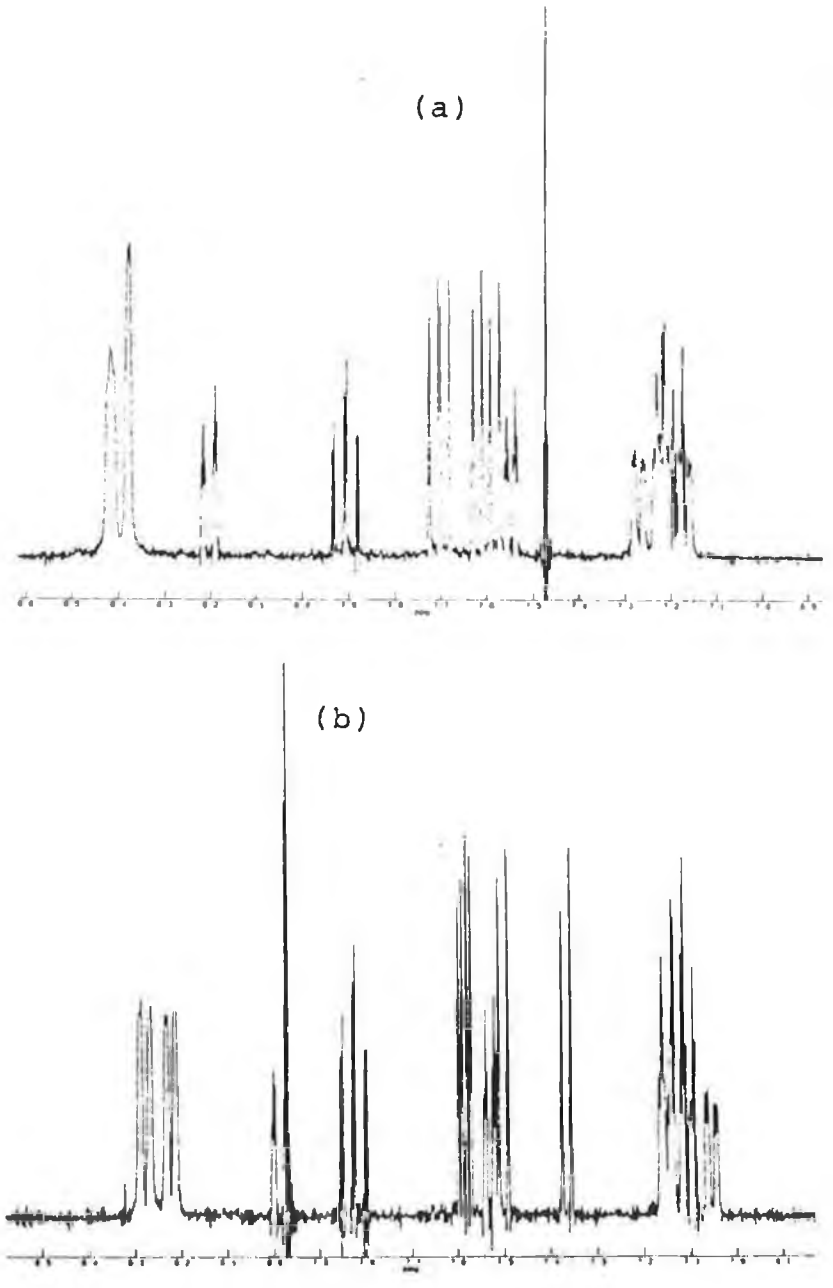

Figure 5.13 ^{1}H NMR spectra of (a) isomer 1 and (b) isomer 2 of $[Ru(dmbpy)_2(ptr)]^+$. Spectra were measured in D_2O with one drop of conc. NaOD to ensure deprotonation.

5.4 Electronic spectra and Redox properties.

The electronic and the electrochemical properties of the complexes are listed in Tables 5.5 - 5.6, together with the data on their bipyridyl analogues, Table 5.7. [1] The absorption bands of lowest energy (highest wavelength) can be assigned to $d\pi$ to π^* MLCT bands. [10] The position of this band is generally taken as a measure of the π-acceptor capacity of the ligand. If the ligand is a good π-acceptor, the $d\pi$ orbitals are stabilised by the back donation of electron density from the filled metal orbitals to the unoccupied π^* orbitals of the ligand. The position of this band may however, also be influenced by the σ-donor properties of the ligand. [11]. The redox potentials presented in Tables 5.5 and 5.6 have been determined by differential pulse polaragraphy. The cyclic voltammetry measurements indicate that all redox processes are quasi-reversible with the difference in peak positions for the oxidation waves in the range 60 - 150 mV. Figures 5.14 and 5.15 are representative diagrams of electrochemical measurements, showing oxidation and reduction processes of the complex $[Ru(dmbpy)_2(4Mptr)]^{2+}$.

Some of the compounds coordinated to the ligands H3Mptr and Hptr required the addition of a few drops of conc. HCl in order to measure the oxidation potential of the protonated species. The reduction potentials could not then be determined in these acidic solutions. For solutions where acid was not added, the electrochemically induced

deprotonation process renders it difficult to determine the reduction potential accurately.

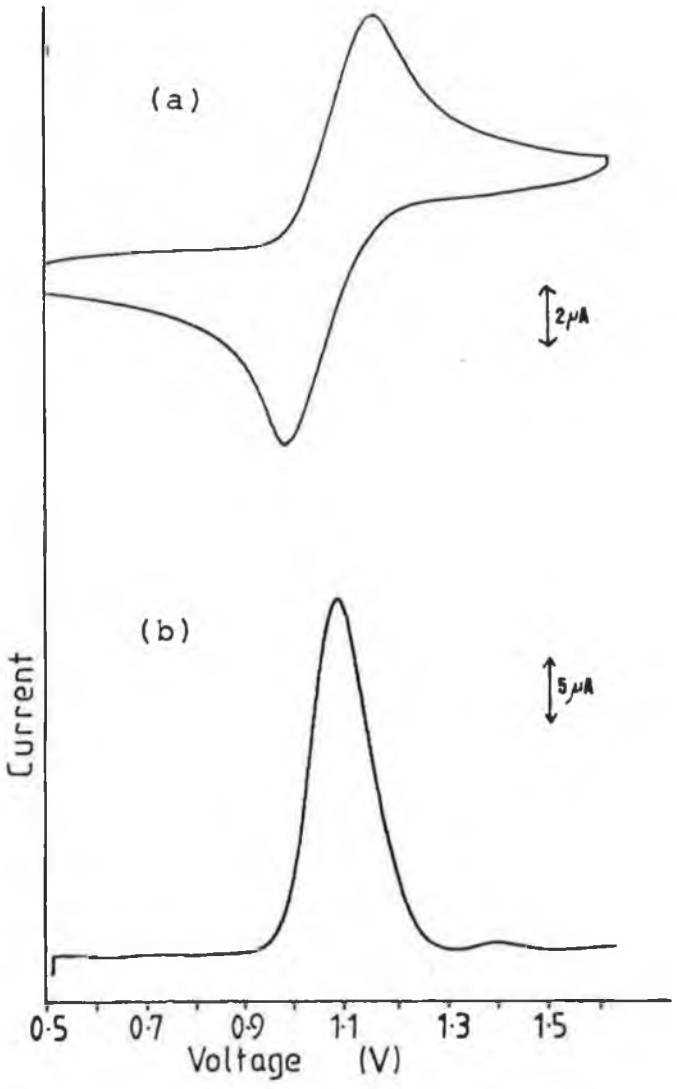

Figure 5.14 Cyclic voltammogram (a) and a differential pulse polarogram (b) showing the oxidation of $[Ru(dmbpy)_2(4Mptr)]^{2+}$ in 0.1 M TEAP / CH_3CN.

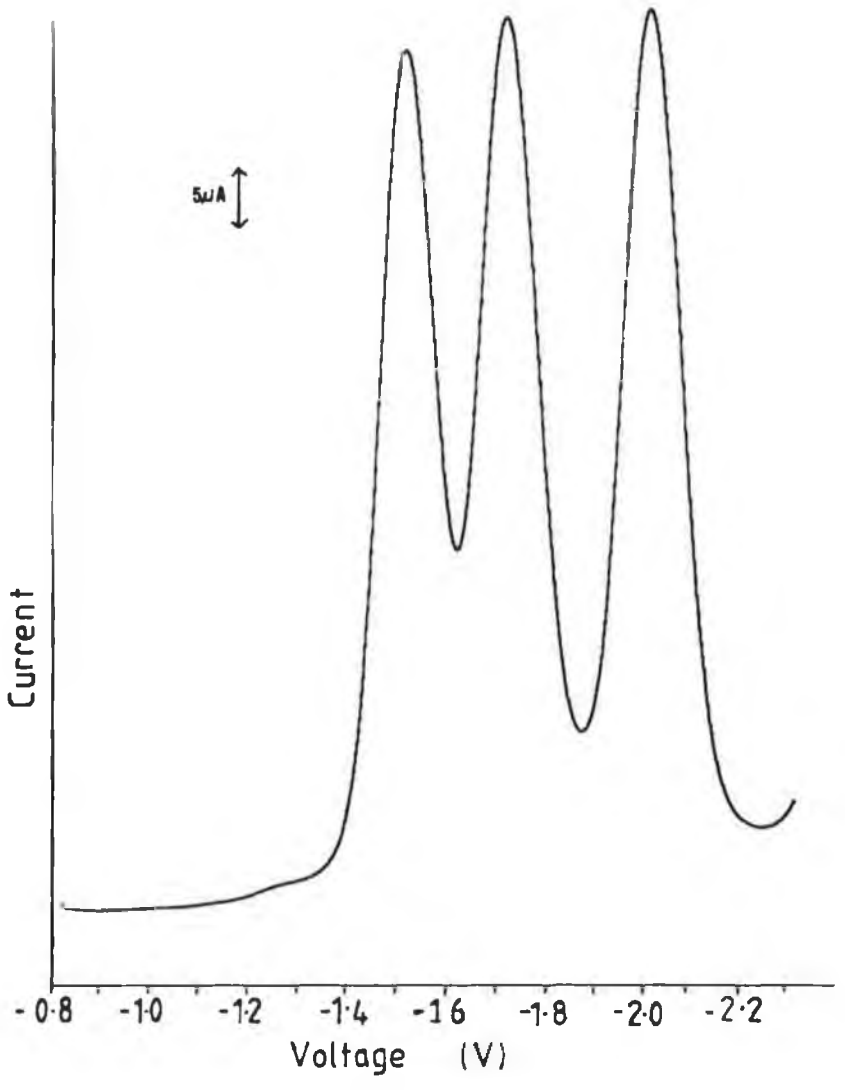

Figure 5.15 Differential pulse polarogram showing the reduction of the complex $[Ru(dmbpy)_2(4Mptr)]^{2+}$ in degassed 0.1 M TEAP / CH_3CN.

Table 5.5 Electronic and electrochemical data for the [Ru(dmbpy)2-(L-L')]n+ complexes.

[Ru(dmbpy)2-(L-L')]n+ where L-L' =		Absorption λmax nm (log ε)(d)	Emission λmax nm 303 K	Emission λmax nm 77 K (e)	Redox Potentials (f) Ru V vs S.C.E.	Redox Potentials (f) Ligand based V vs S.C.E.
Hptr	isomer 1	450(4.00)(a)	624(a)	586	1.08	-1.59, -1.84
Hptr	isomer 2	443(4.02)(a)	621(a)	585	1.09	- -
ptr-	isomer 1	483(3.93)(b)	667(b)	609	0.72	-1.75, -1.85
ptr-	isomer 2	482(3.96)(b)	674(b)	616	0.75	-1.63, -1.83
H3Mptr	isomer 1	452 - (a)	624(a)	590	1.06	-1.58, -1.81
H3Mptr	isomer 2	440(4.14)(a)	629(a)	583	1.09	- -
3Mptr-	isomer 1	484 - (b)	673(b)	623	0.71	-1.64, -1.88
3Mptr-	isomer 2	480(4.02)(b)	682(b)	622	0.72	-1.60, -1.85
1Mptr	isomer 1	450(4.15)(c)	620(c)	582	1.08	-1.54, -1.75
1Mptr	isomer 2	432(4.09)(c)	628(c)	585	1.18	-1.49, -1.69
4Mptr		448(4.21)(c)	622(c)	600	1.09	-1.53, -1.72, -2.02
dmbpy (g)		450	618		1.10	-1.45

(a). Protonated in solvent with one drop 6 M HCl.
(b). Deprotonated in solvent with one drop 6 M NaOH.
(c). Measured in CH_3CN, protonated or deprotonated as appropriate with HCl or NaOH.
(d). Log ε, units M^{-1} cm^{-1}.
(e). Spectra measured at 77 K in EtOH, protonated or deprotonated as appropriate with HCl or NaOH.
(f). Measured in CH_3CN with 0.1 M NEt_4ClO_4 (TEAP), volts vs S.C.E., N.H.E. = S.C.E. +0.2415V; protonated or deprotonated as appropriate with HCl or NaOH.
(g). Ref. 10.

Table 5.6 Electronic and electrochemical data for the $[Ru(phen)_2(L\text{-}L')]^{n+}$ complexes.

$[Ru(phen)_2(L\text{-}L')]^{n+}$ where L-L' =		Absorption λ max nm (log ε)[d]	Emission λ max nm Ru 303 K	77 K [e]		Redox Potentials[f] Ligand based V vs S.C.E.
Hptr	isomer 1	445(4.22)[a]	611[a]	573	1.19	-1.51, -1.76, -2.03
Hptr	isomer 2	416(4.15)[a] also 435 (sh)	607[a]	568	1.18	- - -
ptr-	isomer 1	478(4.08)[b]	651[b]	603	0.84	-1.64, -1.89
ptr-	isomer 2	475(3.99)[b] also 420	663[b]	600	0.86	-1.51, -1.75
H3Mptr	isomer 1	449 -[a]	610[a]	575	1.19	- -
H3Mptr	isomer 2	426(4.21)[a] also 435 (sh)	612[a]	568	1.20	- -
3Mptr-	isomer 1	474 -[b]	651[b]	608	0.87	-1.57, -1.81
3Mptr-	isomer 2	478(4.08)[b]	673[b]	608	0.71	-1.66, -1.90, -1.99
1Mptr	isomer 1	448(4.10)[c]	594[c]	568	1.19	-1.42, -1.65, -1.84
1Mptr	isomer 2	434 -[c]	610[c]	577	1.33	-1.40, -1.56, -1.75
4Mptr		440(4.23)[c]	600[c]	576	1.20	-1.46, -1.64
phen (g)		442	604	568[h]	1.27	-1.35

(a). Protonated in solvent with one drop 6 M HCl.
(b). Deprotonated in solvent with one drop 6 M NaOH.
(c). Measured in CH_3CN, protonated or deprotonated as appropriate with HCl or NaOH.
(d). Log ε , units M^{-1} cm^{-1}.
(e). Spectra measured at 77 K in EtOH, protonated or deprotonated as appropriate with HCl or NaOH.
(f). Measured in CH_3CN with 0.1 M NEt_4ClO_4 (TEAP), volts vs S.C.E., N.H.E. = S.C.E. +0.2415V; protonated or deprotonated as appropriate with HCl or NaOH.
(g). Ref. 10.
(h). Ref. 12.

Table 5.7 Electronic and electrochemical data for the [Ru(bpy)2 (L-L')]n+ complexes. [1]

[Ru(bpy)2 (L-L')]n+ where L-L' =		Absorption λmax nm (log ε)(d)	Emission λmax nm 300 K	77 K (e)	Redox Potentials(f) Ru V vs S.C.E.	Ligand based V vs S.C.E.
Hptr	isomer 1	452(4.05)(a)	616(a)	590	1.20	-1.47, -1.72
HPtr	isomer 2	444(4.11)(a)	625(a)	575	1.10	-1.49, -1.73
ptr-	isomer 1	488(3.97)(b)	670(b)	609	0.90	-1.51, -1.78
ptr-	isomer 2	484(4.04)(b)	670(b)	608	0.83	-1.48, -1.74
H3Mptr		444(4.03)(a)	600(a)	587	1.20	-1.55, -1.81
H3Mptr		476(3.93)(a)	660(a)	610	0.79	-1.50, -1.72
1Mptr		452(4.03)(c)	600(c)	585	1.20	-1.42, -1.64
4Mptr		440(4.16)(c)	600(c)	584	1.21	-1.42, -1.64
bpy (g)		452(4.11)	608	582	1.22	-1.36, -1.53

(a). Protonated in solvent with one drop 6 M HCl.
(b). Deprotonated in solvent with one drop 6 M NaOH.
(c). Measured in CH_3CN, protonated or deprotonated as appropriate with HCl or NaOH.
(d). Log ε , units M^{-1} cm^{-1}.
(e). Spectra measured at 77 K in EtOH, protonated or deprotonated as appropriate with HCl or NaOH.
(f). Measured in CH_3CN with 0.1 M NEt_4ClO_4 (TEAP), volts vs S.C.E., N.H.E. = S.C.E. +0.2415V; protonated or deprotonated as appropriate with HCl or NaOH.
(g). Ref. 10.

For the dications the position of the MLCT band occurs at about the same energy as their $[Ru(dmbpy)_3]^{2+}$ and $[Ru(phen)_3]^{2+}$ analogues and indeed $[Ru(bpy)_3]^{2+}$. The exception was isomer 2 of the $[Ru(L\text{-}L)_2(1Mptr)]^{2+}$ compounds where the MLCT band is found at higher energy, which indicates that in this coordination mode, i.e. via $N^{2'}$ on the pyridyltriazole ring, the ligand may act as a stronger π-acceptor. The oxidation potential of isomer 2 for the 1Mptr coordinated compounds is higher than for the analogous $[Ru(phen)_3]^{2+}$ or $[Ru(dmbpy)_3]^{2+}$ compounds, while the first reduction potential is still more negative than for the tris compounds but slightly less negative than for the other pyridyltriazole compounds. This higher oxidation potential combined with the higher energy MLCT band may indicate a decrease in the σ-donor capacity of the ligand. The effective charge on the ruthenium is decreased which in turn stabilises the metal $d\pi$ orbitals.

Deprotonation of the $[Ru(L\text{-}L)_2(H3Mptr)]^{2+}$ and $[Ru(L\text{-}L)_2(Hptr)]^{2+}$ compounds causes profound changes in their absorption, emission, (see Figures 5.16 - 5.18) and electrochemical properties. Deprotonation leads to a shift to lower energy for the MLCT band and a decrease in the oxidation potential. These effects may be explained by the increase in σ-donor properties due to the increase in electron density in the triazole ring. These effects are also reflected in the shift to lower energy of the emission band upon deprotonation. Deprotonation tends to destabilise the metal d orbitals causing the $d\pi - \pi^*$ band to be

shifted to lower energy. The reduction potentials also shift to a more negative value for the deprotonated compounds.

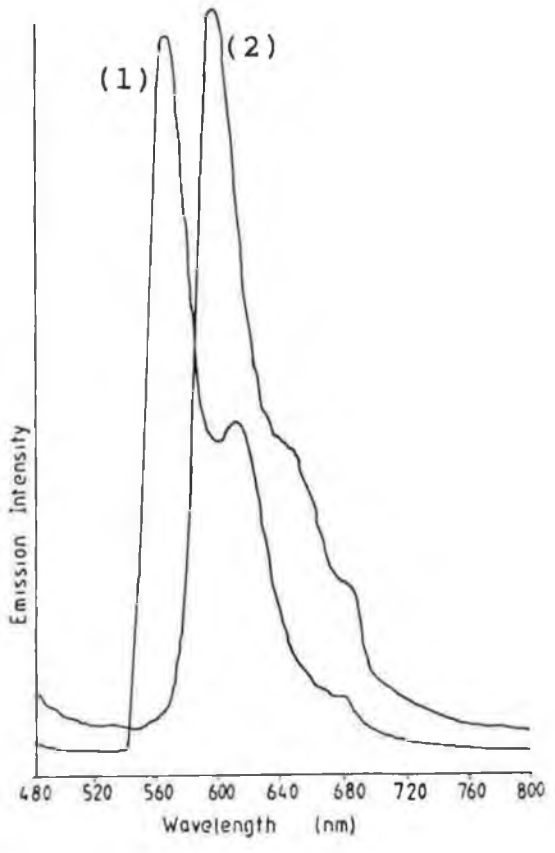

Figure 5.16 Emission spectra at low temperature (77 K), in ethanol of the protonated (1) and deprotonated (2) forms of $[Ru(phen)_2(Hptr)]^{2+}$, isomer 1.

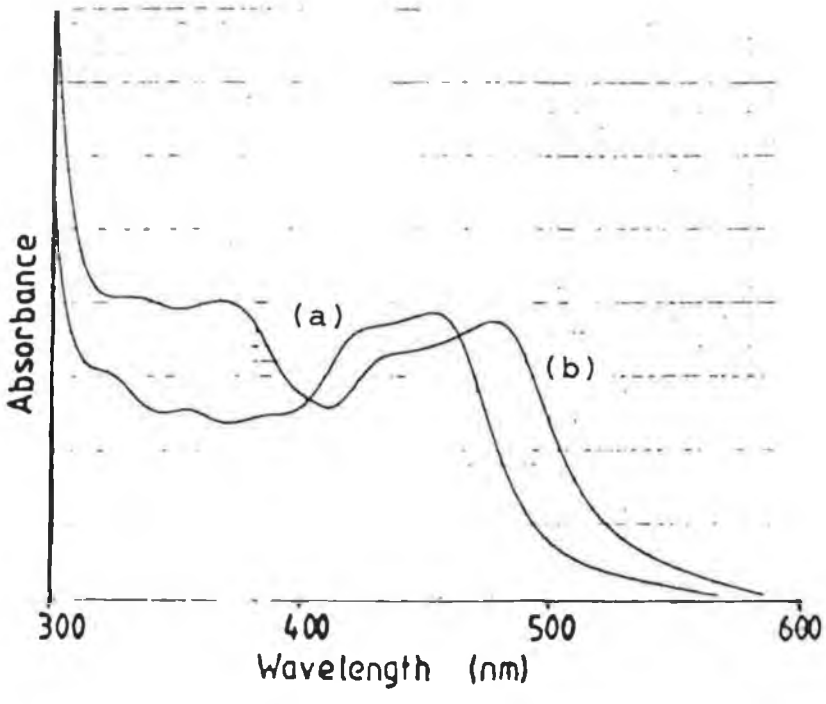

Figure 5.17 Absorption spectra in acetonitrile of (a) the protonated form and (b) the deprotonated form of isomer 1 of $[Ru(dmbpy)_2(H3Mptr)]^{2+}$. One drop of 6 M HCl or 6 M NaOH was added to ensure either protonation or deprotonation.

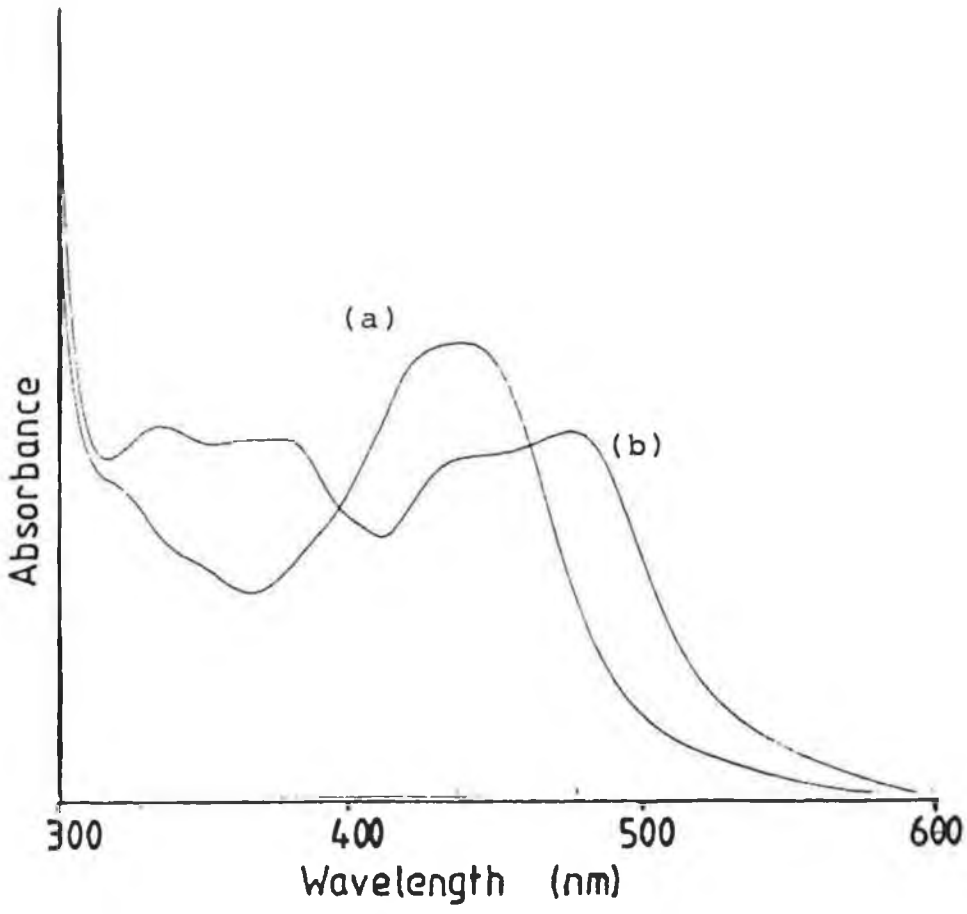

Figure 5.18 Absorption spectra in acetonitrile of (a) the protonated form and (b) the deprotonated form of isomer 2 of $[Ru(dmbpy)_2(H3Mptr)]^{2+}$. One drop of 6 M HCl or 6 M NaOH was added to ensure either protonation or deprotonation.

The first reduction potential of each complex is very similar to the first reduction potential of the appropriate $[Ru(phen)_3]^{2+}$ and $[Ru(dmbpy)_3]^{2+}$ analogues. This suggests that this reduction is dmbpy/ phen based and also indicates that the π^* levels for the pyridyltriazole ligands are at higher energy than those of bpy, dmbpy and phen and therefore, the pyridyltriazole ligands are harder to reduce. This implies that phen and dmbpy act as the emitting ligand whilst the pyridyltriazole ligands act as spectator ligands. In general, the reduction potentials become less negative with increasing π-acceptor abilities of these ligands. [2]

Spectrophotometric titrations have shown that the triazole N-H in isomer 2 for $[Ru(dmbpy)_2(Hptr)]^{2+}$ and $[Ru(phen)_2(Hptr)]^{2+}$ is more acidic by about two orders of magnitude than for isomer 1. This implies that the ligand possesses better σ-donor properties when coordinated in this mode, i.e. via $N^{2'}$ / $N^{1'}$ position.

These results are in agreement with the NMR data discussed earlier where coordination through the $N^{2'}$ / $N^{1'}$ position on the triazole ring for isomer 2 and via the $N^{4'}$ position on the triazole ring for isomer 1, was proposed for the Hptr / H3Mptr coordinated compounds.

The substitution with a methyl group on the $C^{3'}$ position of the triazole ring (H3Mptr) appears to have had little effect on the electronic and electrochemical properties, with data being similar for both the Hptr and H3Mptr coordinated compounds (protonated and deprotonated).

The absorption spectra of the isomers of the deprotonated compounds are very similar, so it would be difficult to differentiate between isomers on the basis of their deprotonated spectra. However, the spectra of the protonated isomers are quite dissimilar which allows the distinction between them. See Figures 5.17 and 5.18 earlier.

The addition of a methyl substituent on either the $N^{1'}$ site of the triazole ring for isomer 2 of $[Ru(L\text{-}L)_2(1Mptr)]^{2+}$ or the $N^{4'}$ site of the triazole ring for $[Ru(L\text{-}L)_2(4Mptr)]^{2+}$ results in spectra which are comparable to the spectra for the protonated isomer 2 of the Hptr and H3Mptr coordinated compounds. The spectrum of $[Ru(L\text{-}L)_2(1Mptr)]^{2+}$ isomer 1 is similar to the protonated spectra of isomer 1 of $[Ru(L\text{-}L)_2(Hptr)]^{2+}$ and $[Ru(L\text{-}L)_2(H3Mptr)]^{2+}$. This would be expected since the isomer 1 compounds are all thought to be bound to ruthenium via the $N^{4'}$ position of the triazole ring and the isomer 2 compounds via the $N^{1'}$/ $N^{2'}$ position of the triazole ring.

All the compounds show emission at 77K and at room temperature. For all compounds, emission at low temperature is stronger than that at room temperature. A number of factors affect the intensity of emission including the energy difference between the deactivating anti-bonding d-d orbital and the emitting ^{3}MLCT state. At room temperature this deactivating state may be thermally populated, thus leading to a decrease in the emission intensity. [11,12,13]

For many $[Ru(bpy)_2(L_2)]^{2+}$ compounds reported in the literature, a linear relationship exists between the energy of the lowest MLCT band and $\Delta E_{1/2}$ and between $\Delta E_{1/2}$ and the emission energy. [11,14] This relationship also holds for the compounds investigated here and indeed for their bisbipyridyl analogues, indicating that emission originates from the same π^* orbitals as observed for other ruthenium polypyridyl complexes. In Figure 5.19, the absorption and emission maxima converted to eV versus $\Delta E_{1/2}$, the difference between the oxidation and reduction potential are plotted. Evidently, the emission / absorption maxima correlate well with the electrochemical measurements. The plots show that the electronic and electrochemical properties of the ruthenium bipyridyl, dimethylbipyridyl and phenthroline compounds are similar. This can be explained by assuming that the same type of orbital plays a role in the absorption and emission processes as well as the oxidation and reduction processes of the compounds.

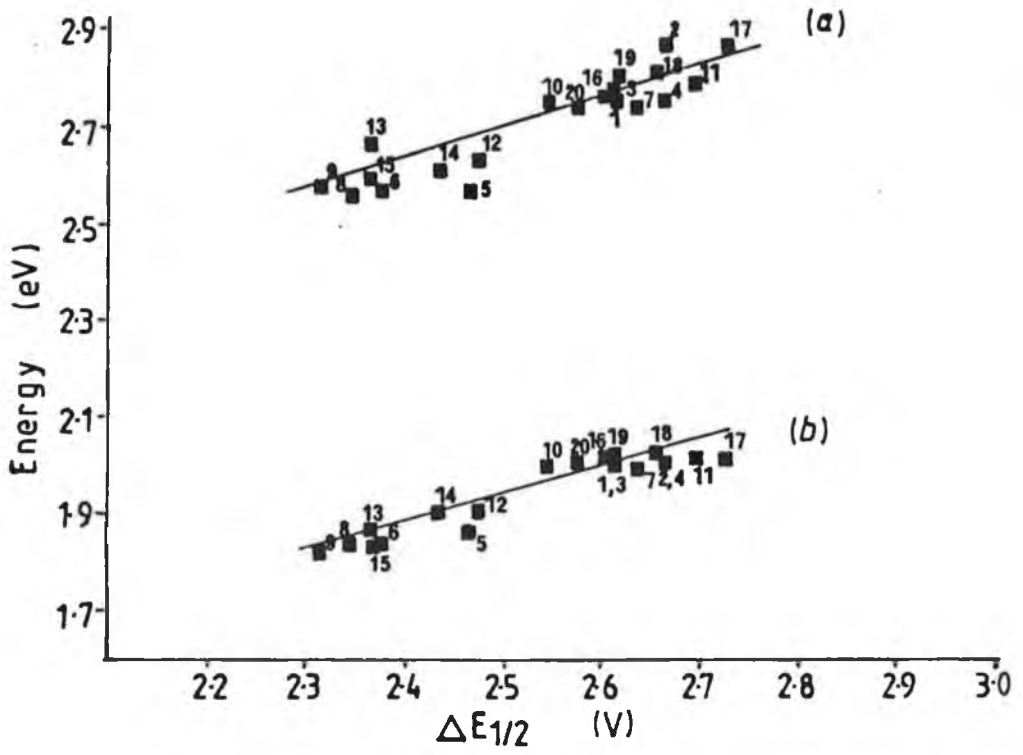

Figure 5.19 Plots of $\Delta E_{1/2}$ vs (a) absorption and (b) emission energies for compounds (1) to (20), as listed below.

(1) $[Ru(dmbpy)_2(1Mptr)]^{2+}$, isomer 1; (2) $[Ru(dmbpy)_2(1Mptr)_{2+}]$, isomer 2; (3) $[Ru(dmbpy)_2(4Mptr)]^{2+}$; (4) $[Ru(dmbpy)_2(Hptr)]^{2+}$, isomer 1; (5) $[Ru(dmbpy)_2(ptr)]^{+}$, isomer 1; (6) $[Ru(dmbpy)_2(ptr)]^{+}$, isomer 2; (7) $[Ru(dmbpy)_2(H3Mptr)]^{2+}$, isomer 1; (8) $[Ru(dmbpy)_2(3Mptr)]^{+}$, isomer 1; (9) $[Ru(dmbpy)_2(3Mptr)]^{+}$, isomer 2; (10) $[Ru(dmbpy)_3]^{2+}$, Ref. 10; (11) $[Ru(phen)_2(Hptr)]^{2+}$, isomer 1; (12) $[Ru(phen)_2(ptr)]^{+}$, isomer 1; (13) $[Ru(phen)_2(ptr)]^{+}$, isomer 2; (14) $[Ru(phen)_2(3Mptr)]^{+}$, isomer 1; (15) $[Ru(phen)_2(3Mptr)]^{+}$, isomer 2; (16) $[Ru(phen)_2(1Mptr)]^{2+}$, isomer 1; (17) $[Ru(phen)_2(1Mptr)]^{2+}$, isomer 2; (18) $[Ru(phen)_2(4Mptr)]^{2+}$; (19) $[Ru(phen)_3]^{2+}$, Ref. 10; (20) $[Ru(bpy)_3]^{2+}$, Ref. 10.

5.5 Acid-Base chemistry

In this section the pH dependence of the ground state and of the excited state of $[Ru(L\text{-}L)_2(Hptr)]^{2+}$ (isomers 1 and 2) and $[Ru(L\text{-}L)_2(H3Mptr)]^{2+}$ (isomer 2) have been studied using UV/vis and luminescence spectrophotometry. There were insufficent quantities of isomer 1 of the $[Ru(L\text{-}L)_2(H3Mptr)]^{2+}$ compounds isolated to allow a pH titration to be carried out.

The acid-base chemistry of the free ligands has already been investigated and also that of the analogous bipyridyl compounds, [1,15], which readily allows comparison with the data obtained for the coordinated ligands.

5.5.1 Electronic spectra and ground state acid-base properties.

The effect of pH on the UV/visible spectra of the ruthenium compounds was investigated. The cations exhibit pH dependence of the lower energy MLCT band. Figures 5.20 - 5.25. All changes are fully reversible and independent of the direction of pH change. The spectroscopic data, pK_a and pK_a^* (excited state pK_a) values are presented in Table 5.8. The observed behaviour can be explained by deprotonation of the pyridyltriazole ligands at higher pH yielding $[Ru(L\text{-}L)_2(ptr)]^+$ and $[Ru(L\text{-}L)_2(3Mptr)]^+$ and has been found for the corresponding bipyridyl compounds.[1].

Table 5.8 Acid-base data for the pyridyltriazole coordinated complexes.

Compound	isomer No.	Abs.[a] λ max		Em.[a] λ max.		pKa[b]	pHi[b]	pKa*[c]	
		acid	base	acid	base			(1)	(2)[e]
$[Ru(phen)_2(Hptr)]^{2+}$	1	444	465	603	639	5.85	5.61	4.03	3.81
$[Ru(phen)_2(Hptr)]^{2+}$	2	416	460 (435,sh)	608	640	4.28	3.84	2.31	1.99
$[Ru(dmbpy)_2(Hptr)]^{2+}$	1	446	468	627	650	6.13	5.93	4.78	4.99
$[Ru(dmbpy)_2(Hptr)]^{2+}$	2	438	466	632	654	4.40	3.40	2.16	2.34
$[Ru(phen)_2(H3Mptr)]^{2+}$	2	418	460 (435,sh)	606	645	5.06	4.25	2.63	-
$[Ru(dmbpy)_2(H3Mptr)]^{2+}$	2	438	466	616	660	5.23	5.13	2.97	-
$[Ru(bpy)_2(Hptr)]^{2+}$	1	450	470	615	650	5.95	5.10	5.20	4.22
$[Ru(bpy)_2(Hptr)]^{2+}$	2	437	465	620	650	4.07	2.70	3.40	2.12
$[Ru(bpy)_2(H3Mptr)]^{2+}$		440	466	612	645	4.87	4.20	4.30	4.44
Hptr [d]						9.20			
H3Mptr [d]						9.80			

(a) Absorption and emission spectra were measured at 303 K, in Britton-Robinson buffer, λ max in nm.

(b) Ground state pK_a and pH_i, obtained from the inflection points of the absorption and emission titration curves respectively, are correct to +/- 0.1.

(c) pK_a^*, the excited state values were obtained from Eqn. 5.2, [16], for those values listed under (1); and from Eqn. 5.1, [17], for those values listed under (2). See Section 5.5.2.

(d) Data obtained from References [1] and [15].

(e) Lifetimes τ , measured in Britton-Robinson buffer at room temperature, $[Ru(phen)_2(Hptr)]^+$: isomer 1, 8 ns, isomer 2, 6 ns; $[Ru(phen)_2(ptr)]^{2+}$: isomer 1, 499 ns, isomer 2, 428 ns; $[Ru(dmbpy)_2(Hptr)]^+$: isomer 1, 11 ns, isomer 2, 7 ns; $[Ru(dmbpy)_2(ptr)]^{2+}$: isomer 1, 95 ns, isomer 2, 80 ns.

$$[Ru(L\text{-}L)_2(Hptr)]^{2+} \underset{H^+}{\overset{pK_a\ (acid)}{\rightleftharpoons}} [Ru(L\text{-}L)_2(ptr)]^{+}$$

The shift to higher wavelength (lower energy) upon deprotonation is consistent with a destabilisation of the metal d orbitals because of increased sigma donor capacities of the triazole ring. As the π^* levels of dmbpy or phen are not altered significantly when the triazole ligand is deprotonated, this leads to a small difference between the filled d orbitals and the empty π^* orbitals of dmbpy / phen. The pK_a values presented in Table 5.8 (obtained from the inflection point of an absorption vs pH plot), show that the ligands act as stronger acids when coordinated to the $Ru(phen)_2$ / $Ru(dmbpy)_2$ moiety which can be attributed to electron donation from the pyridyltriazole ligand to the central metal ion. The pK_a values are higher for the H3Mptr coordinated compounds which is expected from the electron donating properties of the methyl group. This has also been found for $[(NH_3)_5Ru(HMe_2pz)]^{3+}$, ($HMe_2pz$ = 3,5-dimethyl-pyrazole) where the pK_a was found to be higher than the pK_a of $[(NH_3)_5Ru(Hpz)]^{3+}$. [18]

For most compounds the coordinated ligand in the ground state is more acidic than the free ligand. This effect of increased acidity has been found for a number of compounds including recently, $Ru(bpy)_2$ compounds of 3-(2-hydroxy-phenyl)-5-(pyridin-2-yl)-1,2,4 triazole and 3,3-dimethyl-5,5'-bis-1,2,4 triazole. [19,20], and may be attributed to electron donation from the ligand to the central metal atom. The only compound for which acidity has been decreased is $[Ru(NH_3)_5(pyz)]^{3+}$, (pyz = pyrazine), which may be attributed to back donation of electron density from the filled metal based t_{2g} orbitals to the unoccupied π^* orbitals of the ligand. [21].

The results obtained for the compounds discussed here are very similar to the data obtained for the bpy analogues. The pK_a values of the two isomers of the $[Ru(L\text{-}L)_2(Hptr)]^{2+}$ compounds are quite different, the pK_a of isomer 2 is about 2 orders of magnitude lower than for isomer 1. This suggests that the coordinating nitrogen for isomer 2 is a better σ-donor than for isomer 1. This indicates that coordination for isomer 2 occurs via the $N^{2'}$ position of the triazole ring since the presence of a nitrogen adjacent to the coordinating nitrogen is considered a better σ-donor. This supports the NMR evidence discussed earlier.

The pK_a of isomer 2 of $[Ru(L\text{-}L)_2(H3Mptr)]^{2+}$ is slightly higher as would be expected due to the presence of the electron donating methyl group on the triazole ring, which yields a higher electron density on the triazole ring,

but is comparable to the pK_a of isomer 2 of $[Ru(L\text{-}L)_2(Hptr)]^{2+}$ which suggests that coordination is through the $N^{1'}$ position of the triazole ring. No evidence for further protonation was found at very low pH, which suggests that there is a reduction in the basicity of the coordinated ligand. It should be noted that protonation is hindered by coordination of the ligand to the ruthenium ion. Protonation of the free ligand probably occurs at the pyridine ring since pyridine is more acidic than 1,2,4 triazole.

There was insufficient sample available in order to conduct a pH titration curve on isomer 1 of the H3Mptr coordinated complexes, but the pK_a values of the isomer 2 compounds were comparable to those for isomer 2 of the Hptr coordinated complexes, allowing for a slight increase due to the methyl group. It seems likely that the pK_a of isomer 1 of the H3Mptr coordinated complexes would also be comparable to those of isomer 1 of the Hptr coordinated complexes.

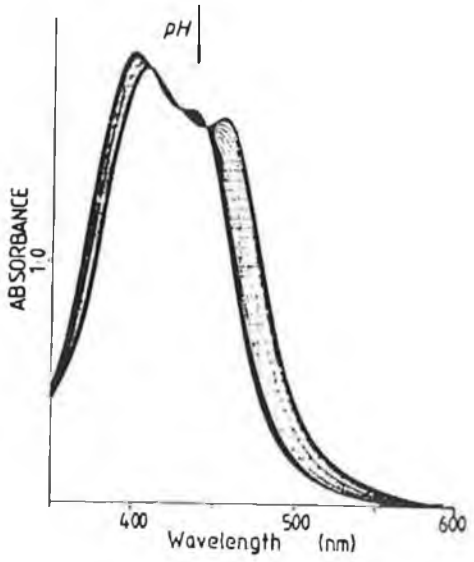

Figure 5.20 pH dependence of the absorption spectrum of $[Ru(phen)_2(Hptr)]^{2+}$, isomer 1, (1)-(31): pH = 1.53, 2.50, 3.07, 3.51, 3.73, 4.06, 4.17, 4.28, 4.39, 4.50, 4.62, 4.75, 4.90, 5.05, 5.22, 5.37, 5.55, 5.73, 5.88, 6.02, 6.22, 6.43, 6.62, 6.85, 7.08, 7.53, 8.01, 9.02, 10.01, 11.02 and 12.02.

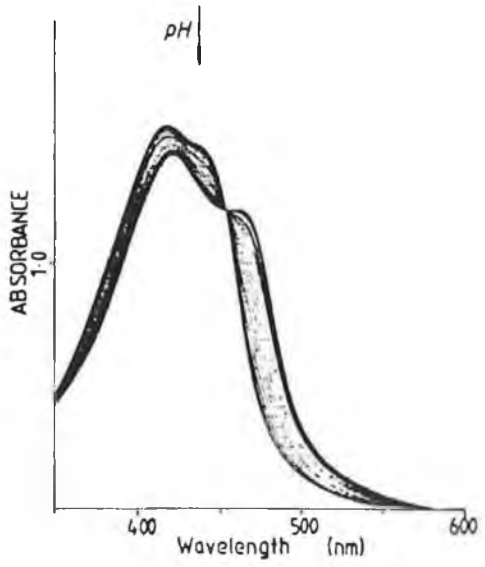

Figure 5.21 pH dependence of the absorption spectrum of $[Ru(phen)_2(Hptr)]^{2+}$, isomer 2, (1)-(25): pH = 1.00, 1.50, 2.01, 2.53, 3.03, 3.55, 3.77, 3.92, 4.14, 4.28, 4.42, 4.60, 4.80, 4.92, 5.07, 5.24, 5.58, 5.73, 6.03, 6.40, 6.85, 7.01, 8.12, 10.06 and 11.10.

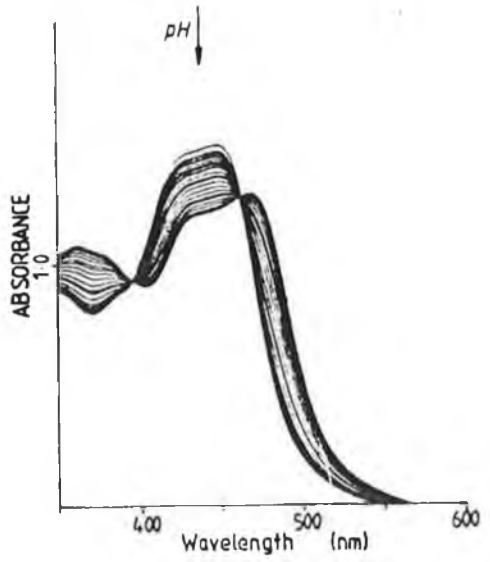

Figure 5.22 pH dependence of the absorption spectrum of $[Ru(dmbpy)_2(Hptr)]^{2+}$, isomer 1, (1)-(33): pH = 1.00, 2.00, 3.05, 3.45, 3.74, 4.02, 4.25, 4.43, 4.61, 4.73, 4.87, 5.02, 5.19, 5.30, 5.56, 5.75, 5.83, 6.00, 6.18, 6.34, 6.50, 6.62, 6.82, 7.01, 7.32, 7.55, 7.86, 8.05, 8.48, 9.05, 9.56, 10.02 and 11.00.

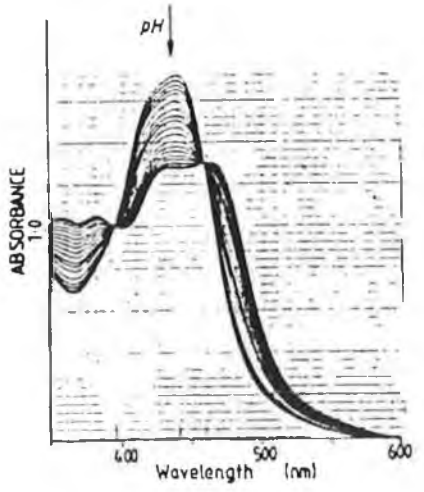

Figure 5.23 pH dependence of the absorption spectrum of $[Ru(dmbpy)_2(Hptr)]^{2+}$, isomer 2, (1)-(29): pH = 1.46, 2.04, 2.53, 3.04, 3.39, 3.62, 3.91, 4.14, 4.27, 4.38, 4.53, 4.68, 4.83, 4.97, 5.12, 5.31, 5.49, 5.76, 6.01, 6.02, 6.44, 6.66, 7.07, 7.52, 7.99, 9.01, 10.03, 11.01 and 12.01.

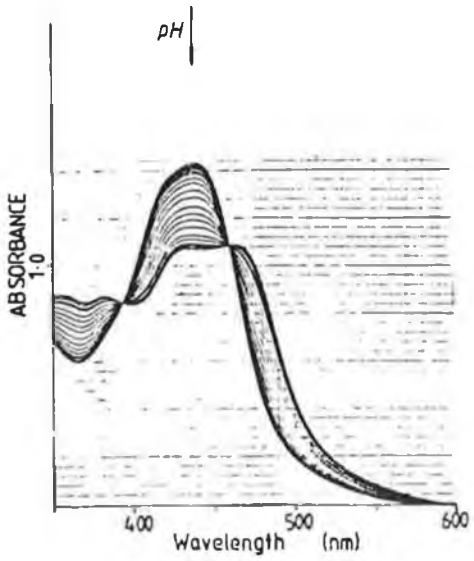

Figure 5.24 pH dependence of the absorption spectrum of $[Ru(dmbpy)_2(H3Mptr)]^2$, isomer 2, (1)-(37): pH = 1.53, 2.05, 2.54, 3.01, 3.33, 3.62, 3.83, 4.01, 4.22, 4.37, 4.47, 4.58, 4.69, 4.79, 4.92, 5.00, 5.07, 5.16, 5.28, 5.35, 5.47, 5.63, 5.79, 5.90, 6.05, 6.15, 6.25, 6.41, 6.64, 6.84, 7.07, 7.48, 8.12, 9.02, 10.06, 11.03 and 12.02.

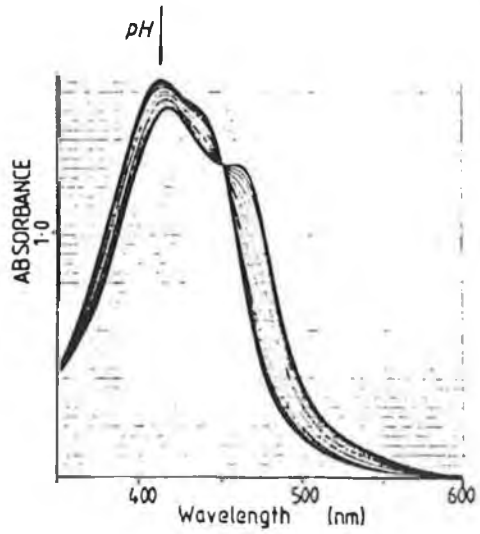

Figure 5.25 pH dependence of the absorption spectrum of $[Ru(phen)_2(H3Mptr)]^{2+}$, isomer 2, (1)-(29): pH = 0.83, 2.01, 2.51, 2.71, 2.93, 3.16, 3.31, 3.53, 3.75, 3.91, 4.14, 4.33, 4.50, 4.74, 4.93, 5.14, 5.30, 5.51, 5.74, 6.04, 6.25, 6.57, 6.79, 7.05, 7.51, 8.02, 9.04, 10.02 and 12.00.

5.5.2 Emission spectra and excited state properties.

The effect of pH on the emission properties of the complexes was also investigated. The emission spectrum as a function of pH of $[Ru(dmbpy)_2(Hptr)]^{2+}$, isomer 1, is presented in Figure 5.26. This spectrum is typical of these compounds, with the emission intensity increasing with increasing pH and the λ max. of emission shifting to lower energy upon deprotonation.

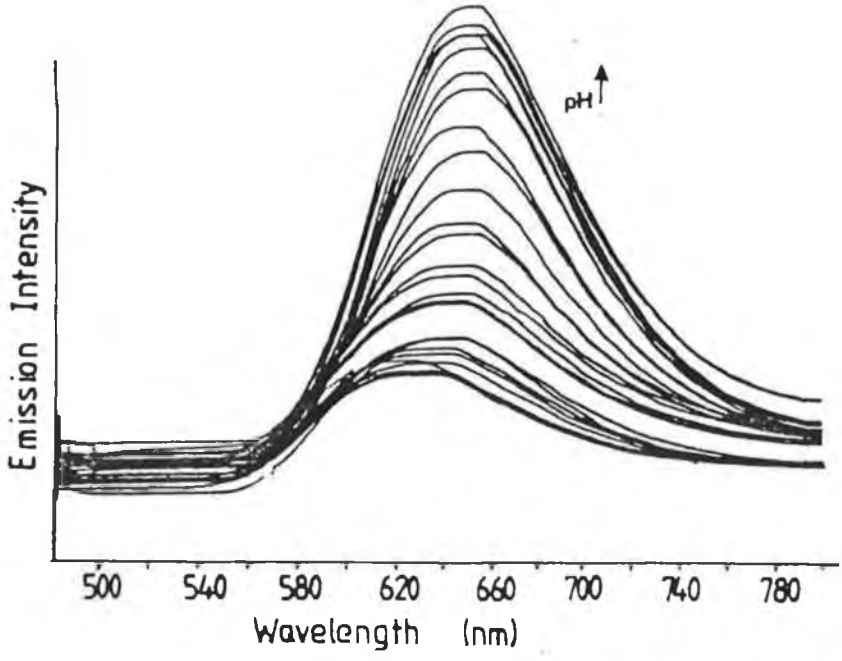

Figure 5.26 pH dependence of the emission spectrum of $[Ru(dmbpy)_2(Hptr)]^{2+}$, isomer 1, (1)-(29): pH = 0.99, 1.21, 1.57, 1.74, 2.00, 2.24, 2.44, 2.62, 2.81, 3.02, 3.23, 3.43, 3.63, 3.83, 4.02, 4.27, 4.51, 4.73, 5.04, 5.27, 5.50, 5.73, 6.55, 7.01, 7.50, 8.06, 9.02, 9.97 and 11.07.

The inflection point in an emission intensity (pH_i) versus pH plot gives an excited state pK_a^* which is called the "apparent pK_a^*" value (given as pH_i in Table 5.8), because these values need to be corrected for the different lifetimes of the protonated and deprotonated complexes, according to equation 5.1, [17].

$$pK_a^* = pH_i + \log (\tau_a / \tau_b) \quad \text{Eqn. 5.1.}$$

where τ_a and τ_b are the excited state lifetimes of the protonated and deprotonated compounds respectively, and pH_i is the inflection point of the emission intensity versus pH curve.
The excited state pK_a^* values may also be determined using the Forster cycle as in equation 5.2, [16].

$$pK_a^* = pK_a + 0.625 (\nu_b - \nu_a) / T \quad \text{Eqn. 5.2}$$

where ν_a and ν_b are the energies of the (0-0) transition from the ground state to the excited state involved in the deprotonation equilibrium, for the protonated and deprotonated forms respectively, obtained using the λ max. emission values measured at 77 K, and pK_a is the ground state pK_a value.

From the results, it may be seen that the

coordinated Hptr and H3Mptr ligands are more acidic in the excited state than in the ground state, (with quite good coorelation between the two methods used for calculating pK_a*). This shows that the pyridyltriazoles act as spectator ligands and do not actively take part in the emission processes. The lifetime values given at the end of Table 5.8, indicates that the emission is strongly deactivated at low pH. This may be caused by population of the d-d level lying above the ^{3}MLCT state, which may become accessible upon protonation of the complexes.

This increased acidity in the excited state has also been found for the bpy analogues and also other ruthenium compounds including [Ru(bpy)$_2$(3-(2-hydroxy-phenyl)-5-(pyridin-2-yl)-H-1,2,4 triazole and [Ru(bpy)$_2$-(3,3'- dimethyl-5,5'-bis-1,2,4 triazole. [19,20], 4,7-dihydroxy-1,10-phenanthroline, 4,4'dicarboxy-2,2'-bipyridine and 2,2'-benzimidazole. [22,23,24,25] The shift to lower energy of the emission λ max. upon deprotonation is consistent with the stronger σ-donation properties of the deprotonated pyridyltriazole ligand.

5.6 Conclusion

A series of pyridyltriazole compounds of the type $[Ru(L\text{-}L)_2\text{-}(L\text{-}L')]^{n+}$ have been synthesised and characterised. (L-L) = dmbpy or phen and (L-L') = 1Mptr, 4Mptr, H3Mptr or Hptr.

For all of the L-L' ligands, with the exception of the 4Mptr, coordination through the $N^{1'}$ / $N^{2'}$ and $N^{4'}$ on the triazole ring is possible. The use of semi-preparative HPLC techniques permitted the separation of these coordination isomers and analytical HPLC was used to determine their purity. New isomers were isolated for the coordinated H3Mptr and 1Mptr complexes, which had not been previously isolated for the bpy analogues. The ratios obtained for these isomers (about 80-90% for one and about 10-20% for the second), substantiate in themselves the coordination mode since the isomer in the lowest yield would be expected to be that isomer where coordination would be hindered sterically.

From the ^1H NMR data on these compounds the coordination mode of the ligands to the $Ru(dmbpy)_2$ and $Ru(phen)_2$ moieties was proposed. The very clear NMR shifts of the methyl groups of the $[Ru(dmbpy)_2(L\text{-}L')]^{n+}$ complexes facilitated in this regard. The coordination modes suggested by NMR data were further substantiated by data on the acid / base chemistry of the compounds incorporating the Hptr and H3Mptr ligands where protonation / deprotonation processes may occur. On the basis of the electronic and electrochemical results for these compounds, it was not

possible to differentiate between the coordination isomers as no substantial differences were found. However, it was proposed on the basis of NMR and acid / base properties that for isomer 1 of the Hptr and H3Mptr coordinated compounds, coordination occurs via the $N^{4'}$ position on the triazole ring. The results for isomer 2 of the lMptr coordinated compound also suggest coordination via the $N^{4'}$ position on the triazole ring. The data obtained for the other isomer 2 compounds implies that coordination occurs through the $N^{2'}$ site on the triazole ring.

Only one coordination mode is possible for the $[Ru(L\text{-}L)_2(4Mptr)]^{2+}$ compounds which is via the $N^{2'}$ position on the triazole ring, due to the presence of a methyl group on the $N^{4'}$ position.

The X-ray studies of $[Ru(bpy)_2(3Mptr)]^{+}$ have substantiated the $N^{1'}$ coordination mode of the 3Mptr ligand for the bpy compound. Although in this case, coordination isomers were not observed or isolated, this site would be the site where coordination would not be sterically hindered and which for the dmbpy / phen compounds would represent the main fraction.

An attempt was made to determine the structure of isomer 2 of $[Ru(dmbpy)_2(Hptr)](PF_6)_2(ClO_4).H_2O$ [26] The R value obtained (which is a measure of how good the expected result compares with the calculated result) was too high to be able to distinguish between a carbon or nitrogen atom and therefore, to differentiate between isomers. There were some indications to suggest that

coordination to the ruthenium atom occurred through the $N^{2'}$ site on the triazole ring but nothing conclusive. The calculated Ru-N distances and N-Ru-N angles were found to be in good agreement with the structure of $[Ru(bpy)]^{3+}$. [27,28]. An ORTEP diagram of the cation is presented in Figure 5.27. [29]

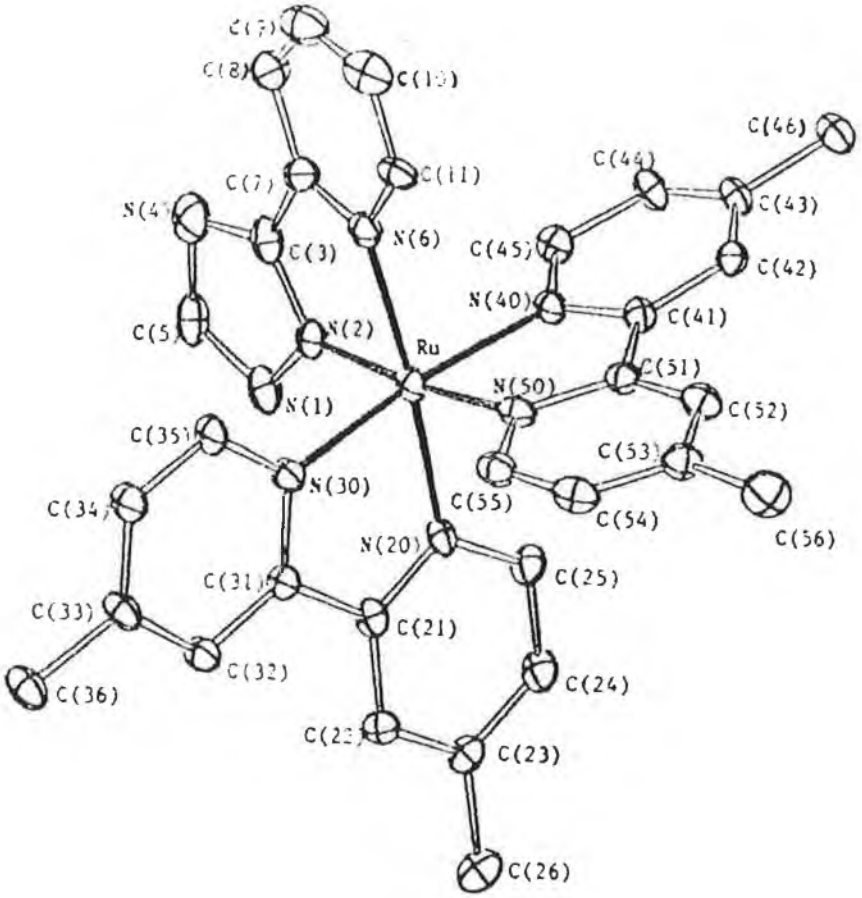

Figure 5.27 ORTEP diagram [29], of the $[Ru(dmbpy)_2(Hptr)]^{2+}$ cation. Atoms are represented by ellipsoids showing a 10% probability of their thermal replacement. Hydrogen atoms, water molecules and the disordered PF_6^- and ClO_4 groups have been omitted for clarity.

Deprotonation was found to have a profound effect on the electronic and electrochemical properties of the $[Ru(L\text{-}L)_2(Hptr)]^{2+}$ and $[Ru(L\text{-}L)_2(H3Mptr)]^{2+}$ compounds. The data shows that upon deprotonation the ligands are better σ-donors / weaker π-acceptors due to destabilisation of the metal d orbitals.

All the compounds investigated were found to emit at both room temperature and at 77 K, with emission intensity increasing with increasing pH for the compounds where protonation / deprotonation processes may occur i.e. the Hptr and H3Mptr coordinated compounds.

The acid-base properties show that the ligands act as stronger acids in the excited state indicating that the pyridyltriazole ligands do not participate in the emission processes. The observed emission for all the compounds is dmbpy / phen based.

In general, the properties of the complexes studied in this work are very similar to those of the analogous bpy complexes. However certain differences are evident for the dmbpy complexes in relation to their electrochemical behaviour. The oxidation potentials for the dmbpy complexes are somewhat lower than those of the phen or bpy complexes, indicating that the metal ion has more electron density, which is caused by strong σ-donating or weak π-accepting ligands. Also the more negative reduction potentials for the dmbpy complexes shows that these complexes are weaker π-acceptors, have higher lying π^* orbitals and consequently are harder to reduce.

The pK_a values determined for the H3Mptr coordinated complexes are generally higher than for the Hptr coordinated complexes. This is caused by the electron donating methyl group which yields a higher electron density on the triazole ring. For the H3Mptr and Hptr coordinated bis dmbpy complexes, the pK_a values are higher than for the phen or bpy analogues, again showing the additional donating effect of the methyl groups present on the dmbpy ligands.

5.7 References

[1] B.E. Buchanan, Ph. D thesis, Dublin City University, Dublin, Ireland, 1990.

[2] R. Hage, R. Prins, J.G. Haasnoot, J. Reedijk and J.G. Vos, J. Chem. Soc., Dalton Trans., 1987, 1389.

[3] L.J. Fitzpatrick, H.A. Goodwin, A. Launikonis, A.W.H. Mau and W.H.F. Sasse, Aust. J. Chem., 1983, 36, 2169.

[4] J.M. Kelly, C. Long, C.M. O'Connell, J.G. Vos and A.H. Tinnemans, Inorg. Chem., 1983, 22, 2818.

[5] C. Marzin, F. Budde, P.J. Steel and D. Lerner, Nouv. J. Chim., 1987, 11, 33.

[6] P. Belser and A. von Zelewsky, Helv. Chim. Acta, 1980, 63, 1675.

[7] E.C. Constable and J. Lewis, Inorg. Chim. Acta, 1983, 70, 25.

[8] P.J. Steel, F. Lahousse, D. Lerner and C. Marzin, Inorg. Chem., 1983, 22, 1488.

[9] J.G. Vos, J.G. Haasnoot and G. Vos, Inorg. Chim. Acta, 1983, 71, 155.

[10] A. Juris, V. Balzani, F. Barigelletti, S. Campagna, P. Belser and A. von Zelewsky, Coord. Chem. Rev., 1988, 84, 85.

[11] J.V. Caspar and T.J. Meyer, Inorg. Chem., 1983, 22, 2444.

[12] K. Kalyanasundaram, Coord. Chem. Rev., 1982, 46, 159.

[13] J. Juris, F. Barigelletti, V. Balzani, P. Belser and A. von Zelewsky, Inorg. Chem., 1985, 24, 202.

[14] E.S. Dodsworth and A.B.P. Lever, Chem. Phys. Lett., 1986, 124, 152.

[15] B.E. Buchanan, J.G. Vos, M. Kaneko, W.J.M. van der Putten, J.M. Kelly, R. Hage, R.A.G. de Graaff, R. Prins, J.G. Haasnoot and J. Reedijk, J. Chem. Soc., Dalton Trans., 1990, 1.

[16] J.F. Ireland, and P.A.H. Whyatt, Adv. Phys. Org. Chem., 1976, 12, 131.

[17] Md. K. Nazeeruddin and K. Kalyanasundaram, Inorg. Chem., 1989, 28, 4251.

[18] G. Yagil, Tetrahedron Lett., 1967, 23, 2855.

[19] R. Hage, J.G. Haasnoot, J. Reedijk, R. Wang, E.M. Ryan, J.G. Vos, A.L. Spek and A.J.M. Duisenberg, Inorg. Chim. Acta, 1990, 174, 77.

[20] B.D.J.R. Fennema, R. Hage, J.G. Haasnoot, J. Reedijk, and J.G. Vos, Inorg. Chim. Acta, 1990, 171, 223.

[21] P. Ford, D.F.P. Rudd, R. Gaunder and H. Taube, J. Am. Chem. Soc., 1968, 90, 1187.

[22] P.J. Giordano, C.R. Bock, M.S. Wrighton, L.V. Interrante and R.F.X. Williams, J. Am. Chem. Soc., 1977, 99, 3187.

[23] T. Shimidzu, T. Iyoda and K. Izaki, J. Phys. Chem., 1985, 89, 642.

[24] M. Haga, Inorg. Chim. Acta, 1983, 75, 29.

[25] A.M. Bond and M. Haga, Inorg. Chem., 1986, 25, 4507.

[26] J.M. de Wolf, Research project in Coordination Chemistry, Leiden University, Leiden, The Netherlands, 1990.

[27] A. Guy Orpen, L. Brammer, F.H. Allen, O. Kennard, P.G. Watson and R.J. Taylor, J. Chem. Soc., Dalton Trans., 1989, S1.

[28] D.P. Rillema, D.S. Jones and H.A. Levy, J. Chem. Soc. Chem. Commun., 1979, 849.

[29] C.K. Johnson, ORTEP Report, ORNL-3794, Oak Ridge National Laboratory, Tennesse, USA, 1965.

CHAPTER 6

FINAL REMARKS

6.1 Final remarks.

This thesis deals primarily with the synthesis and characterisation of ruthenium (II) polypyridyl complexes containing amino and isothiocyanate phenanthroline and pyridine ligands and the application of these complexes as fluorescent probes in biological systems. The secondary concern was the characterisation of a series of bis-(1,10 -phenanthroline) and bis-(4,4'-dimethyl-2,2'-bipyridyl) ruthenium (II) complexes containing various pyridyltriazole ligands and completes the study which was initially conducted on the bis-(2,2'-bipyridyl) analogues.

Chapter 1 begins with a general introduction on the properties of ruthenium polypyridyl complexes relevant to this thesis. The main subject matter of this chapter deals firstly with, the interactions of ruthenium polypyridyls with DNA and secondly, the use of fluorescent probes in immunochemistry. The interactions of ruthenium polypyridyl complexes with DNA are reviewed. This area has been the subject of active investigation over the past few years and concerns both electrostatic and intercalative interactions with DNA. The literature describes the use of ruthenium complexes as probes of DNA helicity which is possible by virtue of their chirality, where both left- and right-handed enantiomers are observed. By a judicious choice of ligand, the complexes may be made specific for different helical forms of DNA.

The spectroscopic properties of DNA bound

ruthenium polypyridyl complexes and the effects on the physical properties of DNA are described. The strong visible absorption band which is distinct from the absorption due to DNA, together with the stronger luminescence and increased excited state lifetimes of the DNA bound complexes, provide a spectroscopic tool for monitoring the binding process.

DNA thermal denaturation measurements can be used to distinguish between those complexes which bind intercalatively and those which bind electrostatically. Also, intercalation causes DNA to unwind and lengthen. This effect may be examined using electrophoretic mobility assays. In addition, intercalation stabilises the DNA helix by substantial structural overlap between the base pairs of the DNA molecule and the intercalated ligand. This effect may be monitored using fluorescence depolarisation and anisotrophic techniques, which indicate if intercalation occurs, that polarisation of emitted light is retained.

The use of ruthenium polypyridyl complexes as sensitisers for the photocleavage of DNA is briefly examined.

The second part of Chapter 1 reviews the use of fluorescent probes in immunochemistry. Conjugation reactions involving the modification of various chemical groups on the protein molecules are described and examples of various types of fluorescent probes are given.

The use of fluorescent probes in fluorescence microscopy and in immunoassay procedures is also discussed and includes the use of time-resolved fluorometric analysis.

This technique is applicable for the use of lanthanide chelates and ruthenium polypyridyl complexes as fluorescent probes. This is due to a combination of long emission lifetimes and large Stokes shifts. The use of ruthenium complexes in this manner has an advantage over the use of lanthanide chelates because fluorescence measurements may be carried out directly. With lanthanide chelates, prior to analysis, the chelate must be destroyed and the lanthanide ion must be embedded into liposomes in order to be detected.

The use of ruthenium complexes as fluorescent probes for biomolecules is reviewed. Various ruthenium (II) complexes have been conjugated to antibodies and albumins. The conjugation reaction has involved mostly, the modification of the ε-amino groups of lysine residues of protein molecules. This has been the subject of a number of patents. The use also, of ruthenium (II) bathophenanthroline complexes to label oligonucleotides has been described.

Chapter 2 deals with the experimental details and includes sections on (a) the synthesis of the complexes described in this work, (b) the instrumentation used to elucidate the various properties of the complexes and (c) the biological procedures, including details of the various conjugation reactions used and methods for determining protein concentration.

Chapter 3 describes the synthesis and characterisation of ruthenium (II) bis-(1,10-phenanthroline) and bis-(2,2'-bipyridyl) complexes containing amino and isothiocyanate phenanthroline and pyridine ligands. These

complexes were characterised using HPLC, UV/vis spectroscopy, electrochemistry, NMR, IR, and emission spectroscopy. HPLC was used to determine the purity of the various complexes. Infra-red spectra were used in a purely qualitative manner, to assess the success of the derivatisation reaction of the amino complex to its isothiocyanate derivative.

The proton resonance signals measured were assigned by comparison with literature data for similar compounds and also by comparison with the NMR spectra obtained for the pyridyltriazole complexes discussed in Chapter 5.

Electronic spectra and electrochemical measurements indicate that most likely, the 2,2'-bipyridyl and 1,10-phenanthroline ligands are the emitting ligands and the amino and isothiocyanate phenanthroline and pyridine ligands act as the spectator ligands.

The complexes described in this chapter were subsequently conjugated to biological materials and this is dealt with in Chapter 4.

In Chapter 4, the conjugation of a number of ruthenium (II) polypyridyl complexes to albumins, immunoglobulins and poly-L-lysine is described. The complexes were bound at different sites on the biomolecules, via the lysine residues, the carbohydrate moieties and via the tyrosine residues, demonstrating the chemical flexibility available for using these complexes as reporter molecules.

The effect of conjugation on the spectroscopic properties of the complexes was examined. The absorption

spectra were found to exhibit changes in the MLCT band with the absorption wavelength maximum experiencing slight red shifts together with general band broadening effects. The emission decay behaviour was also investigated. The unbound complexes were found to exhibit single exponential decay behaviour and the bound complexes exhibited essentially double exponential behaviour. From the double exponential decay fits, the first short-lived species was suggested to be a quenched bound species whilst the second species probably arises from a bound species which is considerably protected from the effects of quenching molecules.

Much of the work described in Chapter 4, represents initial experiments into the use of ruthenium complexes as reporter molecules in biological systems. These investigations show that there are two possible areas of research which may be pursued. One area is the study of these complexes in terms of their emission decay behaviour, with the possibility of their use as probes of protein structure. The second area concerns the use of ruthenium (II) polypyridyl complexes in time-resolved immunoassay methods.

With regard to the emission decay behaviour of the albumin and poly-L-lysine conjugates examined in this thesis, these were high molecular weight conjugates with high F/P ratios. Future studies could involve variation of the F/P ratio and size or structural conformation of the biomolecule. It would be interesting and appropriate to investigate the use of much lower molecular weight conjugates, which could

include the use of amino acids such as lysine or other amino acids which may be covalently bound to the ruthenium polypyridyl complexes and working up to quite large polypeptides consisting of the same or different amino acids. For lysine and poly-L-lysine conjugates (a range of various molecular weight poly-L-lysines are available), the effect of pH on the conformational structure of the poly-L-lysine molecule could lead to interesting effects in the emission decay behaviour.

Only preliminary measurements were made on the emission decay behaviour of antibody bound ruthenium complexes, so this needs further investigation.

The use of ruthenium labelled immunoglobulins as fluorescent probes was examined briefly. However, the retention of immunological activity after conjugation was demonstrated.

The fact that about a 10^{-3}M concentration of a ruthenium (II) polypyridyl complex is required to be bound to a biological molecule before emission is observed under the fluorescence microscope may indicate that these complexes may not be suitable in fluorescence microscopy techniques. However, the successful use of a ruthenium (II) polypyridyl complex in fluorescence microscopy procedures has been described in a patent, so, obviously further investigations are necessary.

The use of ruthenium polypyridyl complexes in time-resolved techniques has been described and hopefully the complexes described in this work will also find application in this way.

Finally, in Chapter 5, the synthesis and characterisation of a number of bis-(1,10-phenanthroline) (phen), and bis-(4,4'-dimethyl- 2,2'-bipyridyl) (dmbpy), ruthenium (II) complexes containing a series of pyridyltriazole ligands are detailed. The ruthenium ion may bind via the $N^{1'}$/ $N^{2'}$ or $N^{4'}$ of the triazole ring. The most favourable coordination mode being dependent on the position of a substituent on the triazole ring. Coordination isomers were obtained and separated by semi-preparative HPLC methods. The electrochemical results suggest that the phen and dmbpy ligands are the emitting ligands and that the pyridyltriazole ligands are the spectator ligands.

The acid-base chemistry of those complexes which can undergo protonation / deprotonation reactions was investigated and the results substantiated the coordination modes proposed using NMR data for the complexes. The ground state pK_a values show that there is a strong σ-donating effect from the triazole ring to the ruthenium ion. Also, the excited state pK_a^* values are lower than the ground state pK_a values which indicates that the pyridyltriazole ligands do not participate in the emission process. As mentioned already, this study completes investigations which were initially conducted on the 2,2'-bipyridyl analogues.

Publications.

E.M. Ryan, J.G. Vos, R. O'Kennedy, J.M. Kelly and M. Feeney.
Covalent linkage of ruthenium polypyridyl amino and isothiocyanate compounds to albumins, immunoglobulin G and poly-L-lysine.
To be submitted to Bioconjugate Chemistry.

R. Hage, J.G. Haasnoot, J. Reedijk, R. Wang, E. Ryan, J.G. Vos, A.L. Spek and A.J.M. Duisenberg.
Synthesis, spectroscopic and electrochemical properties and the X-ray structure of bis(2,2'-bipyridyl){3-(2-hydroxy-phenyl)-5-(pyridin-2-yl)-1,2,4-triazolato}ruthneium(II)hexafluorophosphate
Inorg. Chim. Acta, 1990, 174, 77.